NANYANG TECHNOLOGICAL UNIVERSITY

BEHAVIOURAL STUDY OF COMPLETELY OVERLAPPED TUBULAR JOINTS UNDER MONOTONIC AND CYCLIC AXIAL LOADING

YANG YE

SCHOOL OF CIVIL AND ENVIROMENTAL ENGINEERING

2007

BEHAVIOURAL STUDY OF COMPLETELY OVERLAPPED TUBULAR JOINTS UNDER MONOTONIC AND CYCLIC AXIAL LOADING

YANG YE

2007

Behavioural Study of Completely Overlapped Tubular Joints under Monotonic and Cyclic Axial Loading

Yang Ye

School of Civil and Environmental Engineering

A thesis submitted to the Nanyang Technological University
in fulfillment of the requirement for the degree of
Doctor of Philosophy

2007

ACKNOWLEDGEMENTS

The author is most grateful to his supervisor, Dr. Gho Wie Min, for his patient guidance and constructive advice throughout the research project, and also for his sincere encouragement which has benefited the author towards this interesting research.

The author wishes to acknowledge the financial support received from the School of Civil and Environmental Engineering, Nanyang Technological University in the form of scholarship.

The author expresses his appreciation to Mr. Koh Poh Seng for his help with usage of Unix Workstation and the technical staff in the Construction Technology Laboratory and Protective Engineering Laboratory for their kind assistance and support during the experimental testing. The author would like to thank his colleagues in the school: Dr. Gao Fei, Dr. Liu Dalin, Dr. Yang Zhengmao, Dr. Liu Yu, Dr. Shao Yongbo, Mr. Han Hongsheng, Mr. Sopha Thong for their useful discussions, earnest encouragement and long-standing friendship. Thanks are also made to all staff at NTU and all my friends and colleagues who have in one way or another contributed to this research project.

Special thanks are due to Professor Li Zhenfu, the author's Master degree supervisor, and Professor Zhang Sherong, Head of Department of Hydraulic Engineering, at Tianjin University, China, for their encouragement and recommendation to pursue the PhD degree at NTU.

Last but not least, the author wishes to give special thanks to his parents and his lovely wife for their invaluable encouragement. This would not be possible without their continued support.

TABLE OF CONTENTS

SUMMARY

For the design and construction of an offshore steel jacket, the main structural component to be considered is the joint connecting the chord and braces. The merits of using the completely overlapped tubular joint for the construction of offshore eccentrically braced steel jackets have recently been demonstrated in terms of economic design. This joint configuration shows better static strength and energy dissipation than simple gap joints. It has been commended that the completely overlapped tubular joint could be used in the offshore steel jacket to withstand intense seismic loading. However, the capacity and the behaviour of the joint under static and cyclic loading are still not well understood and the design of such joint configuration is not covered in the current offshore recommendations.

In the current study, the structural behaviour of the completely overlapped tubular joint under monotonic and cyclic loading is experimentally and numerically investigated. Two completely overlapped tubular joint specimens are tested to failure under monotonic and quasi-static cyclic loading. The comparison of the ultimate capacity under monotonic axial compression showed that the existing strength equations under-predict the test result of the joint specimen. The completely overlapped tubular joint specimen shows good ductility performance and energy dissipation capacity under cyclic loading.

In the finite element (FE) analysis, the four-node thick shell finite element is suitable for modelling the completely overlapped tubular joint specimens under both monotonic and cyclic loading. The material post yield property with the effect of strain hardening is adopted. The isotropic and the kinematic hardening rule simulate very well the static and cyclic behaviour of the joint, respectively.

A total of 3888 FE models of the completely overlapped tubular joints are created with various geometrical parameters to investigate the effect of geometrical parameters. The failure mechanism and the ultimate strength of the joint are the two main areas of study. The failure modes of the joint under lap brace axial compression include the through brace wall plastification, the lap brace yielding,

the lap brace local buckling and the lap brace member failure. A combination of these failure modes can be occurred depending on the geometrical parameters of the joint. The lap brace-to-through brace diameter ratio (β_{TL}), through brace-to-lap brace wall thickness ratio (τ_{TL}), through brace radius-to-wall thickness ratio (γ_T), gap size-to-through brace diameter ratio (ξ) and brace angle (θ) are the most crucial geometrical parameters controlling the failure behaviour of the completely overlapped tubular joint. The ultimate strength of the joints increases with increasing β_{TL} and τ_{TL}, but decreases with increasing γ_T, ξ and θ. The existing strength equations of simple T/Y- and gap K-joints which exclude the interactive effects of these geometrical parameters are not suitable for use to predict the ultimate strength of the completely overlapped tubular joints under lap brace axial loading.

A set of parametric equations is proposed for predicting the ultimate capacity of the completely overlapped tubular joint under lap brace axial compression. The reliability of the proposed equations has been verified against the current FE models and the test data. A simplified characteristic strength equation is also proposed for design of tubular joints with complete overlap of braces.

Apart from the ultimate capacity under static loading, the effect of geometrical parameters and load characteristics on the cyclic behaviour of completely overlapped tubular joints is also investigated. It is noted from both the experimental and the numerical study that the geometrical parameters of the chord and the through brace have minimal but the through brace and the lap brace have significant effects on the cyclic behaviour of the joints. The load carrying and the energy dissipation capacity of the joint rapidly deteriorate after the lap brace yielding and local buckling. It is recommended that the dissipative zone of the completely overlapped tubular joint under cyclic loading should be designed at the short segment of the through brace joining the chord. Furthermore, the ultimate capacity of the joint under static loading should not be used for predicting the strength of the joint under cyclic loading as the accumulative effect of strength and energy dissipation under tension and compression of the load cycles have not been considered.

LIST OF TABLES

LIST OF FIGURES

LIST OF SYMBOLS

A	Cross-sectional area
d	Brace outside diameter
d_L	Lap brace diameter
d_T	Through brace diameter
D	Chord diameter
E	Young's modulus
E_i	Energy dissipated in *i*th cycle
E_i^+	Energy dissipated in *i*th tension half-cycle
E_i^-	Energy dissipated in *i*th compression half-cycle
E_y	Energy dissipated at first yield displacement ($E_y = P_y \delta_y / 2$)
E_y^+	Energy dissipated in tension half-cycle with elastic-perfectly plastic material behaviour ($E_y^+ = P_y^+ (\delta_i^+ - \delta_y^+ + \delta_i^- - \delta_y^-)$)
E_y^-	Energy dissipated in compression half-cycle with elastic-perfectly plastic material behaviour ($E_y^- = P_y^- (\delta_i^- - \delta_y^- + \delta_i^+ - \delta_y^+)$)
g	Gap size between braces
l_L	Lap brace length
l_T	Through brace length
L	Chord length
N_c	Total number of load cycles
P_u	Ultimate strength in kN
p_i	Force magnitude at point of unloading in *i*th cycle
p_i^+	Force magnitude at point of unloading in *i*th tension half-cycle
p_i^-	Force magnitude at point of unloading in *i*th compression half-cycle
P_y	First yield load for elastic-perfectly plastic material behaviour
P_y^+	Yield load in tension half-cycle with elastic-perfectly plastic material behaviour
P_y^-	Yield load in compression half-cycle with elastic-perfectly plastic material behaviour
t	Brace wall thickness

t_l	Lap brace wall thickness
t_T	Through brace wall thickness
T	Chord wall thickness
u	Nodal global x displacement
v	Nodal global y displacement
w	Nodal global z displacement
ϕ_x	Nodal rotation about global x axis
ϕ_y	Nodal rotation about global y axis
ϕ_z	Nodal rotation about global z axis
α	Length parameter
t_1, t_2	Normalized vectors
$\bar{s}$, $\bar{d}$	Normalized vectors
V_1	Local coordinate of finite element ($\bar{s}+\bar{d}$)
V_2	Local coordinate of finite element ($\bar{s}-\bar{d}$)
V_3	Local coordinate of finite element ($V_1 \times V_2$)
α_C	Chord length parameter ($2L/D$)
α_L	Lap brace length parameter ($2l_L/d_L$)
α_T	Through brace length parameter ($2l_T/d_T$)
β	Brace-to-chord diameter ratio
β_{CT}	Through brace-to-chord diameter ratio (d_T/D)
β_{TL}	Lap brace-to-through brace diameter ratio (d_L/d_T)
γ_C	Chord radius-to-wall thickness ratio ($D/2T$)
γ_L	Lap brace radius to wall thickness ratio ($d_L/2t_L$)
γ_T	Through brace radius to wall thickness ratio ($d_T/2t_T$)
τ	Brace-to-chord wall thickness ratio
τ_{CT}	Through brace-to-chord wall thickness ratio (t_T/T)
τ_{TL}	Lap brace-to-through brace wall thickness ratio (t_L/t_T)
ξ	Gap size-to-chord diameter ratio (g/D)
ξ_c	constant isoparametric coordinates
θ	Lap brace angle with respect to through brace
ψ	Through brace angle with respect to chord

$\delta_{\max}$	Maximum deformation prior to fracture
δ_y	First yield deformation
δ_i^+	Maximum displacement in *i*th tension half-cycle
δ_i^-	Maximum displacement in *i*th compression half-cycle
δ_y^+	Yield displacement in tension half-cycle with elastic-perfectly plastic material behaviour
δ_y^-	Yield displacement in compression half-cycle with elastic-perfectly plastic material behaviour
μ	Ductility ratio ($\delta_{\max} / \delta_y$)
μ^+	Ductility ratio in *i*th tension half-cycle (δ_i^+ / δ_y^+)
μ^-	Ductility ratio in *i*th compression half-cycle (δ_i^- / δ_y^-)
μ_a	Accumulative ductility ratio ($\sum_{i=1}^{N_c}\left(\mu_i^+ + \left\|\mu_i^-\right\|\right)$)
ω^+	Strength resistance ratio in tension half-cycle (p_i^+ / P_y^+)
ω^-	Strength resistance ratio in compression half-cycle (p_i^- / P_y^-)
η	Energy dissipation ratio (E_i / E_y)
η_i^+	Energy dissipation ratio in *i*th tension half-cycle ($\eta_i^+ = E_i^+ \big/ E_y^+$)
η_i^-	Energy dissipation ratio in *i*th compression half-cycle ($\eta_i^- = E_i^- \big/ E_y^-$)
η_a	Accumulative energy dissipation ratio ($\sum_{i=1}^{N_c}\left(E_i^+ + E_i^-\right) / E_y$)
η_c	Constant isoparametric coordinate
ζ_i^+	Stiffness ratio in *i*th tension half-cycle ($\zeta_i^+ = \tan\alpha_i^+ \big/ \tan\alpha_y^+$)
ζ_i^-	Stiffness ratio in *i*th compression half-cycle ($\zeta_i^- = \tan\alpha_i^- \big/ \tan\alpha_y^-$)
$\tan\alpha_i^+$	Tangential slope of hysteresis loop (load changes from negative to positive at *i*th cycle)
$\tan\alpha_i^-$	Tangential slope of hysteresis loop (load changes from positive to negative at *i*th cycle)
$\tan\alpha_y^+$	Tangential slope of hysteresis loop with elastic-perfectly plastic material behaviour (load increases on positive side)
$\tan\alpha_y^-$	Tangential slope of hysteresis loop with elastic-perfectly plastic material behaviour (load increases on negative side)
σ_{eng}	Engineering stress
σ_{true}	True stress

ε_{true}	Logarithm strain
ε_{eng}	Engineering strain
σ_{max}	Maximum stress in chord
σ_{y}	Yield stress of member
σ_{u}	Tensile stress of member
σ_{cy}	Yield stress of chord
σ_{cp}	Prestress in chord

Abbreviation:

CBF	Concentrically Braced Frame
EBF	Eccentrically Braced Frame
MRF	Moment Resisting Frame
FE	Finite Element

CHAPTER 1

INTRODUCTION

1.1 Steel tubular structures

The installation of the first fixed template type steel structure in the Gulf of Mexico in 1947 marked the first use of welded tubular platforms in the offshore industry. Since then, many offshore platforms have been designed with various configurations to satisfy the need of functionality for the exploration of oil and gas beneath the sea bed in both shallow and deeper waters. Today, majority of offshore structures are found to be steel structures consisting of circular tubular members with one or more bracing members welded directly onto a main structural member. The tubular members are widely used because of their excellent strength and less exposed area to wind and wave loading. Furthermore, they exhibit greater economy in mass as well as possess better hydrodynamic properties than other structural steel open sections.

Offshore steel platforms are generally subjected to large gravity loads and cyclic environmental forces. The important aspect for design and service of these structures is to satisfactorily perform under service conditions and to maintain the requirement of safety under extreme load cases and credible accidents. Hence, the offshore structure should be designed to withstand repetitive loads due to marine forces and should not be suffered from catastrophe collapse due to other load sources such as earthquake and impact.

1.2 Geometrical properties of tubular joints

The geometrical properties of members meeting at a joint vary significantly according to the configuration and size of structures. As shown in Fig. 1.1, a steel jacket can generally be classified as X-, V- or S-braced frame depending on its configuration. Besides the joint can be characterised based on geometry (UEG 1985)

as shown in Fig. 1.2, American Petroleum Institute (API 2000) also classifies the joint according to load transfer mechanism. In the recommendation, a joint is considered as K-joint with the load in a brace balanced by the load on other brace in the same plane of the joint. On the other hand, a T/Y-joint is considered with the load reacted as beam shear in the chord. For X-joint, the load is carried through the chord to braces on the opposite side.

For design purposes, a tubular joint can be classified as one of the four categories (UEG 1985) as shown below.

- Simple welded joints
- Complex welded joints
- Cast steel joints
- Composite joints

The basic dimensions which describe a simple tubular joint are as follows.

- Chord outside diameter, D
- Brace outside diameter, d
- Chord wall thickness, T
- Brace wall thickness, t
- Brace angle, θ
- Gap size between braces, g

In order to facilitate the design and assessment of tubular joints under various types of loading, the following non-dimensional geometrical parameters are adopted. They are also used in the current research of completely overlapped tubular joints under both monotonic and cyclic loads.

- Chord length parameter ($\alpha = 2L/D$) to indicate the effect of boundary conditions and chord beam bending.
- Diameter ratio ($\beta = d/D$) to highlight the compactness of joint.
- Chord radius-to-wall thickness ratio ($\gamma = D/2T$) to show the thickness and radial stiffness of chord.
- Brace-to-chord wall thickness ratio ($\tau = t/T$) to measure the chord wall

failure prior to brace fracture.

- Gap size parameter ($\xi = g/D$) to assess the strength of joints consisting more than one brace.

1.3 Research study of tubular joints

The main component of steel tubular structures is the joint connecting the chord and the braces. Many researches conducted in the past had been concentrated on the fatigue and crack, ultimate capacity, and seismic resistance of the joints. The details of these research areas are briefly described below.

(i) Fatigue and crack

Offshore structures are generally subjected to active loadings with cyclic characteristics such as wind, wave and earthquake. In order to design the structure with a specific life span, the fatigue life is taken into consideration. During in-service inspection, the assessment of the joint with fatigue crack is performed with stress intensity factor input as a parameter in the analysis. The stress intensity factors are calculated from the empirical formulae with a very limited range of validity. For the past two decades, many investigations had been carried out to assess the fatigue life of tubular joints which led to the development of *S-N* curves for design. A number of parametric formulae to determine the stress concentration factors of tubular joints with different configurations had also been developed based on both experimental and numerical studies. The location of high stress concentration at the joint is crucial for the current investigation of completely overlapped tubular joint under cyclic loading as the crack initiation at a specific point along the intersection lines of members can be predetermined.

(ii) Ultimate capacity

For the research of ultimate capacity, the area of study is primarily focused on the prediction of ultimate strength and derivation of accurate formulations for joint design. Many existing design equations for tubular joints are based on a limited number of experimental results performed on simple joints with simple loading

conditions. The numerical simulation of joints using finite element (FE) method is commonly carried out with results compared with experimental data for calibration and verification. A detailed parametric study is subsequently conducted to obtain data for derivation of parametric formulae. In the current research, the ultimate capacity and the failure behaviour of the completely overlapped tubular joint under static loading are investigated in detail with objective to provide a basis for future design recommendation.

(iii) Seismic resistance

In this research, the performance of structures under earthquake excitation and the approaches to improve the ability of structures to dissipate and absorb seismic energy to avoid brittle collapse are assessed. Since 1960s, engineers have noted that the seismic performance of a structure due to large infrequent earthquake depends principally on its inelastic cyclic behaviour. As a result, a series of research on inelastic cyclic behaviour of steel structures as well as their individual members are examined. However, these works mainly focused on the inelastic cyclic response of beams and members of trusses and braced frames as well as moment resisting connections. The research on the cyclic behaviour of connections in braced frames or trusses is not adequately covered. In the current research, the inelastic behaviour of the completely overlapped tubular joint for offshore steel jackets is assessed primarily based on the ductility performance and energy dissipation capacity under cyclic loading. In these aspects, both experimental and numerical investigations of the joint under cyclic loading have been conducted.

1.4 Completely overlapped tubular joint

Presently, the X-braced steel jacket as shown in Fig. 1.1a is the most common type of offshore structures used in earthquake sensitive areas. This type of framing allows the two braces acting as tension members to resist the load while the other two are redundant. However, this conventional X-framing steel jacket can be very expensive to fabricate. For wellhead platforms, Cheung et al (1998) proposed the use of diagonally braced steel jacket with completely overlapped tubular joints to

replace the X-braced steel jacket with concentric joints to effectively dissipate energy under earthquake loading (Fig. 1.1d).

It had been shown from the conceptual study that the steel jacket with completely overlapped tubular joint proposed by Cheung et al (1998) could function as well as the conventional jackets and was found to be lighter, cheaper to fabricate and easier to install. The saving in terms of main steel fabrication man-hours could be as much as 25% in comparison to that of the conventional S-braced jacket (Fig. 1.1c). On the other hand, the saving of fabrication man-hours could be 15% to 20% and 40% to 50% less for static and earthquake design considerations respectively in comparison with that of the X-braced jacket (Fig. 1.1a).

The special feature of the eccentrically braced steel jacket proposed by Cheung et al (1998) is the completely overlapped tubular joint configuration at every connection along the legs of the main structure. This joint comprises a chord, a through brace and a lap brace. The through brace joins the chord while the lap brace is fully welded onto the through brace surface. A gap size on the through brace between the lap brace and the chord outer surfaces is to facilitate welding, non-destructive testing and weld inspection (Fig. 1.3a).

It should be noted that the connections of the conventional offshore steel jackets are usually T/Y-, KT- or K (N)-joints as depicted in Fig. 1.3b. The configuration of the eccentrically braced jacket is found similar in some ways to the eccentrically braced frame (EBF) in the building industry. In EBF, a short member at the joint known as “link” (Fig. 1.3c) has been designed to absorb and dissipate energy through shear mechanism with the structure behaving in ductile mode. The design philosophy of EBF is that under severe earthquake loading, plastic yielding is forced to occur on the link members so that the structure can be prevented from complete collapse. In spite of this similarity, the effectiveness of eccentrically braced steel jacket to resist seismic loading is yet to be verified owing to the use of welded tubular joints.

In capacity considerations, dissipative structures are designed by allowing the

yielding of structural components to ensure that the earthquake resistance is by dissipating energy through hysteretic ductile behaviour. Non-dissipative parts of the dissipative structures are designed with sufficient over-strength to allow cyclic yielding at dissipative zones of structural components. The dissipative zones are often located near the end of structural members. Thus, the ductility of seismic resistant structures is deeply influenced by the behaviour of their connections. For the completely overlapped tubular joint of the eccentrically braced steel jacket, the load is predominantly transferred between the braces without passing via the chord. Because of the failure mechanism shifting from the chord to the through brace, the joint could have a great application potential to prevent the structure from catastrophe collapse under extreme loading (Soh et al 2001).

However the capacity and the behaviour of the completely overlapped tubular joint under static and cyclic loading are still not well understood and the design is not covered in the current offshore design recommendations. Because of the overlapping of braces, the stress distribution at the joint becomes more complicated to be determined and evaluated. Until today, the study of the completely overlapped tubular joints is only limited to two full-scale tests conducted by the researchers from Nanyang Technological University (NTU). One of the tests conducted was to determine the static strength of the joint under monotonic loading (Fung et al 2001a) whilst the other for seismic behaviour under cyclic loading (Soh et al 2001). Thus, an intensive investigation to better understand the capacity and the behaviour of the completely overlapped tubular joints under both static and cyclic loading are essential before a conclusion can be drawn with confidence on the potential application of eccentrically braced steel jacket in practice.

1.5 Objectives of current research

The main objective of the current research is to provide a basis for the design of completely overlapped tubular joints of eccentrically braced offshore steel jacket under both static and cyclic loading. In order to meet this objective, the following areas of research are conducted.

(i) The failure mechanism and the capacity of the completely overlapped tubular joint under monotonic compression and cyclic loading are experimentally investigated. The test results are used for the calibration and verification of FE models.

(ii) The influence of geometrical parameters on the ultimate capacity and the failure behaviour of the completely overlapped tubular joint is examined. A set of parametric formulae is developed for predicting the ultimate strength of the joint under monotonic loading.

(iii) The existing guidelines in the codes and recommendations are reviewed and modified for the design of completely overlapped tubular joints.

(iv) The ductility performance and the energy dissipation capacity of the completely overlapped tubular joint under cyclic large plastic deformation are determined. An assessment on the effectiveness of the joint under seismic loading is proposed.

1.6 Scope of current research

The structural behaviour of the completely overlapped tubular joints under monotonic and cyclic loading is experimentally and numerically investigated. In chapter 1, the use of tubular joints in the offshore construction industry is introduced. The previous research on fatigue, ultimate strength and seismic resistance of tubular joints are briefly summarized. The objectives and the scopes as well as the originality of the current research are also presented.

In chapter 2, the literature with respect to static strength and cyclic behaviour of the completely overlapped tubular joints are reviewed. The existing strength formulae and recommendations for design of tubular joints are described in detail. The existing seismic design requirements of steel structures are also included. In chapter 3, the test set up of the two completely overlapped tubular joint specimens with one subjected to monotonic compression and the other under cyclic loading are presented.

The numerical study of the failure behaviour and the ultimate capacity of the completely overlapped tubular joint under lap brace axial compression are shown in Chapters 4, 5, 6 and 7. In Chapter 4, the test results are used for verifying the FE models. The modelling techniques with respect to element types, weld elements and material properties are discussed. In Chapter 5, the effect of geometrical parameters on the failure mechanism of the joint is examined. The numerical results of the ultimate capacity of the completely overlapped tubular joint are summarised in Chapter 6. A new set of parametric formulae for predicting the ultimate strength of the joint is developed in Chapter 7.

Chapters 8 and 9 present the numerical investigation of completely overlapped tubular joint under cyclic loading. In chapter 8, several behavioural parameters to evaluate the cyclic behaviour of the joint are introduced. A comparison of ultimate behaviour between the completely overlapped joint and gap K-joints is conducted. In Chapter 9, the parametric study of the joint under cyclic loading is carried out. The results of the study include the hyteresis behaviour, strength resistance, ductility capability and energy dissipation capacity of the joint. Finally, in Chapter 10, a conclusion is drawn with respect to the objectives of the current research. The future research proposals on completely overlapped tubular joint are highlighted.

1.7 Originality of current research

The merits of using the completely overlapped tubular joint for the construction of offshore eccentrically brace steel jackets had been demonstrated by Cheung et al (1998) in terms of economic design. This joint configuration also demonstrates better static strength than simple gap joints, and significant potential to resist seismic loading with sufficiently large energy dissipation and zone of plastification. However, these comments are derived based only on experimental results of two large-scale test specimens and a limited numerical study conducted at NTU.

The failure modes of the completely overlapped tubular joint under interactive

effect of geometrical parameters have not been studied. The parametric equations for predicting the ultimate strength of the joint have not been developed. The ductility performance and the energy dissipation capacity of the joint under seismic loading have not been investigated. Thus, in the scope of the current research, an extensive experimental and numerical investigation on the structural behaviour and the ultimate capacity of the complete overlapped tubular joint under static and cyclic loading are carried out.

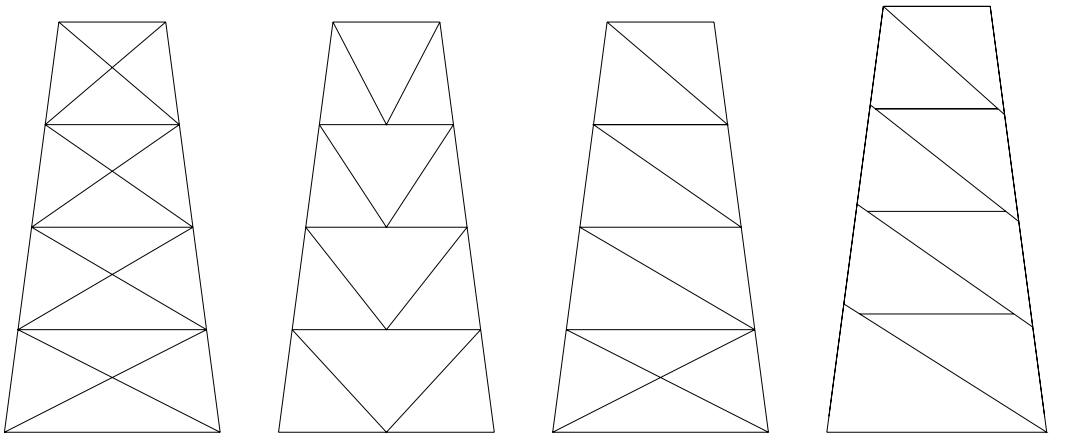

(a) X-braced jacket (b) V-braced jacket (c) S-braced jacket (d) Eccentrically braced jacket

Fig. 1.1 Steel jacket configurations

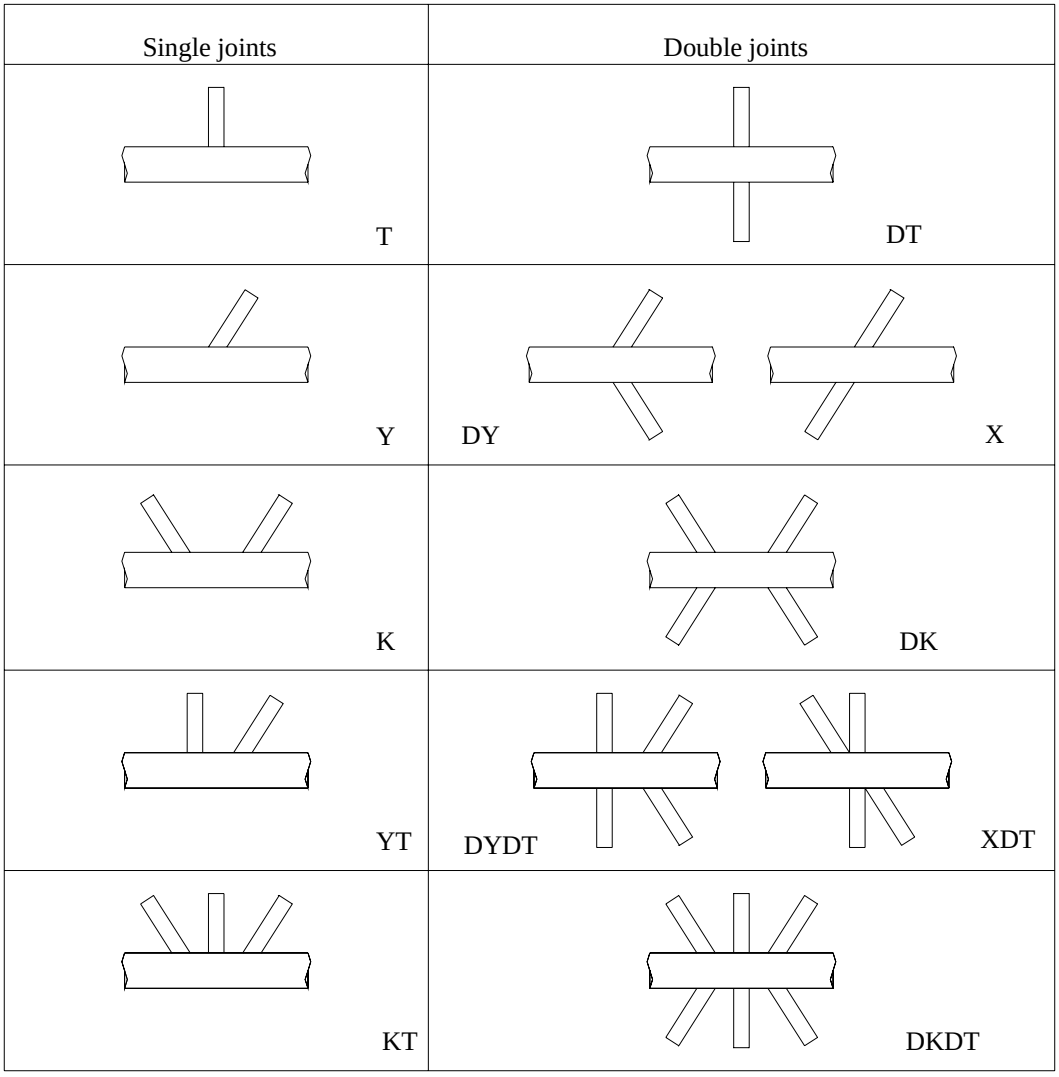

Fig. 1.2 Notations for joint configurations (UEG 1985)

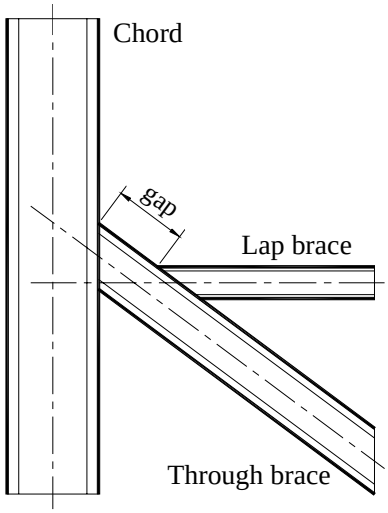

(a) Completely overlapped K(N)-joint

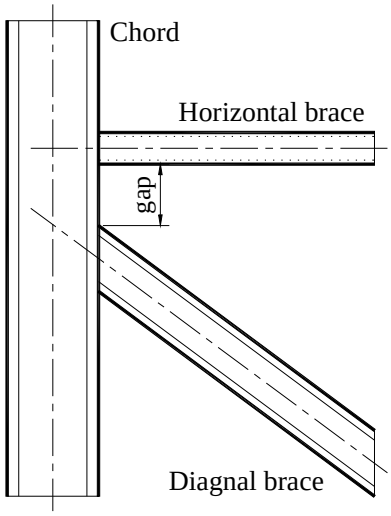

(b) Conventional gap K-joint

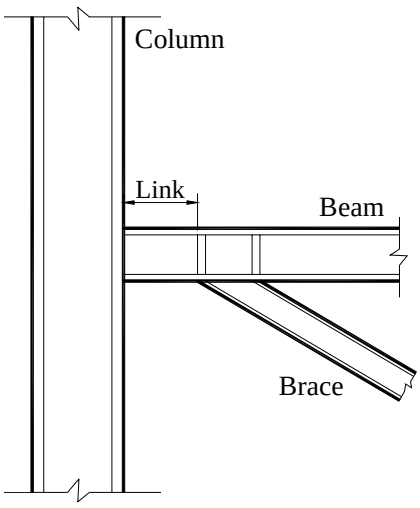

(c) Joint in EBFs

Fig. 1.3 Comparison with column-beam connections

CHAPTER 2

LITERATURE REVIEW

2.1 Static behaviour and strength of welded tubular joints

The ultimate load behaviour of welded tubular connections can be complex and difficult to analyse owing to non-uniform stress distributions at joint intersections. For the past three decades, the analysis and design of welded tubular joints had extensively been conducted for joints with brace end axial loads and subsequently for joints with brace end bending moments, chord pre-stressing and combination of axial, in-plane and out-of-plane loading. Many parametric equations based on these load types had been derived experimentally and numerically for joints with various geometrical configurations. Factors accounting for boundary conditions and materials, geometrical and load variations had also been included to enhance the accuracy and reliability of developed equations for design.

2.1.1 Criteria and modes of failure

Typical load - displacement curves for welded tubular joints under brace end axial compression and tension are shown in Fig. 2.1. For welded tubular joints under brace end axial loading, there are three possible criteria to define the failure namely the ultimate load capacity, the deformation limit and the visually observed crack initiation (Wardenier 1982). However, among these failure criteria, the most accepted criterion of failure for welded tubular joints was the ultimate load capacity under brace end axial compression as it yielded the lowest load capacity. The deformation limit was set to account for overall frame collapse prior to joint failure. This was dependent upon the type of structures being investigated, the level of applied loading and the specifications in design recommendations. Yura et al (1980) proposed a practical deformation limit ($\triangle$) for axially loaded joints with the formulation as shown below.

$$\Delta = 60\sigma_y d / E \tag{2.1}$$

where d, σ_y and E are the diameter, the yield stress and the Young's modulus of the brace, respectively. It was interesting to note that Yura et al's deformation limit was proportional to brace-to-chord diameter ratio (β) for joints with same chord diameter. However, the deformation limit was empirical and was not directly related to the ultimate or serviceability limit state of joint design. Based on the comparison of deformation at brace-chord intersection, Lu et al (1994) concluded that the deformation limit of 3% the chord diameter could be taken as the ultimate strength of welded circular hollow section joints under brace end axial loading.

For welded tension-loaded joints, the failure was generally associated with yielding and ovalising of chord member. As the load increased, the crack initiated at hot spot location of member and then propagated until the brace separated from the chord. However, if the joint was found to be stronger, the brace member would neck and fail in plastic yielding. Because of this failure behaviour, there was no clear sign of peak in the load - displacement curve. For the past research work, Dexter and Lee (1999a) assumed 20% of tensile strain on member outer surface as the onset of cracking in their FE model. The strain value obtained was claimed to be conservative and was a serviceability limit. However, the current experimental study on the completely overlapped tubular joint under cyclic loading revealed that the strain limit of the joint was well below the 20% of that defined by Dexter and Lee. The difference of strain values was due to the load condition where the accumulated strain was considered for joints under cyclic loading.

The failure mode of a tubular joint is generally dependent upon the material properties, geometrical configuration and loading conditions. The typical failure modes of uni-planar simple welded tubular joints as shown in Fig. 2.2 can be commented as follow.

(a) The plastic failure of the chord wall in the vicinity of braces. This failure mode was found common for simple welded tubular joints under axial

compression. In the current experimental study of the completely overlapped tubular joints, the chord wall plastification was observed at the joint intersection of through brace and lap brace.

(b) The rupture of brace due to cracking and large tensile stress at weld. Since the weld was designed to have strength greater than the structural member, and was subjected to non-destructive testing, the weld failure of tubular joint was generally not considered.

(c) The cracking of chord wall at hot spot location of member. This was the most common type of failure mode for joints under axial tension, particularly for joints with brace diameter smaller than chord diameter. The crack initiation would eventually lead to rupture of brace from chord.

(d) The local buckling on compressive area of brace or chord for joints fabricated from thin walled hollow sections.

(e) The lamellar tearing of chord face due to thick chord wall for joints subjected to tension. A good material quality and welding process were necessary to avoid failure.

(f) The shear failure of chord wall at gap location between braces for gap K- and N-joints with large brace-to-chord diameter ratio.

Similar to the current investigation of completely overlapped tubular joints, the gap size of axially loaded gap K-joints between the braces had a significant effect on the failure mechanism. At large gap size, the joint behaved as two independent Y-joints. As the gap size reduced, the load in the compression brace was balanced by that in the tension brace. As a result, the strength of the joint increased with reduced chord ovalization. The plastificaton of chord wall on compression brace and the crack initiation followed by rupture of tension brace were the two most common failure modes for gap K-joints.

For overlap joints, part of the load was made to directly transfer between the two braces through their common weld to enhance the joint strength with reduced chord wall thickness. Dexter and Lee (1999a) concluded from their FE analysis results that the distribution of failure modes of axially loaded tubular overlap K-joints

might be attributed to the interactive effects of geometrical parameters, β, γ, τ and amount of overlap. It was commented that the brace local buckling was the common failure mode for axially loaded tubular overlap K-joints.

The examination of the failure modes of the joints under static loading by Paul (1992) showed that welded tubular joints had enormous reserve capacity beyond yield. The first yield of tubular joints occurred at load level well below the ultimate load capacity. As commented by Marshall (1984), welded tubular joints could be failed at load level of 2.5 to 8 times the magnitude of first yield. Therefore, it was important that the joints should be designed to have adequate rotational and deformation capacity for redistribution of stresses to resist higher loading.

2.1.2 Determination of static ultimate strength

The static ultimate strength of a welded tubular joint should be determined based on the ability of chord wall to resist the loads applied by the braces. These brace loads are resisted by the combined plate and membrane action in the chord wall as shown in Fig 2.3. The plate action occurred at crown region of the joint with brace loads resisted by the transverse shear and bending effect of the chord wall. The membrane action occurred at saddle region for joints with large brace-to-chord diameter ratios where the brace loads were resisted by the axial forces of the chord wall. As the chord wall is found stiffer in membrane than in plate action, this will result in non-uniform stress distribution at the brace-chord intersection as depicted in Fig 2.4.

The static strength of a welded tubular joint could be defined as a function of material strength, geometry of connected members, and applied loading. The material strength could be represented by the tensile strength of the chord or brace member. The geometry of the joint was represented by the non-dimensional parameters such as β, γ, τ, amount of overlap and brace angle.

One of the most important geometrical parameters in determining the ultimate

strength of a welded tubular joint was the brace-to-chord diameter ratio (β). As the diameter of the brace is smaller than that of the chord at small β, the brace load was mainly resisted by the plate action of the chord wall. On the other hand, as the diameter of the brace approached to that of the chord at large β, the brace load was resisted by the membrane action of the chord wall. As a result, the strength of the joint increased. However, it was noted that the strength increase of the joint was not significantly affected until β was larger than 0.6. The strength increase of the joint at large β was also due to longer weld length provided at joint intersection.

The ultimate strength of a welded tubular joint was also affected by the chord diameter to wall thickness ratio (γ). The γ parameter could be used to determine the radial flexibility of the joint. As the chord became thicker in relation to its diameter at small γ, the radial stiffness of the chord increased and so was the strength of the joint. However, it should be aware that many ultimate strength equations developed for design of welded tubular joints did not include γ parameter to account the radial stiffness of the chord. The reason was that the ultimate strength of the joint under various load conditions was controlled by the behaviour at brace-chord intersection. In this connection, the chord wall was stiffened and reinforced by the presence of brace member. As a result, the radial stiffness of the chord did not have any significant effect on the ultimate strength of the joint.

Despite the brace-to-chord wall thickness ratio (τ) was not explicitly expressed in most of the existing ultimate strength equations, it should not be interpreted that τ was unimportant. It was important to note that τ was one of the most important parameters included in the punching shear formula to determine the joint strength under static loading specified in AWS. Furthermore, τ was usually the main parameter to be examined for economic design and failed tubular joints (Marshall 2004).

The strength of the welded tubular joints was also influenced by the brace angle (θ). Owing to the strength of the chord wall in membrane action, only the brace load

component perpendicular to the chord wall need to be considered for joints under axial load case. The inclination of brace with respect to chord with increased length at the brace-chord intersection could have a significant effect on the tensile capacity of a welded tubular joint (Hoadley 1983).

The gap size parameter (ξ) was an important variable to determine the strength of joint comprising more than one braces welded on one side of the chord. For K-joint with sufficiently large gap size between two braces, each brace-chord intersection could be treated as one separate T/Y-joint. As the gap size became smaller, the strength of the joint increased due to increased chord bending stiffness between the braces.

The ultimate strength of a tubular joint under static loading was influenced by the type of loading applied such as axial compression and tension, in-plane bending, out-of-plane bending, and combination of these loadings. The type of loading applied would determine the failure mode of the joint. In most load cases, the failure of the joint was controlled by the brace and not the chord loading. It was important to realise that the type of loading applied determined the dominant action of plate or membrane at the joint to resist brace loading. The membrane action dominated if the brace axial loads were resisted at the saddle of a joint. Furthermore, the tension loaded joint exhibited higher ultimate capacity than the compression loaded joint as the failure mode was governed by the fracture in the heat-affected zone along the weld profile instead the plastic bending or buckling of the chord wall.

For joints under in-plane bending load case, the highest brace load occurred at crown location and thus the plate action dominated. A joint loaded in in-plane bending would have a higher ultimate load capacity with higher stiffness than a joint loaded in out-of-plane bending. However, the joint ultimate capacity under both in-plane bending and out-of-plane bending are not included in the current research work and are recommended for future study.

The presence of compressive stress in the chord significantly affected the ultimate strength of a tubular joint as it drastically reduced the strength of the joint by weakening the plate action of the chord wall (Weinstein and Yura 1986). The presence of the load interaction of more than one brace loading also reduced the strength of the joint.

2.1.3 Ultimate strength formulae

Most of the design guides expressed ultimate strength equations of welded tubular joints in a format of limit states based on strength or failure load. Owing to the complexity of geometrical configurations, the static strength of tubular joints was generally obtained from the experimental study. Several sets of parametric equations had been proposed for predicting the static strength of tubular joints. The main form of these equations was determined by simple analytical models supplement with correction factors to reflect the effect of joint parameters. These correction factors were mathematically derived by fitting a curve to available test data.

One of the primary objectives in developing parametric equations for welded tubular joints was to identify the significant geometrical parameters on joint behaviour. Both experimental and numerical techniques were used to determine the function in relation to the effect of geometrical parameters on joint strength. The impact of parameters α, β, γ, τ, ξ and θ on joint behaviour were studied and included in the parametric equations for predicting the ultimate capacity of the joint. Generally speaking, the strength of a tubular joint could be presented as a non-dimensional function of joint parameters as shown below.

$$P_{nd} = f(\alpha, \beta, \gamma, \tau, \xi, \theta) \tag{2.2}$$

It was assumed that the above parameters had no coupling effect. Thus, EQ (2.2) could be rewritten as follow.

$$P_{nd} = f_1(\alpha)\cdot f_2(\beta)\cdot f_3(\gamma)\cdot f_4(\tau)\cdot f_5(\xi)\cdot f_6(\theta) \tag{2.3}$$

EQ (2.3) could further be expanded to incorporate the material properties and the chord pre-stressing as shown in EQ (2.4) to determine the ultimate strength of the joint under static loading (Wardenier 1982).

$$P_u = \sigma_y \cdot T^2 \cdot f_1(\alpha)\cdot f_2(\beta)\cdot f_3(\gamma)\cdot f_4(\xi)\cdot f_5(\theta)\cdot f_6(\sigma_m/\sigma_y)\cdot f_7(\sigma_y/\sigma_u) \tag{2.4}$$

where P_u was the ultimate strength of the joint expressed in terms of axial load. σ_y, σ_u, σ_m, and T were the yield stress, the ultimate material tensile stress, the maximum applied stress, and the chord wall thickness respectively. These functions could be determined based on a theoretical ring analogy which was related to the plastic moment of a ring model of unit width. The influential functions f_1 to f_7 in EQ (2.4) were determined based on the experimental results. The ultimate strength P_u of the joint under brace end axial loading was non-dimensional using the parameter $\sigma_y T^2$.

Washio et al (1968, 1969) investigated the geometrical parameters influencing the static strength of gap K- and N-joints. A formula was proposed for predicting the ultimate strength of the joint as shown in Table 2.1. The geometrical parameter Q_g was used to model the effect of gap sizes which was defined as follow.

$$Q_g = \begin{cases} 1.75 - 2.65(g/D), 0 \le g/D \le 0.23 \\ 1.15 - 0.06(g/D), \quad g/D > 0.23 \end{cases} \tag{2.5}$$

The formula yielded the strength of T/Y-joints at Q_g = 1. The strength function derived by Washio et al formed the basis for the development of formula in DNV rules (1977). However, it was commented by Wardenier (1982) that the formula used was too conservative for joints with thin-walled chords ($\gamma > 25$).

Based on the computer analysis of stresses of tubular joints and the test correlation

between first yield and failure load of the joint, Reber (1972) proposed a formula to calculate the ultimate strength of T-, Y- and K-joints under brace axial load as shown below.

$$P_u = \frac{5.4\sigma_y}{K \sin^{1.5}\theta} \tag{2.6}$$

where $K = 0.62D^{0.7}/T^{1.6}d^{1.1}$ was the hot spot stress caused by a unit axial load of the brace. Reber's formula can be converted to a non-dimensional form as shown in Table 2.1. Despite the simplicity of the developed equation, the influence of gap size for K-joints and the pre-stressing of chord had been neglected. Additionally, the validity range of β was limited to 0.25 and 0.75. Reber (1972) recommended a safety factor of 1.7 used in the equation for predicting the allowable load of tubular joints for all load cases.

A regression method had been used to derive the ultimate strength formulae for tubular joints by Kurobane et al (1976). Based on the interpretation of test results, the mean strength of T-, Y- and K-joints under compressive load is shown in Table 2.1. The developed formulae also covered joints with overlap of braces and thin-walled chords. On the other hand, Pan et al (1977) analyzed the database of 132 number of simple T-, Y- and X-joints and 214 number of K-joints and proposed a reduction factor for the formula developed by Washio et al (1968, 1969). The developed formulae for predicting the ultimate strength of tubular joints based on the available test data shown in Table 2.1 were regarded as the lower bound with confidence level of 95%.

Similarly, Yura et al (1980) also used the test results of 137 tubular joints to derive lower bound capacity equations for design. Their research work systematically addressed axially and moment loaded T-, DT-, Y- and K-joints. The failure load was taken as the minimum of the peak load in load - displacement curves, the load level of initiating crack and the load corresponding to the deformation limit. The database based on test results was carefully analyzed for the development of formulae as

shown in Table 2.1. These formulae formed the basis of recommendations in the 15th edition API RP2A (1984).

It had been demonstrated from the experiments that the geometrical parameter (*L/D*) of the joint had an influential effect on test results (Kurobane et al 1980a, b). It was also found that the yield to ultimate stress ratio of the joint was the main reason causing the difference of results obtained from the tests conducted in Japan and other countries. Furthermore, the gap size of K-joints was found to be more influential based on *g*/*T* rather than *g*/*D* ratio as it was also dependent upon the γ parameter. The re-analysis of K- and N-joints by Kurobane (1981) established a new design ultimate capacity formula for tubular K-joints (Table 2.1).

Based on the re-analysis of ultimate strength data by Kurobane et al (1980a), International Institute of Welding (IIW) (1981) proposed strength formulae as shown in Table 2.1 for predicting the capacity of tubular joints. In contrast with the previous research conducted by Kurobane et al (1980a), IIW used the characteristic value rather than the lower bound for developing the design equations. The characteristic strength was defined as the value below 5% of the test data. It should be noted that the formulae proposed by IIW were based on a semi-empirical approach derived from joints loaded under brace compression.

In 1984, Kurobane et al presented another new set of design equations for T-, Y-, X- and K-joints based on test results of 747 test specimens (Table 2.1). The developed equations determined the ultimate strength of tubular joints based on a semi-empirical approach. It was assumed that the joint failure was due to excessive plastic deformation. A simple analytical mode comprising a ring model having the same geometrical and material properties as the chord, had been used for predicting the joint behaviour. The joint capacity was computed as the collapse load in the ring model. This load level was defined as the ultimate strength of the joint. Using this method, the yield strength was found approximately 80% of the ultimate strength of the joint. The results of 747 test specimens had been used to calibrate the analytical model.

2.1.4 Review of existing design codes

Presently, there was no standardisation of capacity formulae in various design codes for predicting the ultimate strength of tubular joints. Generally speaking, there were two approaches available to determine the adequacy of the joint based on different analytical models.

The punching shear approach formulated in a working stress design format was based on punching shear model. It was assumed in this model that the ultimate capacity of the joint reached after the chord wall failed in shear. From the equilibrium of forces at joint intersection, as shown in Fig. 2.5, the acting shear stress in the chord wall was given as

$$v_P = \tau f \sin\theta \tag{2.7}$$

where f was the nominal axial, in-plate bending, or out-of-plate bending stress in the brace. In allowable stress design, the shear stress on the potential failure surface of the joint should not exceed the allowable punching shear stress. The allowable shear stress was determined by empirical design equations derived based on the curve fitting of available test data. The punching shear method did not account for membrane action in the chord wall. Thus, the model was not applicable for joints with large β as membrane action could be significant. The basic formulation was calibrated against the experimental data.

The other approach for joint design was based on a limit state format of ring model with the applied load less than the ultimate load. It was assumed in the ring model that the failure mechanism of the joint was due to plastic failure of the chord. This was the most likely failure mechanism for tubular joints subjected to compressive forces. In the ring model, the joint was simulated as a ring with identical geometrical and mechanical properties as the chord member, and with effective length B_e (=3(D-T)), as shown in Fig. 2.6. The brace axial loads were applied as two

line loads equivalent to half the brace vertical load component. The two line loads were separated with a distance equal to the joint diameter at the middle plane of brace wall. The axial and the shear stresses causing the bending of the ring were neglected. The ultimate brace load was computed by assuming plastic hinges as shown below.

$$2m_P = \frac{P_u \sin\theta}{2}\left(\frac{D-d}{2}\right) \tag{2.8}$$

The plastic moment (m_p) for a rectangular section along the effective length of the chord was,

$$m_P = \frac{B_e T^2}{4}\sigma_y \tag{2.9}$$

Thus,

$$P_u = \frac{2B_e}{D}\frac{1}{1-\beta}\frac{\sigma_y T^2}{\sin\theta} \tag{2.10}$$

It was important to realise that no formulae were currently available and suitable for predicting the strength of completely overlapped tubular joints. In the classification according to the load pattern, the lap brace and the through brace carried part of the brace axial load as K- as well as Y-joint. The through brace of the joint was treated as a chord member. In this section of the thesis, nine codes and recommendations for both onshore and offshore concerning the static strength of T/Y- and gap K-joints were reviewed and compared.

The onshore design criteria were as follows.

(a) *CIDECT (Wardenier et al 1993)*

The design strength formulae in CIDECT were developed based on ultimate limit

state with the characteristic load multiplied by appropriate load factors. The design strength of the joint included the safety factor and was governed by two criteria namely the plastification of the chord cross section and the chord punching shear. Most of the design formulae in this code were referenced to the works of Kurobane et al (1984).

(b) *American Welding Institute, AWS (2000)*

In AWS, the simple joints were designed based on the basis of punching shear or ultimate load format. The punching shear was an allowable stress design criterion which included a safety factor of 1.7. The ultimate load was used in load and resistance factor design where the resistance factor was specified.

(c) *American Institution of Steel Construction, AISC-LRFD (2000*)

It was noted in AISC that the design strength of the brace under axial loads was determined from the limit states of chord wall plastification, punching shear rupture, and general collapse. For T-, Y-, and gapped K-joints, the design strength of the brace was taken as the lower value obtained from the limit states of chord wall plastification and punching shear rupture. The criteria specified in AISC-LRFD (2000) were similar to those in AWS (2000). However, AWS did not include a set of applicability limits for tubular joints except an upper limit for yield strength of 414MPa. Marshall (2004) recently reviewed and compared the design criteria of ANSI/AISC-360-05 for tubular joints and commented that "*This is essentially the same as the CIDECT-based IIW document, except that it gives the characteristic ultimate strength without hiding a partial safety factor therein*".

The offshore design criteria were as follows.

(d) *American Petroleum Institute, API RP 2A (API 2000)*

The concept of design criteria in API was similar to that in AWS (2000). Two formats of the formulation were included in the code namely the punching shear and the nominal load. The capacity equations presented in the recommendations were the lower bound of available test data.

(e) *Health and Safety Executive, HSE (2002)*

HSE provided technical information previously contained in the fourth edition of HSE's "*Offshore Installations: Guidance on Design, Construction and Certification*" (HSE 1990) which had been withdrawn in 1998. The relevant sections on tubular joints were published as separate documents in the HSE Offshore Technology Report series. In this guide, an expanded database considered by API formed the basis of static strength equations. The additional data included those with different load and geometrical conditions which gave a more refined set of equations used for design. Furthermore, the design equations in HSE were based on a lower characteristic formulation rather than the lower bound approach as presented in API. However, the overall approach for code checking was based on working stress with characteristic capacities being reduced by a safety factor to yield allowable loads.

(f) *International Standardisation Organization, ISO* (2004)

Despite the first edition of ISO requirement adopted the provisions of API RP2A-LRFD (1993) for strength design of welded tubular joints, it made significant changes in the second edition to account the inconsistency of lower bound formulation in API RP2A-LRFD with respect to rigorous statistical analysis adopted in limit states. In the second edition of ISO, the technical core group included the additional equations of HSE and MSL (Dier and Lalani 1998) as the basis and combined with other design considerations to derive the equations. The requirements were based on the design considerations of the representative strength of tubular joints comparable to lower bound strength.

(g) *Other Standards and Recommendations*

The NORSOK (2004) standard to a very large extent adopted the provisions of ISO standard for the strength design of welded tubular joints. On the other hand, the DNV (2004) guide stated that the strength of tubular joints should be checked against the specifications in API RP 2A-LRFD (1993) and NORSOK (2004). The ABS (2004) guide provided formulations to assess the ultimate strength limit state

of tubular joints.

2.1.5 Comparison of existing design codes

In this section, the existing design equations for welded tubular joints in the codes were expressed in term of nominal load format for comparison. It should be noted that the empirical expression of equations for axial load capacity of tubular joints had the form of

$$\frac{P_u \sin\theta}{\sigma_y T^2} = kQ_u Q_f \tag{2.11}$$

where k, Q_u and Q_f were the multiplier, the factor to account for joint geometry, and the strength reduction factor to account for chord pre-stressing, respectively. In the comparison of the ultimate strength of the joint, all the partial safety factors specified in the equations were removed.

The comparison of Q_u parameter for the axially compression loaded T/Y- and gap K-joints in the design codes is summarised in Table 2.2. For T/Y joints, AWS, AISC (LRFD), HSE, ISO, NORSOK and ABS included Q_β parameter to consider the effect of strengthening for joints with large β.

$$Q_\beta = \begin{cases} 1.0 & \beta \le 0.6 \\ 0.3/\beta(1-0.833\beta) & \beta > 0.6 \end{cases} \tag{2.12}$$

For the joint strengths with respect to β parameter, CIDECT and AISC (Marshall 2004) assumed a parabolic relationship whereas API (21st Ed.) assumed a linear behaviour. The γ parameter was excluded in the joint strength equations in AWS, AISC (LRFD), API (21st Ed.), HSE, ISO and NORSOK. However, AISC, CIDECT and ABS considered the effect of $\gamma^{0.2}$. The proposed 22nd edition of API RP2A gave a different expression of strength formulae which depended on γ parameter (Marshall 2004). HSE considered additional factor (K_a) to account for length

increased at joint intersection. However, it was important to realise that the K_a parameter was regarded as a multiplier in the equation for predicting the ultimate strength of axially loaded welded tubular joints and was not directly related to Q_u.

For joints with low β, the ultimate capacity calculated from the equations in the codes was similar. However, for joints with high β, only AWS, AISC (LRFD), HSE, ISO, NORSOK and ABS yielded the similar ultimate capacity. API, AISC and CIDECT indicated higher whereas API (21st Ed.) showed lower joint ultimate capacity. The difference of the joint ultimate capacity was due to the difference in the relationship of ultimate strength and β parameter.

Similar to simple T/Y-joints, AWS, AISC (LRFD), HSE, ISO, NORSOK and ABS also introduced Q_β parameter in the equation to account for the effect of strengthening for compression loaded gap K-joints with large β. The influence of gap size for gap K-joints was complex and was presented differently in the strength equations. The equations in CIDECT and AISC (Marshall 2004) were expressed in terms of g/T. On the other hand, the equations in API, HSE, ISO, NORSOK and ABS were expressed in terms of g/D. It should be noted that ISO and NORSOK were based on g/T whilst API (21st Ed.) specified g/T or d/D depending on γ parameter. For AWS and AISC (LRFD), the gap size factor was expressed in terms of g/d. The formulation in CIDECT, AISC (Marshall 2004), ISO and NORSOK provided a specific equation to include joints with both gap and overlap configurations. However, Marshall (2004) commented that the strength criteria of gap and overlap K-joints in CIDECT might simply be an artefact of curve fitting. Dexter and Lee (1999b) also commented the abrupt change in behaviour and failure mechanism of K-joints with increasing gap size from gap to overlap. It was important to realise that the failure mechanism of gap K-joints was associated with high shear stresses and cracking in the gap region between braces. For overlap K-joints, the failure was mainly due to the brace local buckling controlled by τ parameter.

The parameter Q_f was derived to account for the effect of chord pre-stressing. For

the existing design codes, the comparison of the chord stress factor (Q_f) for compression axially loaded T-, Y- and gap K-joints is presented in Table 2.3. (Table 2.4 presents Q_f of the existing strength formulae). NORSOK and ABS presented Q_f in the form of stresses whilst other design codes expressed Q_f in terms of forces. In CIDECT, AISC (Marshall 2004), API, ISO and NORSOK, the chord stress effect was independent from γ parameter.

The comparison of validity ranges for design of welded tubular joints in the codes is summarised in Tables 2.5. Despite the strength criteria in AWS were used in AISC (LRFD), AWS did not specify the applicability of equations for design of tubular joints. However, an upper limit of yield stress of 414MPa was stated. Similar to the requirement in AWS, CIDECT imposed an upper limit of yield stress of 355MPa. AISC (LRFD) did not specify any limit of yield strength for joint design and so were API (21st Ed.), HSE, ISO, NORSOK and ABS. However, the range of validity of γ was extended from 25 (specified in AISC and CIDECT) to 50. It should be noted that members with γ parameter less than 30 were the most commonly used in service.

For gap K-joints, only AISC (LRFD) and CIDECT specified a limit of eccentricity whilst other codes did not impose any requirement. In comparison with the specification in HSE, ISO and NORSOK extended the maximum limit of yield stress from 400 to 500MPa. For the parameter τ, only ABS specified a limit of 1.2 whilst other codes did not impose any requirement. However, CIDECT commented that τ should be as low as possible to obtain the necessary efficiency. For the gap size of K-joints, CIDECT, AISC (LRFD) and HSE specified a minimum limit based on brace wall thicknesses whilst ISO, NORSOK and ABS based on chord diameter. On the contrary, API (21st Ed.) required an absolute minimum of 51mm for the gap size of the joint to facilitate welding and non destructive testing.

2.2 Cyclic behaviour of tubular joints

2.2.1 Review of previous work

Steel tubular structures were widely used in the building and offshore industry. They were generally designed to resist earthquake, wind and wave loading. Under these extreme load conditions, the tubular members could be subjected to cyclic inelastic behaviour and lead to damage causing the structure to collapse. For the past few years, many experiments had been conducted to intensively study the inelastic behaviour of steel tubular structures under cyclic loading.

Popov et al (1980) experimentally investigated the behaviour of two one-sixth-scale tubular X-bracing planar frame specimens (offshore tower) under cyclic lateral loading. It was observed that a significant loss of frame capacity was mainly due to brace buckling. The braces with large diameter-to-thickness ratio (D/T) were found to experience earlier and more severe local buckling and failures than those of smaller D/T ratio. The buckling behaviour of the braces showed that the inelastic action was concentrated within the localized plastic region. The localised buckling on the braces leading to the development of plastic hinges was further subjected to high concentration of both compressive and tensile inelastic action under cyclic loading.

Furthermore, the comparison of behaviour of the braces with fix- and pin-ended of the frame specimens was conducted. The results indicated that the braces with pin-ended commonly used in the building construction were not applicable for the design of offshore towers. The local joint flexibility of the frame under inelastic cyclic load reversals was also highlighted.

Zhu et al (1995) studied the structural responses of frame structures with flexible joints under cyclic and dynamic loading conditions. The results from their study showed that the presence of flexible joints significantly affected the vibration characteristics of the structure. The structural response of the frame with the flexible

joints was found dampen and magnified under excitation frequency.

Under extreme loading conditions such as storm and earthquake, the joints of tubular structures could be subjected to loads beyond the design values. In this circumstance, redistribution of loads on the structure could be occurred as a result of buckling and plastic deformation of members. A significant plastic formation on the hot spot region of the joints was noted. Skallerud (1992) carried out detailed study on the relationship of low cycle fatigue with crack growth of welded steel components. The results revealed that the initiation and the growth of crack rapidly occurred for welded components subjected to alternating plasticity. Thus, it was concluded that for a tubular joint exposed to such loading, the crack growth in the hot spot region significantly reduced the stiffness and the strength of the joint. The internal load distribution would be affected and thus the load carrying capacity of the structure.

Several tubular T-joints with chord diameter and wall thickness of 503 mm and 20 mm respectively had been tested to failure under cyclic loading by Skallerud et al (1995). All the test models were found to fracture extensively at the chord weld toe. Owing to cracking at the joint, the applied tensile load was significantly reduced. However, the compressive load was unaffected by the crack at the weld toe. The test was continued into the tensile region to observe the failure behaviour of the joint after through thickness cracking of the chord. Although a significant monotonic crack growth was developed, the tensile load of the test specimen showed good ductility performance of the joint.

Gao et al (2000) conducted cyclic elasto-plastic large displacement analysis of eccentrically loaded steel box and pipe columns of bridge piers under cyclic in-plane loading. The ultimate strength and the ductility capacity of the centrally loaded and eccentrically loaded steel columns subjected to cyclic transverse loading were investigated. The analysis results showed that the load-carrying capacity of the eccentrically loaded columns significantly decreased with increasing eccentricity.

Elchalakani et al (2002) studied a series of tests of fix-ended tubular braces subjected to cyclic concentric axial loading. It showed that the inelastic cyclic behaviour of circular hollow sections was sensitive to both section and member slenderness. The braces with relatively low slenderness ratios still exhibited large ductility index.

From the test results described above, it could be found that the main influencing factors on the inelastic behaviour of steel tubular columns were the cyclic mechanical properties of material, slenderness ratio, radius-to-thickness ratio and magnitude of axial load.

2.2.2 Seismic design requirements

(a) *American Petroleum Institute, API RP 2A (2000)*

In API RP 2A, the strength and the ductility were the two main requirements to be considered for design of offshore platforms under earthquake loading. The strength criteria required the platform to be adequately sized for strength and stiffness so that no significant structural damage occurred in moderate earthquakes. On the other hand, the ductility requirement was to ensure that the platform had sufficient reserve capacity to resist the intense earthquake excitation. This was achieved through the system redundancy to allow for load redistribution and inelastic deformation before the structure completely collapsed.

For tubular members, the ductility and the cyclic degradation characteristics were strongly dependent upon the width-thickness and slenderness ratios. A significant amount of ductility could be implemented on structures with appropriate width-thickness and slenderness ratios. However for tubular joints, they were sized accordingly to the yield and buckling capacity of braces to avoid premature failure so that the ductility performance of the structure could be fully developed.

Based on the energy absorption capacity, API RP2A recommended that the energy

dissipated by inelastic deformation must be at least four times the energy absorbed by structures at first yield under monotonically increasing loads.

(b) *American Institute of Steel Construction, AISC (1997)*

It should be noted that the structural steel building system in a seismic region was expected to dissipate seismic input energy through the controlled inelastic deformation of structures. This provision had been supplemented in "Seismic Provisions Supplement No. 2" (AISC 2000) for the design and construction of structural steel members and connections.

AISC (1997) recommended that the seismic design of beam-to-column joints and connections of Moment Resisting Frame (MRF) should be based on the qualifying cyclic test results with an inelastic rotation of at least 0.03 radians. The qualifying test results should be at least 2 cycles. Although the acceptance criteria of the test usually focused on the level of plastic rotation, the tendency for the strength of connections degraded with increasing deformation was of great concern.

It had been observed from the experiments that the damage of Concentrically Braced Frame (CBF) generally associated with the effect of limited ductility and brittle failure of connections and bracing members. The requirement for the design of ductility and energy dissipation capability of structures had recently been incorporated into the seismic codes. The main objective for the design of CBF was to allow the frame subjected to a relatively large deformation under intense earthquake excitation with bracing members behaved in cyclic tension and compression in post-buckling range.

The Eccentrically Braced Frame (EBF) withstood significant inelastic deformations under intense earthquake excitation with use of short link members at connections to dissipate energy. The columns, diagonal braces, and beam segments outside the links of the frame were designed to remain elastic under the maximum lateral forces. However, the potential occurrence of inelastic behaviour in the columns should be

avoided to prevent the possible failure of the frame due to soft story. It should also be noted that the formation of plastic hinges at column bases of the frame were not allowed in severe earthquake.

(c) *British Standard Institution, BSI (1996)*

In European code EC8, it was specified that the dissipative zone of a structure should be designed to yield or buckle under hysteretic behaviour. The overall stability of the structure must not be affected. The dissipative zone should have adequate ductility and resistance. For the non-dissipative parts of structures, sufficient strength must be allowed for the development of cyclic yielding on the dissipative zone.

The code further specified that the beam-to-column joints for MRF should have adequate strength to allow plastic hinges to be developed on the beams. For the design of CBF, yielding of diagonals in tension should take place before yielding or buckling of the beams and columns as well as connections. On the other hand, they were designed such that the beams were able to dissipate energy by formation of plastic bending as well as plastic shear mechanisms.

(d) *New Zealand Standard, NZS 4203 (1992)*

The New Zealand earthquake code described that a good seismic resistance structural system intended for the dissipation of seismic energy by ductile flexural yielding should have adequate ductility. Furthermore, it commented that an approximate criterion for adequate ductility was that the building as a whole should be able to sustain four cycles of loading with a ductility ratio equal to 4 without the horizontal strength being reduced by more than 20%.

Although the design concepts developed in the United States, Europe and New Zealand had successfully been employed in the building industry, Soh et al (2001) pointed out that the applicability of these building design codes to offshore tubular

structures must thoroughly be investigated owing to a number of features which had not been considered in the building construction. Additionally, relatively little is known about the inelastic seismic behaviour of tubular welded connections. One of the features for the offshore structures was that most members were made from circular hollow section tubes and were welded together. However, in the building industry, structural-I or -H sections were the most commonly used elements for beams and columns. These members were usually connected by bolts. Because of the differences of structural elements and connection details, this had led to some unique mechanical behaviour such as buckling and cracking at the weld toes which significantly influenced the seismic performance of offshore structures.

2.3 Understanding of completely overlapped tubular joints

Simple gap joints were the most commonly used structural connections in tubular structures. The fabrication of the joint was straightforward with the bracing members directly welded onto the chord face. Non-destructive testing and underwater inspections of the joints could easily be conducted. However, due to the gap size between the braces on the chord, longer and thicker joint-cans at connections could be cost ineffective. In order to minimize the footprint length or where the required thickness of joint cans outside the fabrication capability, overlap joints were preferred.

Overlap joints generally referred to joints with two braces partially overlapped and no gap existed on the chord face. The potential cost benefit of overlap joints to reduce the length of joint-cans had been investigated in detail by Zettlemoyer (1988) and Lalani (1992). Additionally, overlap joints generally had higher load capacity than simple gap joints. Healy (1994) reported that the overlap joints could have strength 1.25 to 2.25 times the corresponding gap joints.

More recently, Dexter et al (1994, 1996) performed parametric finite element (FE) study to establish relationship between strength and overlap amount of braces. It was found that the joints were stronger with the through brace in tension than in

compression. However, the behaviour of the fully overlapped joint was opposite. A similar result was also observed in the study of the completely overlapped joints by Gho (2001).

Dexter and Lee (1999a, b) extended their research based on the FE analysis to cover the behaviour of overlap K-joints due to various geometrical parameters. The amount of overlap of the braces was of primary interest in their work. It was concluded that overlapping had an increasingly beneficial effect on strength of axially loaded overlap tubular K-joints. The strength increase was 3 to 4.5 times the strength of gap joints. For the load transfer mechanism of partially overlapped joints, part of the load was made to directly transfer between the braces through their common weld and the chord only transferred a small magnitude of load. This would lead to a reduction of chord wall thickness used at connections of tubular structures. However, the fatigue behaviour of the joints with partial overlapping braces might not be good because of the weld imperfection resulted from complicated welding process. The common weld of the braces had to be designed to partly transmit the shear force and to overcome the stress concentration. Besides, the ends of braces were double coped and the inspection of the hidden weld could be difficult.

On the other hand, complete overlap of braces could provide a more straightforward fabrication than partial overlap joints and better strength behaviour than simple gap joints (Wardenier et al 1993). The use of completely overlapped joints at connections of offshore structures was not uncommon and was usually adopted whenever simple gap and partially overlapped joints were not feasible. For this joint configuration, the through brace joined the chord while the lap brace was fully welded onto the through brace surface. A gap size on the through brace between the outer surfaces of the lap brace and the chord was to facilitate welding, non-destructive testing and inspection of welds. For the past decades, the understanding on the structural behaviour of completely overlapped joint was still very limited.

In the 1980s, if the overlap of two braces was large or complete, the through brace

member was taken as a chord member and considered as such in the analysis of the joint (DEn 1984). It had been shown by Philiastides (1988) that the rectangular hollow section gap joints had an inherent flexibility that could lead to low joint strengths. However, the 100% overlap joints could have the advantage of having a great stiffness.

The investigation of trusses with 100% overlapped joints by Coutie and Saidani (1989) highlighted that the normal shear force was largely transferred through the overlapping members. Thus, the checking of chord shear failure was not necessary in the case of gap joints. Furthermore, they commented that fully overlap joints produced little normal deformation of the chord face and the strength of the joint was much less sensitive to chord axial load than for gap joints. Nevertheless, the design of the fully overlapped joints was regarded simpler than that of gap or partially overlapped joints.

The research on the behaviour of partially overlapped joints by Dexter et al (1996) highlighted that overlapped joints exhibited strength increase with amount of overlap. However, it was noted that the strength of the joint reached the peak at a certain amount of overlap and then decreased until the joint became completely overlapped. This was because the gap region on the through brace was subjected to high shear stresses and the failure was due to cracking at low load level (Dexter and Lee 1999a, b). For more than 100% overlap joints, the behaviour of the gap region of the through brace could have substantial effect on the mode of failure and the strength of the joint. It was commented that under this circumstance the joint behaved as two Y-joints with the through brace acting as a chord.

From construction viewpoint, Cheung et al (1998) conducted a cost analysis between the conventional concentrically and eccentrically braced jackets and concluded that the eccentrically braced frame with use of completely overlapped joint could achieve a 25% reduction in main steel fabrication man-hours. However, if the eccentrically braced frame could be used to replace the conventional X-braced jacket in the earthquake sensitive areas, the cost of fabrication and material could

significantly be reduced. It was important to note that the ability of the eccentrically braced jacket to absorb energy still required intensive investigation.

The experimental investigation on the behaviour of completely overlapped tubular joints under static and cyclic loading had been conducted by the researchers from NTU, Singapore (Fung et al 2001a, b; Soh et al 2001). Their test results revealed that the ultimate capacity of the joint was close to that of the gap K-joint. The failure mode was due to the through brace face plastification with bulging on the through brace saddle vicinity. Bending on the gap region was clearly observed. Furthermore, the joint specimen demonstrated a good ductility performance with a deformation limit of about four times the lap brace yield deformation. The maximum strain concentration was found to occur on the through brace saddle. It was noted from their study that the stress concentration and the local flexibility of the joint decreased with gap size between the outer surfaces of the chord and the lap brace on the through brace. However, the ultimate capacity of the joint increased with decreasing gap size. These results indicated that the completely overlapped joint could have higher ultimate capacity, lower stress concentration and smaller elastic deformation in comparison to simple joints.

Under cyclic inelastic behaviour, Fung et al (1999) found that the buckling and the plastic hinges in the gap region of the through brace was the main mechanism to dissipate seismic energy for the completely overlapped joint. Soh et al (2001) showed that the completely overlapped joint dissipated more energy in the compression than in the tension phase owing to the effect of local buckling on the through brace. The local buckling deformation on the through brace dissipated most of the input energy.

In comparison with the gap K-joint, the completely overlapped joint was able to ensure the safety of the chord member. For the gap K-joint, the critical location was found on the chord wall in the gap region. However for the completely overlapped joint, it was located on the through-brace wall in contact with the lap brace.

The completely overlapped joints showed several merits over simple gap joints with regard to cost, capacity and energy dissipation. However, these conclusions had been drawn only based on a limited study. Despite the joint was of great application potential for the design of eccentrically braced offshore steel jacket in the seismic region, the understanding on the ultimate strength, failure mode, ductility and energy dissipation mechanism of the joint were still needed to be investigated in greater detail.

Table 2.1 Strength formulae for axially compression loaded tubular joints

Authors	Non-dimensional strength $P_u \sin\theta / \sigma_y T^2$		Validity range
	T/Y-joint	Gap K-joint	
Washio et al. (1968,1969)*	$(1+6.52\beta)\gamma^{0.5}(1-0.26\cos^2\theta)Q_g Q_f$		$\gamma \le 25$
Reber (1972)	$11.49\beta^{1.1}\gamma^{0.4}\sin^{-0.5}\theta$		$0.25 \le \beta \le 0.75$
Kurobane et al. (1976)*	$7.14(1+3.79\beta^2)\left[1+3.34(1-10.45\gamma)(1-0.776\beta^2)\left(1+\frac{2/\pi}{\tan(0.4-0.4\gamma)}\right)\right](1+0.0392\cos\theta-0.187\cos^2\theta)Q_f$		N.A.
Pan et al. (1977)	$4.38\beta\gamma^{0.5}$	$\begin{cases} 0.8\gamma^{0.5}(1+6.52\beta)(1-0.26\cos^2\theta), & 0.16 \le g/D \le 0.7 \\ \gamma^{0.5}(1+6.52\beta)(1-0.26\cos^2\theta)(1.05-1.59g/D), & -0.5 \le g/D \le 0.16 \end{cases}$	$30^0 \le \theta \le 90^0$ $9.5 \le \gamma \le 46.5$ $0.19 \le \beta \le 1.0$ (for T/Y-joint)
Yura et al. (1980)	$3.4+19\beta$	$\begin{cases} (3.4+19\beta)(1.8-0.8g/d), & g/d < 1 \\ (3.4+19\beta), & g/d \ge 1 \end{cases}$	N.A.
Kurobane (1981)*	-	$2.57(1+4.67\beta)(2\gamma)^{0.184}(1-0.343\cos^2\theta)\left[1+\frac{0.00613(2\gamma)^{1.41}}{1+\exp[0.394(g-3.11)/T-0.525]}\right]\left(\frac{\sigma_y}{\sigma_u}\right)^{-0.757}Q_f$	N.A.
IIW (1981)*	$(3.3+16.5\beta^2)\gamma^{0.2}Q_f$	$(2.4+11.2\beta)\left(1+\frac{0.012\gamma^{1.5}}{\exp(0.39g/T-0.53)}\right)\gamma^{0.2}Q_f$	$0.25 \le \beta \le 1.0$ $\gamma \le 25$ $-D/2 \le e \le D/4$ (for K joint)
Kurobane et al. (1984)	$4.83(1+4.94\beta^2)\cdot(2\gamma)^{0.233}(L/D)^{-0.45}$	$2.11(1+5.66\beta)(2\gamma)^{0.209}(1-0.376\cos^2\theta)\left[1+\frac{0.00904(2\gamma)^{1.24}}{1+\exp[0.508(g-3.04)/T-1.33]}\right]\left(\frac{\sigma_y}{\sigma_u}\right)^{-0.723}$	N.A.

**Chord stress factor (Q_f) is defined in Table 2.4.*

Table 2.2 Geometric factor (Q_u) in existing design codes

Codes	T/Y-joint	Gap K-joint
CIDECT (1991)	$(2.8+14.2\beta^2)\gamma^{0.2}$	$(1.8+10.2\beta)Q_g$ (g negative for overlap) $Q_g=\gamma^{0.2}\left[1+\frac{0.024\gamma^{1.2}}{1+\exp(0.5g/T-1.33)}\right]$
AWS (2000)	$(3.4+18.8\beta)Q_\beta^{0.5}$	$(3.4+32\beta/\alpha)Q_\beta^{0.7(\alpha-1)}$ $\alpha=1.0+0.7g/d$, $(1.0\le\alpha<1.7)$
AISC-LRFD (2000)	as in AWS	as in AWS
AISC 360-05* (Marshall 2004)	$(3.1+15.6\beta^2)\gamma^{0.2}$	$(2.0+11.33\beta)Q_g$ Q_g as in CIDECT
API RP 2A-WSD (21st, 2000)	$3.4+19\beta$	$(3.4+19\beta)Q_g$ $Q_g=\begin{cases}1.8-0.1g/T, & \gamma\le 20\\ 1.8-4g/D, & \gamma>20\end{cases}$, $(Q_g\ge 1.0)$
API RP 2A-WSD* (Marshall 2004)	$\begin{cases}2.8+(20+0.8\gamma)\beta^{1.6}, & \gamma\le 20\\ 2.8+36\beta^{1.6}, & \gamma>20\end{cases}$	$\begin{cases}(16+1.2\gamma)\beta^{1.2}Q_g, & \gamma\le 20\\ 40\beta^{1.2}Q_g, & \gamma>20\end{cases}$ $Q_g=1+0.2(1-2.8g/D)^3$
HSE** (1990)	$(2+20\beta)Q_\beta^{0.5}K_a$ $K_a=(1+1/\sin\theta)/2$	$(2+20\beta)Q_\beta^{0.5}K_aQ_g$ $Q_g=1.7-0.9(g/D)^{0.5}$, $(Q_g\ge 1.0)$
ISO (1995)	$(1.9+19\beta)Q_\beta^{0.5}$	$(1.9+19\beta)Q_\beta^{0.5}Q_g$ $Q_g=\begin{cases}1.9-(g/D)^{0.5}, & g/T\ge 2.0, Q_g\ge 1.0\\ 0.13+0.65\phi\gamma^{0.5}, & g/T\le -2.0\\ \textit{Interpolation}, & -2.0<g/T<2.0\end{cases}$ $\phi=t\sigma_{yb}/T\sigma_y$
NORSOK (2004)	as in ISO	As in ISO
ABS (2004)	$(0.5+12\beta)\gamma^{0.2}Q_\beta^{0.5}$	$(0.5+12\beta)\gamma^{0.2}Q_\beta^{0.5}Q_g$ $Q_g=1+0.85\exp(-4g/D)$, $(g/D\ge 0.0)$

**Referred from Marshall (2004)*

***K_a is presented as a multiplier rather than an element of Q_u.*

Table 2.3 Chord stress factor (Q_f) in existing design codes

Codes	Chord stress factor (Q_f) **
CIDECT (1991)	$1+0.3(\overline{U}-\overline{U}^2)$, $\overline{U}=P_p/A\sigma_y+M/S\sigma_y$ P_p and M are prestressing load and moment in chord. A is chord cross-sectional area, and S is chord elastic section modulus.
AWS (2000)	$1-0.03\gamma\overline{U}^2$, $\overline{U}^2=(P_c/A\sigma_y)^2+(M_c/S\sigma_y)^2$ P_c and M_c are factored load and moment in chord.
AISC LRFD (2000)	as in AWS
AISC 360-05* (Marshall 2004)	as in CIDECT
API RP 2A-WSD (21st, 2000)	as in AWS
API RP 2A-WSD* (Marshall 2004)	$1-C_1(P_c/A\sigma_y)-C_2(M_c/S\sigma_y)-C_3\overline{U}^2$, $\overline{U}^2=(P_c/A\sigma_y)^2+(M_c/S\sigma_y)^2$
HSE (1990)	Extreme conditions: $1-0.05\gamma\overline{U}^2$; Operating conditions: $1-0.09\gamma\overline{U}^2$ $\overline{U}=\sqrt{(0.23PD)^2+M^2}\,/\,(0.72D^2T\sigma_y)$ Q_f = 1, if chord axial tension force is lager than M/0.23D.
ISO (1995)	$1-0.03\overline{U}^2$, $\overline{U}^2=C_1(P/A\sigma_y)^2+C_2(M/M_p)^2$ M_p is representative plastic moment strength of chord. C_1 = 25 and C_2 = 11 for T/Y joint, C_1 = 14 and C_2 = 43 for gap K joint.
NORSOK (2004)	$1-0.03\overline{U}^2$, $\overline{U}^2=C_1(f_a/\sigma_y)^2+C_2(f_b/(1.27\sigma_y))^2$ f_a and f_b are design axial and bending stresses in chord. C_1 = 25 and C_2 = 11 for T/Y-joint, C_1 = 20 and C_2 = 22 for gap K-joint.
ABS (2004)	$1-0.03\gamma\overline{U}^2$, $\overline{U}^2=(f_a^2+f_b^2)/(\eta\sigma_y)^2$ η is maximum allowable strength utilization factor.

**Referred from Marshall (2004)*

***Only for compression. Q_f = 1 when all extreme fibre stresses in chord are tension.*

Table 2.4 Chord stress factor (Q_f) in published strength formulae

Authors	Chord stress factor Q_f	Remarks
Washio et al. (1968,1969)	$\begin{cases} 1+0.23(n'-n'^2), & n'<0 \\ 1.0, & n'\geq 0 \end{cases}$	$n' = P_p / A\sigma_y$, P_p is prestressing load and A is cross-sectional area of chord. $n = \sigma_a / \sigma_y$, σ_a is axial stress in chord. $U = (\sigma_a+\sigma_b) / \sigma_y$, σ_b is combined in-plane and out-of-plane bending stress in chord. All are tension positive.
Kurobane et al. (1976)	$1+0.24n-0.339n^2$	
Kurobane (1981)	$\begin{cases} 1+0.305n'-0.278n'^2, & n'<0 \\ 1.0, & n'\geq 0 \end{cases}$	
IIW (1981)	$\begin{cases} 1.2-0.5\lVert U\rVert & U\leq -0.4 \\ 1.0 & U\geq -0.4 \end{cases}$	

Table 2.5 Validity ranges of existing design codes

Codes	γ	β	τ	g^{**}	e^{**}	θ	σ_y (MPa)
CIDECT (1991)	≤ 25	0.2-1.0	-	$\geq t_1+t_2$	0.55D-0.25D	30^0-90^0	≤ 355
AWS (2000)	-	-	-	-	-	-	≤ 414
AISC-LRFD (2000)	≤ 25	0.2-1.0	-	$\geq t_1+t_2$	0.55D-0.25D	30^0-90^0	-
API RP 2A-WSD* (21st, 2000)	10-50	0.2-1.0	-	$\geq 51mm$	-	30^0-90^0	333-500
HSE (1990)	9-50	0.15-1.0	-	$\geq 2t_1$	-	30^0-90^0	≤ 400
ISO (1995)	10-50	0.2-1.0	-	$> -0.6D$	-	30^0-90^0	≤ 500
NORSOK (2004)	10-50	0.2-1.0	-	$\geq -0.6D$	-	30^0-90^0	≤ 500
ABS (2004)	10-50	0.2-1.0	< 1.2	$> -0.5D$	-	-	-

* *Not specified in the code and deduced from background of development (Bomel Limited, 2001).*

** *Only for gap K joint; t_1 and t_2 are the wall thickness of braces ($t_1 \geq t_2$).*

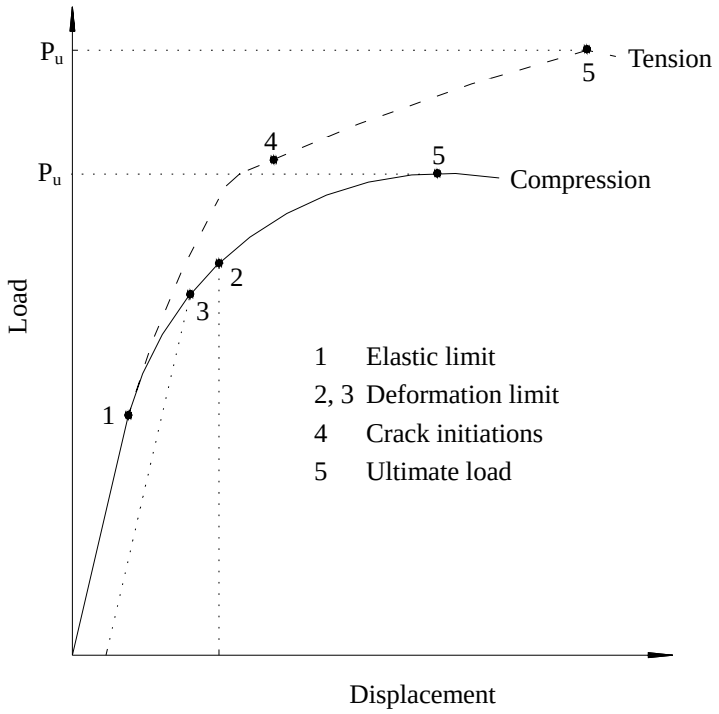

Fig. 2.1 Typical load - displacement curves of axially loaded tubular joints

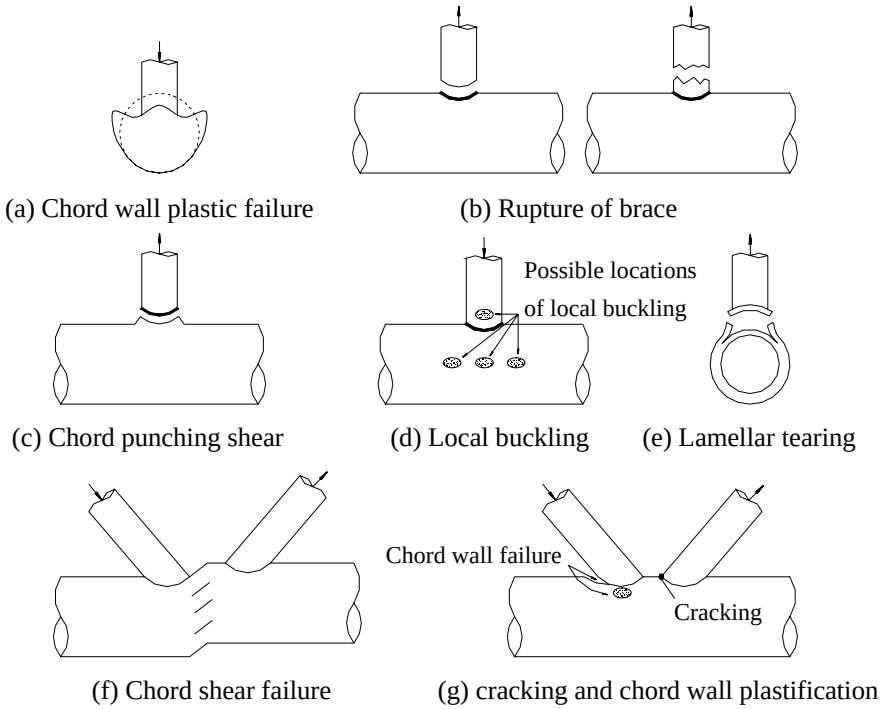

Fig. 2.2 Typical failure modes of simple welded tubular joints

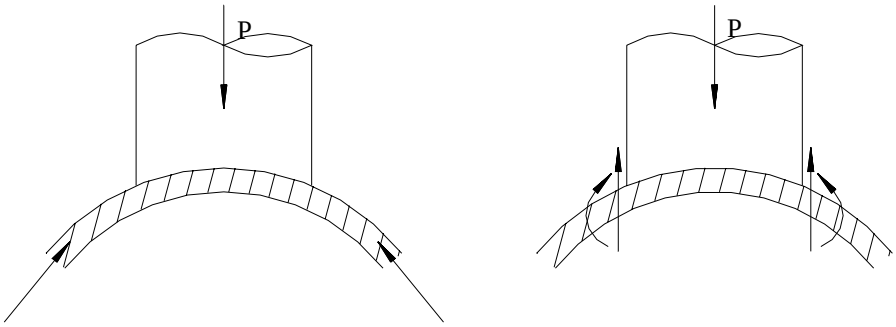

(a) Membrane action (b) Plate action

Fig. 2.3 Plate and membrane action in chord wall

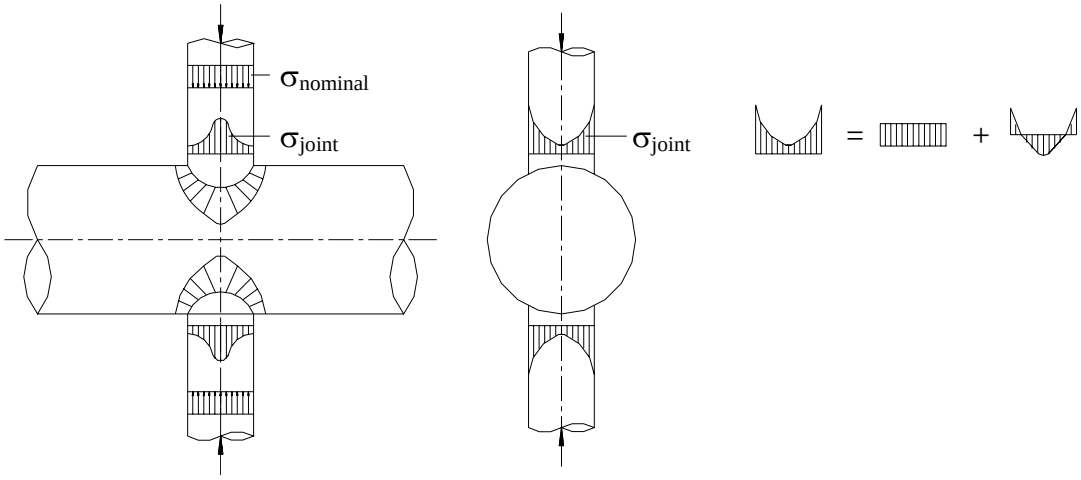

Fig. 2.4 Stress distribution of tubular T-joint under axial compression

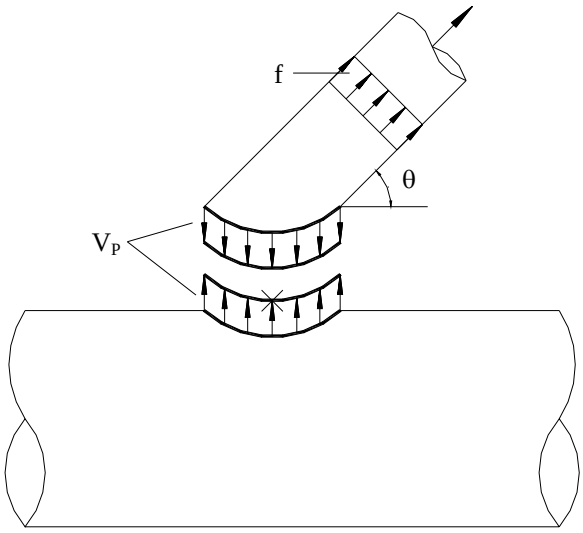

Fig. 2.5 Punching shear model

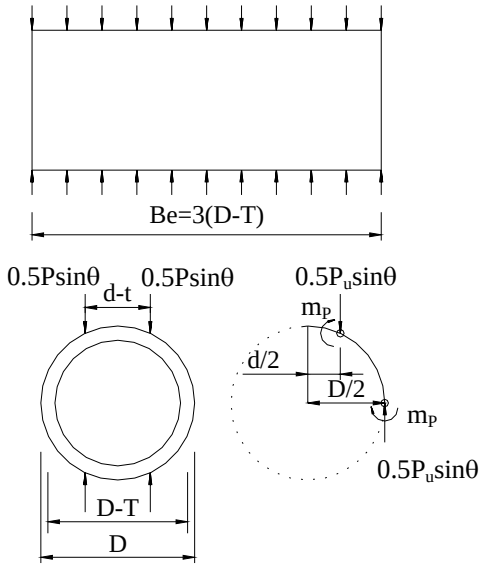

Fig. 2.6 Ring model

CHAPTER 3

EXPERIMENTAL INVESTIGATION

3.1 Introduction

Despite simplified analytical models have been proposed for analysis, the scope of investigation on the behaviour of tubular joints is still very limited owing to the complex geometrical configuration at joint intersections. The most straightforward approach to investigate the behaviour of tubular joints is by testing the joint specimens in the laboratory. In the current experimental study, two completely overlapped tubular joint specimens are tested to failure under monotonic axial compression and quasi-static cyclic loading. The objective of carrying out the monotonic test is to determine the ultimate strength as well as to investigate the failure behaviour of the joint. Furthermore, the test results are used to establish a displacement range for testing the joint under cyclic loading. A relationship of test results between the monotonic and the quasi-static cyclic test is investigated. The failure mode, the ductility performance and the energy dissipation capacity of the joint under cyclic loading are examined.

3.2 Experimental preparation

3.2.1 Test specimens

Two completely overlapped tubular joint specimens were tested to failure. One of the joint specimens was tested under monotonic axial compression and the other was under quasi-static cyclic loading. The two joint specimens have identical geometrical properties with detail as shown in Table 3.1. For the joint specimen tested under monotonic loading, the through brace offsets 300mm from the centre line of the chord. The definition of geometrical parameters of the completely overlapped tubular joint is presented in Fig. 3.1. The detailed configuration of the joint specimens is depicted in Fig. 3.2. Both joint specimens comprised a chord

member, a 30-degree diagonal through brace and a vertical lap brace. The chord length parameter of the test specimens was set at 13.9, larger than 12, to preclude any short chord effects. The brace-to-chord wall thickness ratios were kept less than unity for economic design of members. The joint specimens were designed and fabricated according to the requirements specified by AWS (2000). The welds at the joint intersections of members were complete penetration groove with standard flat profile. All the members were fabricated from API Grade B steel line pipes (API 5L 1991).

Twelve tensile coupon tests were conducted to determine the actual material properties of the joint specimens. All the coupons were prepared and tested according to the requirement specified in BS EN 10002-1:1990 (1998). The coupons were flamed cut in strips in the longitudinal direction of members (two coupons for each member) of each joint specimen before the test. In the preparation of the test coupon, the length of the reduced section for stress and strain measurement is set at 80mm as shown in Fig. 3.3. An extensometer with a standard gauge length of 50mm was clipped onto the coupon to measure the axial displacement. It was removed to prevent damage after the stress level reached the peak in the stress - strain curve. On the surface of the test coupon, two points were marked in the reduced section to determine the elongation.

The tensile coupon test was carried out at the Protective Engineering Laboratory, School of Civil and Environmental Engineering, NTU. The INSTRON 4486 testing machine with a closed loop command and a feedback control is used to fracture the coupon as shown in Fig. 3.4. Both ends of the test coupon were mechanically flattened to ensure a firm support. In the test, the bottom device of the rig was fixed whilst the crosshead was moved upwards at a constant speed of 1.5 mm/min. This was continued until the test coupon broke into two parts. A displacement control mode was set throughout the test to avoid sudden acceleration of the crosshead upon yielding of the coupon. The applied tensile load was recorded via the 300kN load cell installed in the rig. The strains were read via the strain gauges bonded at mid-height of the test coupon before yielding. The displacement was recorded by

the extensometer after strain gauges exceeded the limit. Typical stress-strain relationships of the chord, the through brace and the lap brace of the joint specimens are shown in Fig. 3.5. The detailed results of the coupon tests are summarised in Table 3.2.

3.2.2 Test setup

The test rig is housed in the Heavy Structures Laboratory, School of Civil and Environmental Engineering, NTU, with detailed configuration as shown in Fig. 3.6. The test rig consists of two steel H-section columns and a plate girder. Both ends of the plate girder are directly bolted onto the two steel columns. Each column is firmly supported on the 1.3m thick high strength reinforced concrete cellular floor slab by four 25mm diameter holding down bolts.

In the test setup, both ends of the chord and the end of the through brace of the joint specimen are directly welded onto the flat plate and then bolted onto the rig as shown in Fig. 3.6. A gap size of 143mm was allowed on the face of through brace between the outer surfaces of the chord and the lap brace to avoid overlapping of welds at joint intersections. This gap size was measured after the test specimen was installed in the rig. The measured gap size of the joint specimen satisfied the minimum requirement specified in API RP2A (2000) and CIDECT (Wardenier et al 1993).

The self-weight of the joint specimen was fully supported by the frame and subsequently transferred down through the columns onto the floor. The vertical static and cyclic loads were applied at the end of the lap brace using a double-acting hydraulic controlled cylinder RD10013. This cylinder could apply a maximum static compression and tension of 1000kN and 440kN respectively, with a maximum displacement of 333.5mm. An electrically operated pump PER2045ER with two-speed design was used to power the hydraulic cylinder to exert the load (Fig. 3.7). A 1000KN capacity load cell was placed between the hydraulic controlled cylinder and the joint specimen to measure the magnitude of the load

applied. An adapter was designed to firmly connect the hydraulic cylinder and the load cell so that the joint specimen could steadily be tested (Fig. 3.8). A detailed sketch of the test set up is depicted in Fig. 3.9.

3.2.3 Measurement of strains

Two specific types of standard foil strain gauges (FLA-5-11-5L and YEFRA-2) supplied by Tokyo Sokki Kenkyuio Co Ltd were used to measure the strain values on the outer surface of the joint specimen. The strain gauge type FLA-5-11-5L (Fig. 3.10a) was a general-purpose strain gauge for the measurement of local uni-axial elastic strain in the direction of load measured. It was a single element of 5mm gauge length with strain limit of 3%. On the other hand, the rosette strain gauge type YEFRA-2 (Fig. 3.10b) contained three active elements ($45^0/90^0$) on a common carrier backing made of special plastic carrier base to withstand extreme elongation without creeping and cracking. It was used for strain measurement with maximum strain limit of 15-20% beyond the elastic range.

For the monotonic test, a total of 32 strain gauges of type FLA-5-11-5L were bonded on the outer faces of the joint specimen at locations outside the area of stress concentration to measure the elastic longitudinal strains. The readings from the strain gauges were used to check the eccentricity of load and bending moment acting on the members. The positions of all the strain gauges are shown in Fig. 3.11. There were two sets of strain gauges bonded in the longitudinal direction of the lap brace, the through brace and the chord. For each set, four strain gauges were positioned at 90° intervals around the perimeter of the member. Two of these strain gauges were used to determine the eccentricity in the in-plane whilst the other two were to determine the eccentricity in the out-of-plane direction of the members.

For the cyclic test, a total of 24 strain gauges of type FLA-5-11-5L were used. The arrangement of the strain gauges was similar to that for the joint tested under monotonic loading. However, only one set of strain gauges is used and located at mid-length of each member, as shown in Fig. 3.12.

The post-yield rosette strain gauges of type YEFRA-2 are bonded at the joint intersection of the through brace and the lap brace of the joint specimen under cyclic loading, as illustrated in Fig. 3.13. The strain gauges were placed perpendicular to the weld toe around the joint perimeter at every 45° interval.

In the preparation of strain gauging, soldering was kept at a temperature of about 290°C to connect the strain gauge and the extension lead wire onto the terminal. The extension lead wires were 4 to 5m long. The gauge factors of the strain gauges were reduced accordingly to account for the length effect of lead wires. No temperature compensation was required to eliminate the apparent strain induced over the length as the lead wire was of three-wire system. The connecting terminal of type TF-2SS was used to provide a junction point to connect the strain gauge and the extension lead wire. The rapid adhesive HBM Z70 was used to bond the strain gauge and the terminal on the member outer surface. The coating material, DOW CORNING 3140 silicone rubber, was used to protect the strain gauges and the terminals from dust and corrosion.

3.2.4 Measurement of displacements

The deformation of the joint specimen under loading is measured using the displacement transducers (DTs) of types TML CDP-100, 50 and 25, as illustrated in Fig. 3.14. The magnetic stands and the steel support structures were used to support the DTs to ensure they were secured in positions with no movements. The DTs were positioned in such a way that the shaft was compressed with sufficient length to measure both positive and negative displacements. The amount of displacement of the test specimen had been anticipated from the finite element analysis of the joint model prior to the test. The surfaces of the specimen in contact with the DTs were smoothened to minimize friction.

For both the monotonic and the cyclic tests, a total of 17 DTs were installed around the joint specimens to record the displacement of joints and members. As depicted

in Fig. 3.15, DT-1 to DT-4 and DT-9 are used to determine the member end displacements to assess the actual boundary conditions. DT-5 to DT-7 are placed underneath the joint specimen to determine the chord movement. DT-8 is used to assess the deformation of the through brace. DT-10 to DT-12 are installed to capture the local behaviour at the joint intersections. DT-13 to DT-15 are positioned to determine the bending mode of the lap brace and to monitor any premature failure, such as the compression buckling of members prior to joint failure. DT-16 and -17 are installed to measure the vertical movement of the hydraulic cylinder.

3.2.5 Measuring equipment and computer facilities

Two TML ASW-50C switch boxes with 50 channels each were utilized. All the extension lead wires from the load cells, the DTs and the strain gauges were connected to the switch boxes. A portable data logger TML TDS-302 was used to print all the forces, displacements and strain values. Both the insulation and the stability of the strain gauges were checked prior to testing of the joint specimen. For the insulation, the electrical resistance (in M-Ohms) was kept as large as possible to an infinite value. For the stability, the strain value reading was set within 0 to 2. The data acquisition was done using “Lab Windows” software on a personal computer which was connected to the data logger through an IEEE-488 General Purpose Interface Bus (GP-IB) communication cable. The test control program enabled the strain values of the strain gauges to be directly recorded in a text file and subsequently transferred into a Microsoft Excel file for analysis. The set-up of the data acquisition system can be seen in Fig. 3.16.

3.3 Experimental testing procedure

The joint specimen was first tested to failure under monotonic axial compression with objectives to:

(i) investigate the failure behaviour and the ultimate capacity of the joint;

(ii) check the validity of the FE model for parametric study;

(iii) determine appropriate displacement ranges for cyclic test; and
(iv) assess the test data obtained from the joint tested under cyclic loading.

Prior to the actual test, the joint specimen was subjected to 10 cycles of loading to minimise frictional and lock-in forces. A maximum of 20% of the anticipated failure load was applied (approximately 70kN). This load level was well within the elastic limit of the structural materials. The load was applied in small increment to the maximum load and then unloaded.

During the test, the load control mode was used to capture the elastic load-displacement behaviour and to identify the onset of non-linearity. The loading mode was switched to displacement control after the applied load reached 250kN, approximately 70% of the predicted ultimate capacity of the joint in the FE analysis. The displacement control mode was set so that the peak of the load - displacement curve could be recorded. Furthermore, the overshot of load due to instability of the joint in the inelastic region could be prevented. The joint specimen was unloaded at a displacement of 30mm after it showed a significant plastification on the through brace face in contact with the lap brace. As shown in Fig. 3.17, two displacement values are obtained from the first joint specimen under monotonic loading. δ_y and δ_u are the displacements corresponding to the first yield and the peak load of the tested specimen respectively.

After the monotonic test, the other joint specimen was tested to failure under axial quasi-static cyclic loading. Several load sequences were considered and classified into constant and variable displacement amplitude. It should be noted that the constant axial displacement was adopted by Goh and Grundy (1994), Skallerud et al (1995) and Zhao et al (2002) in their test programme. However, Liu and Goel (1988) defined a load history in terms of yield deformation (δ_y) as the axial deformation in tension corresponding to nominal yield stress. In their test, five load cycles were applied at each axial deflection of $5\delta_y$, $10\delta_y$ and $15\delta_y$. A similar kind of load history was also defined by Walpole (1995) with one cycle applied at each axial deflection of $2\delta_y$, $5\delta_y$, $10\delta_y$, $15\delta_y$, $20\delta_y$ and $25\delta_y$. In the test conducted by Sherman and Sully

(1994), the applied axial displacement was specified as 5mm in any load direction as well as 10mm and 5mm in compression and tension respectively with the load cycles varying from 18 to 40.

In the current experimental programme, the quasi-static cyclic test of the completely overlapped joint specimen was initiated by five elastic displacement amplitudes of $\pm 0.125\delta_y$, $\pm 0.25\delta_y$, $\pm 0.375\delta_y$, $\pm 0.5\delta_y$ and $\pm 0.75\delta_y$. Each of these elastic displacements has a single load cycle as shown in Fig.3.18. This was followed by one load cycle with displacement amplitude of $\pm\delta_y$. Thereafter, the tension displacement was kept constant at amplitude of $\pm\delta_y$ in view of the test rig capacity. The compression displacement amplitudes were increased to $-1.25\delta_y$, $-1.5\delta_y$, $-2.0\delta_y$, and $-2.5\delta_y$. The load control mode was applied in the tension range and was increased from 250kN to 270kN. The compression displacement with three load cycles was kept constant at $-3\delta_y$. Finally, the test terminated with compression displacement equivalent to 1.5 times the peak load (δ_u) of the specimen tested under monotonic loading. The quasi-static cyclic loading protocol used in the current experiment was designed according to the guideline specified by ECCS (1986). However, this guideline had been modified to accommodate the capacity of the test facility in the laboratory.

3.4 Monotonic test results

3.4.1 Failure mode

For the joint specimen tested under monotonic loading, the failure is associated with plastification of the through brace face due to the load exerted from the lap brace, as depicted in Fig. 3.19. The failure mode of the joint specimen was found similar to that of simple T/Y-joints. The through brace ovalised and bulged out on its saddle. The joint specimen showed high shear resistance as no sign of punching shear. During the test, the failure of the joint specimen was gradual and no breaking or snapping noise was heard. In the gap surface, by visual inspection, no sign of

cracking was found at the welds and member surfaces. The chord wall remained intact throughout the test. A similar failure mode was also observed in the test conducted by Fung et al (2001a).

In the test, the out-of-plane bending of the lap brace was negligible with maximum horizontal displacement of only 0.58mm (DT-13). The maximum in-plane horizontal displacements at the middle of the lap brace recorded by DT-14 and DT-15 were determined as 2.32mm and 2.11mm respectively. These deformations were attributed to the rotation effect due to the localized failure at the joint intersection of the through brace and the lap brace. No premature failure due to compression buckling and bending of the lap brace was detected. The strain values obtained from the strain gauges clearly indicated that the members of the joint specimen were symmetrical about the vertical plane before the joint failed.

3.4.2 Load - displacement curve

Four displacement transducers (DT-1 to DT-4), with two at each end of the chord, were placed horizontally against the end plates. At the ultimate load, the displacements of DT-1 and DT-2 were 2.3 and 0.4 mm, and DT-3 and DT-4 were -6.5 and -0.2 mm, respectively. Positive and negative displacements indicated the pushing and pulling of the end plates. After unloading, DT-1 to DT-4 maintained a deformation of 1.1, 0.1, -2.5 and -0.1mm, respectively. These showed that the displacements at both ends of the chord could have a significant effect on the deformation of the joint specimen. DT-5 and DT-7 showed a chord downward displacement of 13.3 and 11.6mm at ultimate load, and 4.6 and 4.3mm after unloading, respectively. However the readings from the strain gauges indicated that the overall beam bending of the chord was very small. The downward rigid movement of the chord was mainly contributed from the deformation of the end plates and the tolerances of the bolt holes between the end plates and the rig. Hence, the lap brace end displacement of the joint specimen was calibrated excluding the rigid movement of the chord.

The load - displacement curve of the test specimen is plotted in Fig. 3.20. The displacement was taken as the average values of DT-16 and –17 minus those of DT-5 and DT-7. The load response was recorded by the load cell. The non-linearity of the curve was initiated at point A with a load of 254.5kN and a displacement of 1.65mm. This was considered as the first yield point for the joint under lap brace axial compression. After yielding, the joint continued to sustain increased load and deformed. An ultimate load of 380.5kN was attained at point B with displacement of 5.83mm. This behaviour revealed that the joint had enormous reserve capacity beyond the first yield. The ultimate load was reached before the excessive deformation limit (point C) of 10.5 defined by EQ (2.1) (Yura et al 1980). After the peak load, the joint continued to yield and the yielding around the intersection between the lap brace and the through brace was rapidly propagated with the joint capacity decreased to 341kN. The displacement of the joint at this load level was 16.8mm. Thereafter, the joint capacity increased with increasing displacement due to the strain hardening of material and the effect of boundary conditions. A permanent deformation of 19.6mm was noted at the joint intersection after the joint was unloaded (point D).

3.4.3 Ductility performance

In the current study, the point A as shown in Fig. 3.20 can be regarded as the first yield with displacement of δ_y = 1.65mm. The lap brace axial displacement at the ultimate load was δ_u = 5.83mm. The ductility ratio could be computed as $\mu = \delta_u/\delta_y$ = 3.53. The joint was considered fully ductile as this ductility ratio was larger than 3 specified in New Zealand Standard (1997).

3.4.4 Deformation at joint intersections

At the joint intersection, DT-10, DT-11 and DT-12 were placed on the chord toe, the gap surface near lap brace and the through brace saddle, respectively. All DTs were positioned perpendicularly with respect to the contact surfaces. The displacement of the three DTs increased with the applied load. At the ultimate load,

the displacements of DT-10, DT-11 and DT-12 were 9.7, 12.3 and 8.0mm respectively. The displacement of DT-10 decreased but those of DT-11 and DT-12 increased with the applied load thereafter. At this load level, the joint buckled but the chord began to move back to its original position to maintain equilibrium. Further increment of the displacement did not cause any increase in the applied load. However, the joint continued to buckle. At this stage, the connection between the braces lost the capability of transferring the additional load to the chord.

3.4.5 Load distribution among members

The bending moment at the connection is determined by linear extrapolation of the bending moments based on the values recorded from the strain gauges in two cross sections (such as the sections La and Lb for lap brace), as shown in Fig. 3.21. The bending moment in a particular cross section of the member could be determined using the following formula.

$$M = \frac{EI}{d}\left(\varepsilon_{\max} - \varepsilon_{\min}\right) \tag{3.1}$$

where $\varepsilon_{\max}$ and $\varepsilon_{\min}$ were the respective maximum and minimum strains recorded by the in-plane strain gauges on the member. The shear force was computed based on the bending moment and the length of each member. The axial load of the member was calculated from the readings recorded by the out-of-plane strain gauges. The axial and the shear force of each member at the ultimate capacity of the joint specimen can be seen in Fig. 3.22. It was noted that the calculated axial load from the strain gauge in the lap brace was almost equivalent to that recorded by the load cell with 0.8% less. In order to ensure the test results were reasonable, the equilibrium of forces at the joint was checked.

$$\sum X = -85 - 61.5 + 189.1 \cdot \cos 30^0 - 18.8 \cdot \sin 30^0 - 7.9 = -0.03 \approx 0 \tag{3.2}$$

$$\sum Y = 172.2 + 86.5 + 189.1 \cdot \sin 30^0 + 18.8 \cdot \cos 30^0 - 377.3 = -7.77 \approx 0 \tag{3.3}$$

It could be seen from the above calculation that the equilibrium of forces was approximately zero. It could therefore be concluded that the test results obtained for analysis was reasonable.

3.4.6 Boundary conditions

In the test setup, the end plates of the chord and the through brace were directly mounted onto the rig through two rows of bolts. Because of the tolerances of the bolt holes, the end condition of the chord should not be fixed or pinned. Based on the simple beam theory, the resistant moment at the end of the chord subjected to a concentrated force *P*, could be determined using the following equation.

$$M_{end} = Pa(l-a)^2 / l^2 \tag{3.4}$$

where *a* was the distance from the end of the chord to the point the concentrated force applied and *l* was the overall length of the chord. If the ends of the chord were assumed fixed, the chord end moment of the current test specimen could be calculated as:

$$M_{end,left} = (172.2+86.5)\times 1.03\times (2.64-1.03)^2/(2.64)^2 = 99.1kNm$$
$$M_{end,right} = (172.2+86.5)\times (2.64-1.03)\times (1.03)^2/(2.64)^2 = 63.4kNm$$

From the measurement taken at the end of the chord during the test as shown in Fig. 3.21, it could be concluded that the actual end conditions are 38% and 35% fixed for the left and the right hand side of the chord, respectively. For the through brace, the end condition could be regarded as pinned.

3.4.7 Comparison with existing codes

It was important to realise that no formulae in the codes and design guides were

currently available and suitable for assessing the ultimate strength of completely overlapped tubular joints. In the joint classification according to the load pattern, the lap brace and the though brace of the completely overlapped joint carry 60% and 40% of the axial brace force as K- and Y-joint respectively, with axial load distribution as shown in Fig. 3.22. Here, the through brace of the joint was treated as a chord member. The comparison of the ultimate capacity between the experiment and the existing T/Y- and gap K-joint equations was conducted for the verification of the existing equations to predict the ultimate strength of the completely overlapped tubular joints.

In the comparison with the current experimental results, five sets of offshore design recommendations namely API RP2A (Marshall 2004), HSE (1990), ISO (1998), NORSOK (2004), and ABS (2004), and three onshore design codes namely CIDECT (1993), AWS (2000) and AISC-360-05 (Marshall 2004) were considered. The chord member of the completely overlapped tubular joint was omitted as the design recommendations and codes only covered the joints with simple T/Y- and gap K-joint. The through brace was taken as the chord member. The actual material property of the through brace of the specimen was used as it showed a significant impact on the failure behaviour. For CIDECT, the characteristic value was obtained by multiplying the design value with the material factor of 1.1. The previous test results obtained from the experimental investigation conducted by Fung et al (2001a) had been included in the study.

The comparison of the ultimate strength of the joints between the experimental data and the existing equations in the recommendations and codes is summarised in Table 3.3. The predicted strength of the joint was computed based on the classification according to load pattern. It should be noted that the strength of the current test specimen was determined as the summation of 40% and 60% the capacity of Y- and K-joints respectively. The axial load distribution was not recorded in the test conducted by Fung et al (2001a). From the FE analysis, the predicted strength of the joint was the summation of 50% the capacity of Y- and K-joints. It could be seen from the comparison of results that the existing strength

equations under-predicted the test results of the completely overlapped tubular joints. The ultimate strength of the joint obtained from the current and the previous tests was closer to that predicted by API RP2A (Marshall 2004) with 18% and 19% less, respectively. On average, the strength obtained from the current and the previous tests were found 29% and 40% higher than that of the existing codes. The results revealed that the existing design equations in the recommendations and codes were too conservative for predicting the ultimate strength of the completely overlapped tubular joints.

3.5 Cyclic test results

3.5.1 Failure behaviour

The relationship of the load response and the axial displacement of the lap brace for the joint specimen tested under cyclic loading are plotted in Fig. 3.23. In the figure, the *x*-axis is the accumulative absolute displacement measured at the end of the lap brace. In the compressive phase of the load applied, a significant local buckling on the through brace face near the chord at 9th load cycle (Point A) was observed. The load and the displacement at this point were found to be 357kN and 15.65mm respectively. The readings obtained from DT-11 and DT-12 at the joint intersection showed permanent deformations of 3.06 and 2.39mm respectively after the joint was unloaded. It was noted that the tension responses of the joint specimen at 5th to 9th load cycles were almost identical with constant displacement amplitude. In the subsequent two load cycles, the tension responses of the joint significantly increased. This behaviour revealed that the compression range of the load - displacement hysteresis curve of the joint specimen had little impact on its tensile strength prior to the displacement at $-3\delta_y$. However, the tensile strength of the joint was significantly affected by the local buckling failure of the compression members.

At 12th load cycle with the compressive load level and the corresponding axial displacement of 220.5kN and 20.3mm (Point B), it is noted that cracks of about 7mm and 5mm occurred at the through brace saddle at points C1 and C2

respectively as shown in Fig. 3.24. These two cracks symmetrically occurred about the vertical plane of the joint specimen. With increasing load cycles, the 7mm crack propagated 15mm and 25mm whilst the 5mm crack propagated 15mm and 10mm along the weld toe toward the heel and the toe of the joint respectively. A loud "bang" was heard at 14th load cycle with the load applied in the tension region (Point C) due to the separation of the lap brace from the through brace. Owing to this failure behaviour, the applied load at the joint was drastically reduced from 201kN to 120kN whilst the corresponding axial displacement increased from 5.1mm to 10.1mm (Point D). At this load level, the joint specimen completely collapses with the lap brace only supported at the heel as shown in Fig. 3.24.

The ultimate capacity of the joint specimen in the tension and the compression phases of the hysteresis behaviour were 270kN and 362kN, respectively. The maximum horizontal and vertical displacements at the ends of the chord were 2.6mm (push) and 4.5mm (pull), and 9mm (upward) and 11.8mm (downward) respectively as indicated in DT-01 to DT-06. DT-08 and DT-09 showed that the maximum displacements at the end of the chord were 5.8mm (push) and 10.2mm (pull) whilst the vertical displacements of the through brace were 3.9mm (upward) and 4.8 (downward). Hence, it could be commented from the measurement that the boundary conditions of the joint specimen tested under cyclic loading was neither fixed nor pinned.

In the test, the out-of-plane bending of the lap brace was negligible with a maximum horizontal displacement of only 1.4mm (DT-13). The maximum in-plane horizontal displacements at the middle of the lap brace recorded by DT-14 and DT-15 were determined as 5.62mm and 5.63mm respectively. These deformations were attributed to the rotation effect owing to the localized failure at the joint intersection of the through brace and the lap brace. No premature failure due to compression buckling and bending of the lap brace was detected. The strain values obtained from the strain gauges clearly indicated that the members of the joint specimen were symmetrical about the vertical plane before the joint failed.

The joint specimen was considered failed in the tension half-cycle at accumulative displacement of 1868.6mm (Point C as shown in Fig. 3.23). At this point of loading, the crack penetrated through the wall thickness of the through brace and resulted in sudden drop of strength by 40.3%. The cracks are initiated at points C1 and C2 as shown in Fig. 3.24. A rough splintered surface was observed at these locations. Significant inelastic local buckling failure behaviour of the through brace was specifically noted. A detailed investigation after the test revealed that there was no crack and no significant damages in other parts of the test specimen outside the joint intersection. It was clearly observed that the failure mode of the completely overlapped joint specimen was different from that of simple Y/T-joints.

The tests of five tubular T/Y-joint specimens under cyclic and three static loading by Goh and Grundy (1994) showed that the failure models of all the test specimens were due to gradual plastic indentation on the chord wall combined with the lateral and some rotational displacement. No significant crack was reported from their test observation and results. However, the test of tubular T-joint specimens under cyclic loading by Skallerud et al (1995) showed that the failure mode was associated with cracking at the weld toe of the chord saddle. It was important to realise that the crack penetrating through the chord wall significantly affected the strength of the joints. For the completely overlapped tubular joint, the crack occurred at the through brace saddle instead the chord. Thus, the chord member of the completely overlapped tubular joint could still be remained intact after the joint failure at the short segment of the through brace.

3.5.2 Strain distribution at joint intersection

From the strain values measured by three-element rosette strain gauges YEFRA-2, the maximum and the minimum principal strain, ε_1 and ε_2, could be obtained. Fig. 3.25 shows the accumulative principal strains at each gauge location. Here the strain values measured after the significant local buckling of the specimen were not considered because some strain gauges were found damaged. It could be seen from Fig. 3.25 that the maximum accumulative value occurs at the crown toe (PY01) of

the through brace. The values decreased when shifted from crown toe to crow heel position of the through brace. For the principal strain ε_2 near the joint intersection, the maximum accumulative value occurred at the saddle (PY03) of the through brace. It should be noted that the crack did not initiate at the position with maximum accumulative principal strain.

3.5.3 Load - displacement hysteresis curve

The load - displacement hysteresis curve of the joint specimen tested under cyclic loading can be seen in Fig. 3.26. An average displacement was taken from the values recorded by DT-16 and DT-17. The load response was recorded by the load cell. In the current study, the load - displacement curve of the joint specimen tested under monotonic loading served as reference for the compressive range of hysteresis curve of the joint specimen tested under cyclic loading.

The comparison of the load - displacement curves showed that the force response of the joint under monotonic compression was higher than that under cyclic loading. The differences of the force response for the two joint specimens could be due to the effect of material deterioration at the joint intersection of the through brace and the lap brace under load reversal. It could be commented based on the comparison of results that the joint specimen under monotonic loading could form a reasonable envelope for the joint under cyclic loading at the first load cycle of $3\delta_y$. In other word, the load - displacement curve obtained from the joint under monotonic loading could be used to predict the strength of the joint under cyclic loading up to the first load cycle with displacement of $3\delta_y$. However, it should be noted that the strength of the joint substantially degraded with further increasing load cycles. The applied load causing failure of the joint under cyclic loading was lowered than that of the joint under monotonic loading.

3.5.4 Ductility performance

The ductility ratio, $\mu\,(=\delta_{max}/\delta_y)$, was the important indicator to assess the seismic

resistance of a structure. δ_{max} denoted the maximum deformation of joints prior to excessive loss of resistance. δ_y was the yield deformation for idealised elastic-perfectly plastic behaviour. ECCS (1986) recommended the yield displacement of a structure corresponding to the intersection of the two tangents from the elastic and inelastic regions of the load - deformation curve. The tangent of the curve in the inelastic range had a slope equivalent to 1/10 the tangent in the elastic region. The yield displacement of the current joint specimen tested under cyclic loading should be determined as δ_y^+ = 9.5mm and δ_y^- = 7.7mm with applied loads of P_y^+ = 338kN and P_y^- = -270kN respectively. The maximum μ in the compression and the tension region of the hysteresis curve were found to be 3.03 and 1.31mm, respectively. Since the applied load in the test did not reach the maximum tensile capacity of the joint, the value of 1.31 should not be taken as a measurement for ductility performance. The accumulative ductility ratio (μ_a,) of the joint specimen at failure was calculated as 33, larger than 24 of the minimum requirement of structural system with good seismic resistance specified in New Zealand Standard (1997).

3.5.5 Strength resistance

It was noted from the load - displacement hysteresis curve that the strength of the joint decreased with increasing load cycles due to local buckling and cracking at large inelastic displacement cycle. The strength reduction of the joint could be evaluated by strength resistance ratio, ω (= P_i/P_y). P_i was the force magnitude of unloading at ith cycle. P_y was the yield force for idealised elastic-perfectly plastic behaviour. For the comparison of strength of the joint, the load at first yield was set as the ultimate capacity of the joint specimen under monotonic loading.

The strength resistance ratios versus the inelastic displacement curves of the joint specimen are shown in Fig. 3.27. The load ratios in the inelastic range were determined as the applied load at the maximum displacement in each load cycle divided by the ultimate load capacity of the joint under monotonic loading. The

load ratios showed the strength capacity of the joint developed at a given deformation level under cyclic loading. Since the applied load in the current study did not reach the maximum tensile capacity, the tension load ratio did not represent the actual capacity of the joint. In the compression range of the hysteresis curve, the load ratio dropped due to local buckling and crack propagation at the joint intersection. It was noted that the maximum compression ratio was close to unity which revealed that the ultimate compression strength of the joint obtained from the cyclic test was similar to that from the monotonic test. It could therefore be commented that the load - displacement curve of the joint under monotonic loading could be used as an envelope for that of the joint under cyclic loading before the crack initiation, but the strength of the joint under cyclic loading could be overestimated due to load reversal.

3.5.6 Energy absorption capacity

The energy absorption capacity of the joint was measured by energy dissipation ratio, η (= E_i/E_y). E_i was the dissipated energy at ith cycle. E_y was the dissipated energy under idealised elastic-perfectly plastic behaviour. The normalized energy absorption capacity of the current joint specimen at each load cycle can be seen in Fig. 3.28. It was noted from Fig. 3.28a that the normalize energy absorption capacity of the joint gradually increased with number of load cycles and was continued until 8th load cycle. Thereafter, the energy absorption capacity of the joint significantly increased due to local buckling on the through brace. As shown in Fig. 3.28b, the inelastic deformation of the joint only dissipates 11.6% of the total energy prior to local buckling. However, it was noticed that 87.7% of the total energy was dissipated prior to crack at the weld toe of the joint. Thus, it could be commented based on this finding that the main contribution of the energy dissipation of the completely overlapped tubular joint was the inelastic local bucking deformation of the though brace. The total dissipated energy of 36.5E_y obtained in the test was found much higher than the minimum requirement of 4E_y specified by API RP2A (1993). However, it is noticed that the normalized energy absorption capacity of the joint decreases at 10th to 11th load cycles as shown in

Fig. 3.28a. These two load cycles had identical displacement amplitude. Thus, the decrease of the energy absorption capacity of the joint specimen could be due to degrading of buckling load with increasing deflection under constant displacement amplitude.

3.6 Concluding Remarks

Two uni-planar completely overlapped tubular joint specimens are tested to failure under monotonic axial compression and quasi-static cyclic loading. For the joint specimen tested under monotonic loading, the failure mode is associated with the through brace face plastification in contact with the lap brace. The ultimate capacity of the joint specimen is determined as 380.5kN. In the joint classification according to the load pattern, the strength of the joint specimen is equivalent to the sum of 60% and 40% the ultimate capacity of K- and Y-joints respectively. All the existing strength equations based on T/Y- and gap K-joints under-predict the test results of the completely overlapped tubular joint specimen.

For the joint specimen tested under cyclic loading, the local buckling failure on the through brace near the lap brace in the compressive phase of 9th load cycle is first observed. It is important to realise that the local buckling on the through brace could have significant effect on the tensile strength of the joint. At 12th load cycle, two cracks along the weld toe symmetrical about the vertical plane of the joint occur at the through brace saddle near the lap brace. The load - displacement hysteresis curve of the joint showed that the peak compression significantly reduced owing to the local buckling and crack initiation at the joint intersection.

It is noted that the load - displacement curve of the joint under monotonic loading can be used as an envelope for that of the joint under cyclic loading before the crack initiation. However, the strength of the joint under cyclic loading can be overestimated because of the severe damage due to load reversal. The accumulative ductility and the accumulative energy dissipation ratio of the joint specimen at failure are found to be 33 and 36.5 respectively. The main contribution of the

energy dissipation of the completely overlapped tubular joint is the inelastic local bucking deformation at the short segment of the through brace.

Table 3.1 Geometrical parameters of test specimens

Geometrical parameters		Non-dimensional parameters
Chord length	L = 2640.0mm	
Chord diameter	D = 219.1mm	$\alpha_C = 2L/D = 24.10$
Chord thickness	T = 7.9mm	$\gamma_C = D/2T = 13.87$
Through brace length	l_T = 1870.0mm	$\beta_{CT} = d_T/D = 0.77$
Through brace diameter	d_T = 168.3mm	$\tau_{CT} = t_T/T = 0.90$
Through brace thickness	t_T = 7.1mm	$\alpha_T = 2l_T/d_T = 22.22$
Lab brace length	l_L = 623.0mm	$\gamma_T = d_T/2t_T = 11.85$
Lap brace diameter	d_L = 88.9mm	$\beta_{TL} = d_L/d_T = 0.53$
Lap brace thickness	t_L = 5.5mm	$\tau_{TL} = t_L/t_T = 0.77$
Gap length	g = 143.0mm	$\xi = g/d_T = 0.85$
Brace angle	$\psi = 30°$, $\theta = 60°$	

Note: see Fig. 3.1 for notation.

Table 3.2 Summary of coupon test results

Specimen	Member	No.	Young's modulus (GPa)	Yield stress (MPa)	Tensile stress (MPa)	Elongation (%)
Monotonic test	Chord	1	196	358	462	30
		2	201	363	462	28
		Mean	199	361	462	29
	Through brace	1	201	405	522	28
		2	200	402	516	26
		Mean	201	403	519	27
	Lap brace	1	193	376	469	31
		2	193	383	468	28
		Mean	193	380	469	29
Cyclic test	Chord	1	202	360	467	32
		2	192	350	450	32
		Mean	197	355	458	32
	Through brace	1	205	378	492	36
		2	205	376	481	32
		Mean	205	377	486	34
	Lap brace	1	190	378	477	26
		2	196	372	457	28
		Mean	193	375	467	27

Table 3.3 Comparison of strength between test results and existing formulae

Test	Strength formulae	Y-joint (kN)	K-joint (kN)	Predicted strength* (kN)	Test/Predicted
Current	API	314.8	329.6	323.7	1.18
	HSE	317.5	317.5	317.5	1.20
	ISO	280.0	280.0	280.0	1.36
	NORSOK	280.0	280.0	280.0	1.36
	ABS	263.0	270.5	267.5	1.42
	CIDECT	286.1	304.2	296.9	1.28
	AWS	312.7	313.0	312.9	1.22
	AISC	286.7	307.1	298.9	1.27
	Mean	292.6	300.2	297.2	1.29
Fung et al. (2001a)	API	793.1	856.2	824.7	1.19
	HSE	786.1	786.1	786.1	1.25
	ISO	618.6	618.6	618.6	1.58
	NORSOK	618.6	618.6	618.6	1.58
	ABS	614.6	765.1	689.9	1.42
	CIDECT	701.5	707.9	704.7	1.39
	AWS	681.2	681.9	681.6	1.44
	AISC	702.4	714.9	708.7	1.38
	Mean	689.5	718.7	707.0	1.40

**Summation of 40% and 60% the capacity of Y- and K-joint respectively for current test, and 50% and 50% the capacity of Y- and K-joints respectively for Fung et al's test.*

Chord and through brace:
$\alpha_C = 2L/D$ $\gamma_C = D/2T$
$\beta_{CT} = d_T/D$ $\tau_{CT} = t_T/T$

Through brace and lap brace:
$\alpha_T = 2l_T/d_T$ $\gamma_T = d_T/2t_T$
$\beta_{TL} = d_L/d_T$ $\tau_{TL} = t_L/t_T$

L : Chord length
L_L : Lap brace length
L_T : Throng brace length
D : Chord diameter
d_L : Lap brace diameter
d_T : Throng brace diameter
T : Chord wall thickness
t_L : Lap brace wall thickness
t_T : Throng brace wall thickness
g : Gap length
θ : Brace angle between lap and through braces
ψ : Brace angle between through braces and chord

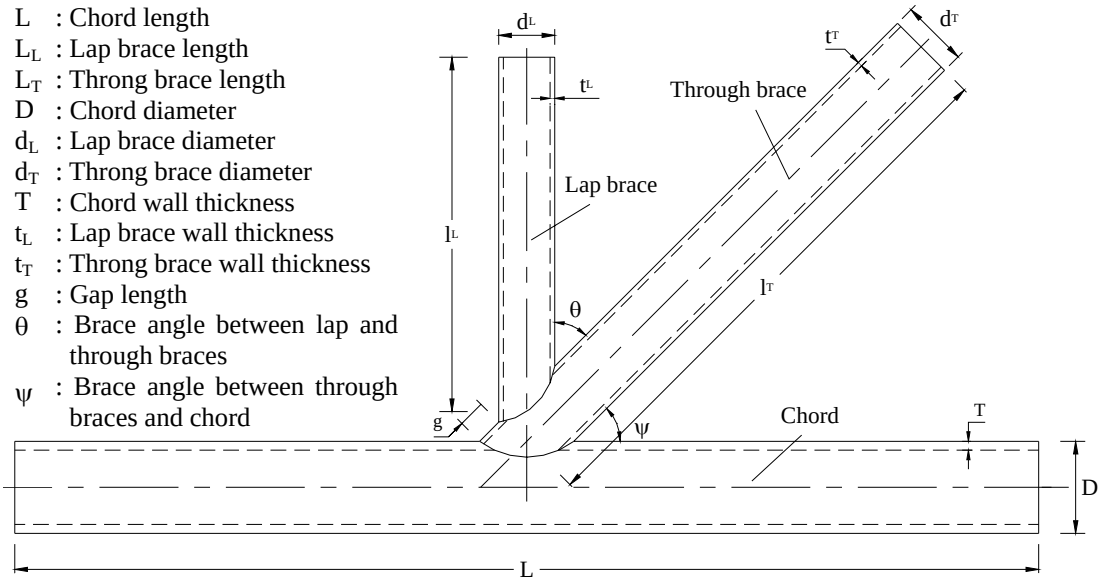

Fig. 3.1 Geometrical parameters of completely overlapped tubular joint

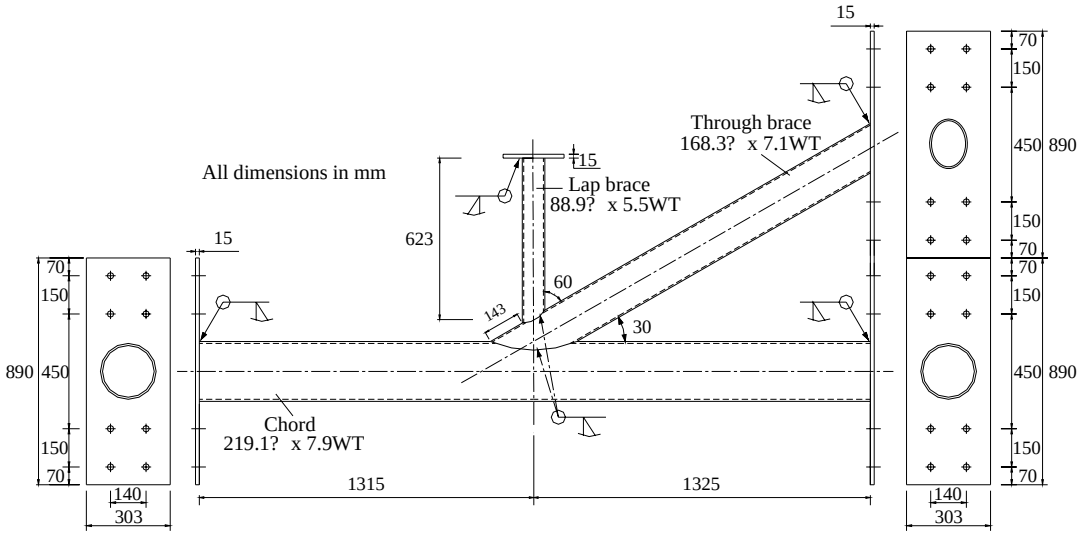

Fig. 3.2 Completely overlapped tubular joint specimen

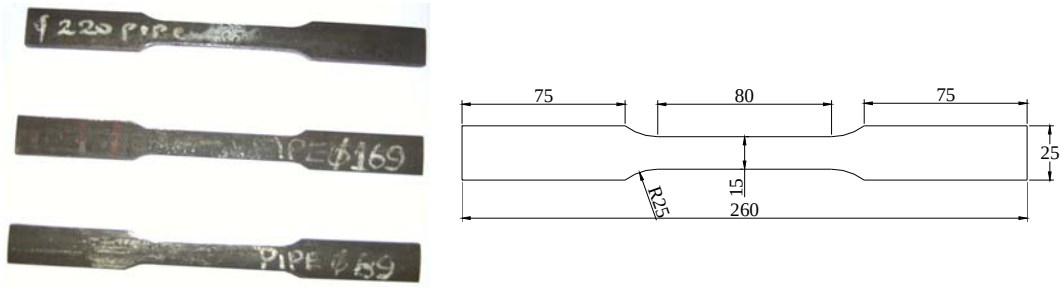

(a) Test specimen (b) Dimension of test specimen

Fig. 3.3 Longitudinal strips for tensile coupon test

(a) INSTRON 4486 testing machine

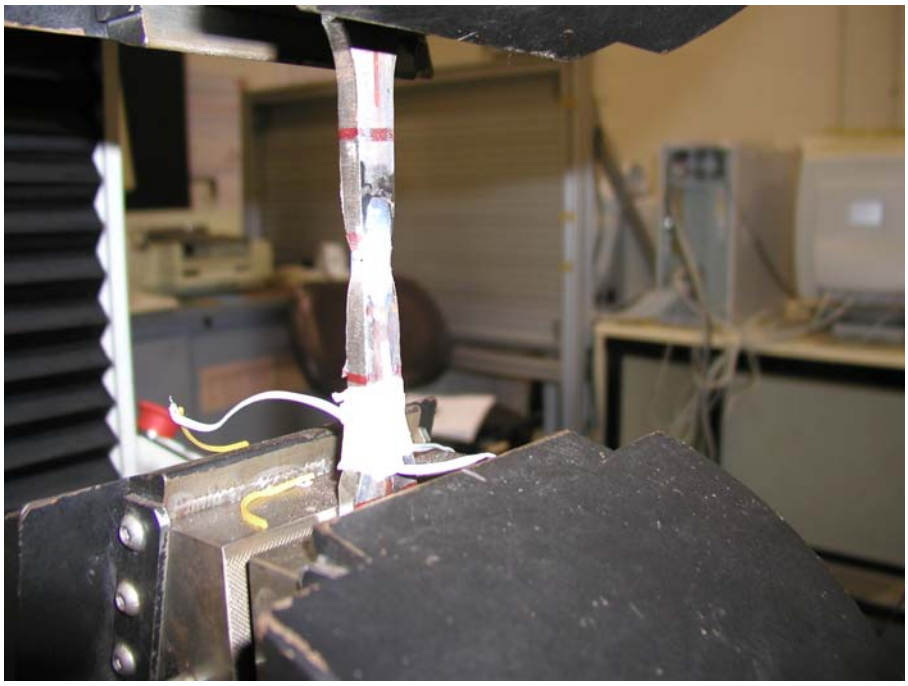

(b) Test specimen after fracture

Fig. 3.4 Tensile coupon test

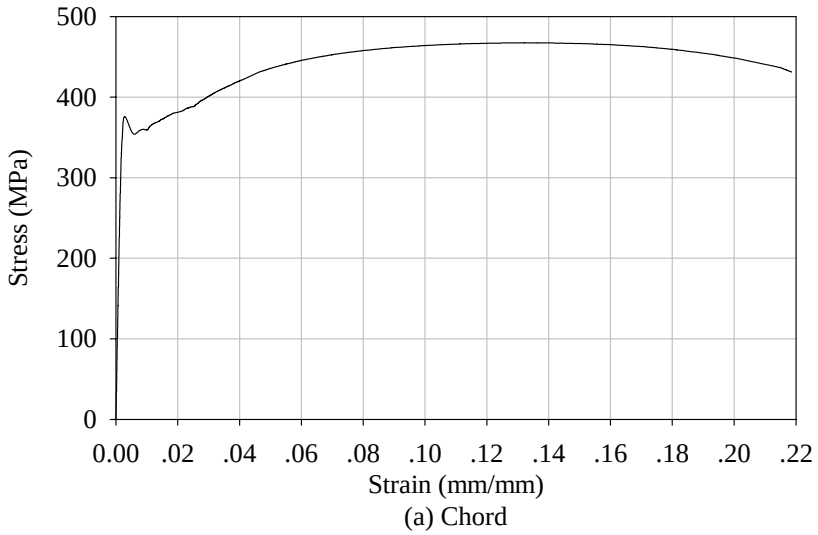

(a) Chord

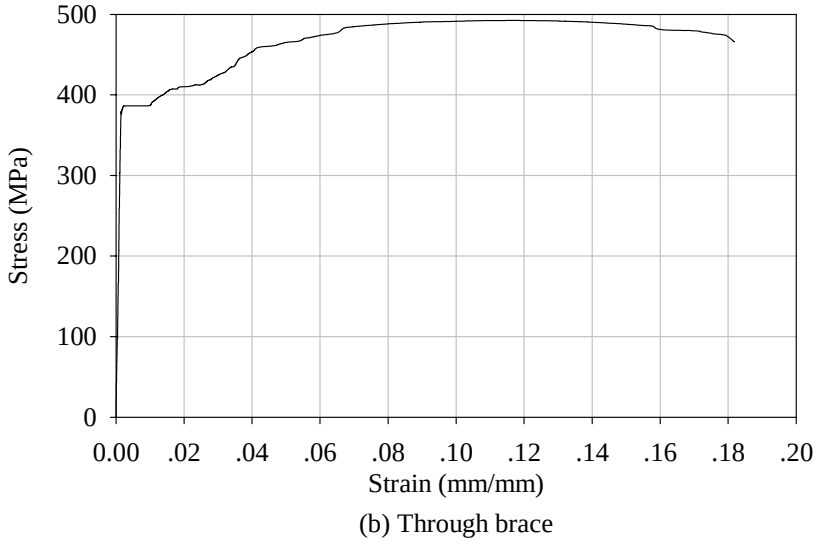

(b) Through brace

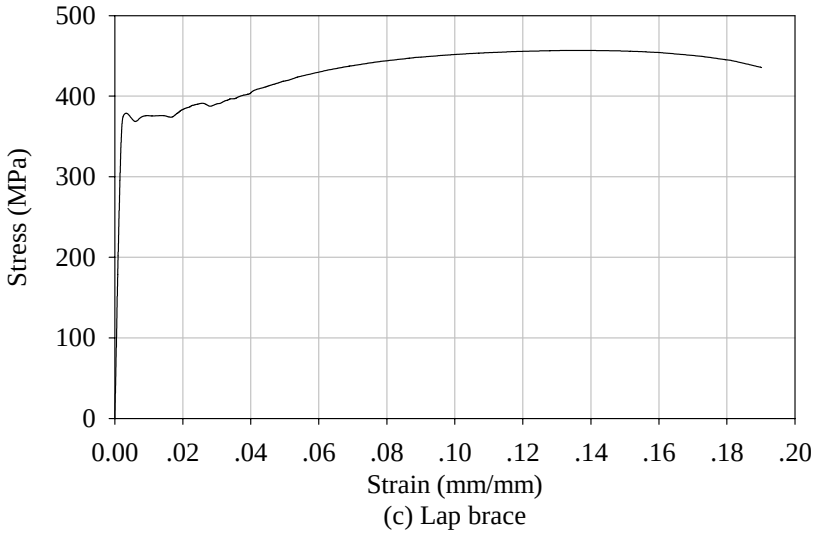

(c) Lap brace

Fig. 3.5 Engineering stress and strain curves

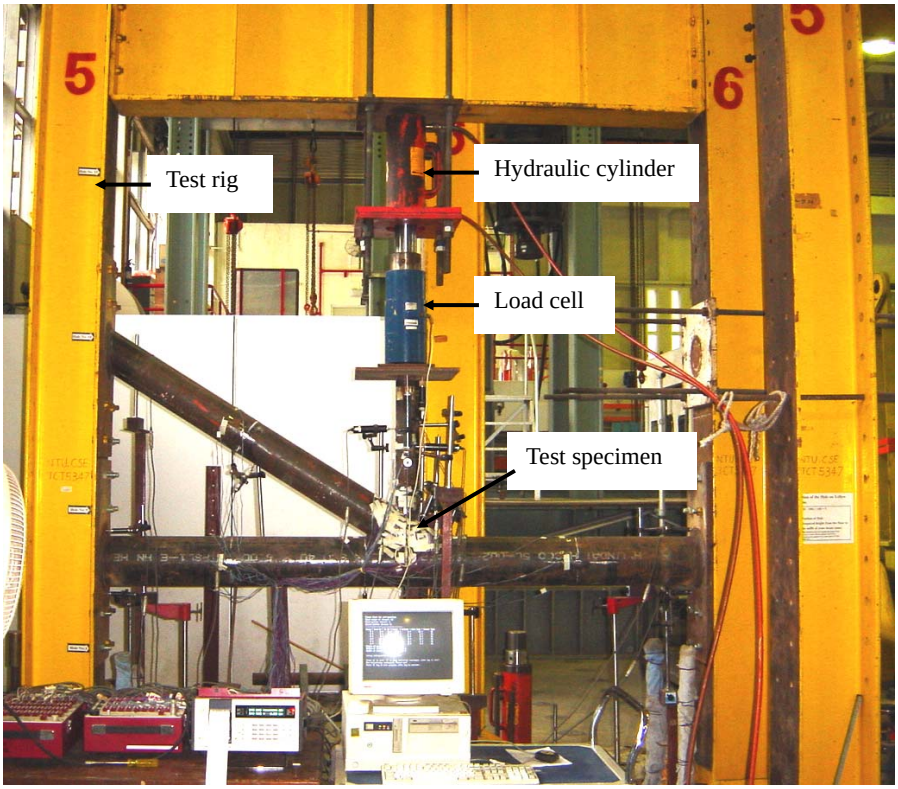

Fig. 3.6 Test rig

Fig. 3.7 Electrically operated pump used in the tests

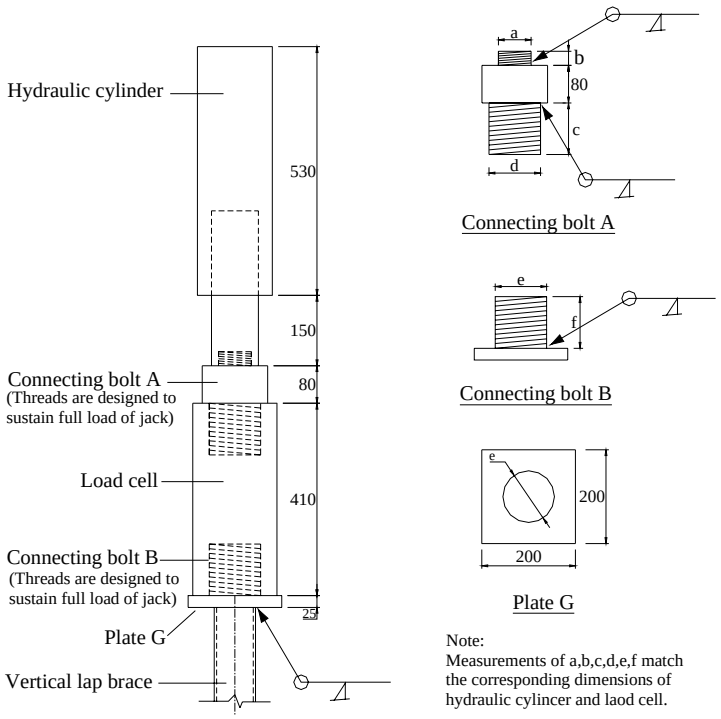

Fig. 3.8 Adapter to connect hydraulic cylinder and load cell

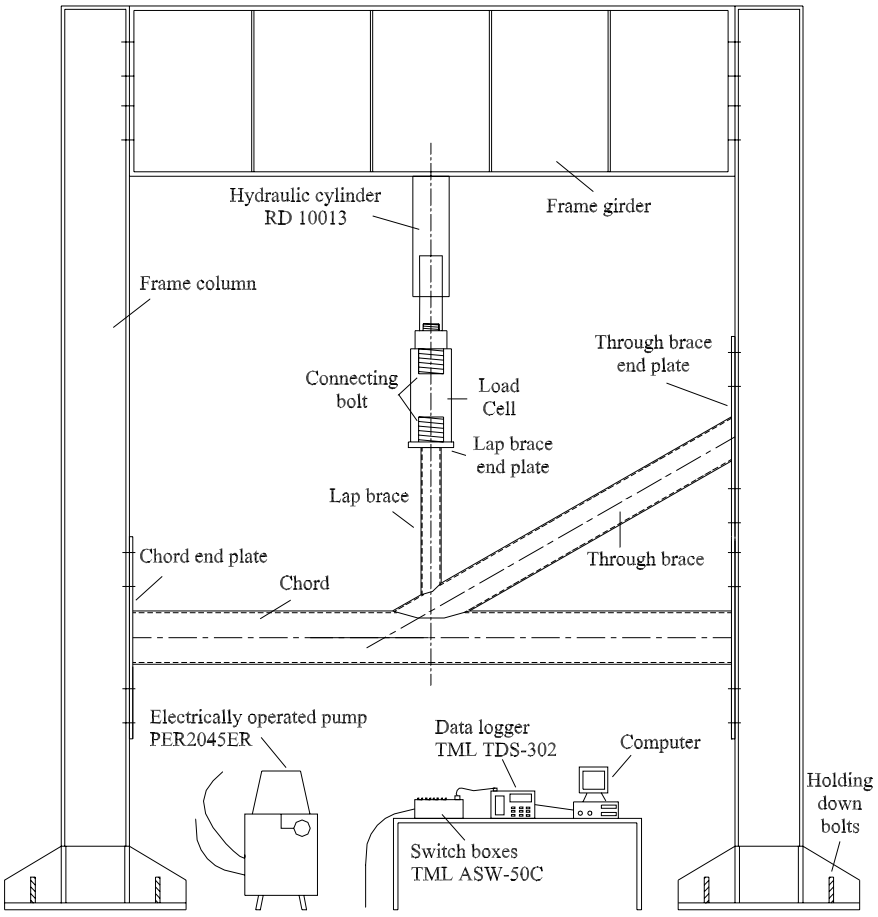

Fig. 3.9 Test set up

(a) Single element gauge (FLA-5-11-5L) (b) Rosette strain gauge (YEFRA-2)

Fig. 3.10 Strain gauges on the test specimens

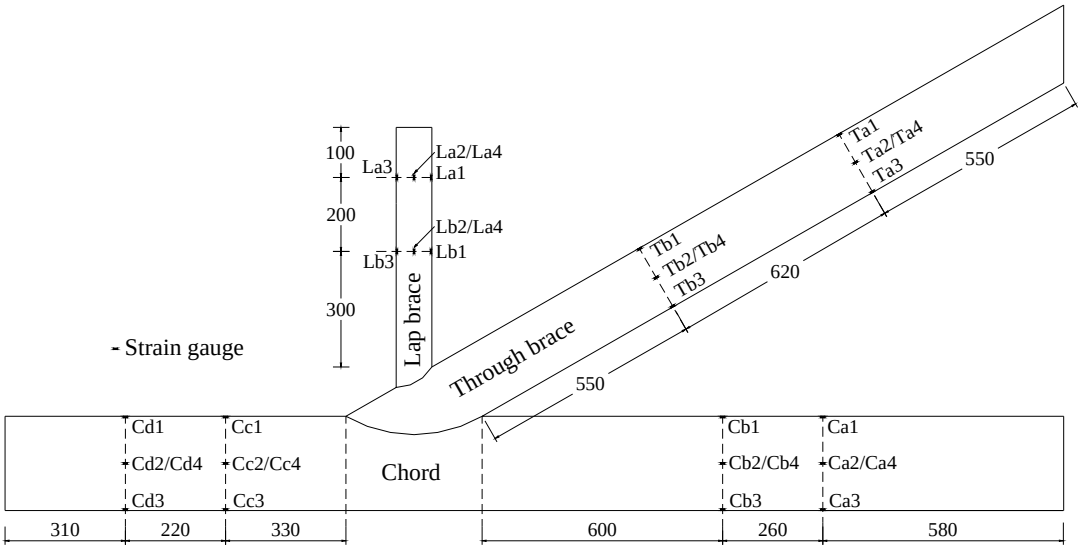

Fig. 3.11 Locations of single element strain gauges (FLA-5-11-5L) on joint specimen tested under monotonic loading

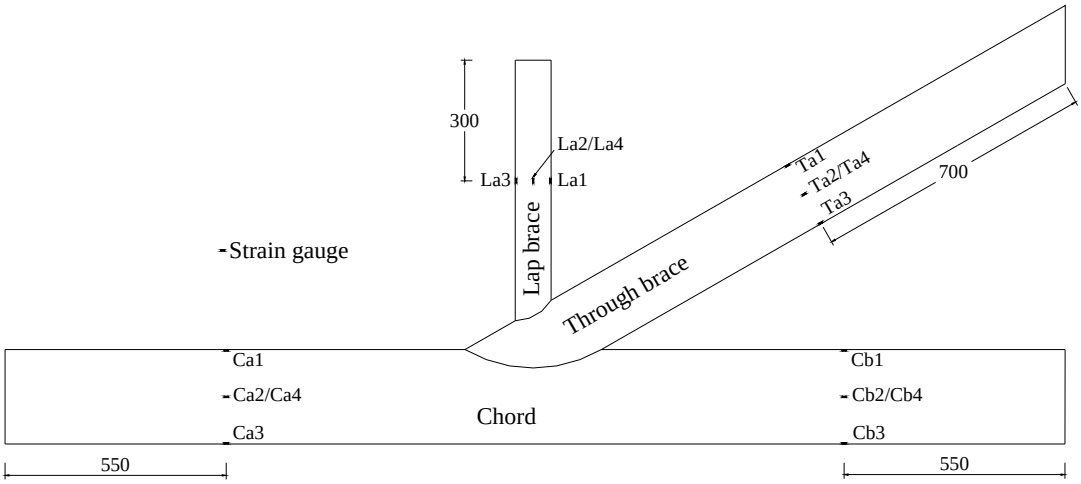

Fig. 3.12 Locations of single-element strain gauges (FLA-5-11-5L) on joint specimen tested under cyclic loading

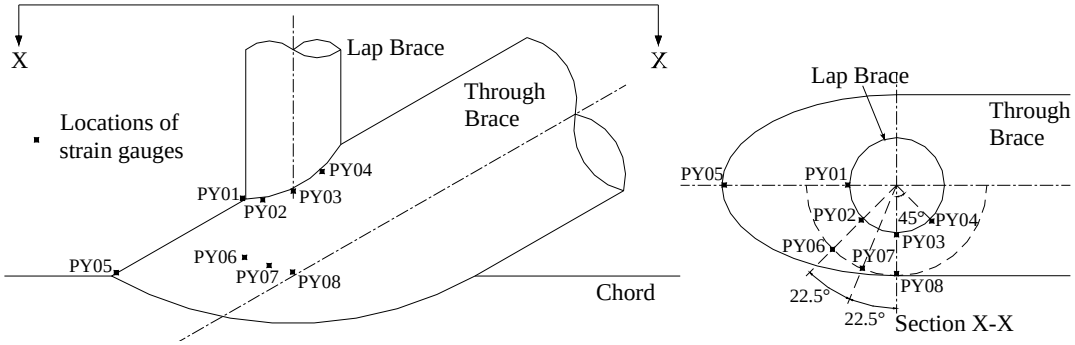

Fig. 3.13 Locations of rosette strain gauges (YEFRA-2) on joint specimen tested under cyclic loading

Fig. 3.14 Displacement transducers used in the tests

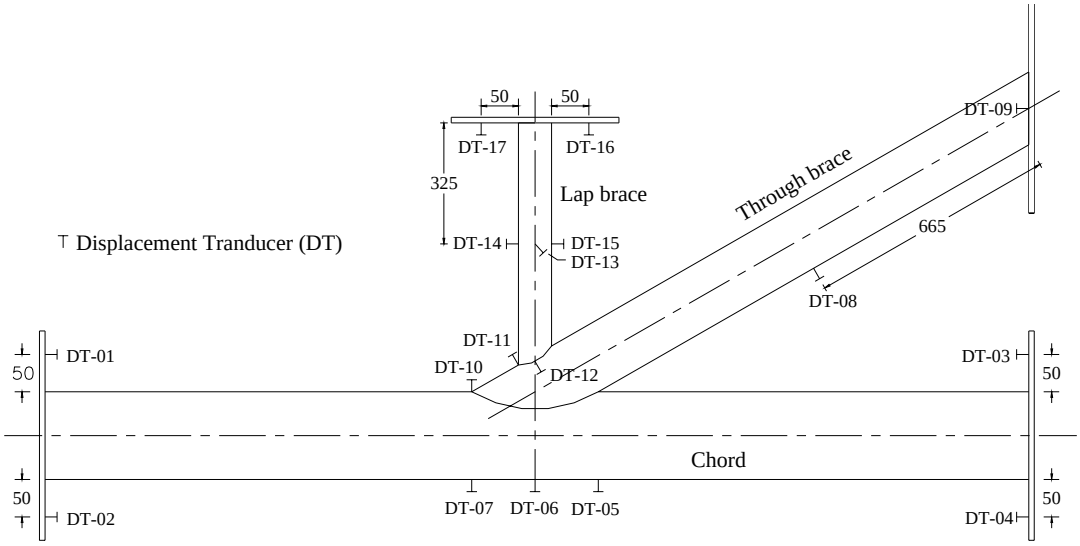

Fig. 3.15 Locations of displacement transducers on joint specimen

Fig. 3.16 Set-up of data acquisition system

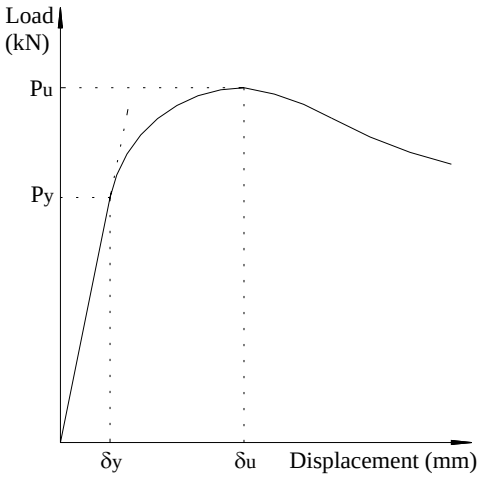

Fig. 3.17 Monotonic axial compression

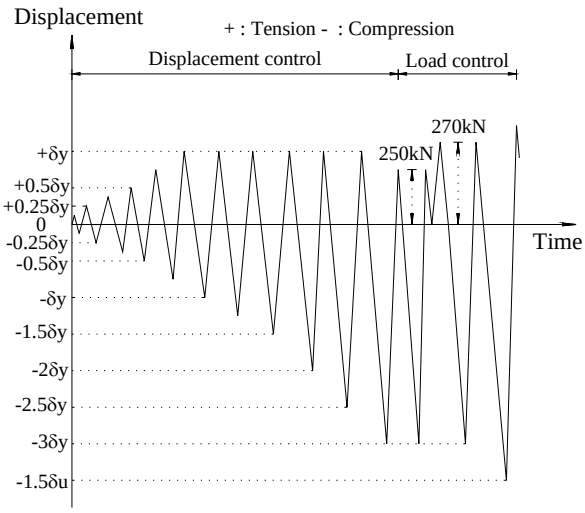

Fig. 3.18 Cyclic loading

(a) Side elevation view

(b) End elevation view

Fig. 3.19 Failure mode of joint specimen under monotonic loading

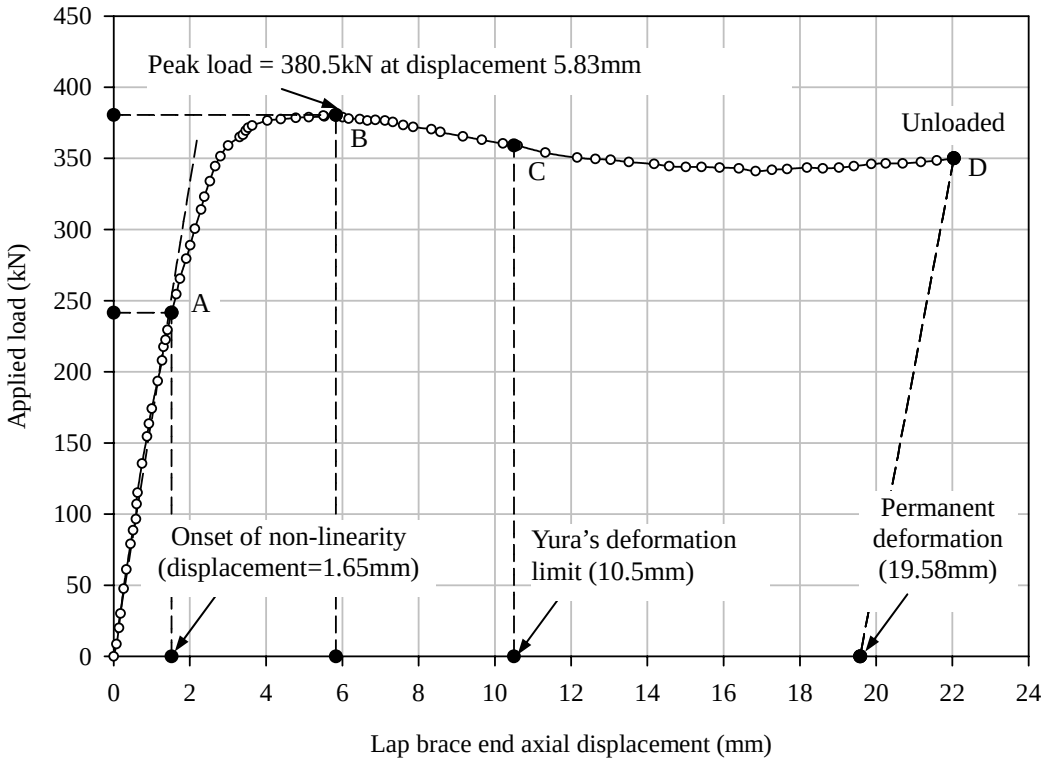

Fig. 3.20 Load - displacement curve of joint specimen under monotonic axial compression

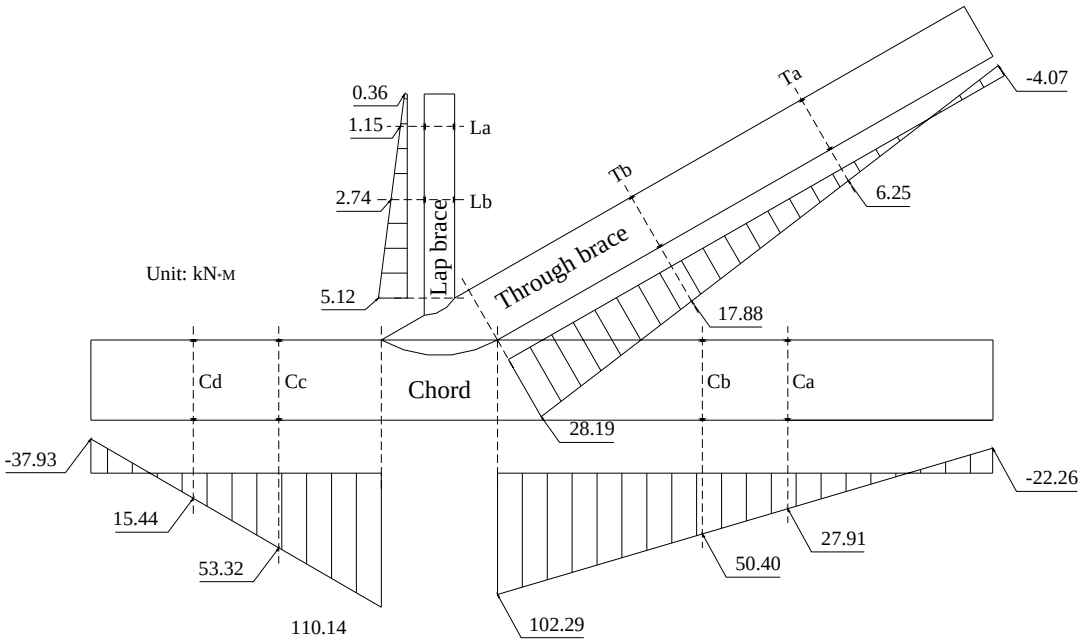

Fig. 3.21 Determination of bending moments by linear extrapolation

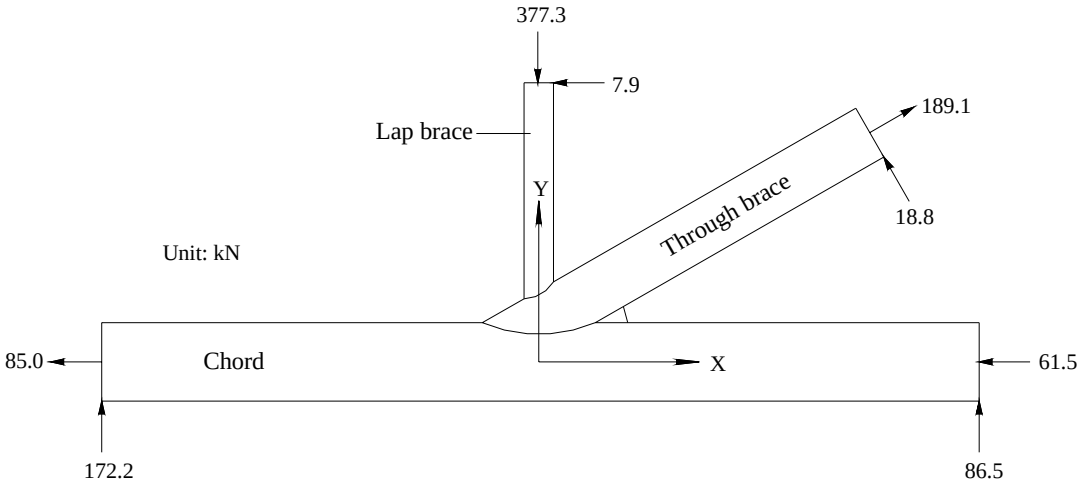

Fig. 3.22 Axial and shear forces in joint specimen

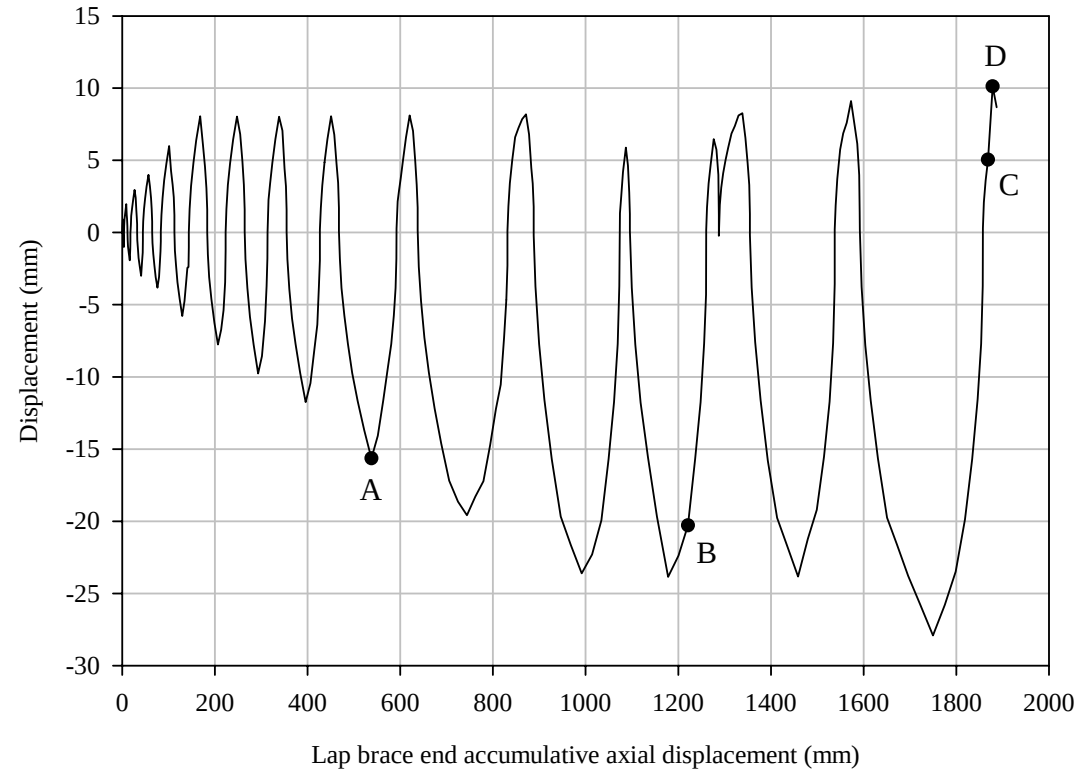

(a) Displacement history

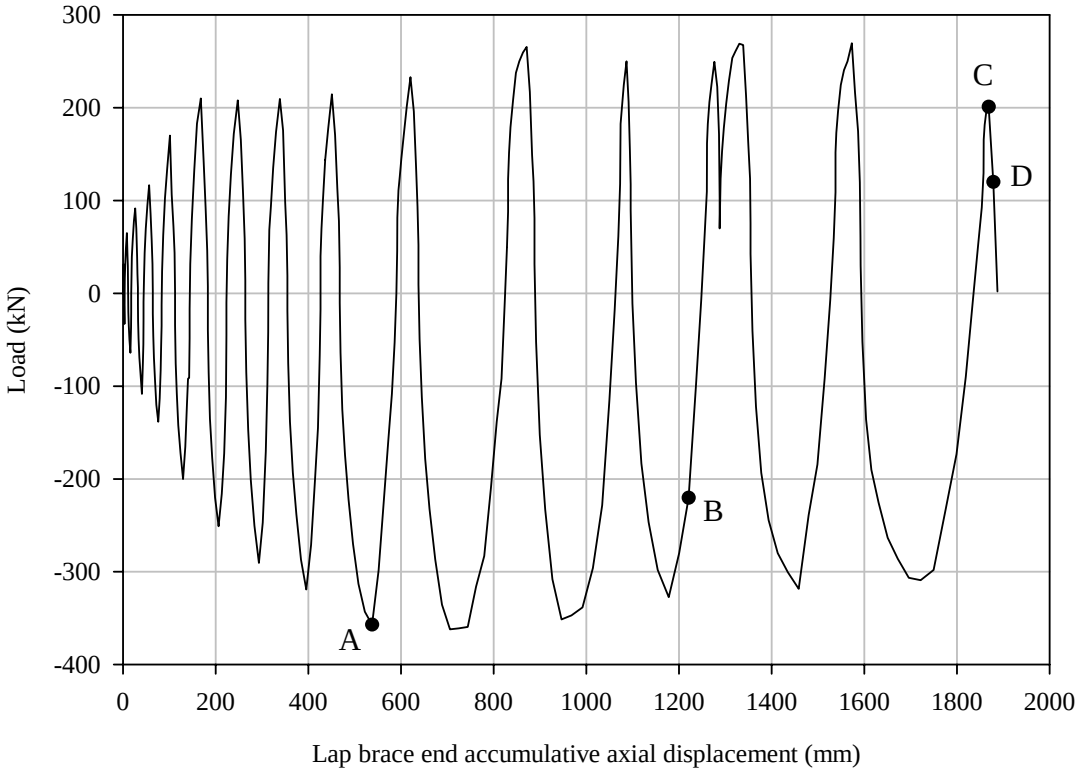

(b) Load reponse

Fig. 3.23 Load response and axial displacement of lap brace

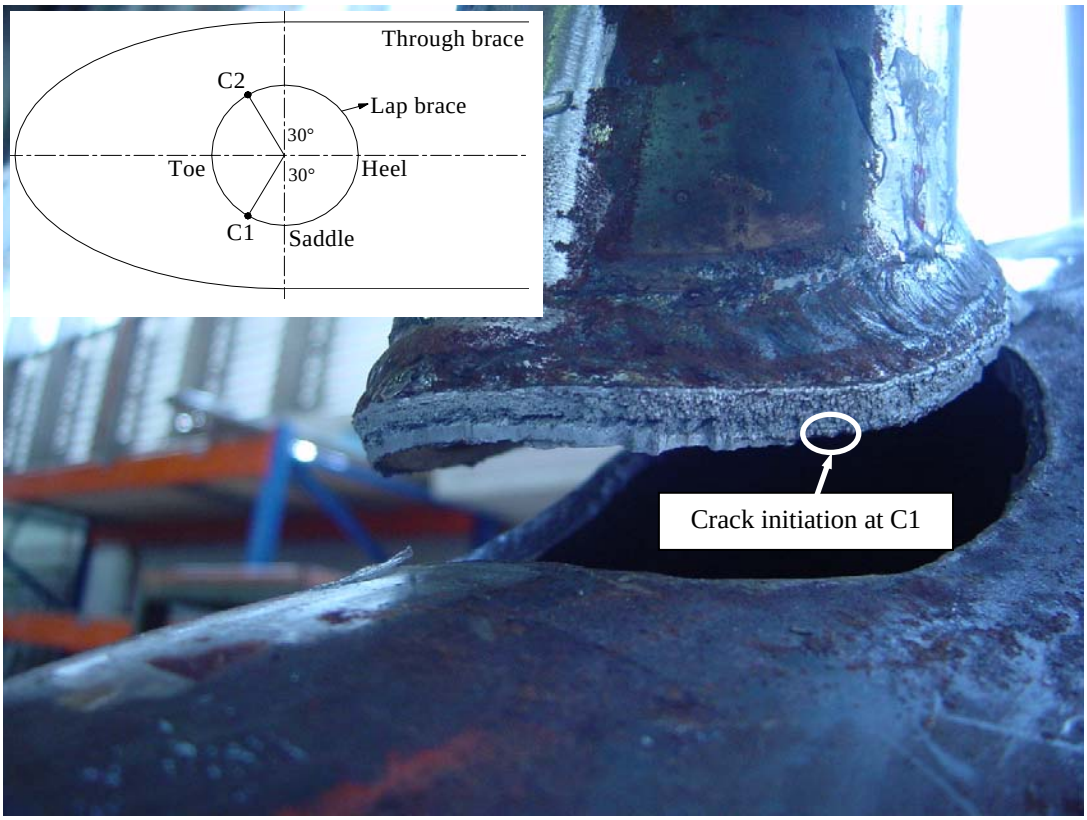

Fig. 3.24 Locations of crack initiation of joint specimen

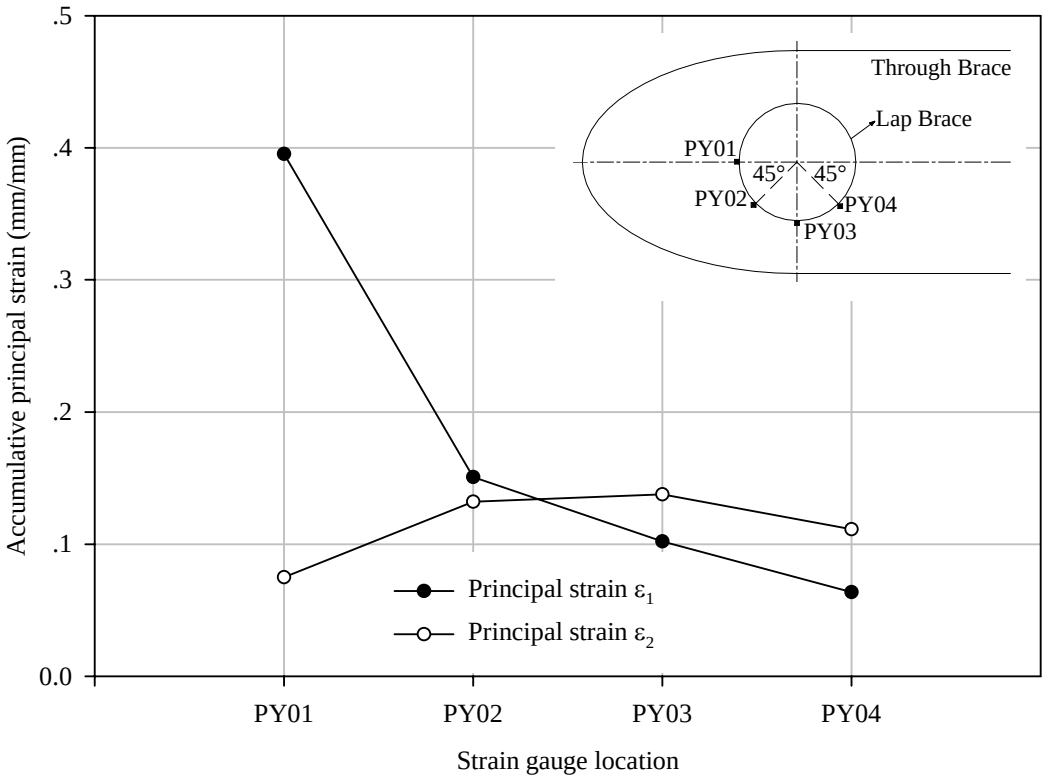

Fig. 3.25 Accumulative principal strain at joint intersection of test specimen

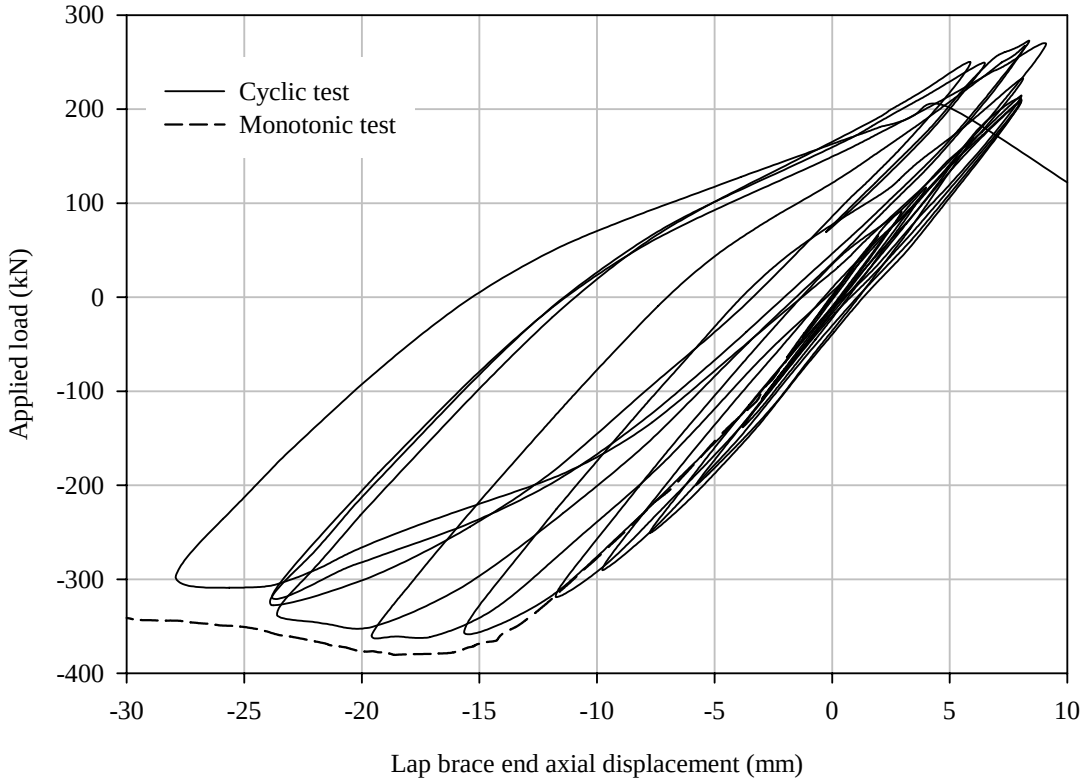

Fig. 3.26 Axial load - displacement curves of joint specimen

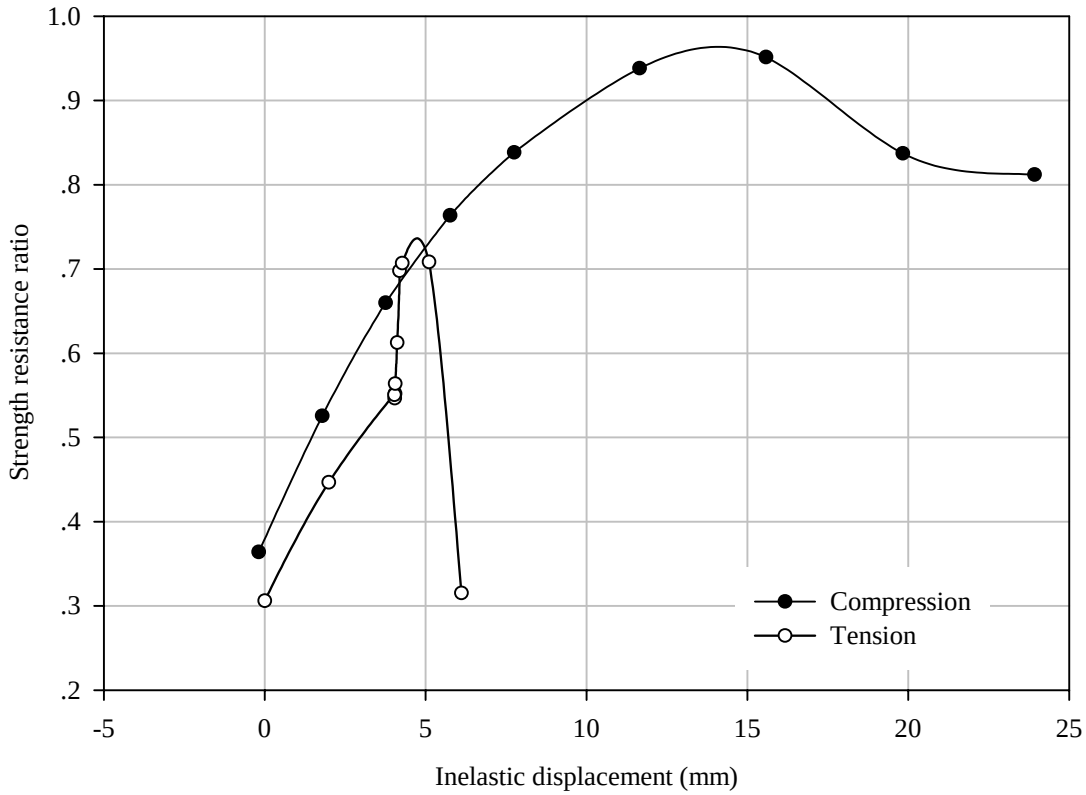

Fig. 3.27 Strength resistance ratio of joint specimen

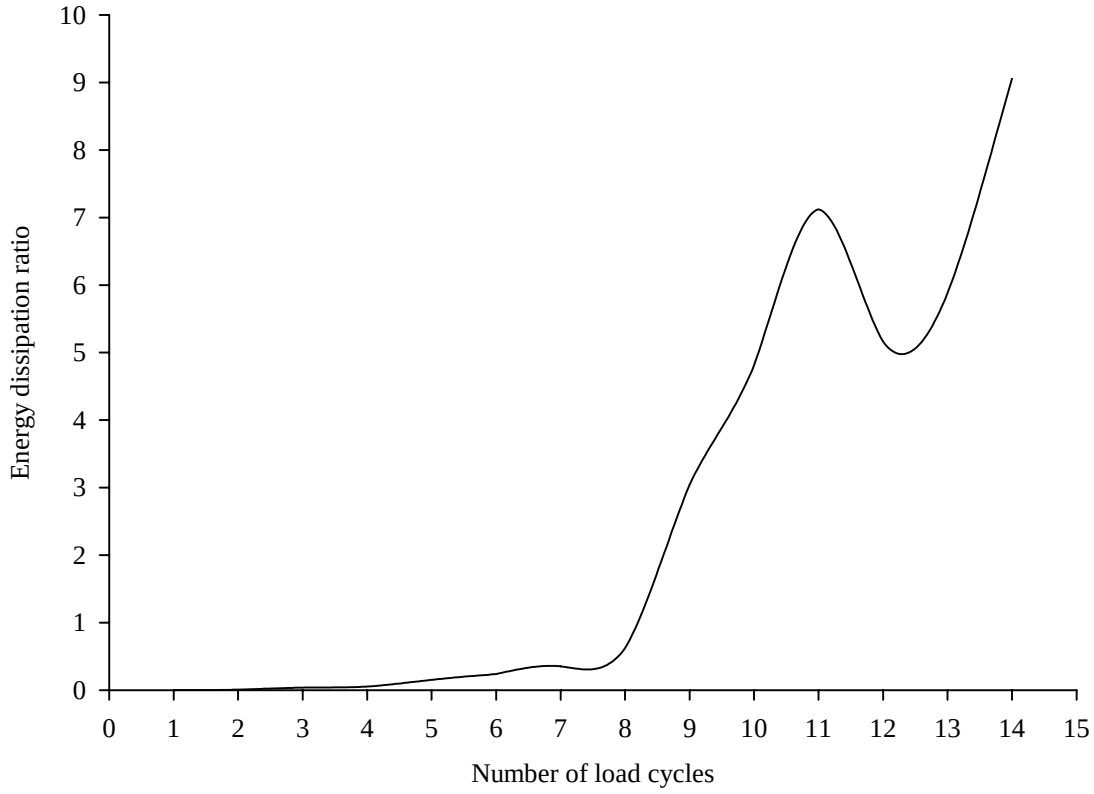

(a) Effect of number of load cycles

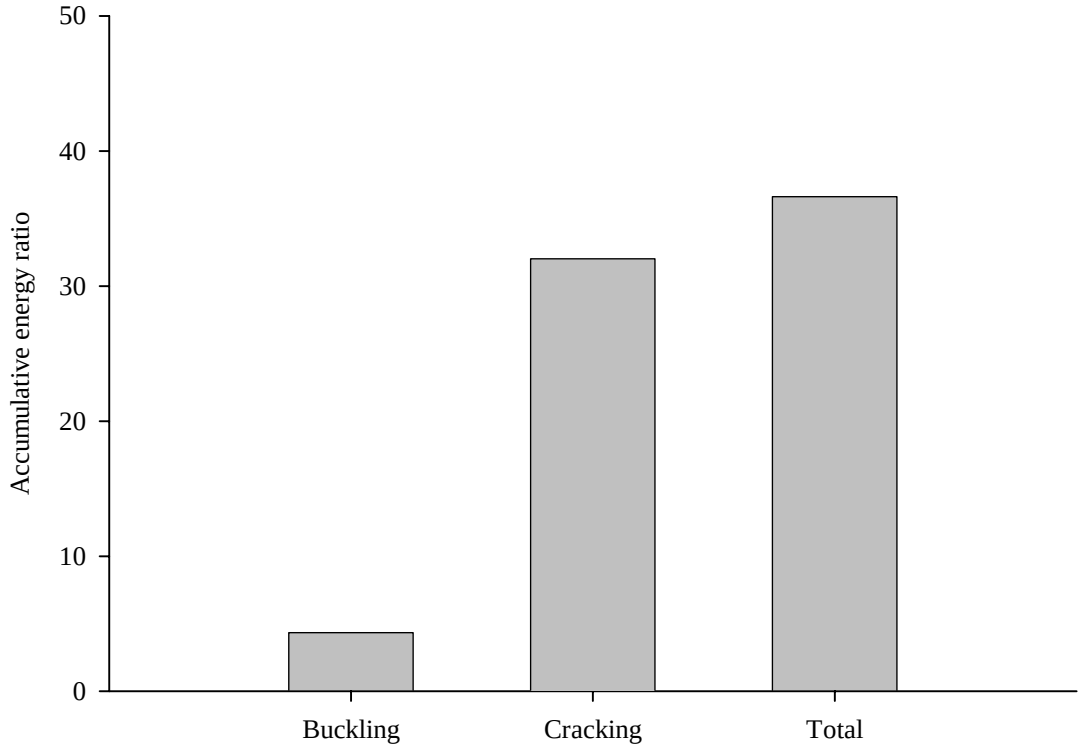

(b) Accumulative energy ratio at buckling and cracking failure modes

Fig. 3.28 Energy absorption capacity of joint specimen

CHAPTER 4
NUMERICAL SIMULATION OF STATIC BEHAVIOUR

4.1 Introduction

In order to obtain realistic behaviour and to identify relevant influencing factors, a series of large-scale tests on the joint specimens are essential. However, the experimental approach to obtain the test data can be very costly and is often impractical for joints with complicated configuration and loading. As such, the need for a reliable numerical technique to supplement the experiments for the analysis of tubular joints under various load combinations had been emphasized by several researchers (Lalani et al 1989, Cofer and Will 1992). The main advantage of conducting numerical analysis for the joint is able to investigate in detail the effect of material and geometrical properties. Furthermore, a database can be set up based on available test data to ensure the reliability of formulation for design and analysis of tubular joints.

The finite element (FE) method is regarded as one of the most suitable numerical approaches for solving problems associated with strength of tubular joints. The reason is that the complicated geometry and boundary conditions of the joint as well as the applied combined loading can be modelled and analysed. In the current study, two completely overlapped tubular joint specimens were tested to failure for the verification of FE models. As the behaviour of the joints was highly non-linear, the following considerations had been included in the FE analysis of the joint model.

- Material non-linearity

  The material properties of tubular joints were modelled with stresses beyond

the elastic limit. The non-linear effect of plasticity and strain hardening of the joint were included.

- Geometric non-linearity

  As the analysis required the buckling failure of the joint to be investigated, a large strain and deflection formulation were adopted.

- Fracture criterion

  A failure criterion was incorporated in the analysis to take account the effect of cracking at weld toe of the joint intersections between the lap brace and through brace for joints failed by fracture mechanism.

4.2 Finite element modelling technique

4.2.1 Finite element programme

Several commercial software packages, such as MARC, PATRAN, FEMGEN, ANSYS, and ABAQUS, are able to successfully generate meshes as well as to carry out analysis for complex tubular joints. Dexter (1996) evaluated the level of capability of PATRAN, FEMGEN and ANSYS and found out that ANSYS was more flexible and easy for use. Both PATRAN and FEMGEN involved complex procedures for modelling. Despite PATRAN was more flexible for meshing, it required excessive amount of memory which was three times higher than that of ANSYS.

Generally speaking, any FE program with shell and solid elements would have the capability for modelling the geometric and material non-linear behaviour of tubular joints for strength analysis. Among the FE packages, the two most commonly used commercial FE packages for tubular joint analysis and research in recent years were ABAQUS and MARC (Lee 1999). In the current study, MARC (2005a) was

adopted to intensively investigate the ultimate capacity of completely overlapped tubular joints. The pre- and post-processing program MENTAT was used to support and to enhance the usage of MARC. Both MARC and MENTAT programs were run on the SUN SPARC workstation in the NTU CADD Laboratory.

4.2.2 Types of finite elements

The type of finite elements used for modelling the tubular joint would determine the layout of the model as well as the mesh density. Most of the tubular joints were modelled using shell elements which considered only the mid-surface of the wall thickness. In the current study, three different shell elements (MARC element type 22, 72 and 75) were available to simulate the test specimen. However, it should be noted that the suitability of the element for modelling the joint specimen was dependent upon several conditions such as the joint configuration, the loading and the area of investigation. Thus, the type of element used was considered on a case-by-case basis and was to be verified against the experimental results. A detailed description of the three types of shell elements available in the FE programme could be found in MARC (2005b). Below was the brief review of the three finite elements for use in the strength analysis of completely overlapped tubular joints.

MARC element type 22 was a higher order doubly curved eight-node thick shell element with reduced integration. The geometry, node location and coordinate system are shown in Fig. 4.1a. This element consists of 4 corner and 4 mid-side nodes. It used a second order interpolation for the coordinates, displacements and rotations. For the corner node, the constant and variable thickness could be defined. For the mid-side node, the thickness was taken as the average of that of the corresponding corner nodes. Each node had six degrees of freedom with three

translational (u, v, w) and three rotational (ϕ_x, ϕ_y, ϕ_z). The stiffness of the element was formed through the four integration points. The transverse shear effect was included in the analysis. At each of the integration points, the vectors tangent to the curves with constant isoparametric coordinates ξ_c and η_c were normalised as follows:

$$t_1 = \frac{\partial x}{\partial \xi_c} \Big/ \left| \frac{\partial x}{\partial \xi_c} \right|, \quad t_2 = \frac{\partial x}{\partial \eta_c} \Big/ \left| \frac{\partial x}{\partial \eta_c} \right| \tag{4.1}$$

A new basis could then be defined as

$$s' = t_1 + t_2, \quad d' = t_1 - t_2 \tag{4.2}$$

After normalizing these vectors by

$$\bar{s} = s' / \sqrt{2}\left|s'\right|, \quad \bar{d} = d' / \sqrt{2}\left|d'\right| \tag{4.3}$$

The local orthogonal directions could be obtained as

$$V_1 = \bar{s} + \bar{d}, \quad V_2 = \bar{s} - \bar{d}, \quad V_3 = V_1 \times V_2 \tag{4.4}$$

On the other hand, MARC element type 72 was an eight-node doubly curved thin shell element, which used bilinear interpolation functions for coordinates and displacement. The global rotations were quadratically interpolated from the rotation vectors at the centre and mid-side nodes. As shown in Fig. 4.1b, the element is defined geometrically based on the coordinates of four corner nodes. Although coordinates could be specified at mid-side nodes, they were ignored and the edges were treated as straight lines. There were three translational degrees of freedom for the four corner nodes and one rotational about the edge axis for the mid-side nodes. There were four integration points at the plane and seven integration points through the thickness of the element. Unlike the thick shell MARC element type 22, the transverse shear effect was not included.

The capability of MARC element type 75, as shown in Fig. 4.1c, is quite similar to that of MARC element type 22 except that it is a four-node doubly curved thick shell element, which uses bilinear integration functions for the coordinates, displacements and rotations.

4.2.3 Modelling and mesh generation

The FE model of the joint is first modelled according to the geometrical configuration and dimensional properties of the test specimen, as shown in Fig. 3.1 and Table 3.1. It should be noted that the centrelines of the chord, the through brace and the lap brace as well as the applied loads and supports were symmetrical about the middle plane of the joint. Hence, by taking advantage of symmetry, one-half the joint model was sufficient to investigate the behaviour. In the modelling, fine meshes were generated at the vicinity of joint intersection of members and the gap regions to account for the effect of high stress gradients. In the areas outside the joint, coarse meshes are adopted as shown in Fig. 4.2.

The boundary conditions of the joint model were constrained at the out-of-plane displacement, out-of-plane moment and torsion. Both ends of the chord were fixed and the end of through brace was pinned. At the end of the lap brace, the rotations were released to simulate the pinned support condition. The two shear translations were fixed with the axial translation released to allow for the applied load.

4.2.4 Weld modelling

For the static strength analysis of T/Y-joints, the overall behaviour of the joint could adequately be simulated using the shell element by modelling the mid-plane of the member wall thickness without considering the extra stiffening effect of welds.

However, for joints with notable gap size between braces, the bending stiffness of the chord wall in the gap region could have an appreciable effect on the strength behaviour. The lack of weld element in the model might result in strength reduction of the joint, so the overall behaviour could significantly be changed (Lee 1999). It was recommended by van der Vegte et al (1991) that the weld in the gap region could be modelled as a ring of shell elements at joint intersections (Fig. 4.3). The size of weld element in the model was simulated according to the actual weld size of the joint specimen.

4.3 Finite element analysis procedure

In the FE analysis, apart from the geometry and boundary conditions of the joint, other relevant data were also examined to define the material properties, solution methods and controls.

4.3.1 Material non-linearity

The non-linear property of steel material was included in the current FE model of the joint to account for the effect of load applied after the elastic limit. In the study, the Young's modulus of steel material and the stress-strain curves of members are obtained from the tensile coupon tests as shown in Table 3.2 and Fig. 3.4. The Poisson's ratio was assumed as 0.28. The true stress (σ_{true}) and logarithm strain (ε_{ln}) relationship was adopted in the FE analysis of the joint to account for the effect of large strain. The logarithm strain (ε_{ln}) was to consider the change in the length of the tensile coupon during the test. The true stress (σ_{true}) was to take account the change of the actual cross sectional area of the tensile coupon prior to the next load increment. As the volume change of the tensile coupon was small and only associated with the elastic strain with no contribution from the plastic strain and

creep, two relationships could be derived by assuming a constant volume of the tensile coupon as shown below (Dowling 1997).

$$\varepsilon_{\ln} = \ln(1+\varepsilon_{eng}) \tag{4.5}$$

$$\sigma_{true} = \sigma_{eng}(1+\varepsilon_{eng}) \tag{4.6}$$

where ε_{eng} and σ_{eng} were the engineering strain and stress respectively. However, the use of the above two equations were limited to the strength before the coupon fracture. As shown in Fig. 4.4, the true stress is assumed to constantly behave after the peak value. This was applied for the chord, the through brace and the lap brace of the joint specimen. It should be noted that the assumption of constant stress after the peak had little impact on the determination of joint capacity as the plasticity occurred at localised area around the joint intersections (Gho 2001).

4.3.2 Geometric non-linearity

In the experimental investigation, a significant local buckling was found to develop on the through brace face in contact with the lap brace. The geometric non-linearity was included in the FE analysis so that the finite element could be formulated in the loading history based on the immediate load condition instead the original configuration for the next load increment. To accurately simulate the geometric non-linearity, the large displacement, the updated Lagrange procedure and the finite strain plasticity were activated in the current FE analysis for a complete large strain plasticity formulation.

4.3.3 Loading and solution control

In the current FE analysis, a displacement control had been applied in a number of small increments to determine the ultimate capacity of the joint. In contrast to the

load control with the load directly applied onto the nodes of finite element, the displacement at the nodes of finite element was prescribed in the displacement control mode. The displacement control had resulted in nodal reaction forces at the nodes of the finite element with displacements prescribed. The summation of these reaction forces gave the applied external load. There was no preference on the load types used in the control of analysis from a physical viewpoint. However, the displacement control was generally preferred to the load control mode because of better conditioned tangent stiffness matrix (Borst 1991). In the current analysis, the displacement control mode was adopted to determine the ultimate strength of the joint.

In the solution control, the iteration process of the non-linear analysis of the problem was activated. A full Newton-Raphson method was adopted to reassemble the stiffness matrix at each of the iteration. For the convergence criteria of the joint model, the residual force and the moment relative to the reaction force and moment was set at 5%. A modified Riks-Ramm method (Crisfield 1981, Ramm 1985) was used to adaptively apply the load step in the analysis.

4.4 Finite element analysis results

4.4.1 Convergence study

A large number of FE models of the completely overlapped tubular joint were created for parametric study. A convergence study was conducted with main objective to optimise the mesh density at the joint intersections of the chord and through brace and the through brace and lap brace for accurate solutions with minimal computational time.

In the study, six different mesh densities of the joint model to simulate the joint specimen were created for comparison. The weld element was not included. The number of finite elements and nodes of the joint models are summarised in Table 4.1. It could be seen from Fig. 4.5 that the ultimate capacity of the joint converges with finer meshes at the joint intersections. The difference of the ultimate capacity of the joint models with meshes D, E and F was small with maximum discrepancy of less than 1%. However, the CPU time for running the joint models with meshes E and F were about 155% and 356% greater than that of mesh D. It could be concluded from the comparison of ultimate load that the joint model with mesh D was most efficient. Thus, this mesh density had been adopted in the current study to assess the ultimate behaviour of tubular joints with complete overlap of braces.

4.4.2 Boundary conditions and chord pre-stresses

In the current test program, both ends of the chord and the end of the through brace of the joint specimen were directly welded onto the flat plates and bolted on the test rig. As the movement at the end of members was found small, the connections were considered fixed. However, owing to the bending effects of end plates and the tightness of bolted connections, the end of members provided certain degree of flexibility which might affect the overall behaviour of the joint. This implied that the boundary conditions of the joint specimen were neither pinned nor fixed.

In the current FE modelling of the joint, various boundary conditions and chord pre-stresses are investigated with results shown in Fig. 4.6. The boundary support condition BC1 simulated the behaviour of the joint in the test. BC2 was used to compare with BC1 to investigate the differences of support conditions of pinned and fixed at the end of the through brace. BC3 and BC4 yielded net compressive and tensile load in the chord respectively. BC5 and BC6 were used to investigate

the effect of chord pre-stresses. Eight chord pre-stressed levels at σ_{cp}/σ_{cy} = ±0.1, ±0.3, ±0.5, ±0.7 and ±0.9 were considered in the FE analysis. σ_{cp} and σ_{cy} were the pre-stress and the yield stress of the chord, respectively. The negative sign convention showed a compressive stress applied on the chord. The ultimate strength of the joint under different boundary conditions and chord preloads are summarised in Table 4.2. It was found that the change in the ultimate capacity of the joint due to different end supports and chord preloads was insignificant.

4.4.3 Chord and through brace length parameters

A large chord length resulted in beam bending action whilst a small chord length caused an excessive ovalisation. In the study, a range of chord and through brace length parameters (α_C and α_T) from 6 to 30 was considered to investigate the effect of length parameters. The gap size of the joint model was fixed at 143mm according to the measurement taken during the test set up. It could be seen from Fig. 4.7 that the chord length parameter has an insignificant effect on the ultimate load of the completely overlapped tubular joint. The maximum difference of ultimate load at the chord length parameter of 6 and 30 was only 0.34%. For the through brace length parameter, the ultimate load of the joint decreased with increasing length parameter. The difference of the length parameters was found less than 1% with parameter α_T greater than 14. However, as the failure mode of the joint was associated with through brace wall plastification, a sufficient through brace length parameter should be provided to prevent the localized ovalisation of the cross section.

4.5 Comparison of experimental and finite element analysis results

4.5.1 Verification of finite element model

The FE model of the joint was calibrated against the test results obtained in the current experimental study (Test 1) and the previous experimental study conducted by Fung et al (2001a) (Test 2). The comparison of the load - displacement curves in Fig. 4.8 showed that the results obtained from the FE analysis compare very well with those from the experimental study. The joint stiffness in the elastic region of the load - displacement curves was well simulated. The FE model showed lower ultimate load of 1.52% but with higher corresponding displacement of 1.72% in comparison to that of Test 1. On the other hand, the FE model showed close simulation of ultimate load with difference of only 0.16% but with higher corresponding displacement of 3.5% in comparison to that of Test 2. The failure modes predicted by the FE model match those of the joint specimens as depicted in Fig. 4.9. It was therefore concluded from the comparison of ultimate strength and failure modes that the current FE model was suitable for elastic-plastic large deformation analysis of tubular joints with complete overlap of braces.

4.5.2 Effect of element types

To determine the effect on the type of elements used in the FE analysis, the joint specimen had been modelled using the eight-node thick shell, eight-node thin shell and four-node thick shell elements for comparison. The load - displacement curves and the numerical results obtained from the joints modelled using the above-mentioned finite elements are presented in Fig. 4.10 and Table 4.3. The comparison with the experimental results revealed that the eight-node thin shell FE model was unsuitable for analysis as it over predicted the test result by 89.1%. Furthermore, it did not consider the effect of transverse shear deformation which resulted in excessive stiffness of the joint.

The FE model using the four-node thick shell element showed 1.52% lower ultimate load with 1.72% higher corresponding displacement in comparison with that of the test. For the model with eight-node thick shell element, the ultimate load and the corresponding displacement were found to be 5.0% and 3.8% lower. Despite the eight-node thick shell FE model yielded a more conservative ultimate capacity and corresponding displacement, the CPU time required to run the analysis was 3.5 times more than the four-node thick shell FE model. In the current FE analysis, the four-node thick shell FE model was adopted as it compared very well with the test results with slight discrepancy of the ultimate capacity and the corresponding displacement.

4.5.3 Effect of weld elements

The effect of weld elements at joint intersections is illustrated in Fig. 4.11. The FE model without the weld elements gave lower ultimate strength with difference of 7.7% in comparison to that of the experimental value. On the other hand, the results of the FE model with weld elements agreed very well with the experiment data. The difference of ultimate loads between the FE models with and without the weld elements was found less than 8%. It should be noted that the absence of weld element in the completely overlapped joint model caused the bending stiffness of the short segment of the through brace reduced and so the strength of the joint. Despite the differences, the FE model without the weld element was recommended to obtain more conservative ultimate strength for the study.

4.5.4 Effect of material behaviour

The effect of material property of the joint is analysed using two different material post-yield properties as shown in Fig. 4.12. Material type 2 used a simple

linear-elastic perfectly plastic stress-strain relationship which did not include the effect of strain hardening. The detail of the load - displacement curves of the joints with two different material types are depicted in Fig. 4.12. It could be seen from the figure that the model without the strain hardening exhibits lower load in comparison to that with strain hardening. In comparison with the experimental result, the difference in the ultimate load and the corresponding displacement was found 7.6% and 25.6% respectively. A small difference of ultimate load was due to plasticity in a localized area of the joint. In the current study, the material with the strain hardening was included in the joint model for FE analysis.

4.6 Discussions

It should be noted in the FE analysis that the transverse shear effect was important for the finite element with thickness greater than 1/15 its characteristic length. If the diameter of the joint member was to be taken as the characteristic length, thick shell elements should be used for joints with diameter to wall thickness ratio (γ) less than 7.5. This implied that for tubular joints with geometrical parameters within the practical range of limit, thin shell elements were sufficient for FE analysis of the joint. Lee (1999) highlighted that both thick and thin shell elements produced similar results but the processing time of using thick shell could be doubled that of thin shell elements. Van der Vegte (1995) indicated that eight-node thick shell element gave higher accuracy whilst eight-node thin shell and four-node thick shell element showed the best performance in terms of CPU time and disk storage. It was therefore recommended that eight-node thick shell element should be used for modelling the tubular joints.

In general, thin shell elements were used for modelling a large number of tubular joints with radius-to wall-thickness ratio of members greater than 10. The use of

eight-node thick shell element required more CPU time. However, in the current study, thin shell element was found unsuitable for modelling the completely overlapped tubular joint. In view of the accuracy and computational time, four-node thick shell element was adopted throughout the FE analysis.

The joint model without the weld elements showed conservative result and close comparison with the experimental value. Despite the modelling of weld element at the joint produced accurate estimate of strength, the dimensioning of the weld profile could be arbitrary as the actual weld size at the joint was practically larger than the minimum requirement specified in AWS (2000). Thus, in the parametric study presented in the next Chapter, the area of investigation on the strength and the ultimate behaviour of the joint were focused on the effect of geometrical properties. The weld element was excluded at the joint intersections of the FE models to obtain more conservative result for comparison.

4.7 Concluding remarks

The four-node thick shell element is found suitable and most efficient for modelling the joint specimen with complete overlap of braces. The weld element at the joint intersections is excluded from the FE model to obtain more conservative result for comparison. The post yield property of material with the effect of strain hardening is used. The comparison of the load - displacement curves and the failure behaviour shows that the FE model simulates very well the joint specimen. As the FE model is verified to be reliable and accurate, a detailed parametric study is carried out to assess the behaviour and the strength of the completely overlapped tubular joint in the next two Chapters 5 and 6.

Table 4.1 Results of convergence study

Mesh reference	No. of elements	No. of nodes	*Element l / t ratio			Peak load (kN)	CPU time (s)
			Chord	Through brace	Lap brace		
A	161	195	14.0	9.0	4.5	565.3	46
B	417	479	7.0	3.5	2.0	415.8	135
C	959	1045	4.0	2.5	1.2	368.1	306
D	1900	2019	3.0	2.0	1.0	351.0	682
E	4115	4263	2.0	1.0	0.5	349.8	1736
F	7948	8113	1.5	0.5	0.5	348.9	3110

**In the region of joint intersection; l: length of element; t: thickness of element*

Table 4.2 Effect of boundary conditions and chord pre-stresses

Boundary conditions	Ultimate strength*	Boundary conditions	Ultimate strength*
BC1	374.71	BC3	373.91
BC2	374.70	BC4	375.03
BC5-1	0.9984	BC6-1	0.9998
BC5-3	0.9984	BC6-3	0.9979
BC5-5	0.9983	BC6-5	0.9943
BC5-7	0.9979	BC6-7	0.9888
BC5-9	0.9973	BC6-9	0.9795
BC5+1	0.9981	BC6+1	1.0025
BC5+3	0.9978	BC6+3	1.0033
BC5+5	0.9971	BC6+5	1.0039
BC5+7	0.9965	BC6+7	1.0039
BC5+9	0.9960	BC6+9	1.0035

*For BC5 and BC6 the ultimate strength is normalized by the joint strength without chord stress. The negative sign means a compressive stress, and positive sign means a tensile stress applied on the chord. The number after the sign means the level of chord pre-stress.

Table 4.3 Summary of numerical results for different element types

FE Model	Number of elements	Number of nodes	CPU time (s)	Ultimate Strength (kN)	Numerical/Test
4-node thick shell element	1943	2019	682	374.7	0.985
8-node thin shell element	1943	5983	799	719.4	1.891
8-node thick shell element	1943	5983	2323	361.3	0.950

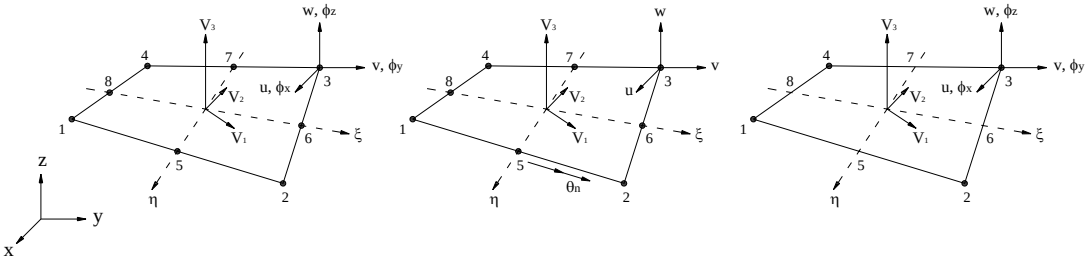

(a) Element 22 (b) Element 72 (c) Element 75

Fig. 4.1 Types of finite elements

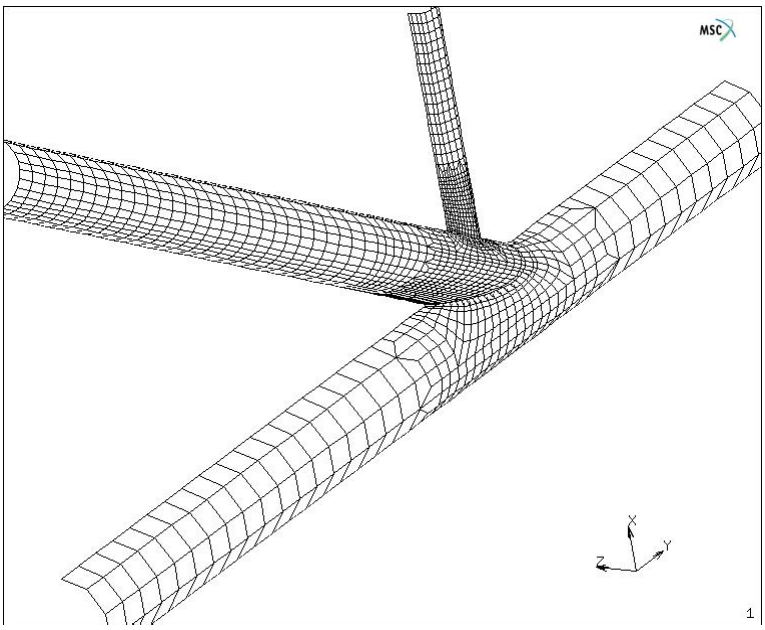

Fig. 4.2 FE model of completely overlapped tubular joint specimen

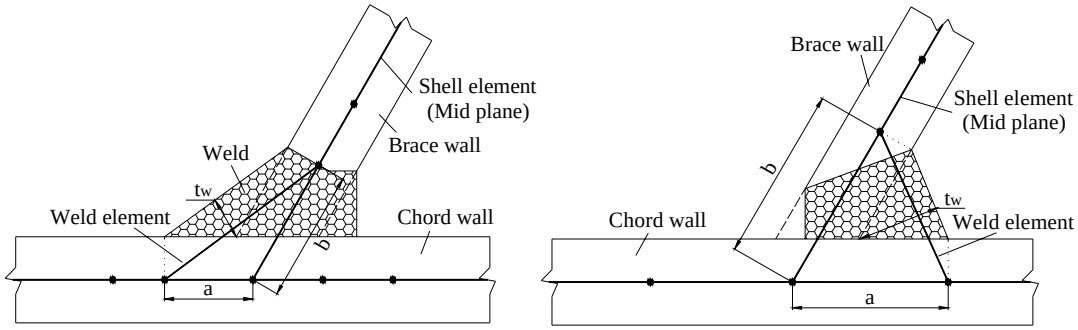

(a) Member crown toe and saddle (b) Member crown heel

Note: a, b - FE sizes, t_w -weld thickness

Fig. 4.3 Weld modelling at joint intersection

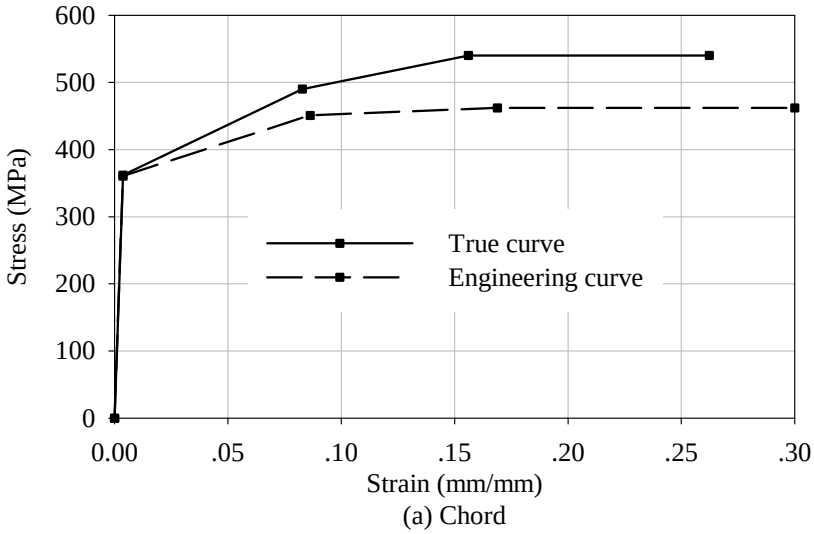

(a) Chord

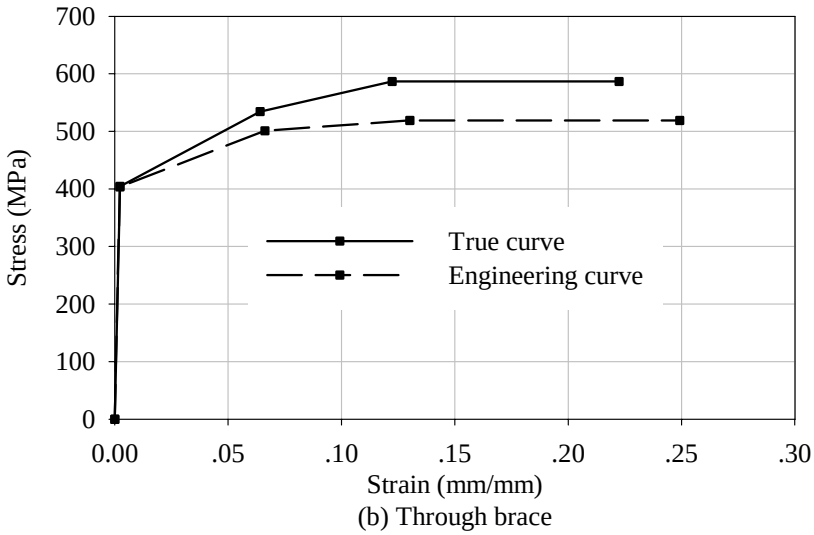

(b) Through brace

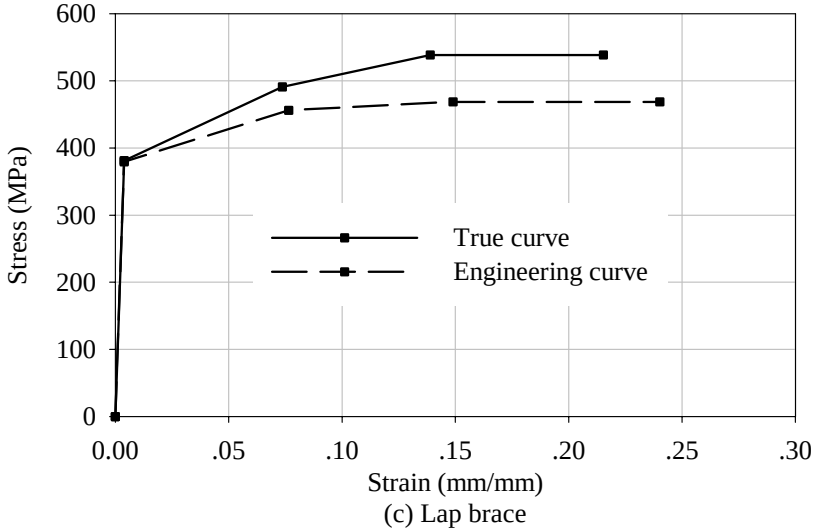

(c) Lap brace

Fig. 4.4 True stress - logarithmic strain curves

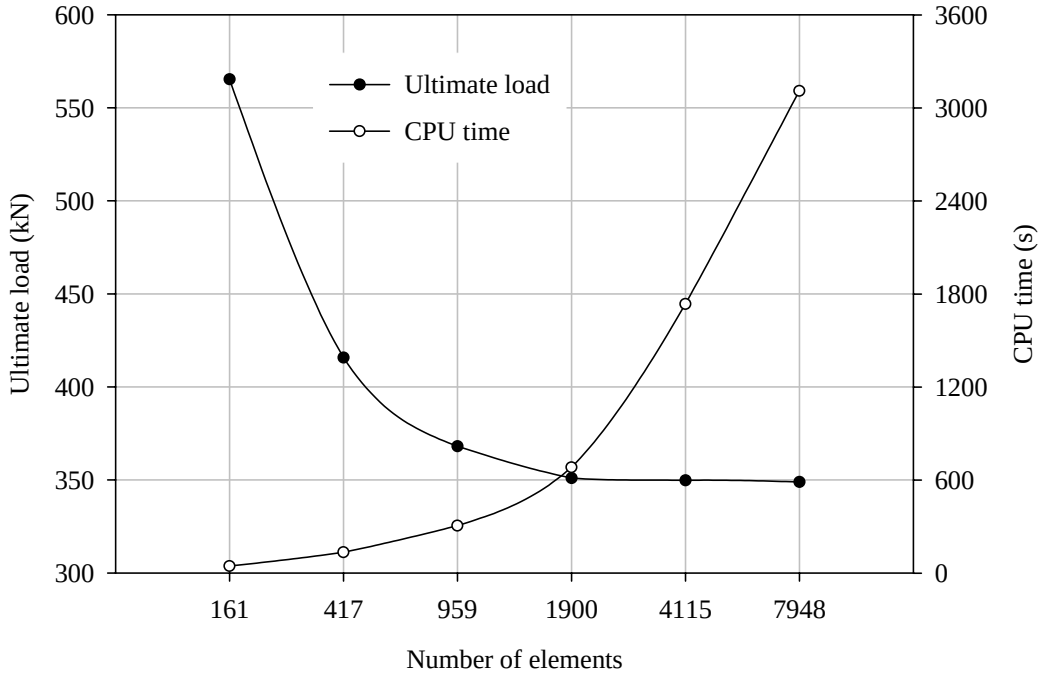

Fig. 4.5 Convergence study of FE models

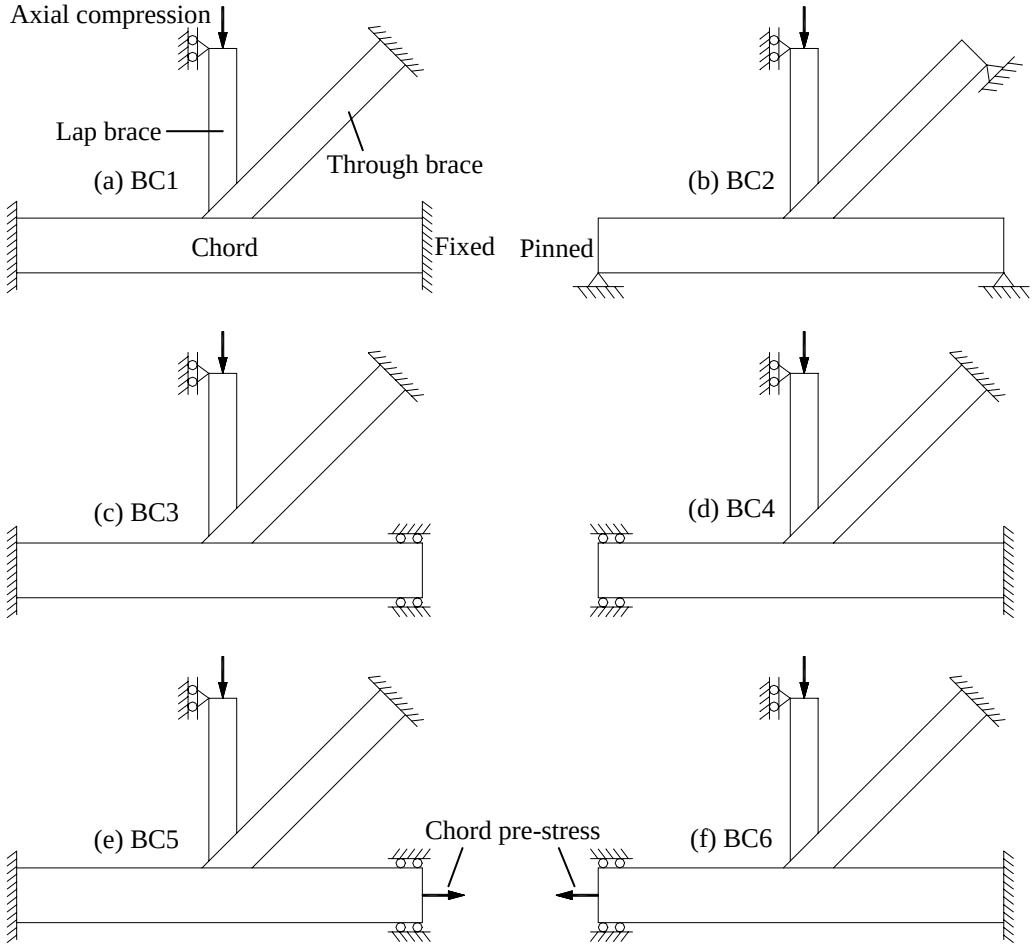

Fig. 4.6 Boundary conditions of FE models

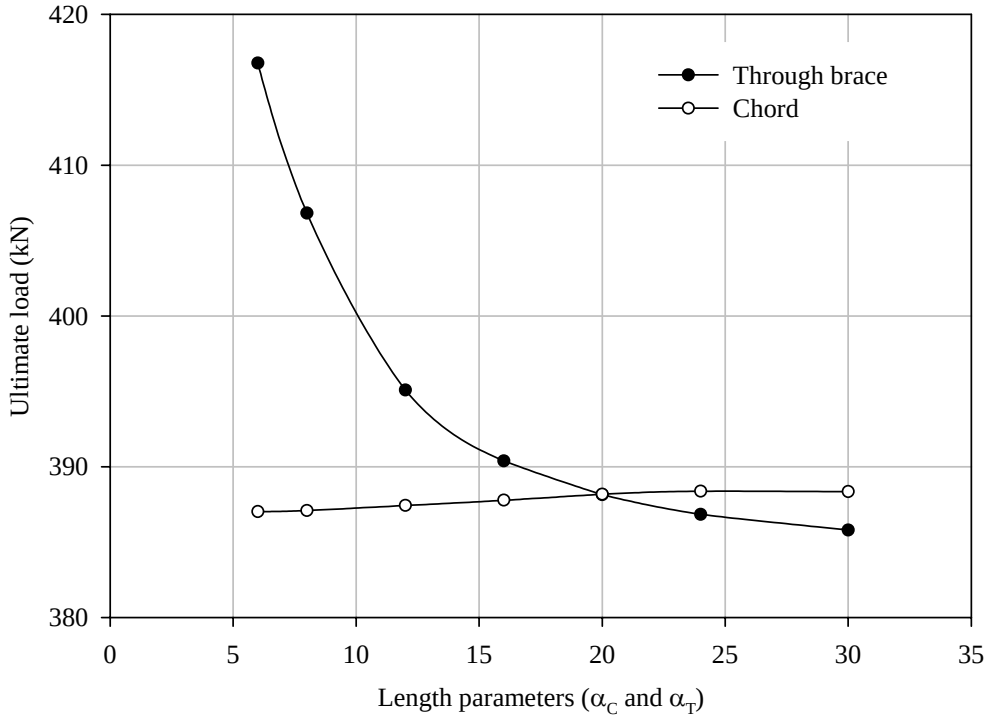

Fig. 4.7 Effect of chord and through brace length parameters

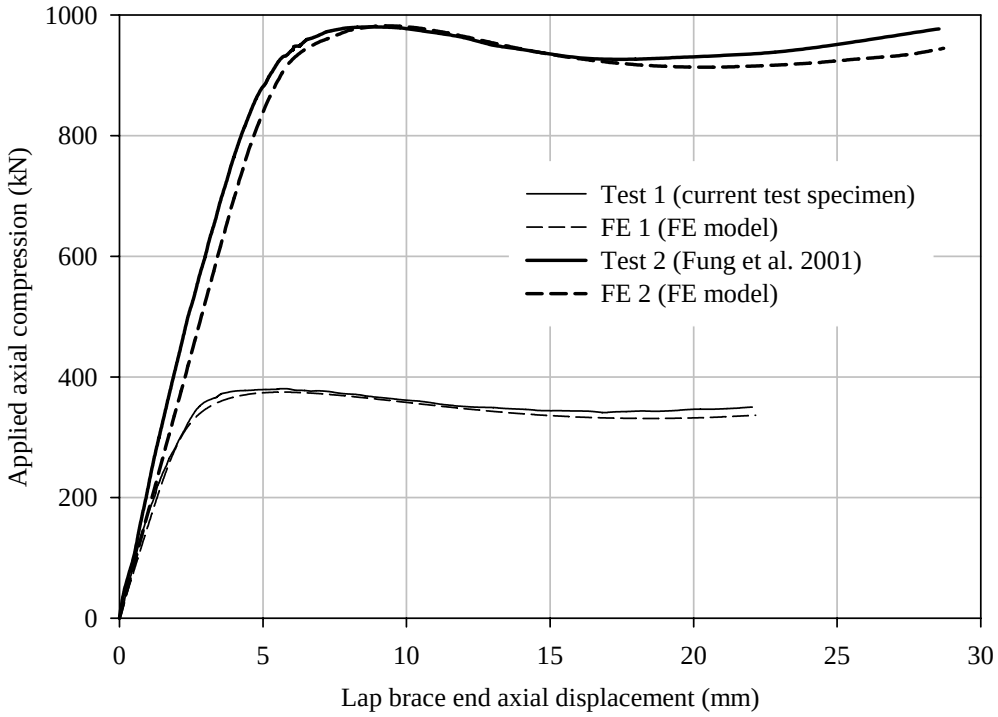

Fig. 4.8 Comparison of axial load - displacement curves

(a) Test 1 (current test specimen)

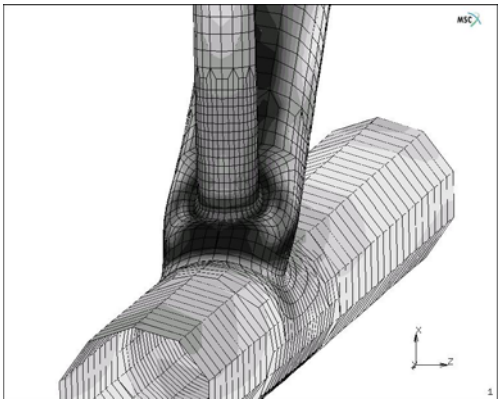

(b) FE 1 (FE model)

(c) Test 2 (Fung et al. 2001)

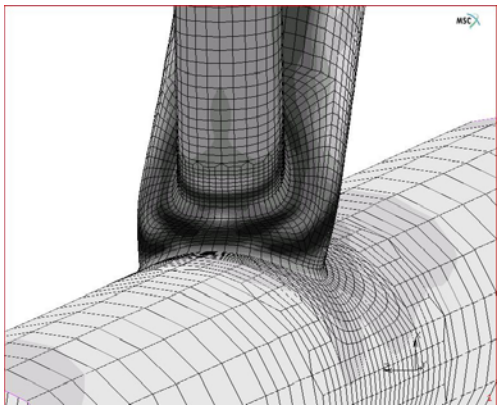

(d) FE 2 (FE model)

Fig. 4.9 Failure modes of joint specimens and FE models

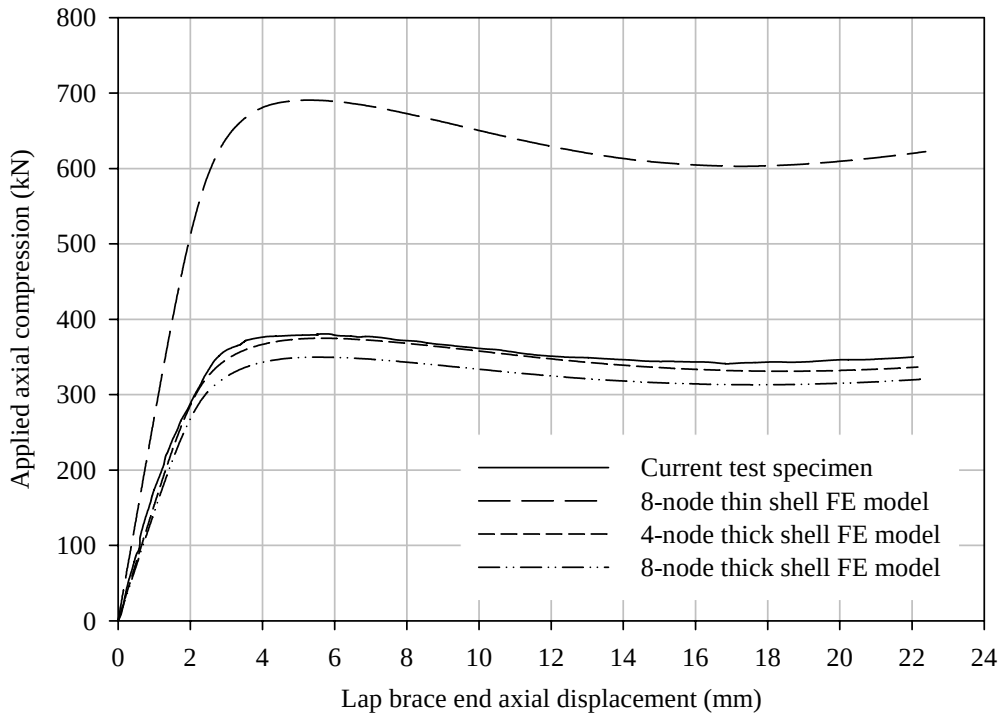

Fig. 4.10 Effect of element types

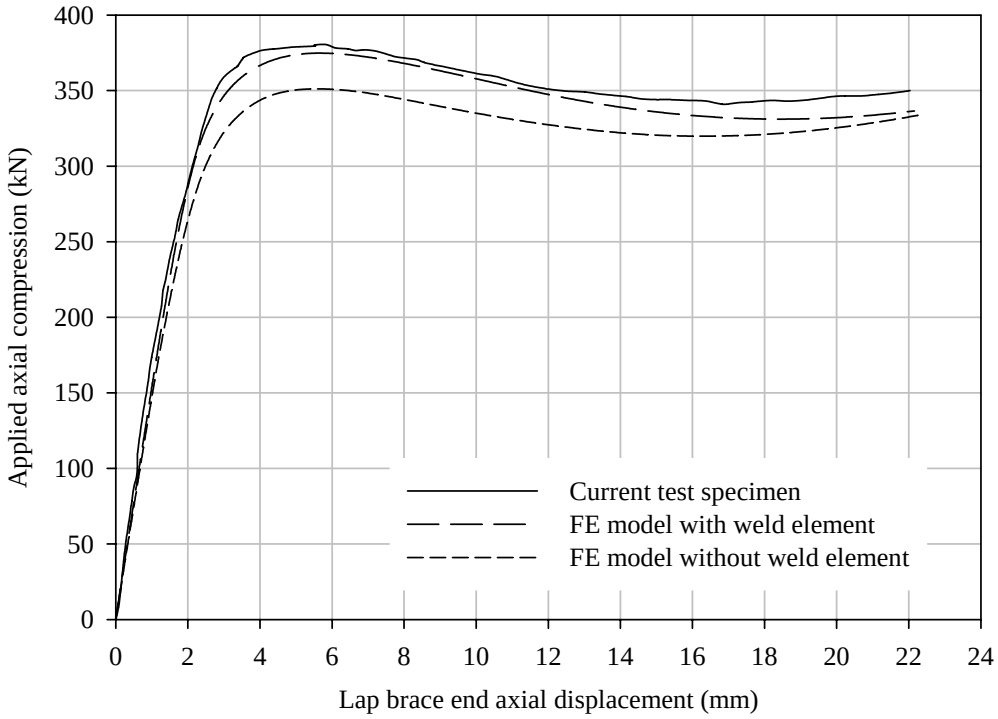

Fig. 4.11 Effect of weld elements

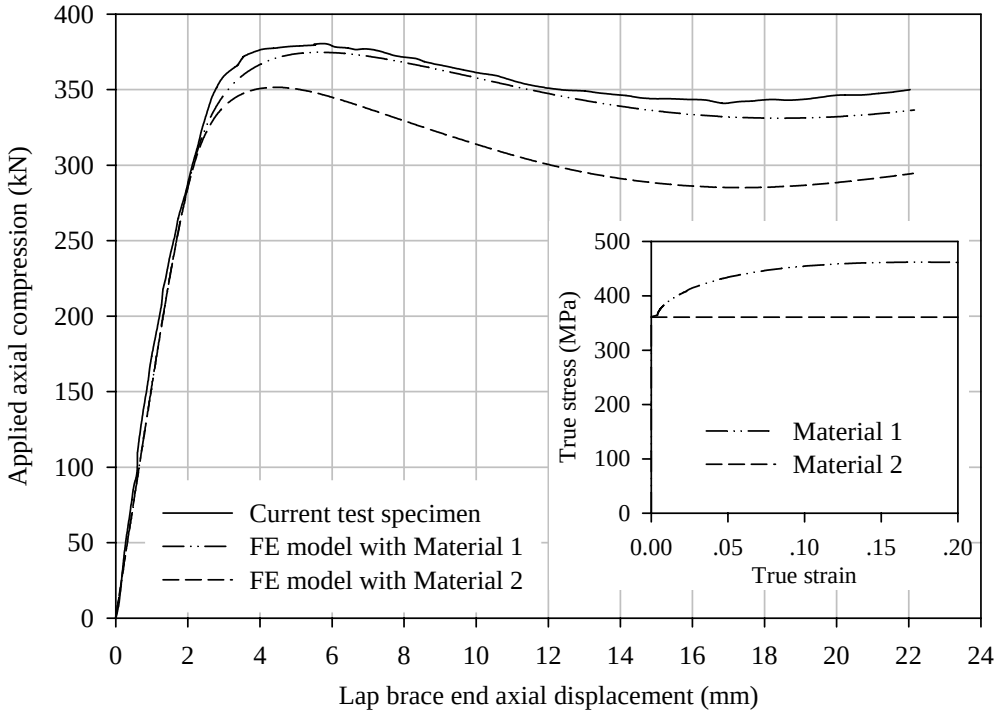

Fig. 4.12 Effect of material post yield properties

CHAPTER 5

FAILURE MECHANISM

5.1 Introduction

The behaviour of tubular joints under static loading is highly affected by the geometrical configurations, the member sizes, and the material properties. These factors have been considered and included in the design parameters as discussed in Chapter 2. Some design parameters are found more important for certain joint configurations and load types such as the parameter γ which could have a significant effect on the ultimate strength of T-joints under bending but not axial loading.

For simple gap joints, the parameters β and γ are the main geometrical parameters to be considered for strength design. For overlapped joints, apart from β and γ, τ is also considered an important parameter as it influences the joint capacity with failure due to brace local buckling. Thus, a parametric study is generally conducted to identify the most influential geometrical parameters on the failure behaviour of the joints. In the current study, the ultimate load behaviour of the completely overlapped joints is investigated in terms of failure mechanism and load - displacement relationship. All the FE models of the completely overlapped tubular joints were generated using the pre-processing program MENTAT. The FE analyses were performed using the general FE package MARC (2005a). Both MARC and MENTAT programs were run on the SUN SPARC workstation.

5.2 Finite element models

In Chapter 4, the comparison with the experimental results showed that the FE model predicted very well the ultimate load behaviour of completely overlapped tubular joints. However, prior to the parametric study of the completely overlapped

tubular joints under axial loading, some assumptions and standardisation of geometrical parameters for analysis are necessary to ensure the data obtained is useful for comparison with previous research results and for future reference.

5.2.1 Validity ranges

The geometrical parameters of the completely overlapped tubular joint considered in the current study are limited as follow.

$$
\begin{aligned}
&0.4 \leqslant \beta_{CT} \leqslant 0.8 \text{ (0.4, 0.6 and 0.8)} \\
&0.4 \leqslant \beta_{TL} \leqslant 0.8 \text{ (0.4, 0.6 and 0.8)} \\
&0.4 \leqslant \tau_{CT} \leqslant 1.0 \text{ (0.4, 0.7 and 1.0)} \\
&0.4 \leqslant \tau_{TL} \leqslant 1.0 \text{ (0.4, 0.7 and 1.0)} \\
&12 \leqslant \gamma_C \leqslant 50 \text{ (12, 20, 30 and 50)} \\
&0.5 \leqslant \xi_T \leqslant 1.0 \text{ (51mm, } 0.5d_T\text{, } d_T \text{ and } 2d_T\text{)} \\
&30^\circ \leqslant \theta \leqslant 60^\circ \text{ (30º, 45º and 60º)} \\
&30^\circ \leqslant \psi \leqslant 60^\circ \text{ (30º, 45º and 60º)} \\
&\alpha_C = \alpha_T = 14
\end{aligned}
\qquad (5.1)
$$

For all the joints under investigation, the chord diameter was taken as D = 762mm. A chord length of 7 times its diameter was used to avoid excessive beam bending and effect of end conditions. It had been discussed in previous Chapter 4 that the chord length had negligible effect on the ultimate capacity of the completely overlapped tubular joint. However, the through brace length was crucial to accurately determine the ultimate strength of the joint as it acted as a chord member supporting the lap brace.

As the failure mode of the completely overlapped tubular joint was associated with through brace face plastification, the through brace length of 7 times its diameter was found sufficient to avoid localised ovalisation of cross section. It should also be noted that the overall length of the chord and the through brace was taken as 7 times the diameter to preclude any short chord effect due to boundary conditions. The

length of the lap brace was 4 times its diameter to ensure a smooth transition of nominal stress from the load point onto the face of the through brace. This satisfied the requirement of Saint Venant's principle having a nominal stress applied on the lap brace. Furthermore, the length of the lap brace was designed to prevent buckling before member squash load according to buckling curves highlighted by Wardenier (1982).

Based on the formulation $\gamma_C \cdot \beta_{CT} / \tau_{CT}$, the through brace radius-to-wall thickness ratio (γ_T) of the joint was set in the range of 5 to 100. Generally speaking, the structural circular hollow sections of tubular structures could have radius-to-thickness (γ) ratio less than 30. However, γ in the range of 30 to 50 were still considered acceptable if the bucking resistance of the section was within the allowable limit. It was important to note that γ was one of the most important geometrical parameters used for the design of completely overlapped tubular joints to achieve the cost saving.

5.2.2 Modelling of welds

The weld elements were not included in the FE model as the joint model without the welds yielded conservative results with small discrepancy in comparison with the experimental values (see Fig. 4.8).

5.2.3 Loading and boundary conditions

The load applied and the boundary conditions of the joint are depicted in Fig. 5.1. The load condition was unbalanced with the joint subjected to lap brace axial compression. For partially overlapped tubular joints under balanced axial loading, the tension loaded lap brace and the compression loaded through brace yielded the lowest ultimate capacity. On the contrary, for joints with complete overlap of braces, the compression loaded lap brace and the tension loaded through brace gave the lowest ultimate load with the failure behaviour similar to simple Y-joint (Gho 2001). Thus, in the current parametric study of the joint with complete overlap of braces, the compression loaded lap brace was considered to yield the lowest ultimate

capacity among all the load cases. In the FE analysis, the incremental compressive load was applied at the end of the lap brace under displacement control mode.

In the actual offshore structures, the end conditions of members was generally between pinned and fixed. It had been shown from the FE analysis that the boundary conditions of the chord and the through brace had insignificant impact on the ultimate strength of the completely overlapped tubular joint. The applied load was predominately transferred between the lap brace and the through brace through truss action. In the current parametric study, it was assumed that both ends of the chord were fixed and the end of the through brace was pinned.

5.2.4 Material post yield properties

The completely overlapped tubular joint specimen was fabricated from the steel pipe of API Grade B. The average Young's modulus, the yield stress and the ultimate tensile stress obtained from the tensile coupon tests were 197kN/mm^2, 355N/mm^2 and 458N/mm^2, respectively. The Poisson's ratio of the steel material was assumed as 0.28. The material post yield property was input as a multi-linear relationship of the true stress and the logarithm strain. For the joint specimen, the yield strength of the steel material was found 78% of the ultimate tensile strength, which was greater than the minimum requirement of 67%. The geometrical and the material properties of the joint specimen satisfied the requirement in API RP2A (2000).

5.3 Failure criteria of joint under axial compression

In the analysis, the lowest load among the three failure criteria was defined as the ultimate capacity of completely overlapped tubular joints under lap brace axial compression. These criteria were,

(i) First peak load of load - displacement curve

The first peak load of the applied load - lap brace end axial displacement

curve was the most important basic criterion to determine the joint strength as it usually yielded the lowest ultimate capacity among the failure criteria. The failure mode of the joint was associated with the yielding, local buckling and plastic deformation of through brace member.

(ii) Yura et al's excessive deformation limit

The excessive deformation limit ($\Delta = 60\sigma_y \cdot d_L/E$) proposed by Yura et al (1980) was commonly used to determine the ultimate strength of tubular joints isolated from a frame. This limit was specifically considered for brace load - displacement response which did not exhibit any sign of peak load. It did not serve as a serviceability limit but reflected as a joint strength in the frame collapse. It should be noted that the applied load and the second-order effect of the joint at very large deflections in isolated tests probably could not reflect conditions during the collapse of a frame (Zettlemoyer 1988).

(iii) Lap brace member squash load

The structural member yielded prior to joint collapse if the ultimate strength of the joint was stronger than that of member. In such a situation, the ultimate load of the joint was determined based on the material yield strength of member defined as $\sigma_y \cdot A$, where σ_y and A were the yield stress and the cross-sectional area of member respectively. For the completely overlapped tubular joint, the bearing failure of the lap brace due to material yielding could be occurred.

5.4 Influence of geometrical parameters

5.4.1 Failure mechanisms

The type of failure modes for joints with complete overlap of braces under lap brace axial compression was mainly dependent upon its geometrical properties. The failure modes of completely overlapped tubular joint observed in the current numerical investigation is summarized in Tables 5.1 to 5.3. Generally speaking, the

failure of the joints with complete overlap of braces under lap brace axial compression could be categorised as follows.

(i) Mode 1: Through brace wall plastification (TBWP)

This is the most common type of failure modes in the FE analysis of the completely overlapped tubular joint which is also observed in the current experimental study with detail as shown in Fig. 5.2. The failure of the joint was governed by the localized plastic bending of the through brace face in contact with the lap brace. The failure was associated with high shear deformation and high plastic strains at the joint intersection area of the through brace and the lap brace under lap brace axial compression. It was first initiated at the through brace saddle and propagated towards the crown toe and heel as the brace load increased. The ovalisation of the through brace at the vicinity of joint intersection with the lap brace and the short segment of the through brace joining the chord was specifically noted.

(ii) Mode 2: Lap brace yielding (LBY)

This failure mode was first observed on the lap brace joining the through brace with the applied stress exceeded the yield stress of steel material. The failure was subsequently extended and caused the through brace yielding as the applied load increased. It is noticed that the rate of plastic zone formation on the through brace face is faster than that of the lap brace as shown in Fig. 5.3.

(iii) Mode 3: Lap brace local buckling (LBLB)

The premature failure of the lap brace prior to completely collapse of the joint were generally not accepted in the current design practice. However, the brace local buckling was considered a valid and a common type of failure mode for partially overlapped joints. This failure mode was also observed for completely overlapped tubular joints under lap brace axial compression. The stability of the lap brace wall was strongly correlated with the axial compressive stress on the member. The failure mode of lap brace

local buckling is found similar to that of lap brace yielding in Mode 2 except that the failure is associated with the localised buckling due to axial compressive stress on the member which occurs at the crown toe of the joint as shown in Fig. 5.4.

(iv) Mode 4: Lap brace member failure (LBMF)

This type of failure mode occurs for joints with ultimate capacity greater than flexure capacity of lap brace member as shown in Fig. 5.5. In other word, the lap brace member collapsed due to overall bending prior to joint failure. Thus, the failure mode was considered as member failure associated with high stress distribution. The joint could be commented to attain 100% strength efficiency with failure on the member instead the joint. In this failure mode, the joint was resisted by the membrane action of shear more than the bending at the through brace face in contact with the lap brace. The through brace saddle near the lap brace acted as firm support to resist the compressive load which was similar to the behaviour of axially loaded column.

Apart from the four failure modes described above, a combination of these failure modes for joints with complete overlap of braces could be occurred depending on the material and the geometrical properties of the joint.

5.4.2 Effect of through brace-to-chord diameter ratio, β_{CT}

The distribution of failure modes of the completely overlapped tubular joints with respect to the parameter β_{CT} is shown in Fig. 5.6. It could be seen from the figure that the number of joints failed by through brace wall plastification increased whilst the joints failed by lap brace member failure decreased with increasing β_{CT}. However, it was noted that this change of failure mode distribution was small. Furthermore, the parameter γ_T also increased with increasing β_{CT} with other geometrical parameters remained constant. The change of failure modes from the lap brace member failure to the through brace wall plastification with increasing β_{CT}

could be due to increasing γ_T. It could therefore be concluded that the parameter β_{CT} showed insignificant effect on the failure modes of the joints under lap brace axial compression.

5.4.3 Effect of through brace-to-chord wall thickness ratio, τ_{CT}

The distribution of failure modes of the completely overlapped tubular joints with respect to the parameter τ_{CT} is shown in Fig. 5.7. In contrast with the effect of β_{CT} described in Section 5.4.2, the number of joints failed by through brace wall plastification decreased whilst the joints failed by lap brace member failure increased with increasing τ_{CT}. The decreasing parameter γ_T with increasing τ_{CT} mainly resulted in the change of failure modes. It could therefore be concluded that the parameter τ_{CT} showed insignificant effect on the failure modes of the joints under lap brace axial compression.

5.4.4 Effect of chord radius-to-wall thickness ratio, γ_C

The failure modes of the completely overlapped tubular joints with varying γ_C for different cases of γ_T are shown in Fig. 5.8. The distribution of failure modes under constant γ_T was found identical for joints with different γ_C. Thus, the parameter γ_C was commented to have insignificant effect on the failure modes of the joints under lap brace axial compression. It was noted with increasing γ_T that the failure modes of the joint changed from the lap brace member failure to the though brace wall plastification.

5.4.5 Effect of lap brace-to-through brace diameter ratio, β_{TL}

The distribution of failure modes of the completely overlapped tubular joints with respect to the parameter β_{TL} is shown in Fig. 5.9. The parameter β_{TL} showed significant impact on the failure mode of the joint by lap brace local buckling. The possible joint failure by lap brace local buckling increased with increasing β_{TL}.

However, the lap brace local buckling was not a common failure mode for the completely overlapped tubular joint.

5.4.6 Effect of lap brace-to-through brace wall thickness ratio, τ_{TL}

The distribution of failure modes of the completely overlapped tubular joints with respect to the parameter τ_{TL} is shown in Fig. 5.10. The parameter τ_{TL} played a crucial role in the failure mechanism of the joint under lap brace axial compression. For the joints with high τ_{TL}, the failure mode mainly associated with through brace wall plastification or in combination with lap brace yielding. More than 98% and 66% of the joints at τ_{TL} =1.0 and 0.7 respectively failed by through brace wall plastification in the region in contact with the lap brace. For the joints at τ_{TL} = 1.0, there was no lap brace member failure. The failure mode of the joint changed from the through brace wall plastification to the lap brace member failure with decreasing τ_{TL}. 65% of the joints at τ_{TL} = 0.4 attaining 100% efficiency. Only 13% of the joints at τ_{TL} = 0.4 failed by through brace wall plastification in combined with lap brace yielding. It was noted that the through brace wall plastification failure was not observed but the lap brace local buckling was the dominant failure mode for 14% of the joints at τ_{TL} = 0.4. However, the lap brace local buckling did not occur for the joints with medium and high τ_{TL} (= 0.7 and 1.0).

5.4.7 Effect of through brace radius-to-wall thickness ratio, γ_T

The distribution of failure modes of the completely overlapped tubular joints with respect to the parameter γ_T is shown in Fig. 5.11. Apart from the parameter τ_{TL}, γ_T was also considered a crucial parameter influencing the failure mechanism. For the joints with high γ_T, the failure occurred at the joint intersection in the region in contact with the lap brace. On the other hand, for the joints with low γ_T, the lap brace member failed. It was noted at γ_T = 34 that about 67% of the joints failed by through brace wall plastification. The lap brace member failure was not observed. For the joints at low γ_T = 5, 67% and 22% of the joints failed by lap brace member

failure and through brace wall plastification respectively. The lap brace local buckling occurred for the joints with high γ_T. More than 22% of the joints at $\gamma_T = 57$ failed by lap brace local buckling. However, the lap brace local buckling was not observed for the joints at $\gamma_T = 5$ and 14.

5.4.8 Effect of gap size parameter, ξ

The distribution of failure modes of the completely overlapped tubular joints with respect to the parameter ξ is shown in Fig. 5.12. It was important to realise that the possible lap brace failure increased with decreasing gap size. At small gap size, the chord wall acted as a diaphragm restraining the through brace from ovalisation. Thus, the bending stiffness of the short segment of through brace joining the chord enhanced and so did the joint capacity. As a result, the lap brace member failed prior to joint failure. However, the strengthening effect due to chord wall support reduced and so the joint capacity as the gap size increased. At sufficiently large gap size, the behaviour of the joint was similar to that of simple T/Y-joint and the plastic failure at joint intersection became the most common failure mode. It should also be noted that the possible lap brace local buckling reduced with increasing gap size.

5.4.9 Effect of brace angle, θ

The distribution of failure modes of the completely overlapped tubular joints with respect to brace angle (θ) between the lap brace and the through brace is shown in Fig. 5.13. The possible lap brace failure increased with decreasing θ whilst the lap brace remained in vertical position. In the current study of the completely overlapped tubular joints, the number of joint failure associated with the lap brace member for the joints with brace angle of 30^0 was about two and three times the joints with that of 45^0 and 60^0, respectively.

5.4.10 Interactive effect of geometrical parameters

From the above analysis of geometrical parameters of the joints, the parameters β_{CT},

τ_{CT} and γ_C showed insignificant effects whilst the parameters τ_{TL} and γ_T played crucial roles on the failure behaviour of completely overlapped tubular joints. The interactive effect of the parameters τ_{TL} and γ_T for the joints with brace angle of 60^0 at two different gap sizes is shown in Fig. 5.14. The through brace wall plastification in the region in contact with the lap brace or combined with the lap brace yielding was found most prominent for the joints with high τ_{TL} (=1.0 or 0.7) and low γ_T. However, the joints with low τ_{TL} (=0.4) was not failed by the through brace wall plastification. The failure mode of the joints with low τ_{TL} and high γ_T was due to yielding and buckling of the lap brace. In the current parametric study, 84 out of 3888 FE joint models failed by lap brace local buckling. All these joints were associated with high γ_T (>30), low τ_{TL} (= 0.4) and high β_{TL} (= 0.8 and 0.6). Most of the joints with low τ_{TL} (=0.4) and large γ_T (>30) failed by lap brace yielding or local buckling combined with through brace wall plastification.

For the joints at τ_{TL} = 0.4 and γ_T between 20 and 30, the overall buckling failure of the lap brace occurred at β_{TL} = 0.8. For partially overlapped joints, the brace local buckling occurred at joint intersection owing to the load transfer mechanism between the braces and the chord. For joints with complete overlap of braces, the brace local buckling occurred at small gap size (ξ). It was noted in the current parametric study that no local buckling failure occurred for joints with large gap sizes at ξ = 2.0. The failure modes of the joint with complete overlap of braces changed from the lap brace local buckling to the through brace face plastification with increasing ξ.

5.5 Load - displacement characteristics

In the current parametric study, the failure mode of the joints with complete overlap of braces was also assessed based on load - displacement curves. Some typical load - displacement curves of the joints under lap brace axial compression were illustrated. However, it should be noted that the axial load and the corresponding displacement of the joint were applied at the end of the lap brace. Three failure criteria previously described in Section 5.3 were used as a guide to determine the

ultimate capacity of the completely overlapped tubular joints.

The curves showing the typical failure modes of the joints with the through brace wall plastification are depicted in Fig. 5.15. This failure mode was associated with the first peak load and Yura et al's excessive deformation limit failure criteria. It should be noted that significant post peak reserve capacity of the joint was obtained for this type of failure mode. This behaviour was attributed to the excessive plastic deformation on the through brace face in contact with the lap brace of the joint.

There were two different types of load - displacement curves describing the failure of lap brace member as shown in Fig. 5.16. The joints with minimum gap size (g = 51mm), low τ_{TL} (= 0.4) and low γ_T (< 12) exhibits approximately bilinear curves prior to Yura et al's excessive deformation limit as depicted in Figs. 5.16(a) and (b). A high stress contour which was greater than the material yield stress of the lap brace was specifically noted. The ultimate capacity of the joints was defined as the strength of the lap brace acted as an axially loaded column.

From Figs. 5.16(c) and (d), it is noted in the load - displacement curves that sharp fall of load is observed for the joints with γ_T greater than 12. Some of the joints at γ_T =12 exhibit sudden drop of load at the later stages of load history but this was limited to the joints with large β_{TL} and gap size (Fig. 5.16(f)). The failure modes of the joints with this type of load - displacement curve involved the global buckling and the collapse of lap brace member after the ultimate load. However, there was no failure on the through brace and the chord member. The first peak load of the joint was almost equivalent to the yield strength of the lap brace. The comparison of the curves as shown in Figs. 5.16(c) and (d) indicated that the failure mode of the joint changes from the lap brace member to the through brace wall yielding with increasing gap size. It could therefore be commented from the comparison of the failure behaviour that the buckling failure of the lap brace for the joints with complete overlap of braces could be avoided with increasing gap size on the through brace face between the outer faces of the chord and the lap brace.

The joints failed by lap brace local buckling also exhibit sudden fall of load in the load - displacement curve as shown in Fig. 5.17(a). The peak load occurred at low displacement. There was no failure on the through brace member throughout the load history. The sudden failure of the lap brace member occurred at high displacement with decreasing β_{TL}. The failure of these joints was mainly due to combined through brace wall plastification and lap brace local buckling. It could be seen from Fig. 5.17(b) that the joints at β_{TL} = 0.6 show similar load - displacement behaviour prior to load shedding with those failed by through brace wall plastification.

5.6 Discussions

For axially loaded simple gap K-joint with small gap size between braces, the chord wall plastificaton due to compression-loaded brace and the crack initiation by rupture of the tension-loaded brace were the most common failure mode. However, this type of joints behaved as two independent Y-joints at large gap size.

For partially overlapped K-joints, the failure modes were attributed to the interactive effect of geometric parameters β, γ, τ and amount of overlap. The general failure mode of this type of joints was found to be chord wall plastification, brace local buckling of compression-loaded brace or the combination of these failure behaviours. However, for the joints with more than 100% overlap of braces under balanced axial load cases, the chord wall plastification would not occur as most of the load was directly transferred between the braces. Cracking of the gap region around the tensioned-loaded brace was the most common failure mode.

It should be noted that cracking did not occur in the current study of completely overlapped joints as the joint was only loaded by lap brace axial compression. The failure mechanism of the completely overlapped tubular joint was similar to that of simple Y-joint but not partially overlapped K-joint. However, the lap brace member could be failed at member squash load or local buckling prior to the joint strength at small gap size.

5.7 Concluding remarks

From the results of the parametric study, the failure modes of the tubular joints with complete overlap of braces under lap brace axial compression can be characterised as the through brace wall plastification, the lap brace yielding, the lap brace local buckling and the lap brace member failure. A combination of these failure modes can be occurred depending on the geometrical parameters of the joint. However, the through brace wall plastification is found the most common type of failure mode for joints with high through brace-to-lap brace wall thickness ratio (τ_{TL}). The load - displacement behaviour indicated that significant post peak reserve capacity of the completely overlapped joint is obtained. This type of failure mode of the joint is associated with the first peak load and the Yura et al's excessive deformation limit failure criteria.

The lap brace failure mainly occurs for the joints with low τ_{TL}, low through brace radius-to-thickness ratio (γ_T), small gap size parameter (ξ) and small brace angle (θ). The lap brace yielding and localised buckling combined with the through brace wall plastification is the most prominent failure for the joints with high γ_T and lap brace-to-through brace diameter ratio (β_{TL}) but with low τ_{TL} and ξ. The lap brace local buckling failure only occurs for the joints with small τ_{TL} and large β_{TL}. The joints failed by the lap brace local buckling exhibits sudden fall of load in the load - displacement curve with the peak load occurs at low displacement. Overall, τ_{TL}, γ_T, ξ and θ are the most crucial geometrical parameters controlling the failure behaviour of the completely overlapped tubular joints.

Table 5.1 Failure modes of joints with $\theta = 60^0$

Failure modes	β_{TL}		0.4								0.6								0.8							
	τ_{TL}		0.4				0.7				1.0				0.4				0.7				1.0			
β_{CT}	γ_C	τ_{CT} \ ξ	0.2	0.5	1.0	2.0	0.2	0.5	1.0	2.0	0.2	0.5	1.0	2.0	0.2	0.5	1.0	2.0	0.2	0.5	1.0	2.0	0.2	0.5	1.0	2.0
0.4	12	0.4	4	4	4,1	4,1	4,1	1	1	1	1	1	1	1	4	4	4	4	4,1	1	1	2	1	1	1	1	4	4	4	4	4,1	1	1	1	1	1	1	1
		0.7	4	4	4	4	4	4,1	4,1	4,1	1	1	1	1	4	4	4	4	4	4,1	4,1	4,1	1	1	1	1	4	4	4	4	4	4,1	4,1	4,1	1	1	1	1
		1.0	4	4	4	4	4	4	4,1	4,1	1	1	1	1	4	4	4	4	4	4	4	4,1	1	1	1	1	4	4	4	4	4	4	4,1	4,1	1	1	1	1
	20	0.4	2	2	2	2	1	1	1	1	1	1	1	1	4	2	2	2	1	1	1	1	1	1	1	1	4	4	2	4,1	1	1	1	1	1	1	1	1
		0.7	4	4	4,1	4,1	4,1	4,1	1	1	1	1	1	1	4	4	4	4	4,1	4,1	1	1	1	1	1	1	4	4	4	4	4,1	4,1	1	1	1	1	1	1
		1.0	4	4	4	4,1	4,1	4,1	4,1	4,1	1	1	1	1	4	4	4,1	4,1	4,1	4,1	4,1	4,1	1	1	1	1	4	4	4	4	4,1	4,1	4,1	4,1	1	1	1	1
	30	0.4	2	2	2	2	1	1	1	1	1	1	1	1	2	2	2	2	1	1	1	1	1	1	1	1	4	2	2	2	1	1	1	1	1	1	1	1
		0.7	4,1	2	2	2	1	1	1	1	1	1	1	1	4	4,1	2	2	1	1	1	1	1	1	1	1	4	4	4,1	4,1	2	1	1	1	1	1	1	1
		1.0	4	4	4,1	2	4,1	1	1	1	1	1	1	1	4	4	4,1	2	4,1	1	1	1	1	1	1	1	4	4	4	4,1	4,1	1	1	1	1	1	1	1
	50	0.4	2	2	2	2	1	1	1	1	1	1	1	1	1,3	2	2	2	1	1	1	1	1	1	1	1	3	3	2	2	1	1	1	1	1	1	1	1
		0.7	2	2	2	2	1	1	1	1	1	1	1	1	2	2	2	2	1	1	1	1	1	1	1	1	4	2	2	2	2	1	1	1	1	1	1	1
		1.0	2	2	2	2	1	1	1	1	1	1	1	1	4	2	2	2	1	1	1	1	1	1	1	1	4	2	2	2	1	1	1	1	1	1	1	1
0.6	12	0.4	4	4,1	2	2	1	1	1	1	1	1	1	1	4	2	2	2	1	1	1	1	1	1	1	1	4	4,1	2	2	1	1	1	1	1	1	1	1
		0.7	4	4	4	4,1	4,1	4,1	1	1	1	1	1	1	4	4	4,1	4,1	4,1	4,1	1	1	1	1	1	1	4	4	4	4,1	4,1	4,1	1	1	1	1	1	1
		1.0	4	4	4	4	4,1	4,1	4,1	4,1	1	1	1	1	4	4	4	4,1	4	4,1	4,1	4,1	1	1	1	1	4	4	4	4,1	4	4,1	4,1	4,1	1	1	1	1
	20	0.4	2	2	2	2	1	1	1	1	1	1	1	1	2	2	2	2	1	1	1	1	1	1	1	1	4	2	2	2	1	1	1	1	1	1	1	1
		0.7	4	2	2	2	1	1	1	1	1	1	1	1	4	2	2	2	1	1	1	1	1	1	1	1	4	4	2	2	1	1	1	1	1	1	1	1
		1.0	4	4	4,1	2	4,1	1	1	1	1	1	1	1	4	4	4,1	4,1	4,1	1	1	1	1	1	1	1	4	4	4,1	4,1	4,1	1	1	1	1	1	1	1
	30	0.4	2	2	2	2	1	1	1	1	1	1	1	1	1,3	2	2	2	1	1	1	1	1	1	1	1	3	3	2	2	1	1	1	1	1	1	1	1
		0.7	2	2	2	2	1	1	1	1	1	1	1	1	2	2	2	2	1	1	1	1	1	1	1	1	4	2	2	2	1	1	1	1	1	1	1	1
		1.0	4	2	2	2	1	1	1	1	1	1	1	1	4	2	2	2	1	1	1	1	1	1	1	1	4	4,1	2	2	1	1	1	1	1	1	1	1
	50	0.4	2	2	2	2	1	1	1	1	1	1	1	1	1,3	2	2	2	1	1	1	1	1	1	1	1	3	3	2	2	1	1	1	1	1	1	1	1
		0.7	2	2	2	2	1	1	1	1	1	1	1	1	1,3	2	2	2	1	1	1	1	1	1	1	1	3	2	2	2	1	1	1	1	1	1	1	1
		1.0	2	2	2	2	1	1	1	1	1	1	1	1	2	2	2	2	1	1	1	1	1	1	1	1	4	2	2	2	1	1	1	1	1	1	1	1
0.8	12	0.4	2	2	2	2	1	1	1	1	1	1	1	1	4,1	2	2	2	1	1	1	1	1	1	1	1	4	2	2	2	1	1	1	1	1	1	1	1
		0.7	4	4,1	2	2	2	1	1	1	1	1	1	1	4	4	4,1	2	2	1	1	1	1	1	1	1	4	4	4,1	4,1	2	1	1	1	1	1	1	1
		1.0	4	4	4	4,1	4,1	4,1	1	1	1	1	1	1	4	4	4	4,1	4,1	4,1	1	1	1	1	1	1	4	4	4	4,1	4,1	4,1	1	1	1	1	1	1
	20	0.4	2	2	2	2	1	1	1	1	1	1	1	1	1,3	2	2	2	1	1	1	1	1	1	1	1	3	2	2	2	1	1	1	1	1	1	1	1
		0.7	2	2	2	2	1	1	1	1	1	1	1	1	4,1	2	2	2	1	1	1	1	1	1	1	1	4	2	2	2	1	1	1	1	1	1	1	1
		1.0	4	2	2	2	1	1	1	1	1	1	1	1	4	2	2	2	1	1	1	1	1	1	1	1	4	4	4,1	2	1	1	1	1	1	1	1	1
	30	0.4	2	2	2	2	1	1	1	1	1	1	1	1	1,3	2	2	2	1	1	1	1	1	1	1	1	3	3	2	2	1	1	1	1	1	1	1	1
		0.7	2	2	2	2	1	1	1	1	1	1	1	1	1,3	2	2	2	1	1	1	1	1	1	1	1	3	2	2	2	1	1	1	1	1	1	1	1
		1.0	2	2	2	2	1	1	1	1	1	1	1	1	4,1	2	2	2	1	1	1	1	1	1	1	1	4	2	2	2	1	1	1	1	1	1	1	1
	50	0.4	2	2	2	2	1	1	1	1	1	1	1	1	1,3	2	2	2	1	1	1	1	1	1	1	1	3	3	2	2	1,3	1	1	1	1	1	1	1
		0.7	2	2	2	2	1	1	1	1	1	1	1	1	1,3	2	2	2	1	1	1	1	1	1	1	1	3	3	2	2	1	1	1	1	1	1	1	1
		1.0	2	2	2	2	1	1	1	1	1	1	1	1	1,3	2	2	2	1	1	1	1	1	1	1	1	3	3	2	2	1	1	1	1	1	1	1	1

Note: 1=Through brace wall plastification; 2=Combination of through brace wall plastification with lap brace yielding; 3=Lap brace local buckling; 4=Lap brace member failure

Table 5.2 Failure modes of joints with $\theta = 45^0$

Failure modes	β_{TL}		0.4												0.6												0.8											
	τ_{TL}		0.4				0.7				1.0				0.4				0.7				1.0				0.4				0.7				1.0			
β_{CT}	γ_C	τ_{CT} \ ξ	0.2	0.5	1.0	2.0	0.2	0.5	1.0	2.0	0.2	0.5	1.0	2.0	0.2	0.5	1.0	2.0	0.2	0.5	1.0	2.0	0.2	0.5	1.0	2.0	0.2	0.5	1.0	2.0	0.2	0.5	1.0	2.0	0.2	0.5	1.0	2.0
0.4	12	0.4	4	4	4	4	4,1	1	1	1	1	1	1	1	4	4	4	4	4,1	1	1	2	1	1	1	1	4	4	4	4	4,1	1	1	1	1	1	1	1
		0.7	4	4	4	4	4	4,1	4,1	4,1	1	1	1	1	4	4	4	4	4	4	4,1	4,1	1	1	1	1	4	4	4	4	4	4,1	4,1	4,1	1	1	1	1
		1.0	4	4	4	4	4	4	4,1	4,1	4,1	1	1	1	4	4	4	4	4	4	4,1	4,1	1	1	1	1	4	4	4	4	4	4	4,1	4,1	1	1	1	1
	20	0.4	4	2	2	2	1	1	1	1	1	1	1	1	4	4	4,1	2	1	1	1	1	1	1	1	1	4	4	4	4,1	1	1	1	1	1	1	1	1
		0.7	4	4	4	4	4,1	4,1	1	1	1	1	1	1	4	4	4	4,1	4	4,1	1	1	1	1	1	1	4	4	4	4,1	4,1	4,1	1	1	1	1	1	1
		1.0	4	4	4	4	4	4,1	4,1	4,1	1	1	1	1	4	4	4	4	4,1	4	4,1	4,1	1	1	1	1	4	4	4	4	4,1	4,1	4,1	4,1	1	1	1	1
	30	0.4	2	2	2	2	1	1	1	1	1	1	1	1	1,3	2	2	2	1	1	1	1	1	1	1	1	4	3	4	4	1	1	1	1	1	1	1	1
		0.7	4	4,1	2	2	1	1	1	1	1	1	1	1	4	4	4,1	4,1	1	1	1	1	1	1	1	1	4	4	4	4,1	2	1	1	1	1	1	1	1
		1.0	4	4	4	4	4,1	1	1	1	1	1	1	1	4	4	4	4,1	4,1	1	1	1	1	1	1	1	4	4	4	4	4,1	1	1	1	1	1	1	1
	50	0.4	2	2	2	2	1	1	1	1	1	1	1	1	1,3	2	2	2	1	1	1	1	1	1	1	1	3	3	3	2	1	1	1	1	1	1	1	1
		0.7	2	2	2	2	1	1	1	1	1	1	1	1	2	2	2	2	1	1	1	1	1	1	1	1	4	4,1	4,1	4,1	2	1	1	1	1	1	1	1
		1.0	4	2	2	2	1	1	1	1	1	1	1	1	4	4,1	4,1	2	1	1	1	1	1	1	1	1	4	4	4,1	4,1	1	1	1	1	1	1	1	1
0.6	12	0.4	4	4,1	2	2	1	1	1	1	1	1	1	1	4	4	4,1	4,1	2	1	1	1	1	1	1	1	4	4	4	4,1	1	1	1	1	1	1	1	1
		0.7	4	4	4	4,1	4	4,1	1	1	1	1	1	1	4	4	4	4,1	4	4,1	1	1	1	1	1	1	4	4	4	4,1	4,1	4,1	1	1	1	1	1	1
		1.0	4	4	4	4	4	4	4,1	4,1	1	1	1	1	4	4	4	4,1	4	4	4,1	4,1	1	1	1	1	4	4	4	4,1	4	4	4,1	4,1	1	1	1	1
	20	0.4	2	2	2	2	1	1	1	1	1	1	1	1	1,3	2	2	4,1	1	1	1	1	1	1	1	1	4	4,1	4	4,1	1	1	1	1	1	1	1	1
		0.7	4	4,1	4,1	4,1	1	1	1	1	1	1	1	1	4	4,1	4,1	2	2	1	1	1	1	1	1	1	4	4	4	4,1	2	1	1	1	1	1	1	1
		1.0	4	4	4,1	4,1	4,1	1	1	1	1	1	1	1	4	4	4,1	4,1	4,1	1	1	1	1	1	1	1	4	4	4	4	4,1	1	1	1	1	1	1	1
	30	0.4	2	2	2	2	1	1	1	1	1	1	1	1	3	2	2	4,1	1	1	1	1	1	1	1	1	3	3	1,3	2	1	1	1	1	1	1	1	1
		0.7	2	2	2	2	1	1	1	1	1	1	1	1	4	2	2	2	1	1	1	1	1	1	1	1	4	4,1	4,1	4,1	1	1	1	1	1	1	1	1
		1.0	4	4,1	2	2	1	1	1	1	1	1	1	1	4	4,1	4,1	2	1	1	1	1	1	1	1	1	4	4	4,1	4,1	2	1	1	1	1	1	1	1
	50	0.4	2	2	2	2	1	1	1	1	1	1	1	1	3	2	2	2	1	1	1	1	1	1	1	1	3	3	1,3	2	1,3	1	1	1	1	1	1	1
		0.7	2	2	2	2	1	1	1	1	1	1	1	1	1,3	2	2	2	1	1	1	1	1	1	1	1	3	3	3	2	1	1	1	1	1	1	1	1
		1.0	2	2	2	2	1	1	1	1	1	1	1	1	1,3	2	2	2	1	1	1	1	1	1	1	1	4	4,1	4,1	4,1	1	1	1	1	1	1	1	1
0.8	12	0.4	4	4,1	2	2	1	1	1	1	1	1	1	1	4	2	2	2	1	1	1	1	1	1	1	1	4	4	4,1	4,1	1	1	1	1	1	1	1	1
		0.7	4	4	4	4	4,1	1	1	1	1	1	1	1	4	4	4	4,1	4,1	1	1	1	1	1	1	1	4	4	4	4,1	2	1	1	1	1	1	1	1
		1.0	4	4	4	4	4,1	4,1	1	1	1	1	1	1	4	4	4	4	4,1	4,1	1	1	1	1	1	1	4	4	4	4,1	4,1	4,1	1	1	1	1	1	1
	20	0.4	2	2	2	2	1	1	1	1	1	1	1	1	1,3	2	2	2	2	1	1	1	1	1	1	1	3	3	3	2	1	1	1	1	1	1	1	1
		0.7	4	2	2	2	1	1	1	1	1	1	1	1	4	2	2	2	1	1	1	1	1	1	1	1	4	4	2	2	1	1	1	1	1	1	1	1
		1.0	4	4	4	2	1	1	1	1	1	1	1	1	4	4	4,1	4,1	1	1	1	1	1	1	1	1	4	4	4	4,1	1	1	1	1	1	1	1	1
	30	0.4	2	2	2	2	1	1	1	1	1	1	1	1	3	2	2	2	2	1	1	1	1	1	1	1	3	3	3	2	2	1	1	1	1	1	1	1
		0.7	4,1	2	2	2	1	1	1	1	1	1	1	1	1,3	2	2	2	1	1	1	1	1	1	1	1	3	3	2	2	1	1	1	1	1	1	1	1
		1.0	4	2	2	2	1	1	1	1	1	1	1	1	4,1	2	2	2	1	1	1	1	1	1	1	1	4	4,1	4,1	2	1	1	1	1	1	1	1	1
	50	0.4	2	2	2	2	1	1	1	1	1	1	1	1	3	2	2	2	1,3	1	1	1	1	1	1	1	3	3	3	2	1,3	1	1	1	1,3	1	1	1
		0.7	1,3	2	2	2	1	1	1	1	1	1	1	1	3	2	2	2	1	1	1	1	1	1	1	1	3	3	2	2	1,3	1	1	1	1	1	1	1
		1.0	2	2	2	2	1	1	1	1	1	1	1	1	3	2	2	2	1	1	1	1	1	1	1	1	1,3	3	2	2	1	1	1	1	1	1	1	1

Note: 1=Through brace wall plastification; 2=Combination of through brace wall plastification with lap brace yielding; 3=Lap brace local buckling; 4=Lap brace member failure

Table 5.3 Failure modes of joints with $\theta = 30^0$

Failure modes		β_{TL}	0.4								0.6								0.8							
		τ_{TL}	0.4				0.7				1.0				0.4				0.7				1.0			
β_{CT}	γ_C	τ_{CT} \ ξ	0.2	0.5	1.0	2.0	0.2	0.5	1.0	2.0	0.2	0.5	1.0	2.0	0.2	0.5	1.0	2.0	0.2	0.5	1.0	2.0	0.2	0.5	1.0	2.0
0.4	12	0.4	4	4	4	4	4	4,1	4,1	4,1	1	1	1	1	4	4	4	4	4	4,1	4,1	4,1	1	1	1	1	4	4	4	4	4	4	4,1	4,1	1	1	1	1
		0.7	4	4	4	4	4	4	4	4,1	4,1	4,1	4,1	4,1	4	4	4	4	4	4	4	4,1	4,1	4	4	4,1	4	4	4	4	4	4	4	4,1	4,1	4	4	4,1
		1.0	4	4	4	4	4	4	4	4	4	4,1	4,1	4,1	4	4	4	4	4	4	4	4,1	4	4,1	4,1	4,1	4	4	4	4	4	4	4	4,1	4	4,1	4,1	1
	20	0.4	4	4	4	4	1	2	1	1	1	1	1	1	4	4	4	4	2	2	1	1	1	1	1	1	4	4	4	4	4,1	2	2	2	1	1	1	1
		0.7	4	4	4	4	4	4	4,1	4,1	1	1	1	1	4	4	4	4	4	4	4,1	4,1	1	1	1	1	4	4	4	4	4	4	4,1	4,1	4,1	1	1	1
		1.0	4	4	4	4	4	4	4,1	4,1	4,1	4	4,1	1	4	4	4	4	4	4	4,1	4,1	4,1	4	1	1	4	4	4	4	4	4	4	4,1	4,1	4,1	4,1	1
	30	0.4	4	4	4,1	4,1	1	1	1	1	1	1	1	1	4	4	4,1	4,1	1	1	1	1	1	1	1	1	4	4	4	4	1	2	2	1	1	1	1	1
		0.7	4	4	4	4	4,1	2	1	1	1	1	1	1	4	4	4	4	4,1	2	1	1	1	1	1	1	4	4	4	4	4	2	2	2	1	1	1	1
		1.0	4	4	4	4	4	4,1	4,1	4,1	1	1	1	1	4	4	4	4	4	4,1	4,1	4,1	1	1	1	1	4	4	4	4	4	4	4,1	4,1	1	1	1	1
	50	0.4	4,1	4,1	4,1	4,1	1	1	1	1	1	1	1	1	4	4,1	4,1	4,1	1	1	1	1	1	1	1	1	3	3	3	1,3	1,3	1	1	1	1	1	1	1
		0.7	4	4	4,1	4,1	1	1	1	1	1	1	1	1	4	4	4,1	4,1	1	1	1	1	1	1	1	1	4	4	4	4	2	2	2	2	1	1	1	1
		1.0	4	4	4	4,1	4,1	1	1	1	1	1	1	1	4	4	4	4	2	2	1	2	1	1	1	1	4	4	4	4	4,1	2	2	2	1	1	1	1
0.6	12	0.4	4	4	4	4	4,1	1	1	1	1	1	1	1	4	4	4	4	4,1	2	2	2	1	1	1	1	4	4	4	4	4,1	4,1	4,1	2	1	1	1	1
		0.7	4	4	4	4	4	4	4,1	4,1	4,1	1	1	1	4	4	4	4	4	4,1	4,1	4,1	4,1	1	1	1	4	4	4	4	4	4	4	4,1	4,1	1	1	1
		1.0	4	4	4	4	4	4	4	4	4,1	4,1	4,1	4,1	4	4	4	4	4	4	4,1	4,1	4,1	4,1	4,1	1	4	4	4	4	4	4	4	4	4,1	4,1	4,1	4,1
	20	0.4	4	4	4,1	4,1	1	1	1	1	1	1	1	1	4	4	4,1	4,1	1	1	1	1	1	1	1	1	4	4	4	4	2	2	2	2	1	1	1	1
		0.7	4	4	4	4	4,1	1	1	1	1	1	1	1	4	4	4	4	4,1	2	2	2	1	1	1	1	4	4	4	4	4	1,3	4,1	2	1	1	1	1
		1.0	4	4	4	4	4	4,1	4,1	4,1	1	1	1	1	4	4	4	4	4	4,1	4,1	2	1	1	1	1	4	4	4	4	4	4,1	4,1	4,1	2	1	1	1
	30	0.4	4	4,1	4,1	4,1	1	1	1	1	1	1	1	1	4	1,3	1,3	1,3	1	1	1	1	1	1	1	1	3	4	4	4,1	1,3	2	1	1	1	1	1	1
		0.7	4	4	4,1	2	1	1	1	1	1	1	1	1	4	4	4	4,1	1	1	1	1	1	1	1	1	4	4	4	4	1,3	4,1	2	2	1	1	1	1
		1.0	4	4	4	4,1	4,1	1	1	1	1	1	1	1	4	4	4	4	4,1	2	2	2	1	1	1	1	4	4	4	4	4	4,1	4,1	4,1	2	1	1	1
	50	0.4	2	2	2	2	1	1	1	1	1	1	1	1	3	3	2	2	1	1	1	1	1	1	1	1	3	3	3	1,3	1,3	1	1	1	1	1	1	1
		0.7	4	2	2	2	1	1	1	1	1	1	1	1	4,1	4,1	4,1	4,1	1	1	1	1	1	1	1	1	3	3	3	4	1,3	1	1	1	1	1	1	1
		1.0	4	4	4,1	4,1	1	1	1	1	1	1	1	1	4	4	4,1	4,1	1	1	1	1	1	1	1	1	4	4	4	4	2	2	2	2	1	1	1	1
0.8	12	0.4	4	4	4	4	2	2	2	1	1	1	1	1	4	4	4	4	1,3	1	1	1	1	1	1	1	4	4	4	4	1,3	2	1	1	1	1	1	1
		0.7	4	4	4	4	4	4,1	4,1	1	1	1	1	1	4	4	4	4	4	4,1	4,1	2	1	1	1	1	4	4	4	4	4	4,1	4,1	4,1	1	1	1	1
		1.0	4	4	4	4	4	4	4	4,1	4,1	1	1	1	4	4	4	4	4	4	4,1	4,1	4,1	1	1	1	4	4	4	4	4	4	4,1	4,1	4	1	1	1
	20	0.4	4	4,1	4,1	4,1	1	1	1	1	1	1	1	1	4	4	4	1,3	2	1	1	1	1	1	1	1	3	3	3	1,3	1,3	1	1	1	1	1	1	1
		0.7	4	4	4	4	2	2	2	1	1	1	1	1	4	4	4	4	1	1	1	1	1	1	1	1	4	4	4	4	1,3	1	1	1	1	1	1	1
		1.0	4	4	4	4	4,1	2	2	2	1	1	1	1	4	4	4	4	4	2	2	2	1	1	1	1	4	4	4	4	4	1	1	1	1	1	1	1
	30	0.4	4,1	1,3	1,3	1,3	1	1	1	1	1	1	1	1	3	3	2	1,3	2	1	1	1	1	1	1	1	3	3	3	1,3	1,3	1	1	1	1	1	1	1
		0.7	4	4,1	4,1	4,1	1	1	1	1	1	1	1	1	4	4,1	4,1	4,1	1	1	1	1	1	1	1	1	3	3	3	1,3	1,3	1	1	1	1	1	1	1
		1.0	4	4	4	4,1	1	1	1	1	1	1	1	1	4	4	4	4,1	1	1	1	1	1	1	1	1	4	4	4	4,1	1,3	1	1	1	1	1	1	1
	50	0.4	1,3	2	2	2	1	1	1	1	1	1	1	1	3	3	1	2	1,3	1	1	1	1	1	1	1	3	3	3	2	1,3	1	1	1	1,3	1	1	1
		0.7	1,3	1,3	1,3	1,3	1	1	1	1	1	1	1	1	3	3	1,3	2	1	1	1	1	1	1	1	1	3	3	3	1,3	1,3	1	1	1	1,3	1	1	1
		1.0	4	4,1	4,1	4,1	1	1	1	1	1	1	1	1	4	4	1,3	1,3	1	1	1	1	1	1	1	1	3	3	3	1,3	1,3	1	1	1	1	1	1	1

Note: 1=Through brace wall plastification; 2=Combination of through brace wall plastification with lap brace yielding; 3=Lap brace local buckling; 4=Lap brace member failure

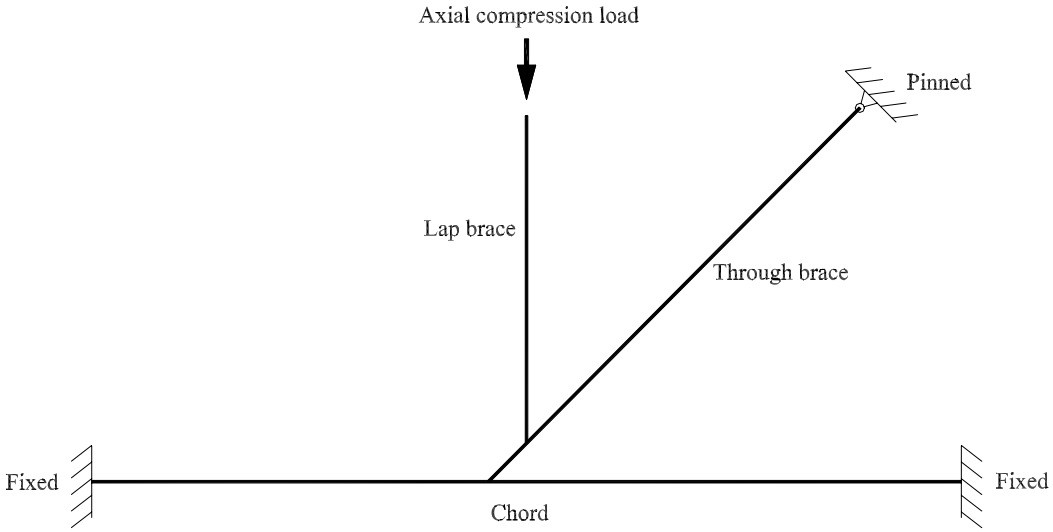

Fig. 5.1 Loading and boundary conditions

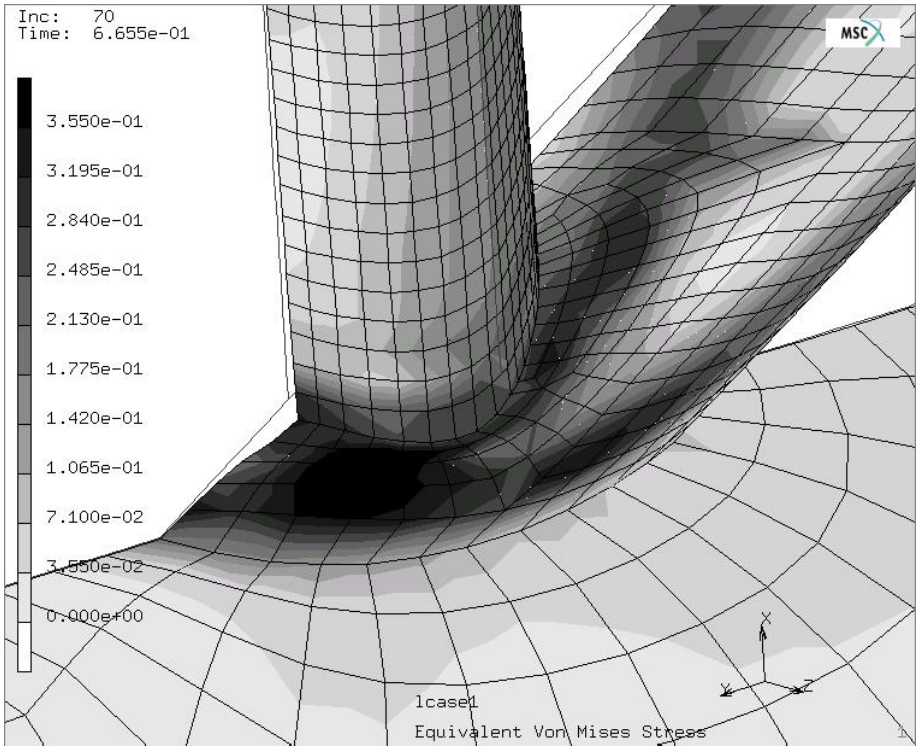

(Constants: $\beta_{CT} = 0.4$, $\beta_{TL} = 0.8$, $\tau_{CT} = 0.4$, $\tau_{TL} = 1.0$, $\gamma_C = 30$, $\xi = 0.5$ and $\theta = 60^0$)

Fig. 5.2 Through brace wall plastification

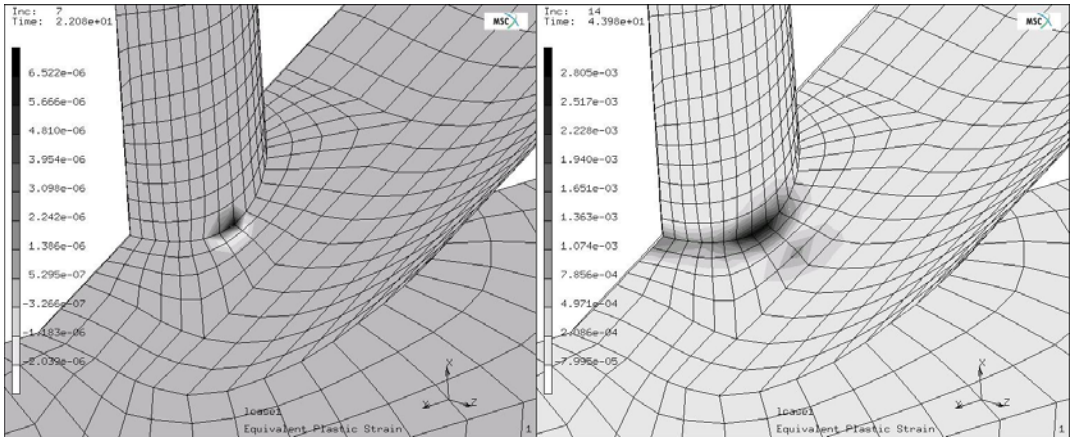

(a) Displacement of 3.14mm (b) Displacement of 6.26mm

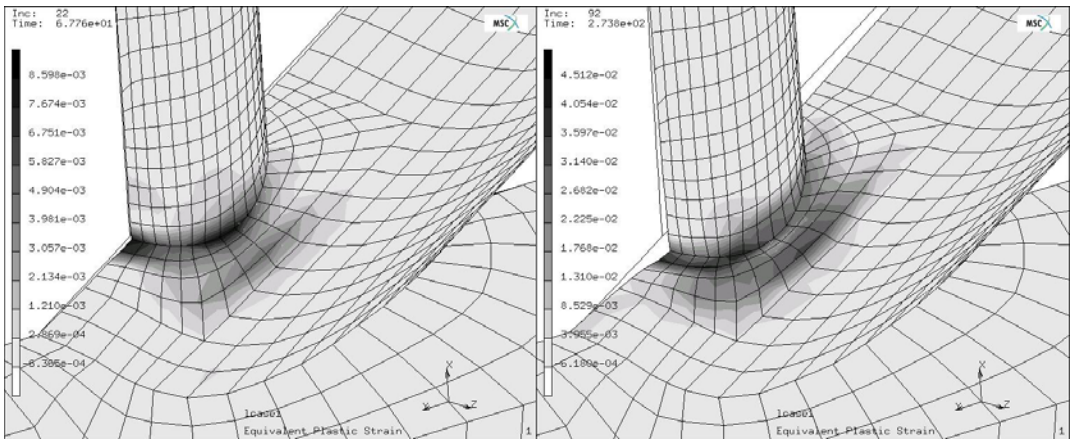

(c) Displacement of 9.65mm (first peak load)

(d) Displacement of 39.3mm (Yura et al.'s deformation limit)

(Constants: $\beta_{CT} = 0.8$, $\beta_{TL} = 0.6$, $\tau_{CT} = 0.7$, $\tau_{TL} = 0.4$, $\gamma_C = 50$, $\xi = 0.5$ and $\theta = 60^0$)

Fig. 5.3 Plastic zone formation for joint with lap brace yielding

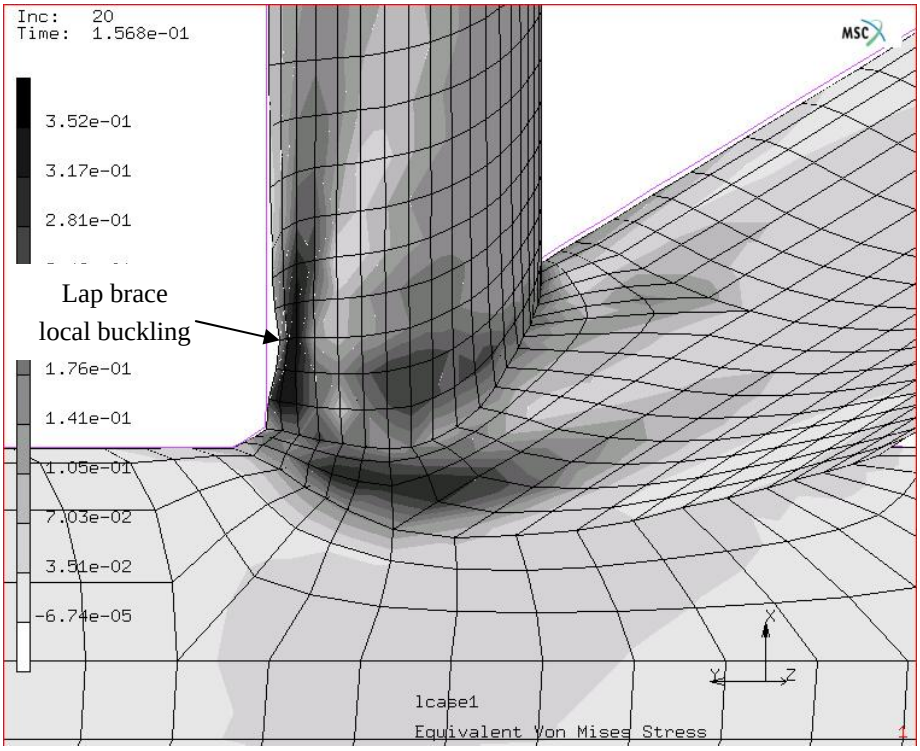

(Constants: $\beta_{CT} = 0.8$, $\beta_{TL} = 0.8$, $\tau_{CT} = 0.4$, $\tau_{TL} = 0.4$, $\gamma_T = 40$, $g = 51$mm and $\theta = 60^0$)

Fig. 5.4 Lap brace local buckling

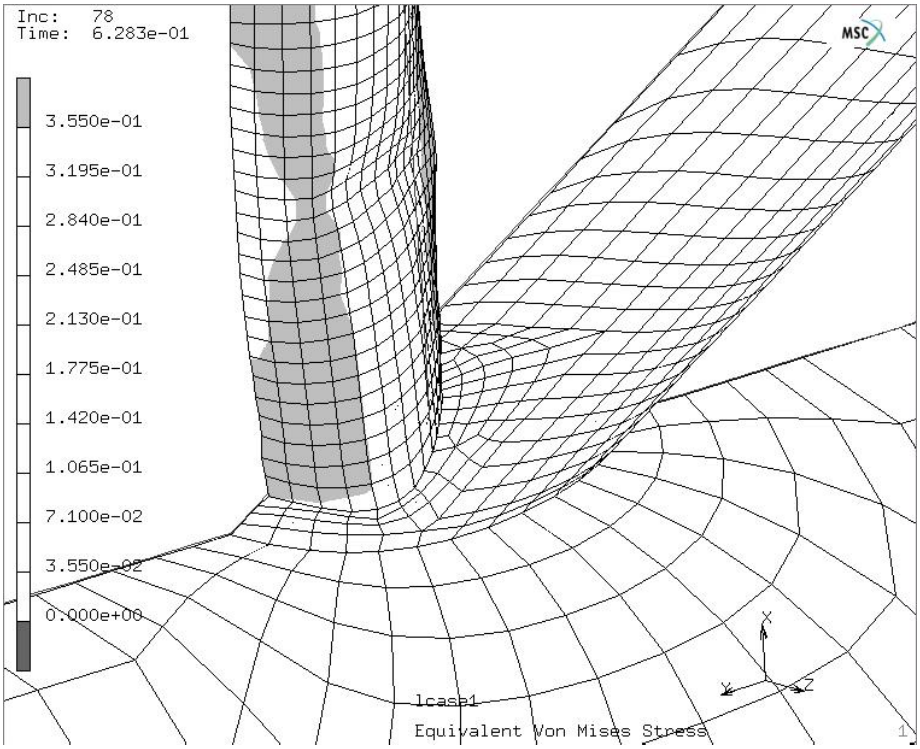

(Constants: $\beta_{CT} = 0.4$, $\beta_{TL} = 0.8$, $\tau_{CT} = 0.4$, $\tau_{TL} = 0.4$, $\gamma_T = 20$, $g = 51$mm and $\theta = 60^0$)

Fig. 5.5 Lap brace member failure

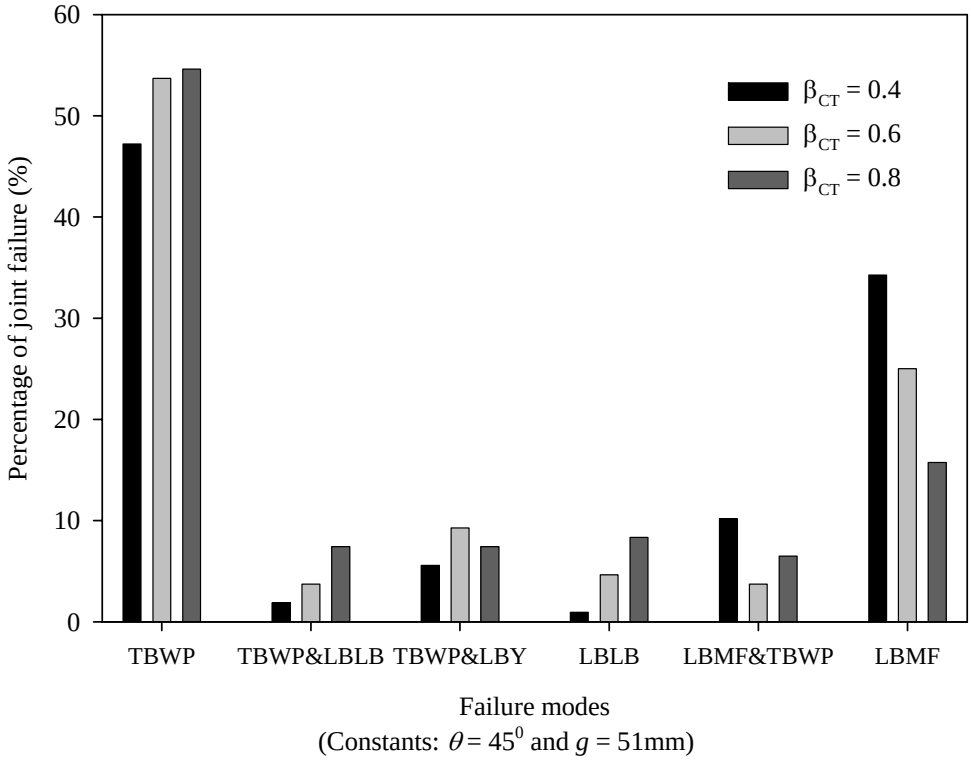

Fig. 5.6 Failure modes (through brace-to-chord diameter ratio, β_{CT})

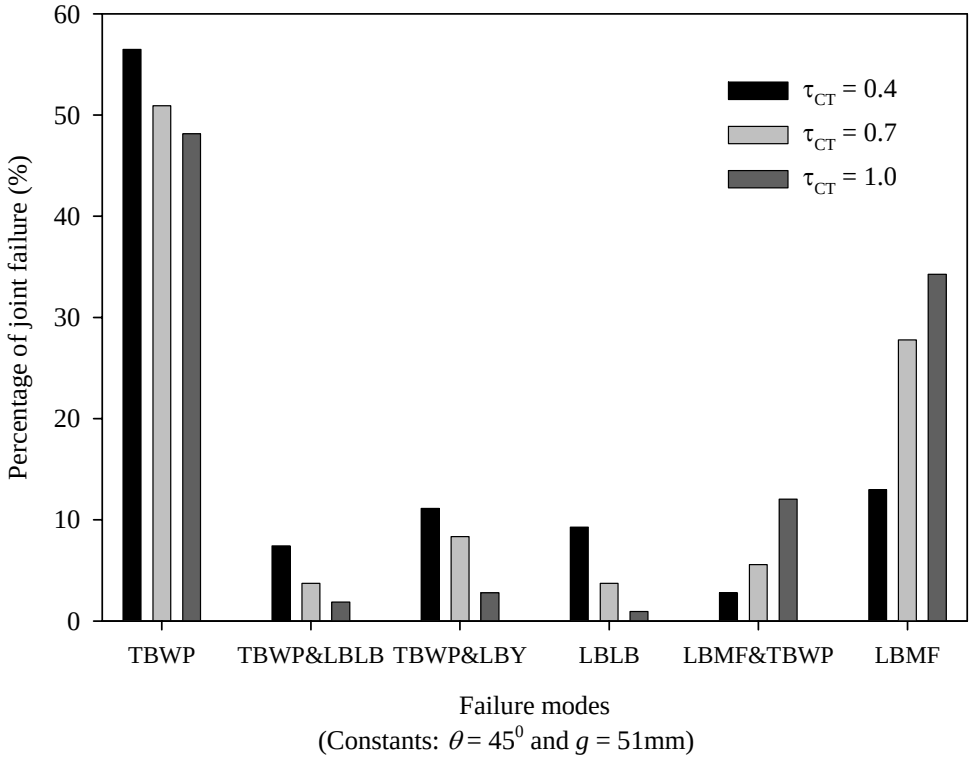

Fig. 5.7 Failure modes (through brace-to-chord wall thickness ratio, τ_{CT})

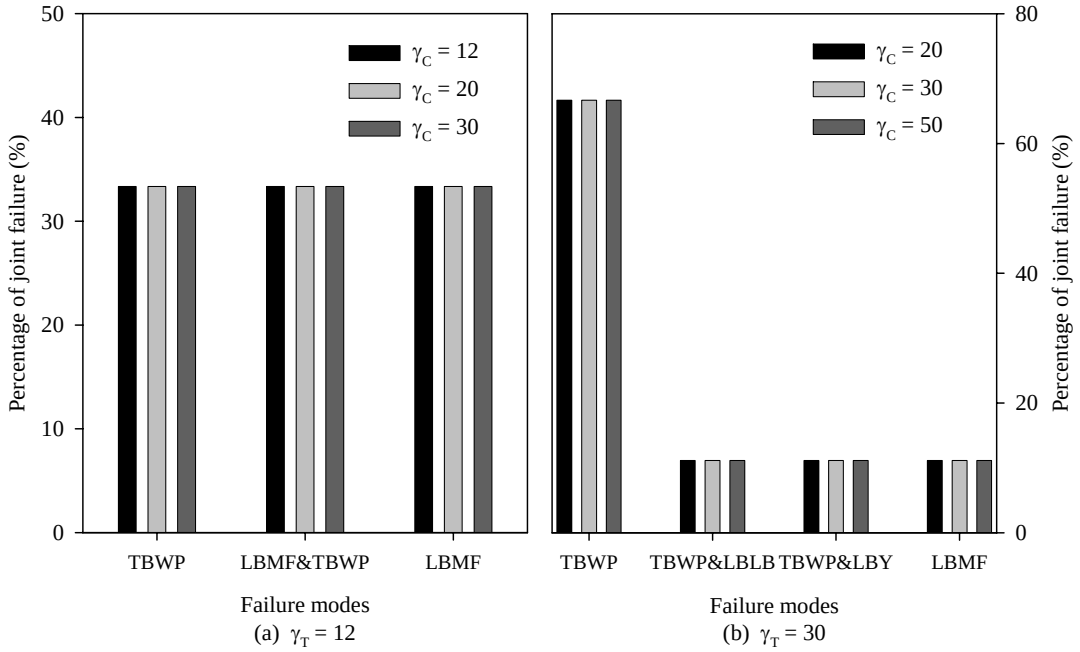

(Constants: $\theta = 45^0$ and g = 51mm)

Fig. 5.8 Failure modes (chord radius-to-wall thickness ratio, γ_C)

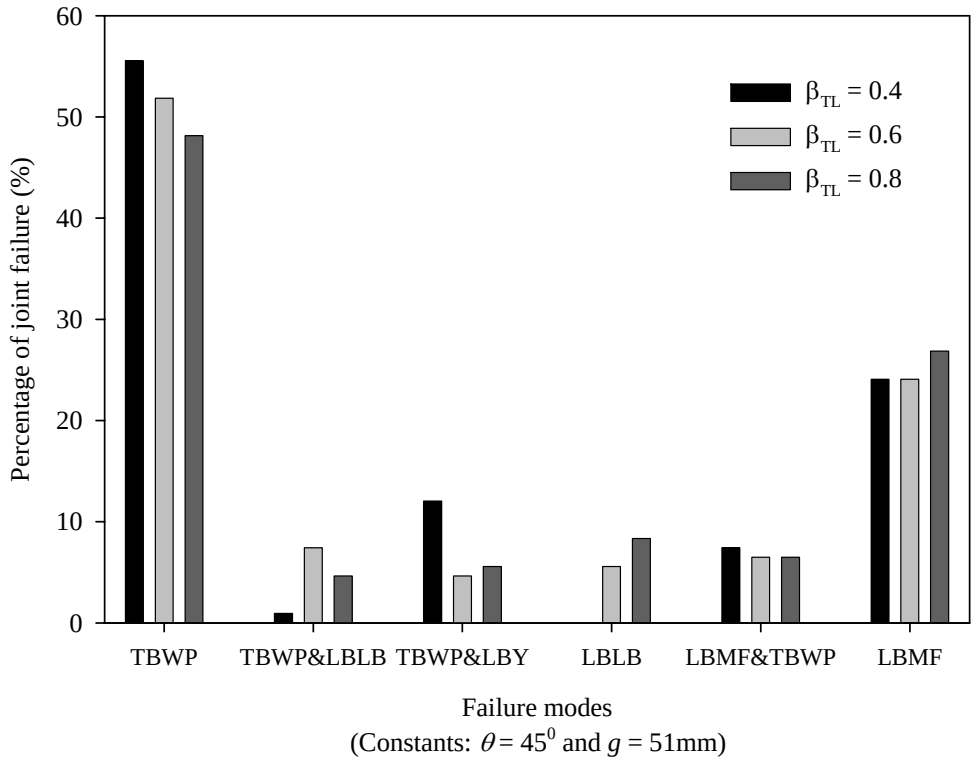

(Constants: $\theta = 45^0$ and g = 51mm)

Fig. 5.9 Failure modes (lap brace-to-through brace diameter ratio, β_{TL})

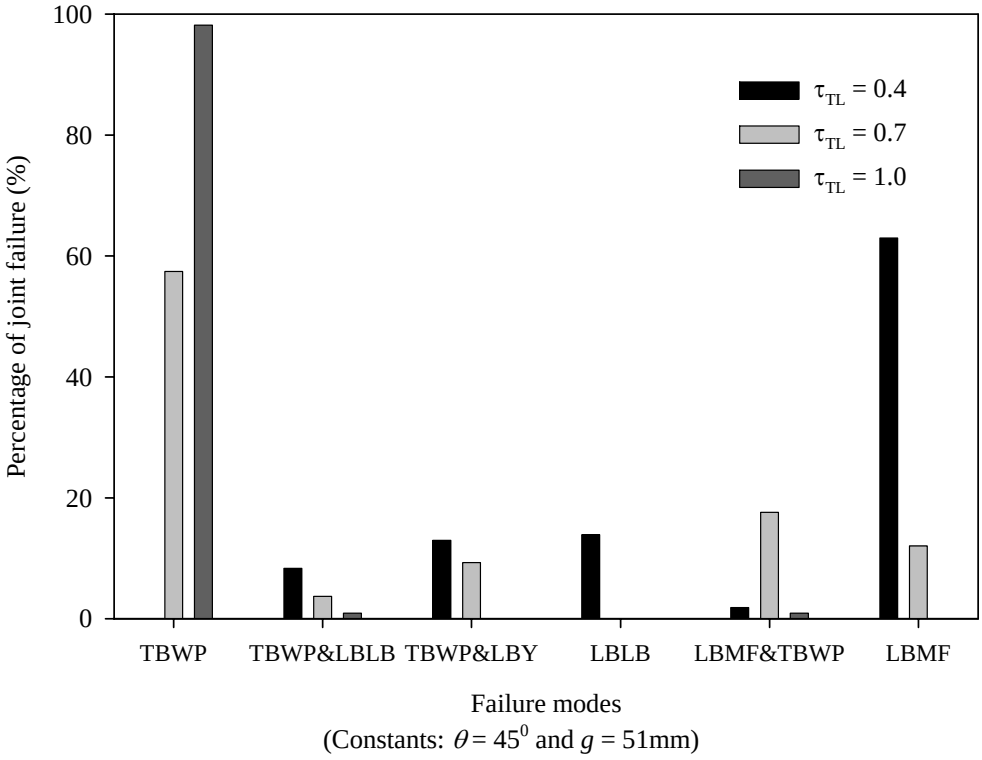

Fig. 5.10 Failure modes (lap brace-to-through brace thickness ratio, τ_{TL})

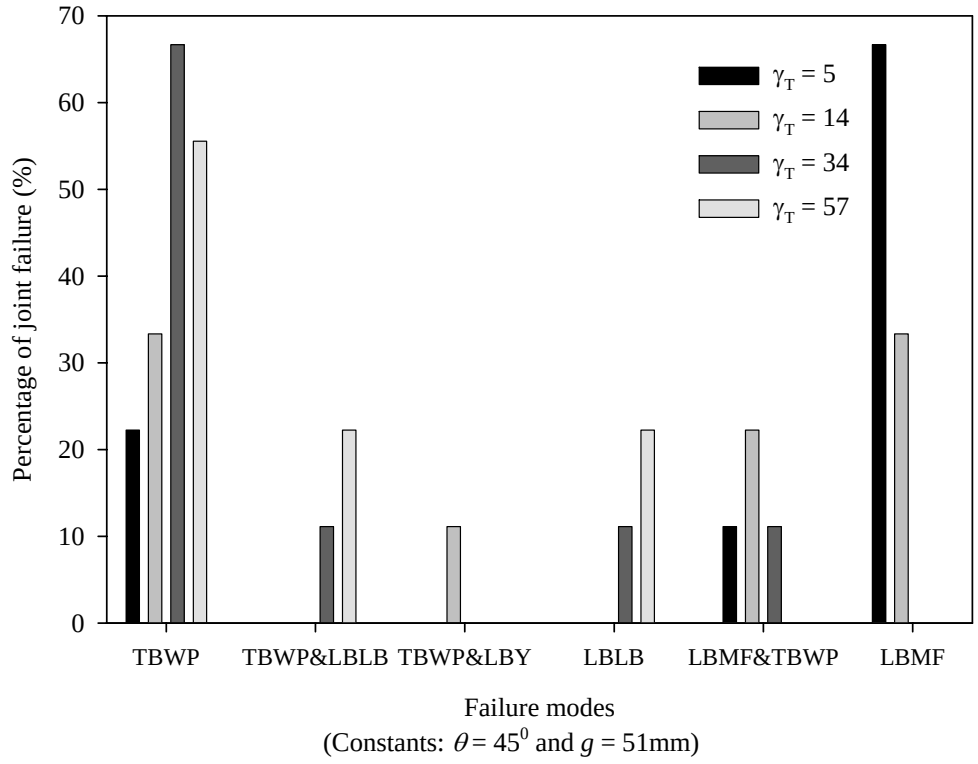

Fig. 5.11 Failure modes (through brace radius-to-wall thickness ratio, γ_T)

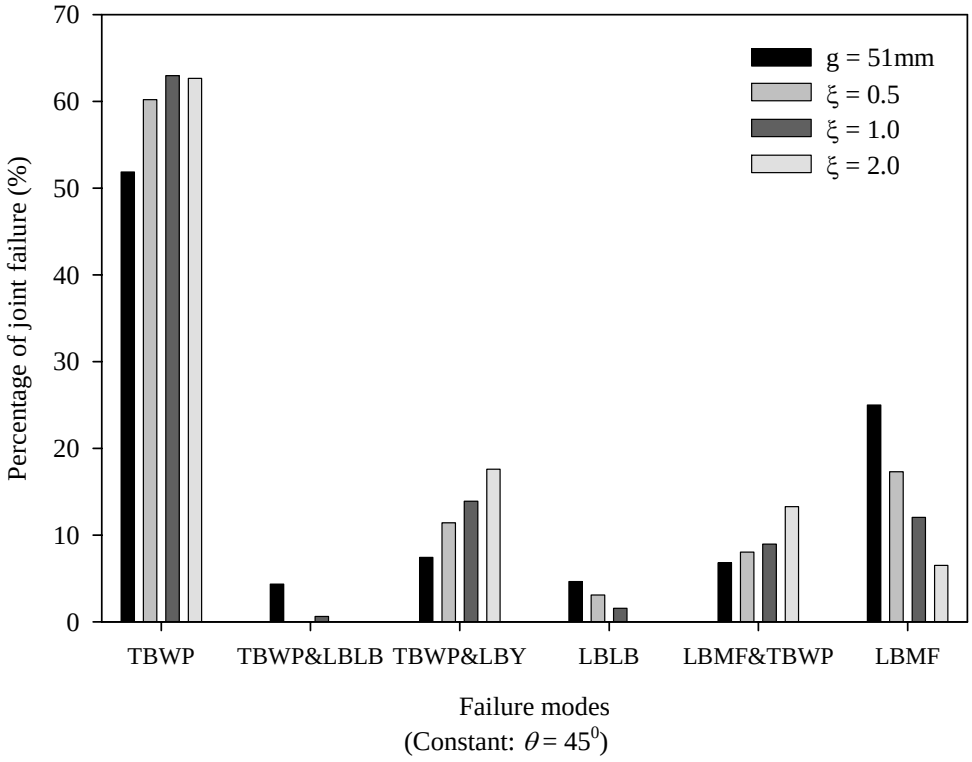

Fig. 5.12 Failure modes (gap size, ξ (g))

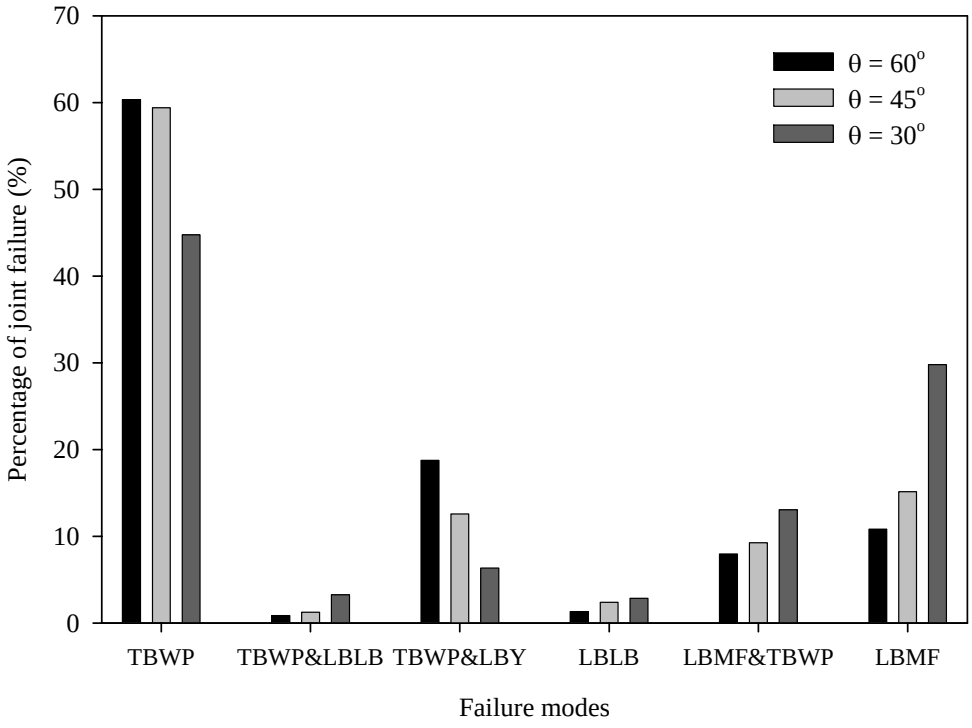

Fig. 5.13 Failure modes (brace angle, θ)

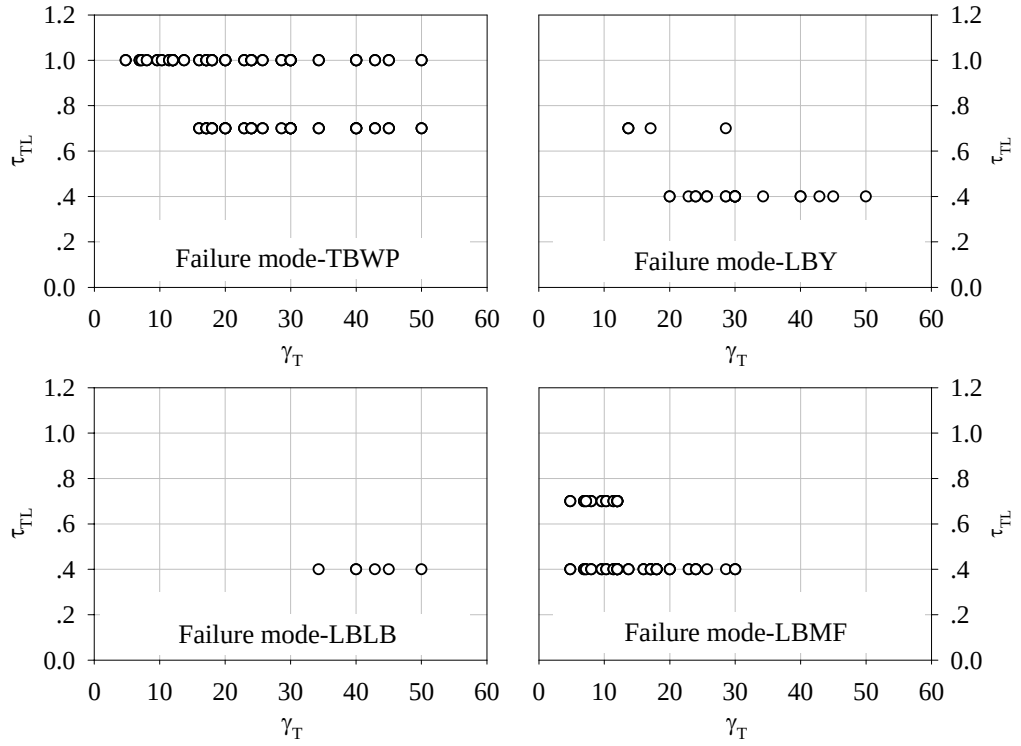

(a) g = 51mm

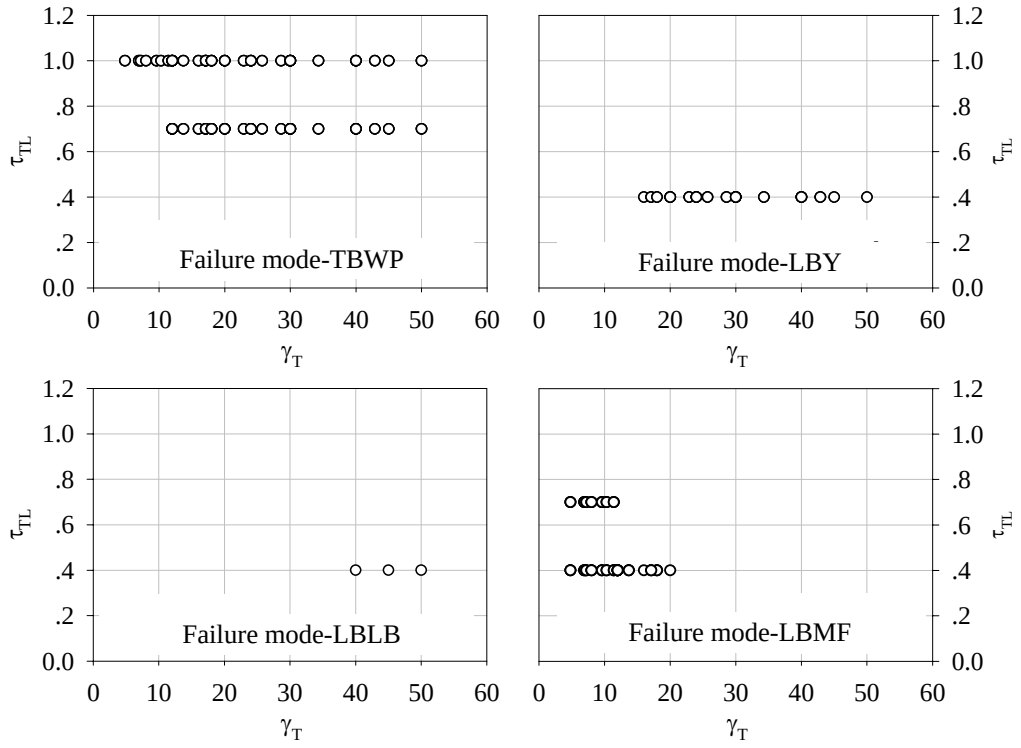

(b) ξ = 0.5

(Constant: $\theta = 60^0$)

Fig. 5.14 Failure modes with varying τ_{TL} and γ_T

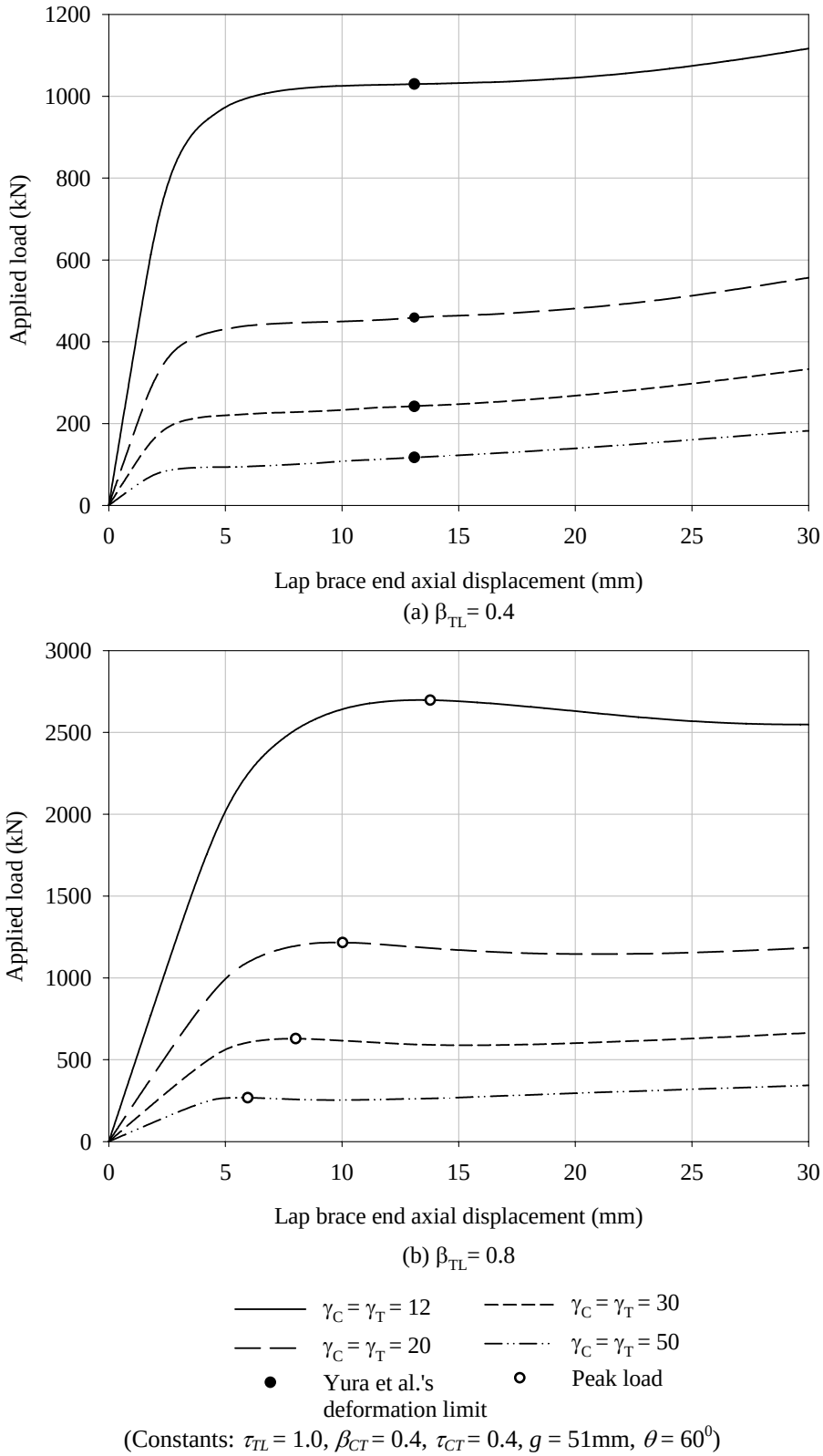

Fig. 5.15 Axial load - displacement curves of joints with through brace wall plastification

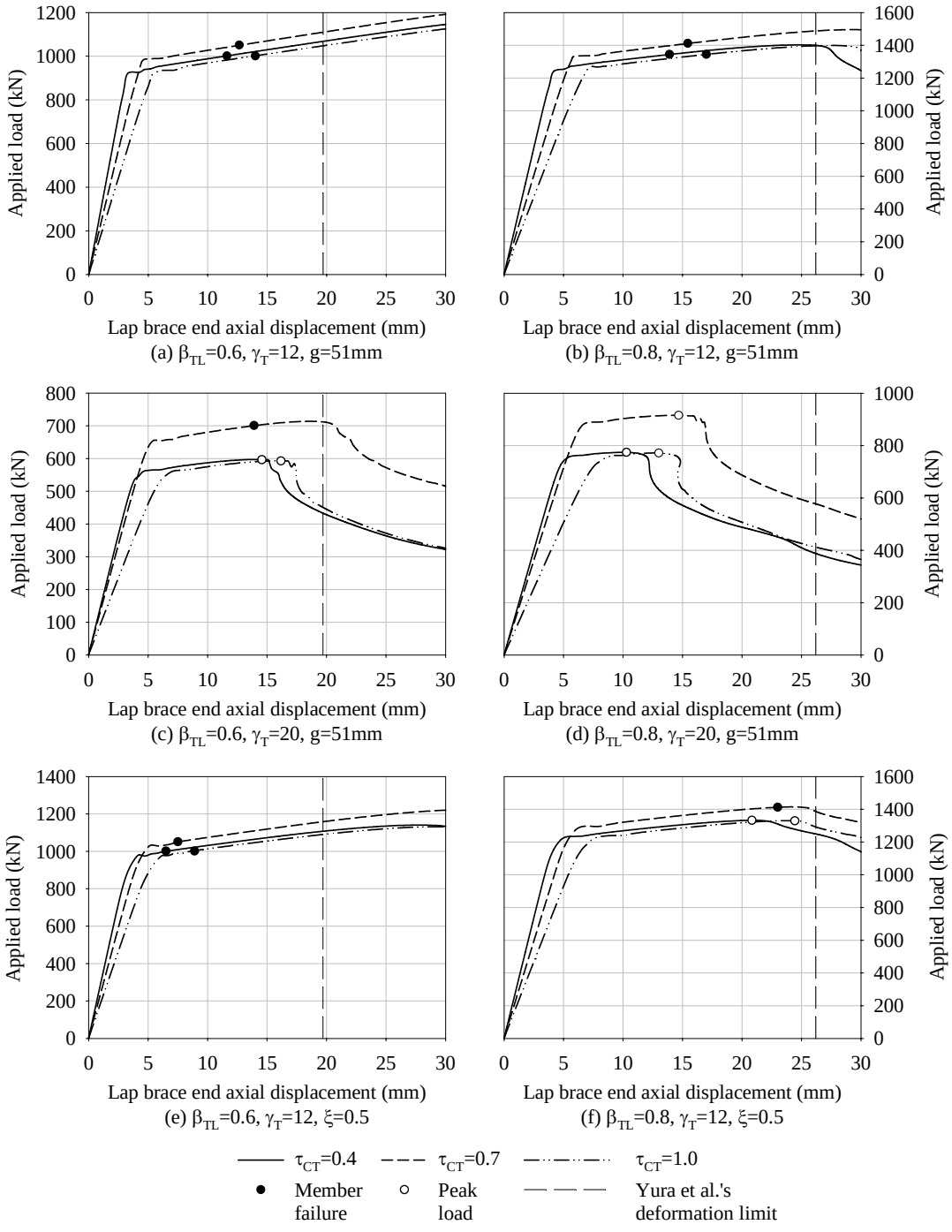

(Constants: β_{CT} = 0.4, τ_{IL} = 0.4, θ = 60^0)

Fig. 5.16 Axial load - displacement curves of joints with lap brace failure

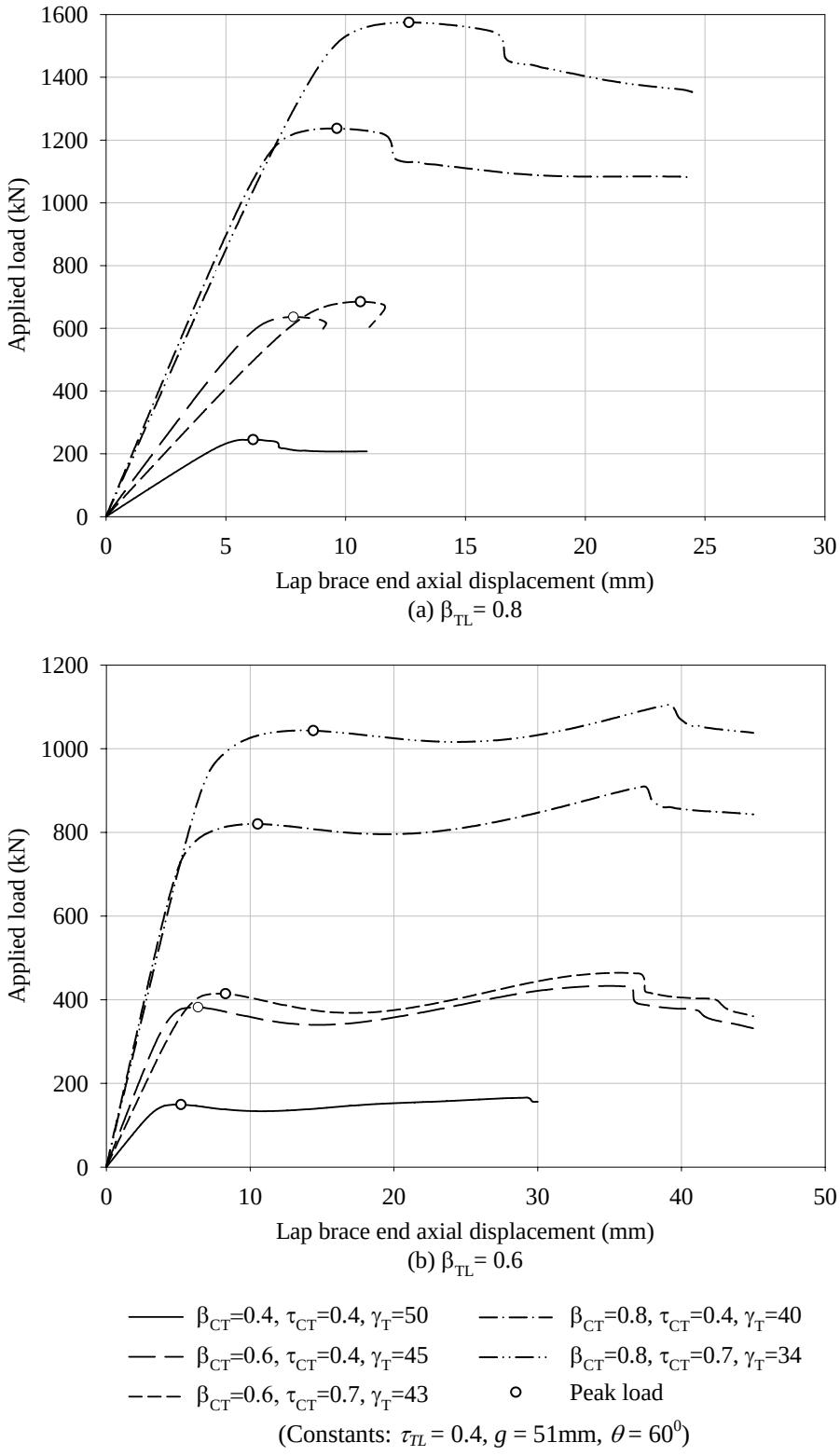

Fig. 5.17 Axial load - displacement curves of joints with lap brace local buckling

CHAPTER 6

ULTIMATE CAPACITY

6.1 Introduction

Ultimate capacity is one of the basic criteria to design a joint. For offshore tubular structures, the joints must be sized for all the possible load cases so that they can be performed satisfactorily under service conditions and to achieve a reasonable balance between economy and risk of failure. It has been shown from several research studies that a tubular joint with complete overlap of braces provides more straightforward fabrication than partial overlap joints and better strength behaviour than simple gap joints. As the loads of the joint are predominantly transferred between the two braces, it is further commended that the punching shear stress on the chord can be reduced and thus the wall thickness. However, the structural behaviour of the joint with complete overlap of braces under static loading is yet to be investigated in detail as the research information of this joint configuration is still very limited.

To estimate the ultimate capacity of a tubular joint based only on analytical approach can be very difficult due to the complexity of geometrical configuration at joint intersection. Generally speaking, the most appropriate method to determine the ultimate capacity of a tubular joint is by testing a full-scale joint specimen in the laboratory. However, the high cost of fabricating a large capacity test rig and specimens has prevented the comprehensive study of the joints under various geometrical parameters and load conditions. As a result, the FE method becomes the most widely used technique for modelling the joint to determine the ultimate capacity.

In the current study, the test of the joint specimen was carried out to verify the reliability of the FE model for detailed parametric analysis of the joint with complete overlap of braces. Three failure criteria discussed in Chapter 5 are used to

determine the ultimate capacity of the joints. The detailed results of the ultimate capacity and the failure criteria of the joints can be seen in Appendix A. All the FE models are generated and analyzed using the commercial FE package MARC (2005a) with pre- and post-processing programs MENTAT. A simple computer program written in Visual C language is developed to directly obtain the ultimate capacity of the joint from the FE models for investigation (Appendix B).

6.2 Influence of geometrical parameters

6.2.1 Effect of through brace-to-chord diameter ratio, β_{CT}

In Fig. 6.1, the ultimate capacity of the joints with four varying gap sizes (g = 51mm, ξ = 0.5, 1.0 and 2.0) are expressed in terms of β_{CT}, τ_{CT} and γ_C. The parameters β_{TL} (= 0.6), τ_{TL} (= 0.7) and θ (= 45°) were kept constant. The parameter γ_T was not constant throughout the analysis as it was expressed in the form of $\gamma_C \cdot \beta_{CT} / \tau_{CT}$. The joint strength was normalized with respect to $\gamma_T^{0.5}$ so that γ_T effect could be excluded. The results from the FE analysis showed that the joint strength with small γ_C and large τ_{CT} (γ_C = 12, τ_{CT} = 1.0) was significantly affected by β_{CT}. For the joints with small γ_C and large τ_{CT}, the capacity could be taken as the lap brace column strength as it failed prior to joint collapse. It was noticed that τ_{CT} increased with γ_C in order to maintain the joint capacity. The effect of β_{CT} increased with decreasing gap size as the chord wall acted as diaphragm restraining the through brace from ovalisation. However, the parameter β_{CT} at ξ = 0.5, 1.0 and 2.0 in the non-dimensional format of $P_u \sin\theta / \sigma_y t_T^2 \gamma_T^{0.5}$ showed little influence on the joint strength (Fig. 6.2). At minimum gap size of 51mm, the non-dimensional strength of the joint increased with β_{CT}.

For the joints with varying β_{TL} and τ_{TL}, a similar trend of behaviour described above is observed as shown in Figs. 6.3 and 6.4. The geometrical parameters of FE models in these figures are summarised in Table 6.1 excluding the lap brace member failure. It could be seen from Fig. 6.3 that the strength of the joint at minimum gap size of

51mm increased with increasing β_{CT} but the impact of strength increment was not crucial. Fig. 6.4 indicated that the effect of β_{CT} is small for the joints with large gap size. It could therefore be concluded from the above study that the joint strength at small gap size was significantly affected by large β_{CT}.

6.2.2 Effect of through brace-to-chord wall thickness ratio, τ_{CT}

As shown in Fig. 6.5, the ultimate capacity of the joint increases with τ_{CT}. The parameters β_{TL} (= 0.6), τ_{TL} (= 0.7) and θ (= 45°) remained constant throughout the analysis. It was noted that the increase of joint strength with τ_{CT} was dependent upon γ_C. The increment of joint strength with smaller γ_C was found larger. A similar effect of parameter τ_{CT} with various gap sizes was observed.

6.2.3 Effect of chord radius-to-wall thickness ratio, γ_C

As shown in Fig. 6.6, the ultimate capacity of the joint decreases with increasing γ_C. The joints with $\gamma_C \leq 20$ showed greater rate of strength decreases and became insignificant with decreasing τ_{CT}. The joint strength with varying γ_C was not affected by gap sizes. For the joints with varying β_{TL} and τ_{TL}, a similar trend of behaviour described above was specifically noted (Figs. 6.7, 6.8 and Table 5.2). The parameter γ_C shows little influence on the non-dimensional strength of the joint, as depicted in Fig. 6.9.

6.2.4 Effect of lap brace-to-through brace diameter ratio, β_{TL}

The ultimate capacity of the joint with varying β_{TL} is presented in Fig. 6.10. In the figures, the parameters β_{CT} (= 0.6), τ_{CT} (= 0.7) and θ (= 45°) remained constant throughout the analysis. For any given geometry, it showed that the joint strength increased with β_{TL} as a result of increased support at the saddle of the through brace and the lap brace which inhibiting the punching action of braces. The strength increase with β_{TL} was dependent upon the parameter γ_T but this impact was found

greater at lower γ_T.

The relationship of the non-dimensional strength $P_u \sin\theta / \sigma_y t_T^2 \gamma_T^{0.5}$ versus β_{TL} at different gap sizes is plotted in Fig. 6.11. It could be seen from this figure that the non-dimensional strength increased with β_{TL}. At minimum gap size of 51mm, the trend line showed higher tangent owing to the effect of γ_C on the joint strength. A similar effect for the joints at β_{CT} = 0.4 and 0.8 is also observed as shown in Fig. 6.12.

6.2.5 Effect of lap brace-to-through brace wall thickness ratio, τ_{TL}

The ultimate capacity of the joint with varying τ_{TL} is presented in Fig. 6.13. The parameters β_{CT} (= 0.6), τ_{CT} (= 0.7) and θ (= 45°) remained constant throughout the analysis. The joint strength was significantly affected by τ_{TL} at γ_T = 11 and $\tau_{TL} \leq 0.7$. As shown in Fig. 6.14, the non-dimensional strength of the joint increases with τ_{TL}. For the joints at high β_{TL} = 0.8, the strength increase at minimum gap size of 51mm was found greater. A similar behaviour for the joints with varying gap sizes and β_{CT} is observed as shown in Figs. 6.15 and 6.16.

6.2.6 Effect of through brace radius-to-wall thickness ratio, γ_T

The non-dimensional strength of the joint at minimum gap size (51 mm) and $0.5d_T$ with varying γ_T are shown in Figs. 6.17 and 6.18 respectively. The strength of the joint in the form of $P_u \sin\theta / \sigma_y t_T^2 \gamma_T^{0.5}$ was found not affected by γ_T. It was noted at minimum gap size of g = 51mm that some points deviated from the trend line plotted due to the effect of chord dimensions. The joints considered were modelled with varying parameters β_{CT} and τ_{CT}. However, the effect of chord dimensions becomes minimal with increasing gap sizes as shown in Fig. 6.18.

6.2.7 Effect of gap size parameter, ξ

The ultimate capacity of the joint with varying gap size parameter ξ is plotted in Fig. 6.19. As shown in these figures, the joint strength decreased with increasing ξ. A sharp drop of load level at gap sizes between 51mm and $0.5d_T$ was specifically noted. This load level gradually reduced with increasing gap size after $0.5d_T$. It was noticed that the ultimate capacity of the joint with small γ_C and τ_{TL} was equivalent to that of the lap brace member. The joint strength remained constant with increasing gap size. However, the ultimate capacity of the joint with small γ_C and medium τ_{TL} was only found equivalent to that of the lap brace member at minimum gap size of 51mm. It was important to realise that the failure modes of the joint changed from the lap brace member to the through brace face plastification with increasing gap size.

6.2.8 Effect of brace angle, θ

The ultimate capacity of the joint with varying brace angle, θ, is shown in Figs. 6.20 and 6.21. In these figures, it showed that the joint strength decreased with increasing θ. The joints failed by lap brace member were marked in bold in the figure. The ultimate capacity of some of the joints remained constant with increasing θ as they reached the capacity of the lap brace member. The decrement of joint strength with brace angle between $30^o < \theta \le 45^o$ was found greater than that between $45^o \le \theta \le 60^o$. However, this was limited to the joints with $\tau_{TL} \ge 0.7$. The joint strength with varying θ was not significantly affected with the change of gap sizes.

In the design recommendations, the effect of brace angle at a joint was included as a load component perpendicular to the chord axis (= $P_u \sin\theta$). In the current study, the ultimate capacity of the completely overlapped tubular joints (excluding the joints with member failure) is multiplied by the parameter $\sin\theta$ and plotted as shown in Fig. 6.22. In the figure, most of the points were well fitted on the solid

line. For the joints with brace angles of 30^0 and 60^0, the data points were found slightly higher and lower with respect to the line plotted, respectively. It was concluded that the $\sin\theta$ factor could be used to compute the ultimate capacity of the completely overlapped tubular joint with varying brace angle.

6.3 Comparison with existing strength formulae

In the current design guidance, there was no formula suitable for predicting the ultimate capacity of tubular joints with complete overlap of braces. In the classification according to load pattern, the completely overlapped tubular joint should be considered to transfer part of the axial brace force of K- and Y-joint. In order to determine the difference of the ultimate capacity of the joint with that specified in the recommendations, the completely overlapped tubular joint was interpreted as two T/Y-joints with the through brace considered as a "chord" member. In the study, four different sets of offshore design recommendations namely API RP2A (2000) (Marshall 2004), HSE (1990), NORSOK (2004) and ABS (2004), and two onshore design guides namely CIDECT (Wardenier et al 1993) and AWS (2000) were considered for comparison. The formulae proposed by IIW (1981) and Kurobane et al (1980a, 1984) for predicting the ultimate capacity of T/Y- and K-joints were also included.

6.3.1 Comparison with API RP 2A (2000) (Marshall 2004)

The ultimate capacity of the completely overlapped tubular joints obtained from the current FE analysis was compared with that of Y- and K-joints specified in API RP2A (2000). The non-dimensional strength of the joint ($P_u\sin\theta/\sigma_y t_T^2$) versus the parameter β_{TL} is shown in Fig. 6.23. Two cases of the joint configurations with minimum and maximum gap sizes were considered for comparison. The joint strength with varying γ_T at β_{TL}= 0.6 is presented in Fig. 6.24. The geometrical parameters at the joint intersection of the through brace and the chord and the brace angle remained constant. It could be seen from Figs. 6.23 and 6.24 that the Y- and K-joints' equations specified in API RP2A (2000) under predict the ultimate

strength of the completely overlapped tubular joints except those with member failure. The data marked in bold in Fig. 6.24 indicated that the member stresses exceed the allowable limits specified in the recommendation. It was noted that API RP2A (2000) was unable to reasonably predict the ultimate capacity of the joint with high β_{TL} and γ_T. Furthermore, API RP2A (2000) did not include the effect of γ_T in the equation for predicting the ultimate capacity of Y-joint. As a result, the predicted ultimate strength of the joint with varying γ_T remained constant. For K-joints, API RP2A (2000) predicted a constant ultimate strength for the completely overlapped tubular joint with $\gamma_T > 20$.

An updated formulation in API RP2A, twenty-second edition (Marshall 2004), included the nonlinear function of β and parameter γ in the strength equations for tubular joint design. It predicts higher ultimate capacity in comparison with that of API RP2A, twenty-first edition (2000), except for K-joints with $\gamma < 20$ and small gap size as shown in Figs. 6.23 and 6.24. At large gap size, it predicted the ultimate capacity of Y-joints not identical to that of K-joints. This was otherwise for API RP2A, twenty-first edition (2000).

The strength of the completely overlapped tubular joint at small gap size was underestimated by API RP2A (Marshall 2004). At large gap size, the joint strength was over predicted with use of K-joint's equation but this was limited to joints with low γ_T and τ_{TL}. It should be noted that the inclusion of nonlinear function of β in API RP2A (Marshall 2004) formulation better predicted the ultimate capacity of the joint with varying β_{TL} despite the combined effect of high γ_T and τ_{TL} were not captured. However, the effect of γ_T was considered in the formulae for joints at low $\gamma_T < 20$. The good agreement of the ultimate capacity for the joints at large gap size between the predicted values and the current FE data suggested that the strength of the completely overlapped tubular joints at large gap size could be predicted using the available formulae in API RP2A.

6.3.2 Comparison with HSE (1990) and NORSOK (2004)

The equations specified in HSE (1990) and NORSOK (2004) for predicting the ultimate capacity of tubular joints used similar geometrical functions. The joint capacities predicted by these two recommendations versus the parameters β_{TL} and γ_T are shown in Figs. 6.25 and 6.26 respectively. For K-joints, the formulations in HSE and NORSOK yielded the same ultimate capacity. For Y-joints, the predicted ultimate capacity was slightly different. It was noted that the strength increase with increasing β_{TL} was better predicted with the inclusion of nonlinear function β in the formulations. The joint strength with varying γ_T predicted by HSE and NORSOK remained constant. The results of the current study showed that the non-dimensional strength ($P_u \sin\theta / \sigma_y t_T^2$) of the completely overlapped joint was significantly affected by γ_T. It was therefore recommended that the parameter γ_T should be included in the equation for predicting the ultimate capacity of the completely overlapped tubular joint.

6.3.3 Comparison with ABS (2000)

The joint capacity predicted by ABS (2000) versus the parameters β_{TL} and γ_T are shown in Figs. 6.27 and 6.28 respectively. The nonlinear function β_{TL} was included in the formulation to better predict the joint capacity. ABS predicted very well the joint capacity as the effect of parameter γ was included in the equation. Generally speaking, the ABS formulae of Y- and K-joints under estimated the capacity of the completely overlapped tubular joint.

It should be noted that the ABS formulae specified a different Q_g (= 0.13 + 0.65 · ($\sigma_{y,\ \text{brace}} / \sigma_{y,\ \text{chord}}$)· $\tau \cdot \gamma^{0.5}$) based on simple joints for predicting the strength of overlapping joints. From Fig. 6.28, the ABS formula of overlapping joint at low γ_T better predicts the joint capacity. However, the formula over predicts the capacity of the joint at higher τ_{TL}, as shown in Fig. 6.29. It was important to realise that the ABS formulae for predicting the ultimate capacity of overlapped joint was

developed based on database of partially overlapped K-joints. Dexter and Lee (1999b) commented that the capacity of more than 100% overlapped joint should be less than that of the corresponding 90% overlapped joints.

6.3.4 Comparison with CIDECT (1993) and AWS (2000)

The joint capacity predicted by onshore design guide CIDECT (1993) and AWS (2000) versus the parameters β_{TL} and γ_T, as shown in Figs. 6.30 and 6.31 respectively. In CIDECT's strength equation, the ultimate load, P_u, included the resistance factor and the characteristic load was obtained by multiplying the design values with partial safety factor of 1.1. The CIDECT's equation assumed parabolic behaviour of β for predicting the strength of Y-joint. It predicted very well the strength increase of completely overlapped tubular joint with increasing β_{TL}. For the effect of γ_T, the joint strength predicted by AWS was constant. On the other hand, the strength increase of joint with increasing γ_T was well predicted by CIDECT. It could be seen from Fig. 6.31 that the K-joint's equation with $\gamma_T > 25$ in CIDECT showed strength decrease with increasing γ_T. It was important to note that the joints with $\gamma_T > 25$ were outside the validity range specified in CIDECT. The ultimate capacity of the completely overlapped tubular joint with the joint failure was under predicted by CIDECT and AWS.

6.3.5 Comparison with IIW (1981) (Kurobane et al 1980, 1984)

The strength equation developed by Kurobane et al (1980, 1984) precisely estimated the joint capacity without considering the factors due to uncertainties such as material and load variations. It showed only the actual ultimate strength of the joint failed by chord wall plastification. The characteristic strength formula in IIW (1981) was based on the re-analysis of ultimate strength data presented by Kurobane et al (1980a).

The joint capacity predicted by Kurobane et al and IIW versus the parameter β_{TL} is shown in Fig. 6.32. The Y-joint's equation with parabolic relationship of β predicted

very well the joint capacity. However, the K-joint's equation with linear function of β was unable to capture the effect of high β_{TL}. At large gap size, the strength increase of the joint with increasing γ_T was well captured. However, at small gap size, both the Y- and the K-joints' equations were unable to accurately capture the effect of high γ_T. It could therefore be commented from the study that the equations proposed by Kurobane et al and IIW were not suitable for predicting the ultimate capacity of the completely overlapped tubular joint particularly with large γ_T (>30).

The joint capacity predicted by Kurobane and IIW versus the parameter ξ is shown in Fig. 6.34. In the figure, the parameter γ_T was ranged between 8 and 30. The joint with lap brace member failure was not included in the study. The equations derived by Kurobane and IIW for predicting the ultimate capacity of Y-joints underestimated the strength of completely overlapped tubular joints. However, the strength difference between the FE data and the predicted values using equations became smaller with increasing ξ. On the other hand, the equations for predicting the ultimate capacity of K-joint overestimated the strength of completely overlapped tubular joint. The gap size parameter, ξ, showed less impact with use of K-joint's equations for predicting the strength of completely overlapped tubular joint. This meant that the geometrical function of gap size in the formula derived by Kurobane and IIW could be used for predicting the ultimate capacity of the completely overlapped joint.

6.4 Discussions

For a simple tubular joint, the geometrical parameter β was considered to have a crucial effect on the strength of the joint. The ultimate capacity of a tubular joint was also affected by its radial flexibility expressed in terms of chord thickness parameter $\gamma (= D/2T)$. Many ultimate strength equations were derived without the parameter γ as the joint under various load conditions was mainly controlled by the chord behaviour near the joint intersection of members. At the joint intersection, the chord wall was stiffened and reinforced by the brace and thus the radial stiffness of the chord did not significantly affect the ultimate strength of the joint.

However, for partially overlapped joints, apart from the geometrical parameters β and γ, the parameter τ was commented to have large influence on the ultimate capacity of the joint. It should be noted that the parameter τ was not included in most of the ultimate strength equations. The importance of this parameter to determine the ultimate capacity of the joint in the punching shear format had been highlighted in AWS (2000). Furthermore, it was usually the first parameter to be examined for joint failure (Marshall 2004).

For the completely overlapped tubular joint, the chord parameters β_{CT}, τ_{CT} and γ_C showed to have insignificant effects on the strength of the joint ($P_u \sin\theta / \sigma_y t_T^2 \gamma_T^{0.5}$). The chord parameters were only critical for the joints with large β_{CT} and small gap size. On the other hand, the through brace parameters β_{TL} and γ_T played significant roles in controlling the strength of the completely overlapped tubular joint which was found to be similar to that of simple joints. The strength increase of the joint was affected by parameter τ_{TL} and it was found to be more prominent for the joints with small gap size. The gap size parameter, ξ, was an important parameter which influenced the strength of the completely overlapped tubular joint. However, the enhancement of joint strength with increasing ξ with the gap size larger than the through brace diameter became insignificant. Under this circumstance, the ultimate capacity of the completely overlapped tubular joint was equivalent to that of the simple Y-joint.

It was important to realise that the existing equations did not include all the effects of geometrical parameters β_{TL}, γ_T, τ_{TL} and ξ for predicting the strength of completely overlapped tubular joint. Some of the recommendations interpreted the completely overlapped tubular joint as two T/Y joints. This interpretation was found inappropriate as the T/Y-joint equations under predicted the strength of completely overlapped tubular joint at small gap size. Despite Kurobane's K-joint equation estimated very well the strength of completely overlapped tubular joint, it over predicted the strength of the joint at high γ_T. All other existing formulae of simple

T/Y-joints showed to excessively under predict the ultimate capacity of the completely overlapped joints at small gap size. Despite the use of T/Y-joint equations for predicting the strength of completely overlapped joints was considered conservative, the under prediction of the joint strength could be three times that might lead to uneconomical design of tubular connections.

6.5 Concluding remarks

A total of 3888 FE models with various geometrical parameters have been created for investigation. Eight geometrical parameters, β_{CT}, τ_{CT}, γ_C, β_{TL}, τ_{TL}, γ_T,. ξ, and θ, are considered in the study to examine the impact on the ultimate capacity of completely overlapped tubular joints.

The parametric study showed that the joint strength increases with increasing β_{CT}, τ_{CT}, β_{TL} and τ_{TL}, but decreases with increasing γ_T, γ_C, ξ and θ. The effects of these geometric parameters are interactive. The joint strength is significantly affected by β_{CT} only at small γ_T. The strength increase with τ_{CT} and β_{TL} is found dependent upon γ_C and γ_T respectively. The strength decrease with increasing γ_C for joints with large τ_{CT} and small γ_C is drastic. The parameter τ_{TL} could have a significant effect on the ultimate capacity for the joints with small γ_T and τ_{TL}. The interaction of these parameters becomes more significant with decreasing gap size. A completely overlapped tubular joint could be considered as a simple Y-joint with the gap size larger than the through brace diameter.

The strength of the completely overlapped tubular joint obtained from the FE analysis is compared with that predicted by existing equations in the design recommendations. All the existing equations fail to accurately predict the strength of the completely overlapped tubular joint as the effects of geometrical parameters β_{TL}, γ_T, τ_{TL} and ξ are not fully considered. Thus, a new strength equation for predicting the ultimate capacity of completely overlapped tubular joint is proposed and presented in the next chapter of this thesis.

Table 6.1 Geometrical parameters of FE models used in Figs. 6.3 and 6.4

Model No.	1	2	3	4	5	6	7	8	9	10	11	12
β_{CT}	0.4											
γ_C	12			20			30			50		
τ_{CT}	0.4	0.7	1.0	0.4	0.7	1.0	0.4	0.7	1.0	0.4	0.7	1.0
Model No.	13	14	15	16	17	18	19	20	21	22	23	24
β_{CT}	0.6											
γ_C	12			20			30			50		
τ_{CT}	0.4	0.7	1.0	0.4	0.7	1.0	0.4	0.7	1.0	0.4	0.7	1.0
Model No.	25	26	27	28	29	30	31	32	33	34	35	36
β_{CT}	0.8											
γ_C	12			20			30			50		
τ_{CT}	0.4	0.7	1.0	0.4	0.7	1.0	0.4	0.7	1.0	0.4	0.7	1.0

Table 6.2 Geometrical parameters of FE models used in Figs. 6.7 and 6.8

Model No.	1	2	3	4	5	6	7	8	9	10	11	12
τ_{CT}	0.4											
β_{CT}	0.4				0.6				0.8			
γ_C	12	20	30	50	12	20	30	50	12	20	30	50
Model No.	13	14	15	16	17	18	19	20	21	22	23	24
τ_{CT}	0.7											
β_{CT}	0.4				0.6				0.8			
γ_C	12	20	30	50	12	20	30	50	12	20	30	50
Model No.	25	26	27	28	29	30	31	32	33	34	35	36
τ_{CT}	1.0											
β_{CT}	0.4				0.6				0.8			
γ_C	12	20	30	50	12	20	30	50	12	20	30	50

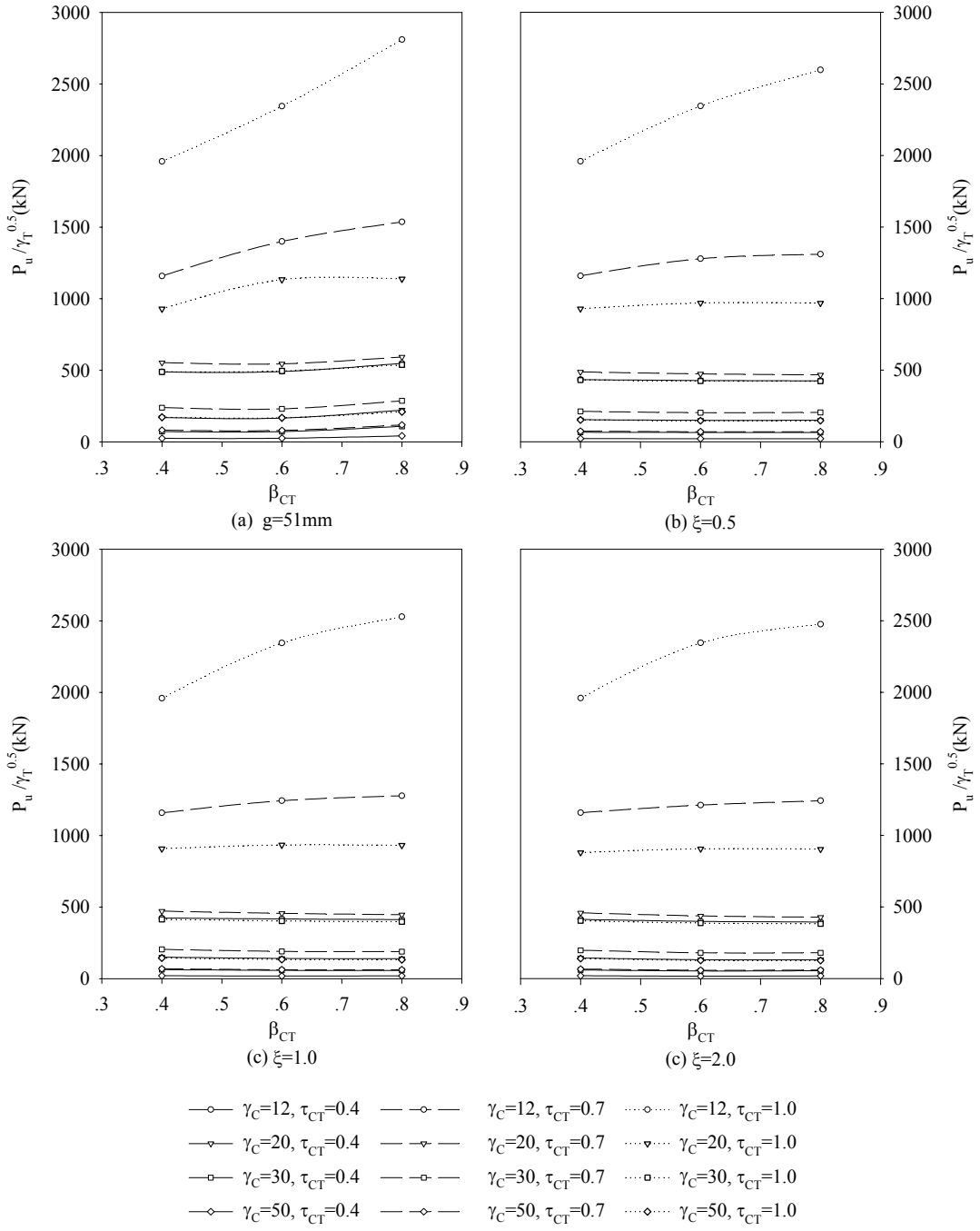

(Constants: β_{TL} = 0.6, τ_{TL} = 0.7, θ = 45°)

Fig. 6.1 Ultimate strength (through brace-to-chord diameter ratio, β_{CT})

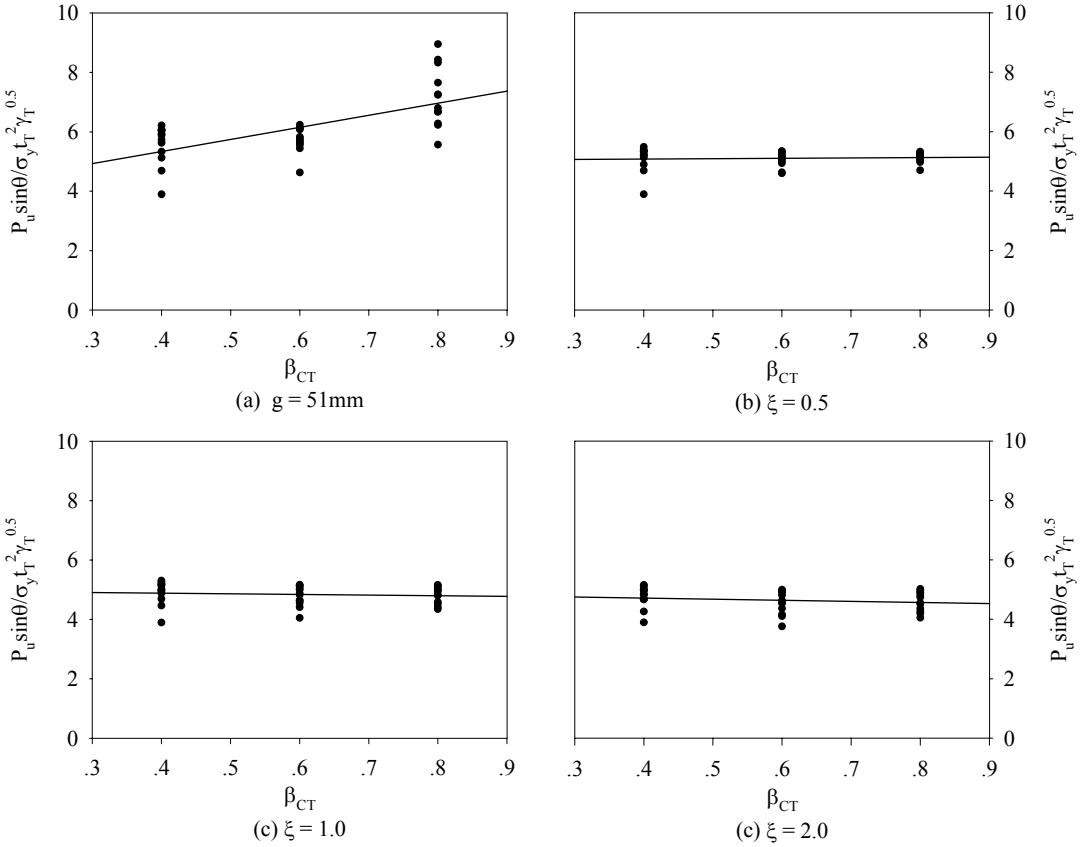

(Constants: $\beta_{TL} = 0.6$, $\tau_{TL} = 0.7$, $\theta = 45^o$)

Fig. 6.2 Non-dimensional ultimate strength of joints with varying β_{CT}

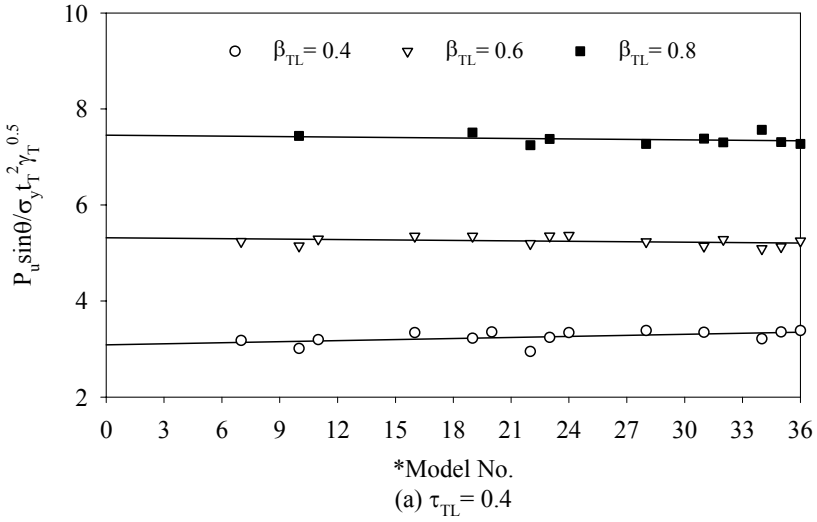

(a) τ_{TL}= 0.4

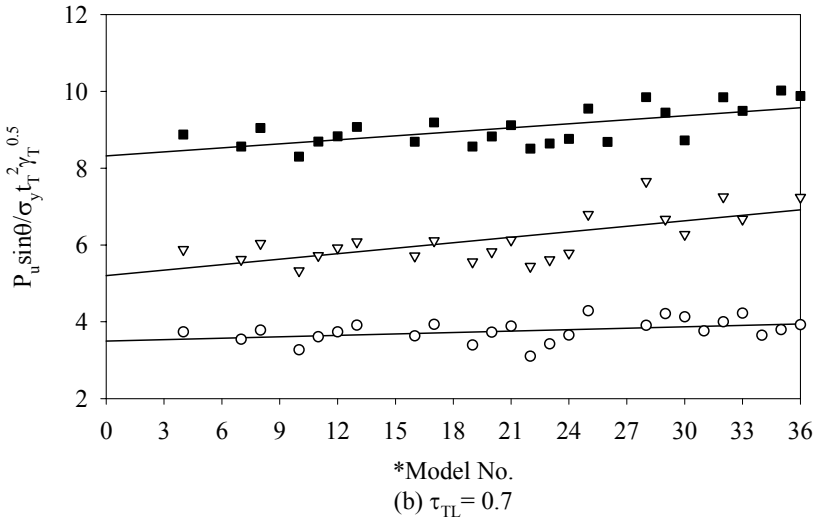

(b) τ_{TL}= 0.7

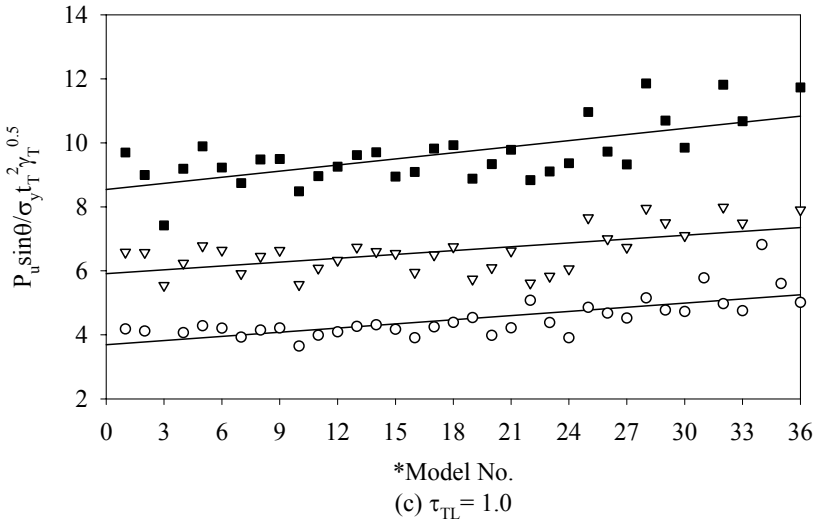

(c) τ_{TL}= 1.0

* Geometrical parameters of FE models shown in Table 6.1. (Constants: g = 51mm, θ= 45°)

Fig. 6.3 Non-dimensional ultimate strength of joints with varying β_{TL} and τ_{TL} (g = 51mm)

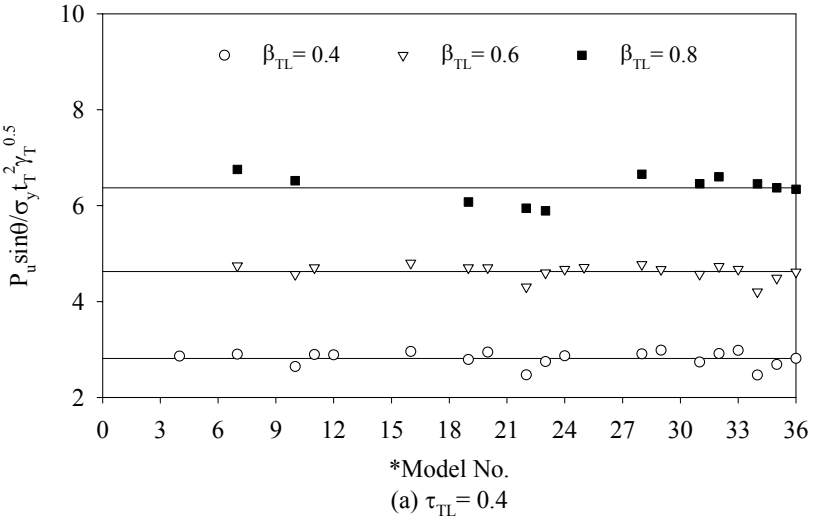

(a) τ_{TL}= 0.4

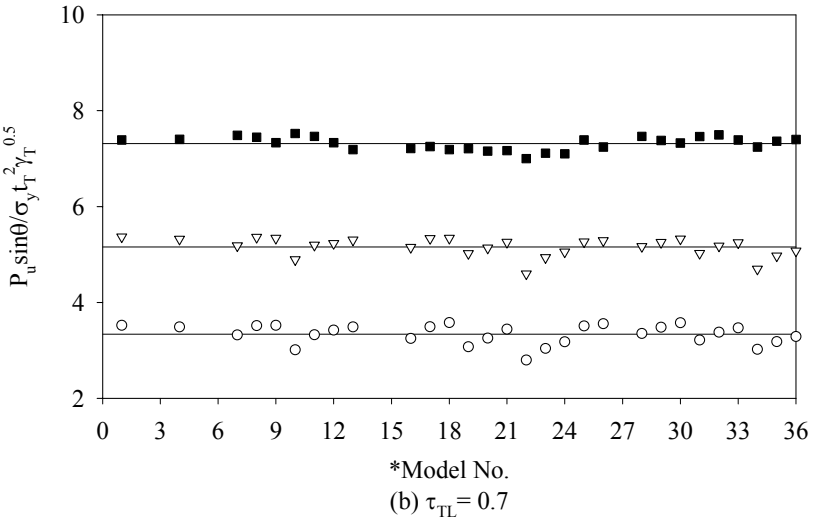

(b) τ_{TL}= 0.7

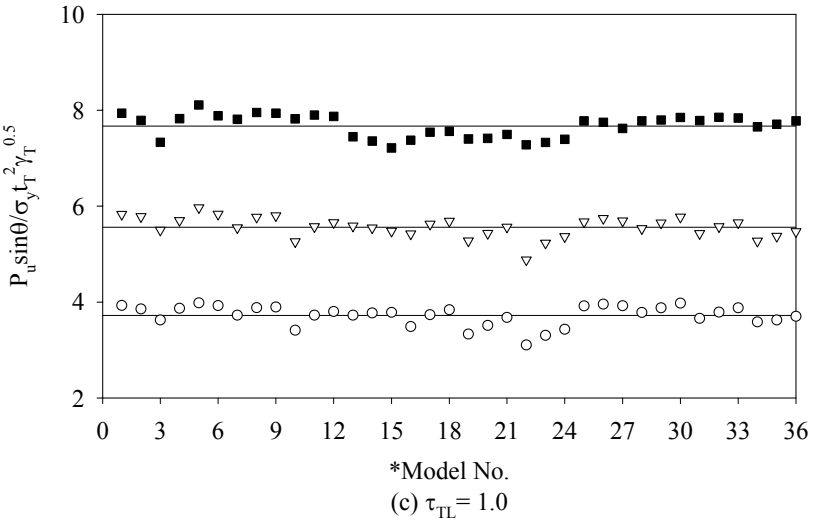

(c) τ_{TL}= 1.0

* Geometrical parameters of FE models shown in Table 6.1. (Constants: $\xi = 0.5$, $\theta = 45^{o}$)

Fig. 6.4 Non-dimensional ultimate strength of joints with varying β_{TL} and τ_{TL} (ξ = 0.5)

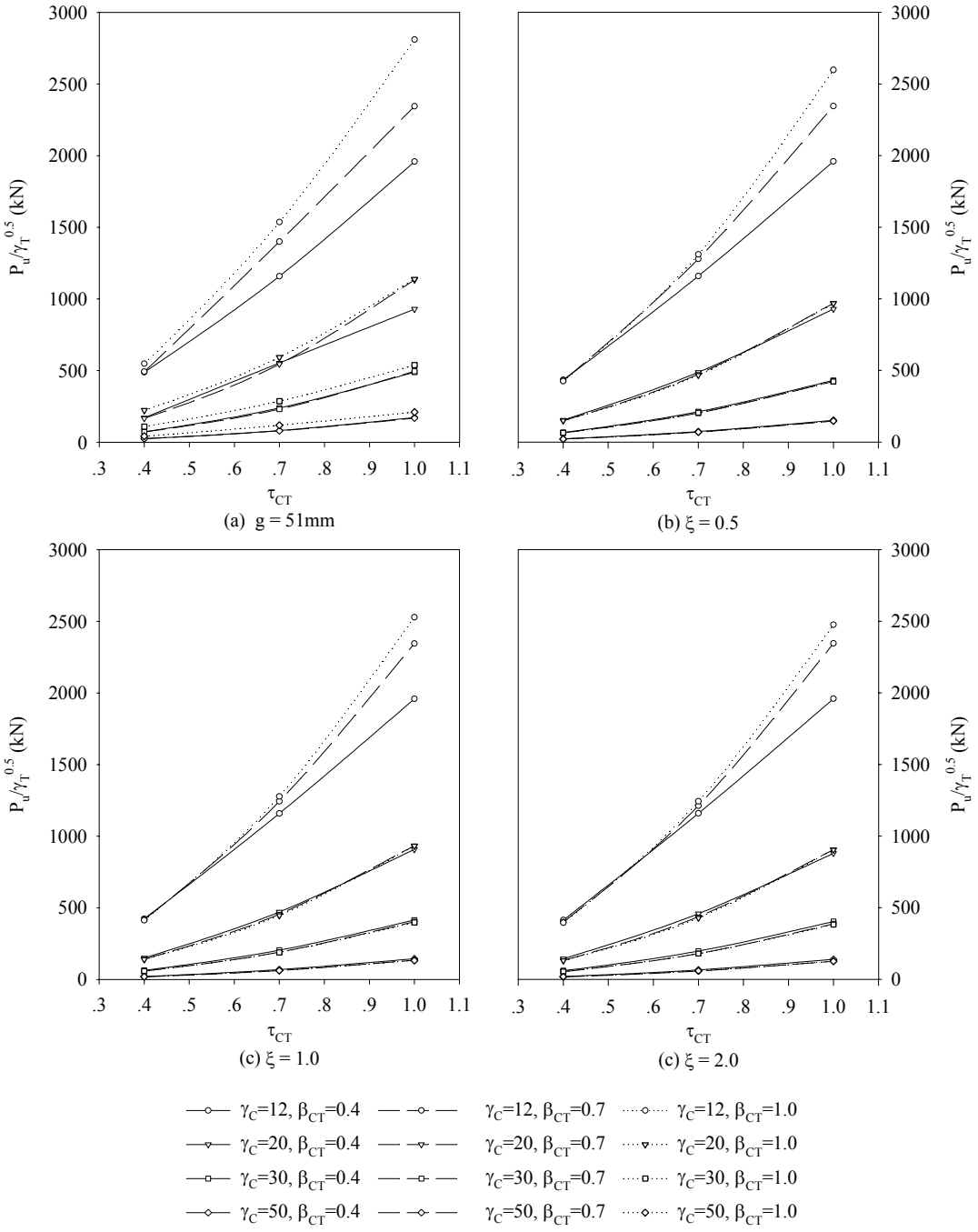

(Constants: β_{TL} = 0.6, τ_{TL} = 0.7, θ = 45°)

Fig. 6.5 Ultimate strength (through brace-to-chord thickness ratio, τ_{CT})

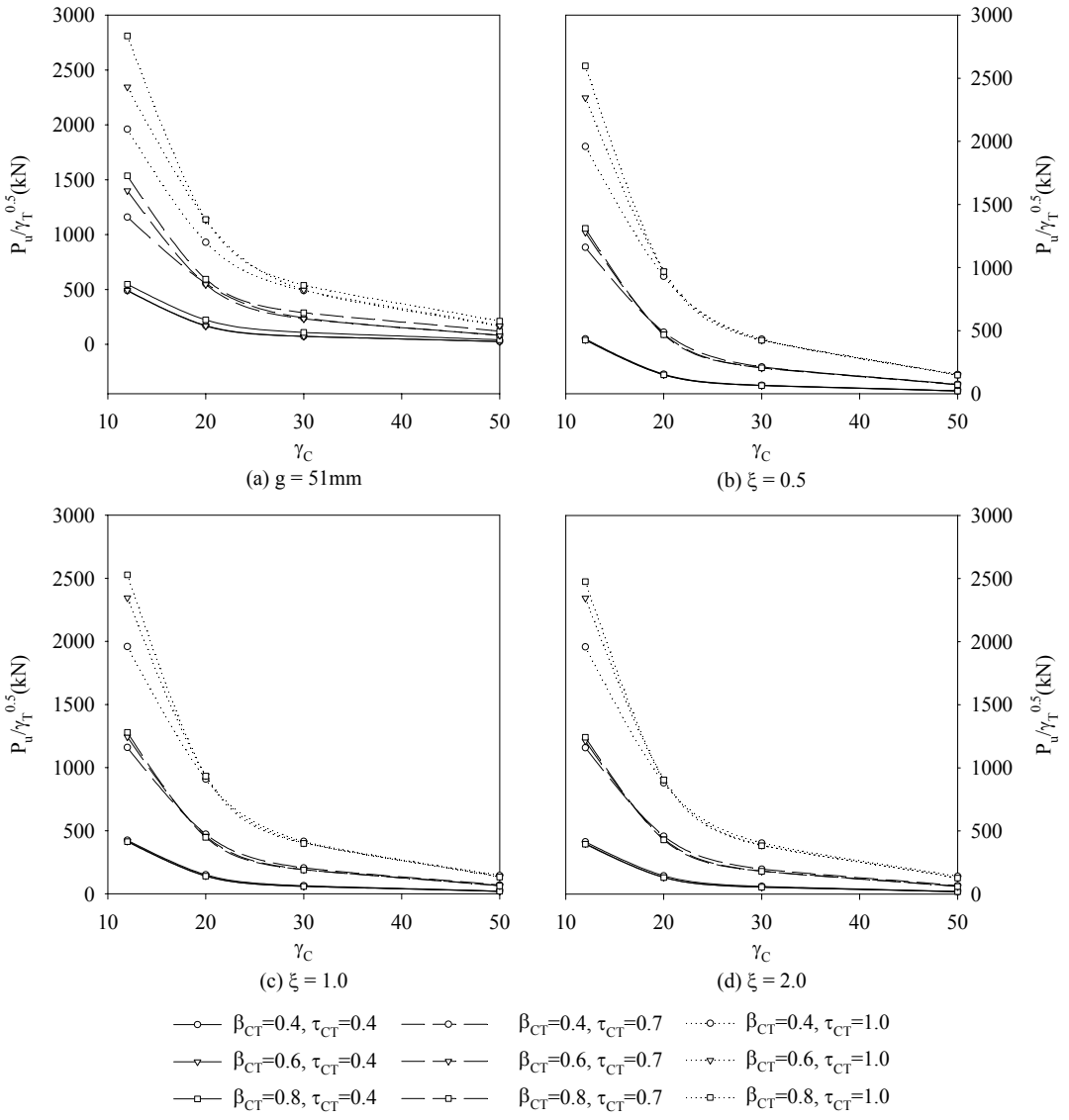

(Constants: $\beta_{TL} = 0.6,\ \tau_{TL} = 0.7,\ \theta = 45^{o}$)

Fig. 6.6 Ultimate strength (chord radius-to-wall thickness ratio, γ_C)

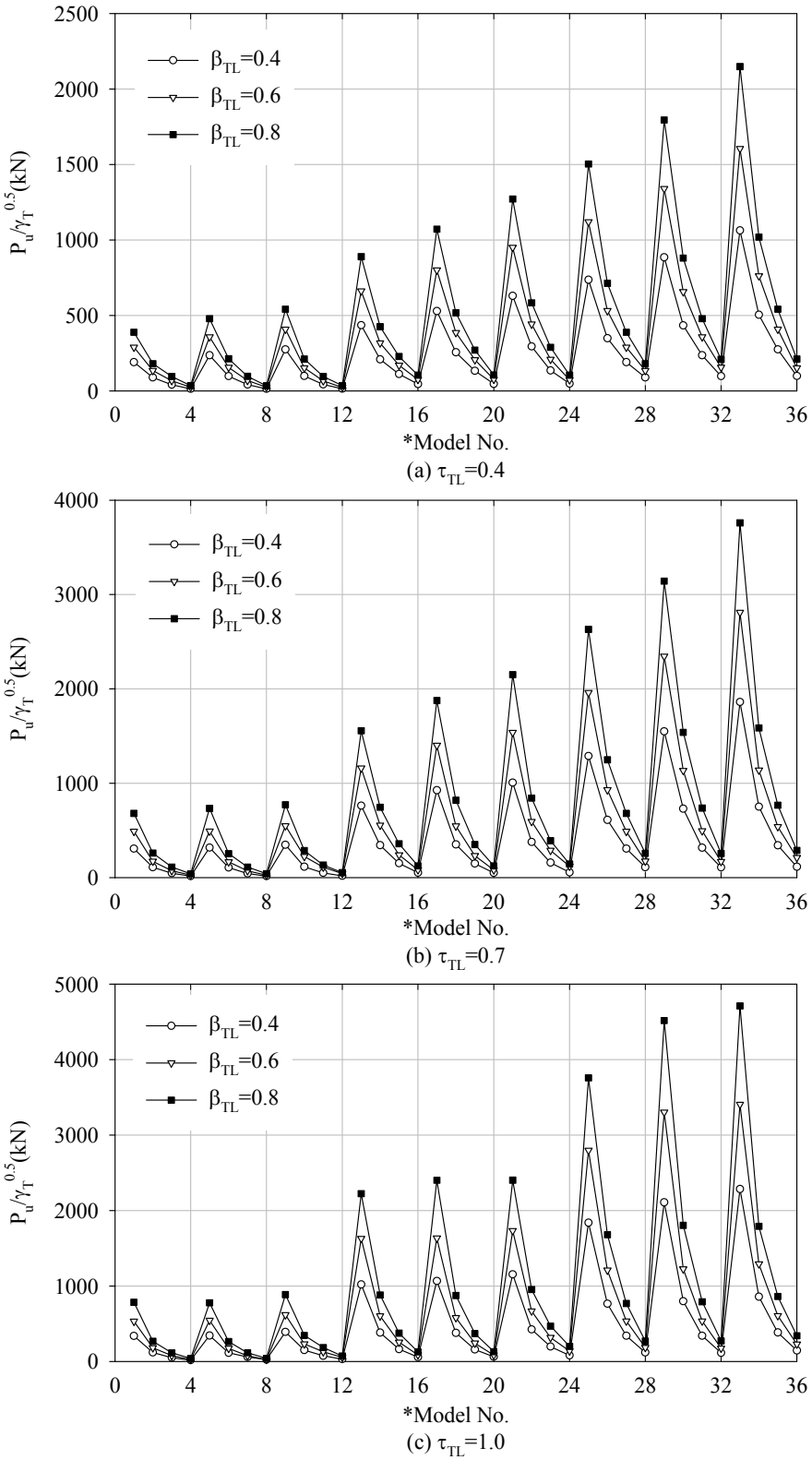

* Geometrical parameters of FE models shown in Table 6.2. (Constants: g = 51mm, θ = 45°)

Fig. 6.7 Ultimate strength of joints with varying β_{TL} and τ_{TL} (g = 51mm)

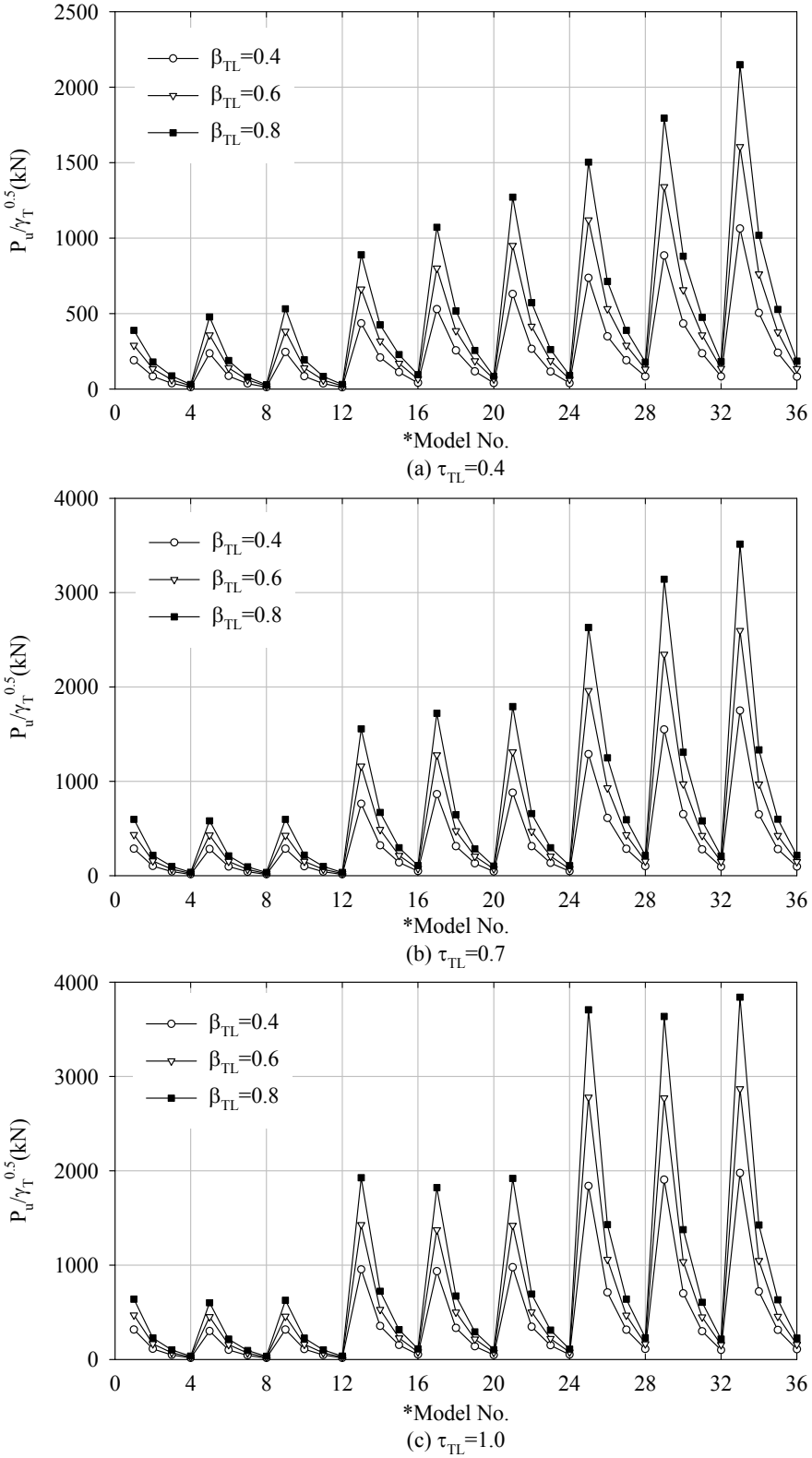

* Geometrical parameters of FE models shown in Table 6.2. (Constants: $\xi = 0.5$, $\theta = 45^o$)

Fig. 6.8 Ultimate strength of joints with varying β_{TL} and τ_{TL} (ξ = 0.5)

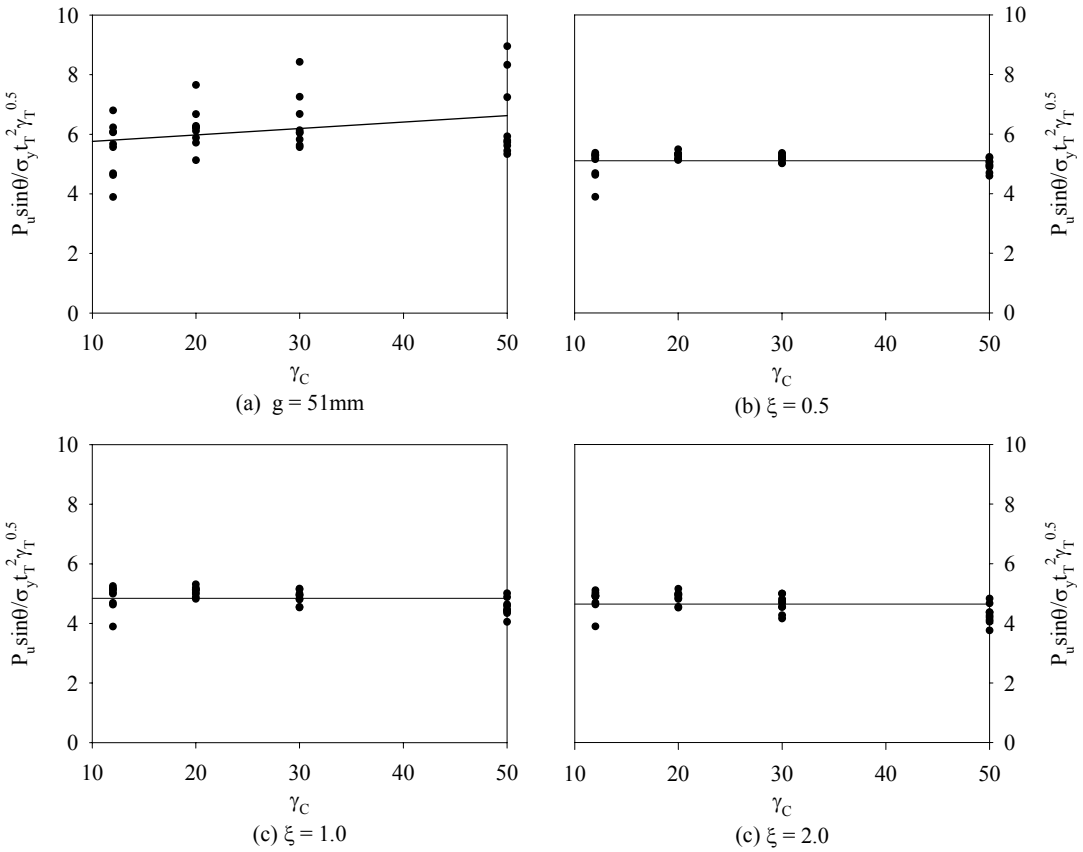

(Constants: $\beta_{TL} = 0.6$, $\tau_{TL} = 0.7$, $\theta = 45^o$)

Fig. 6.9 Non-dimensional ultimate strength of joints with varying γ_C

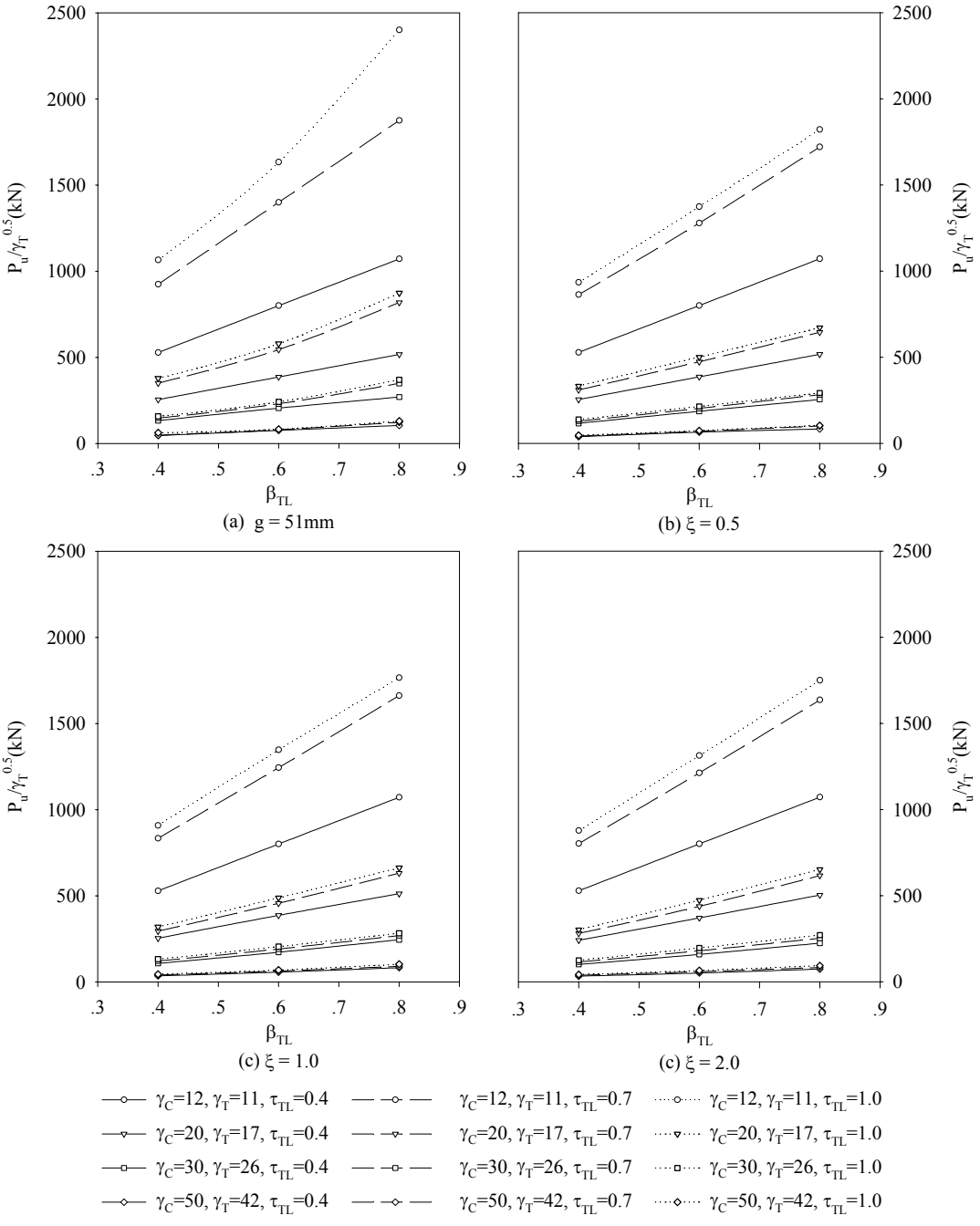

Fig. 6.10 Ultimate strength (lap brace-to-through brace diameter ratio, β_{TL})

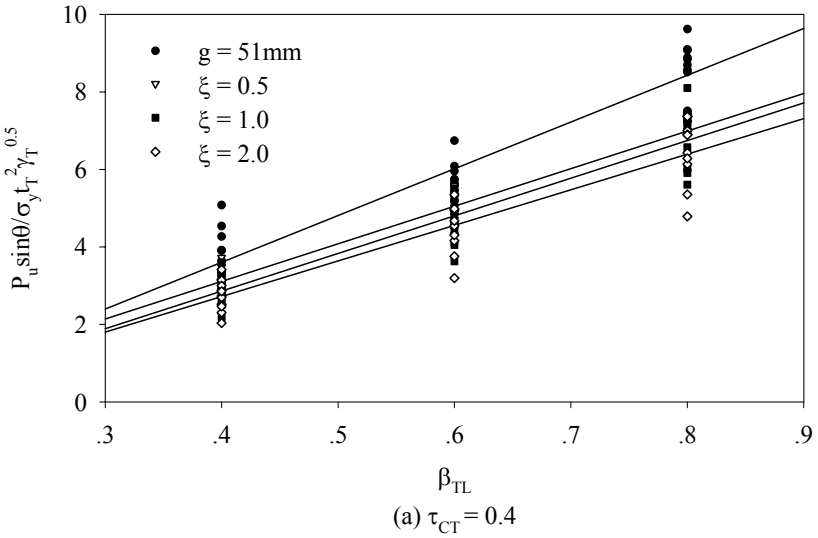

(a) $\tau_{CT} = 0.4$

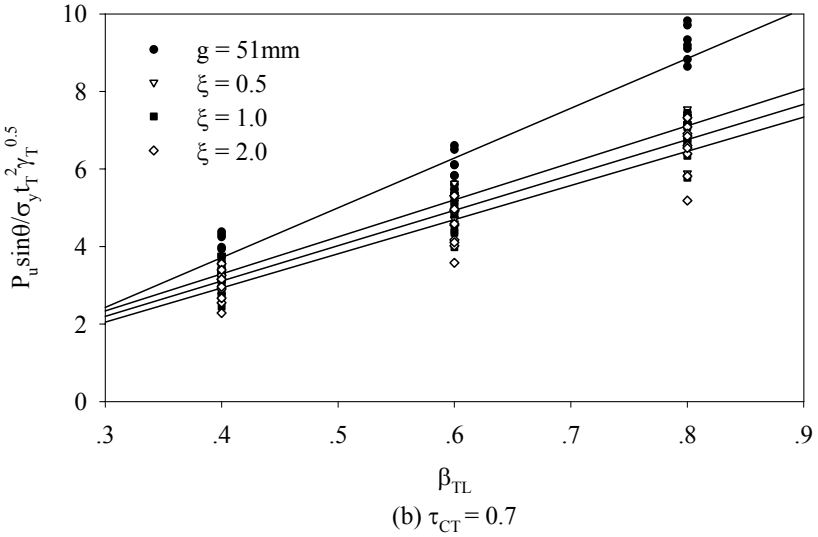

(b) $\tau_{CT} = 0.7$

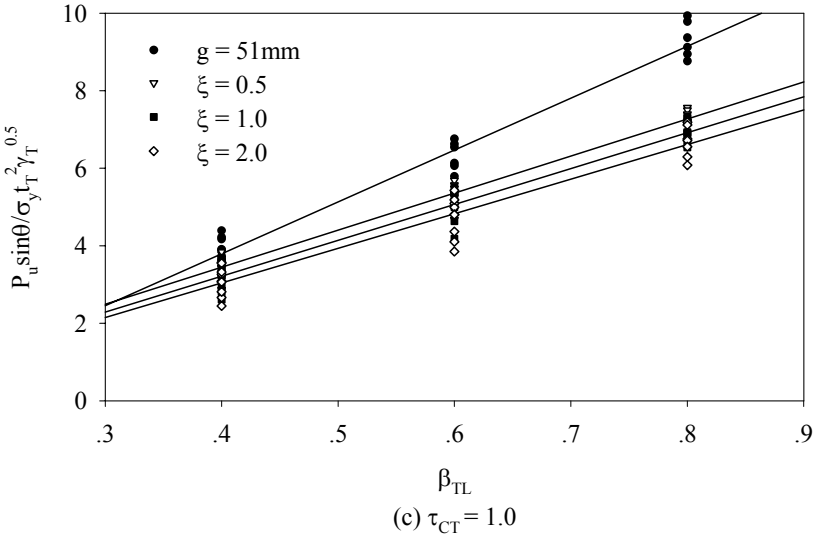

(c) $\tau_{CT} = 1.0$

(Constants: $\beta_{CT} = 0.6$, $\theta = 45^o$)

Fig. 6.11 Non-dimensional ultimate strength of joints with varying gap size and β_{TL}

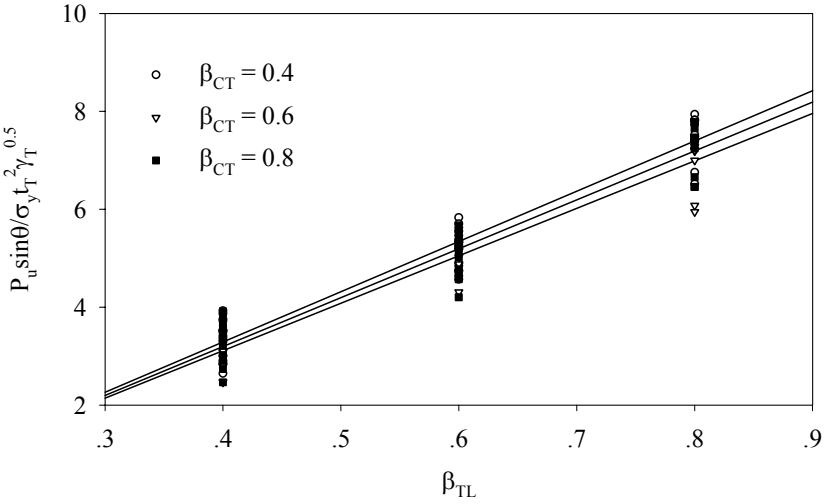

(a) τ_{CT} = 0.4

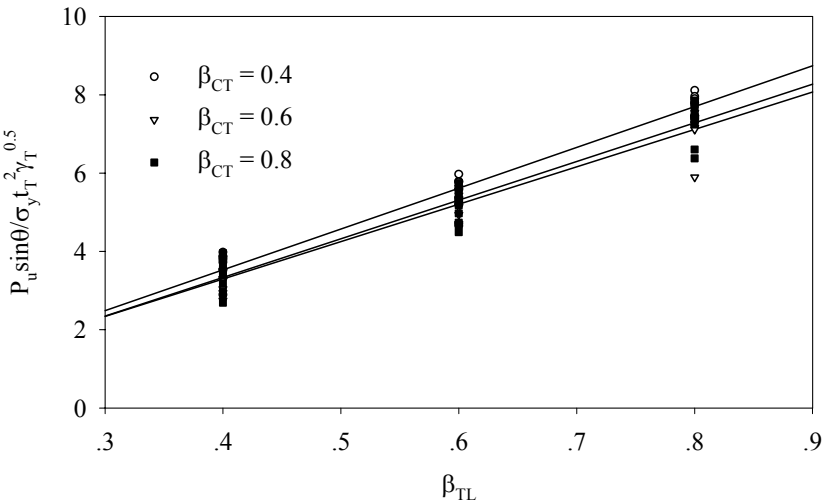

(b) τ_{CT} = 0.7

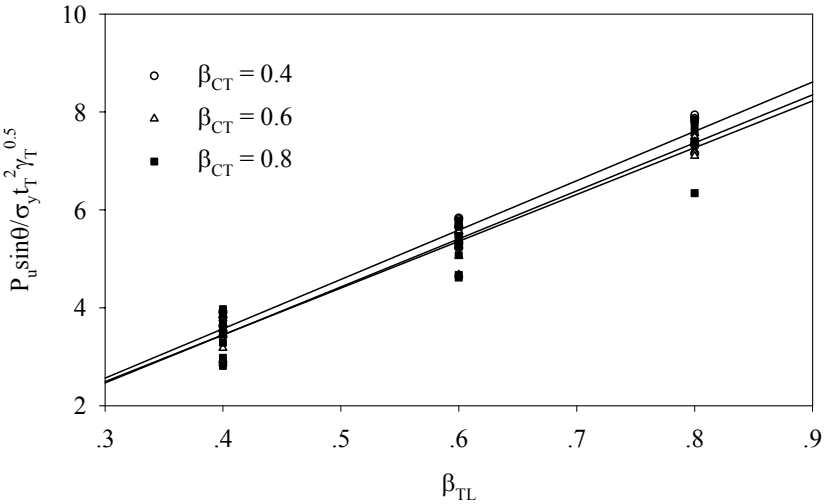

(c) τ_{CT} = 1.0

(Constants: ξ = 0.5, θ = 45°)

Fig. 6.12 Non-dimensional ultimate strength of joints with varying β_{CT} and β_{TL}

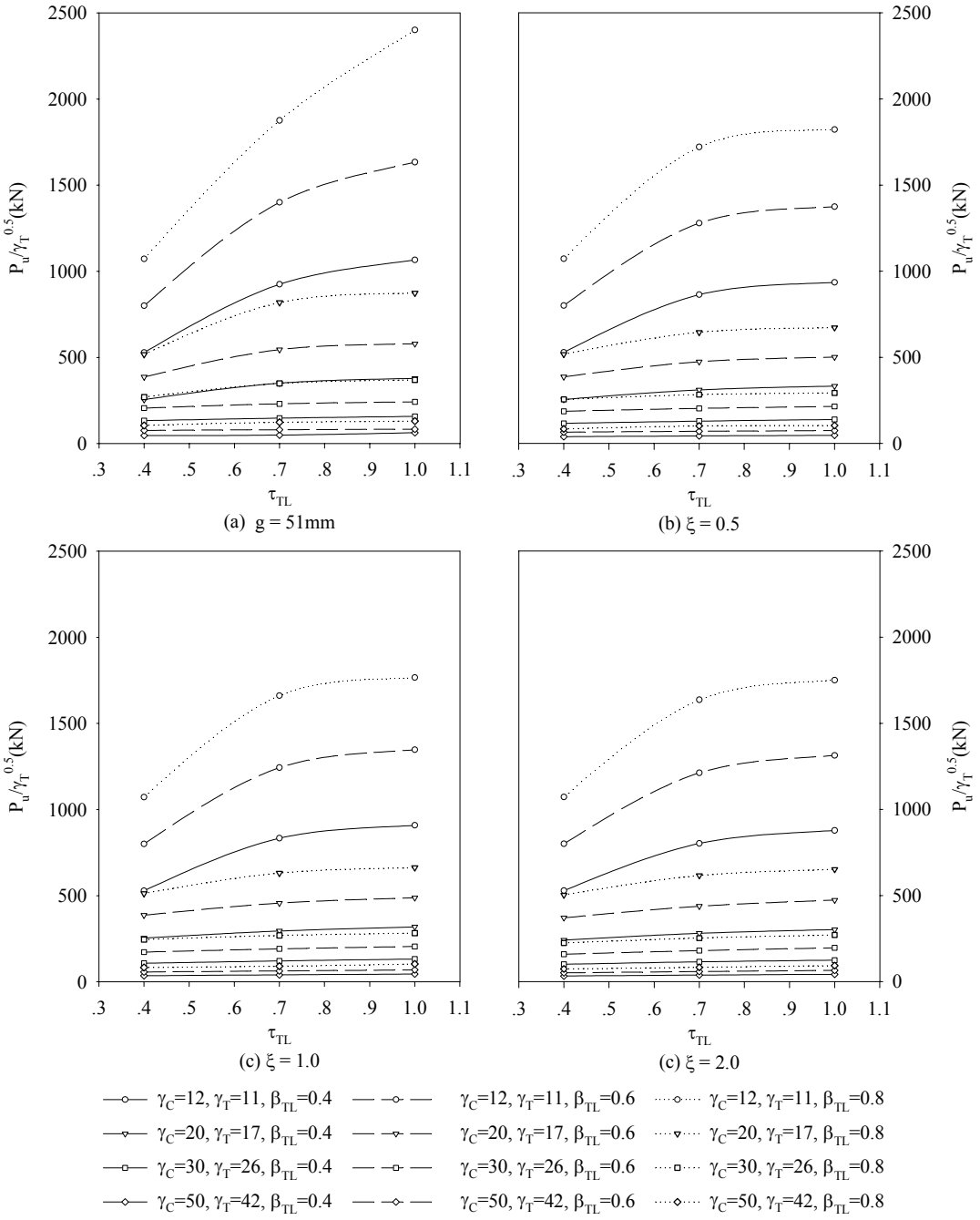

(Constants: $\beta_{CT} = 0.6,\ \tau_{CT} = 0.7,\ \theta = 45^{o}$)

Fig. 6.13 Ultimate strength (lap brace-to-through brace thickness ratio, τ_{TL})

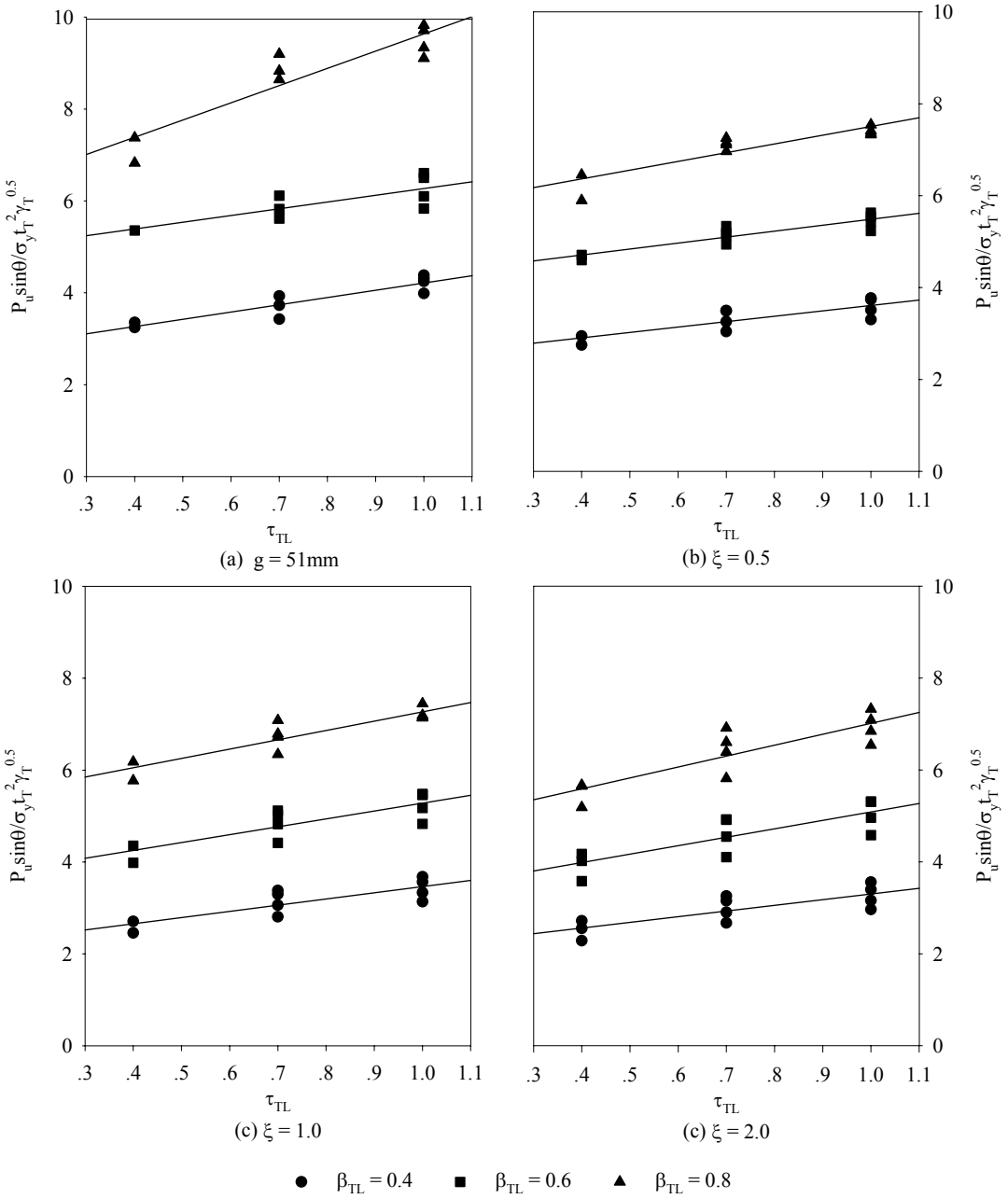

(Constants: $\beta_{CT} = 0.6$, $\tau_{CT} = 0.7$, $\theta = 45^o$)

Fig. 6.14 Non-dimensional ultimate strength of joints with varying τ_{TL}

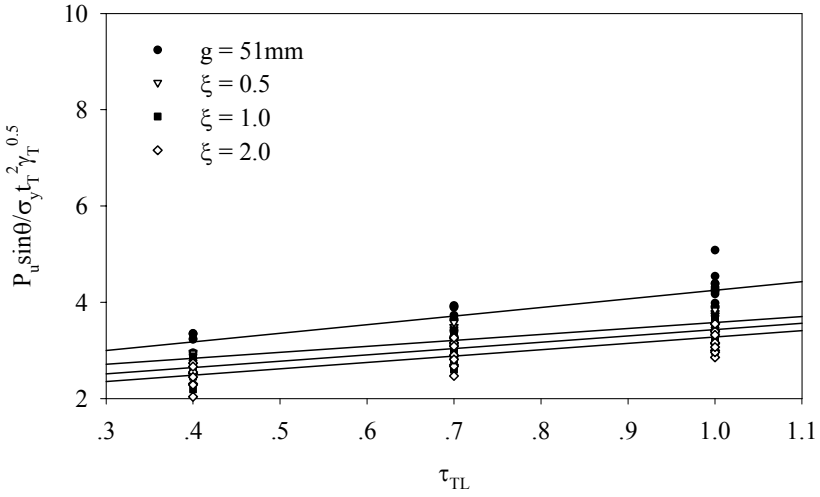

(a) $\beta_{TL} = 0.4$

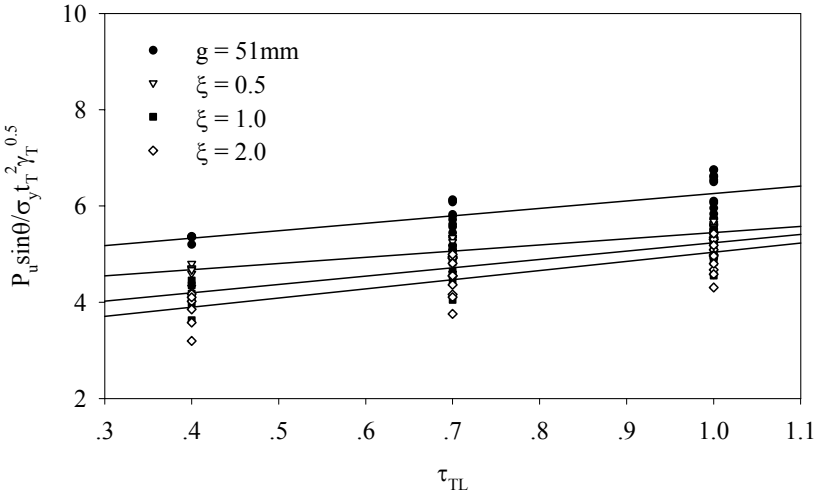

(b) $\beta_{TL} = 0.6$

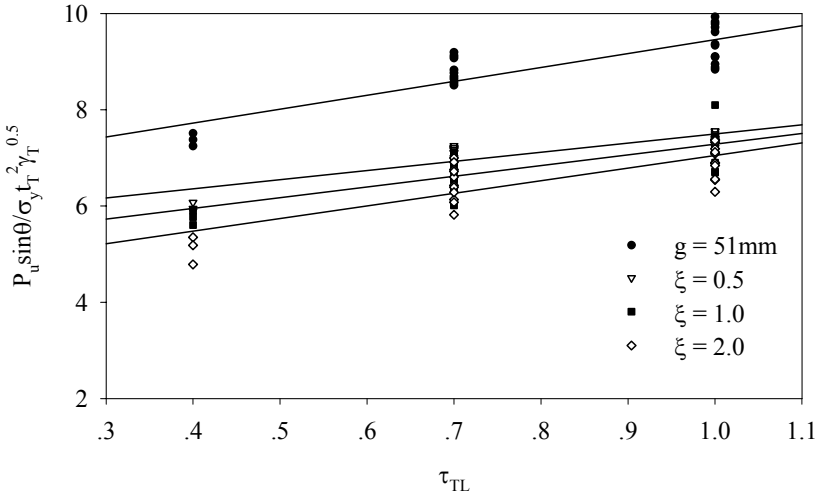

(c) $\beta_{TL} = 0.8$

(Constants: $\beta_{CT} = 0.6$, $\theta = 45^o$)

Fig. 6.15 Non-dimensional ultimate strength of joints with varying gap size and τ_{TL}

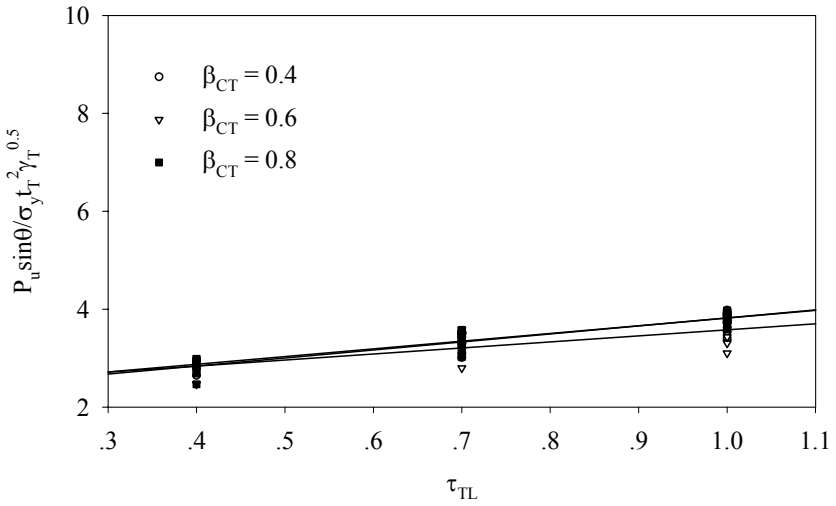

(a) β_{TL} = 0.4

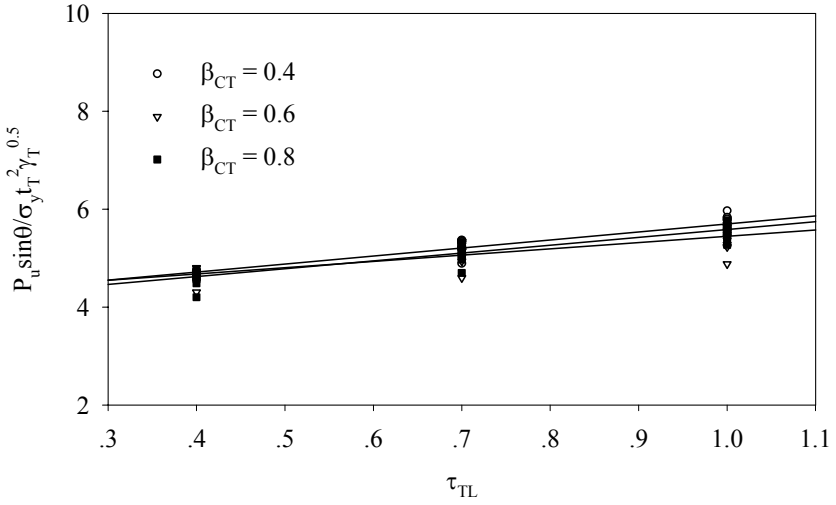

(b) β_{TL} = 0.6

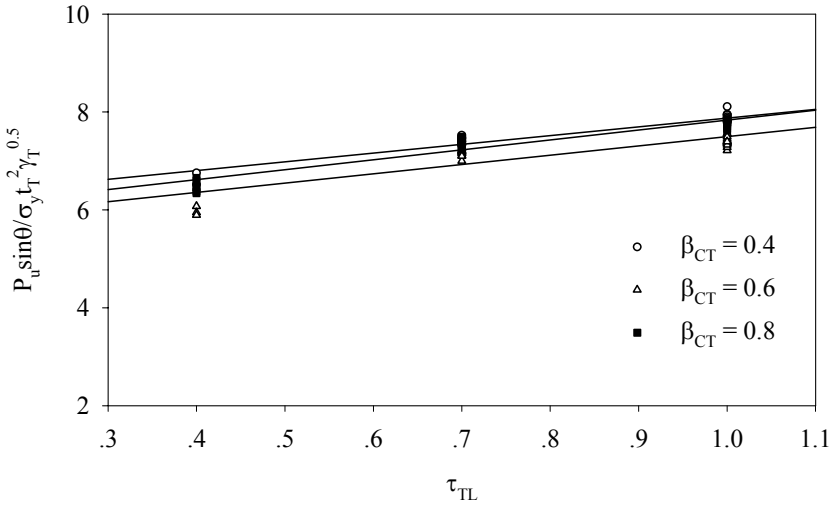

(c) β_{TL} = 0.8

(Constants: $\xi = 0.5$, $\theta = 45^o$)

Fig. 6.16 Non-dimensional ultimate strength of joints with varying β_{CT} and τ_{TL}

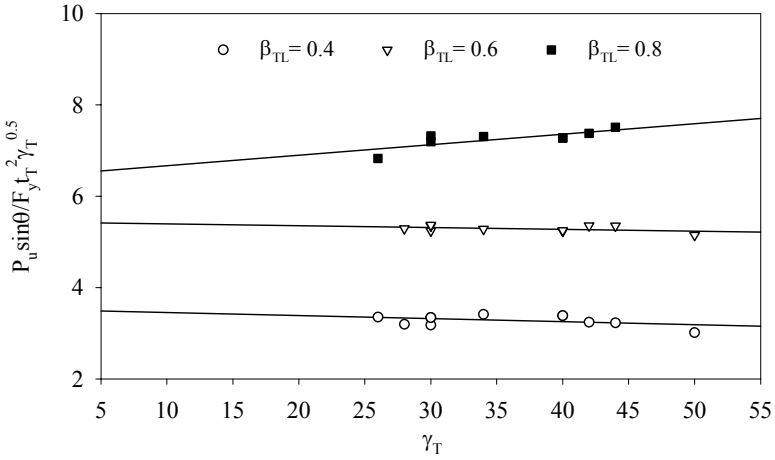

(a) τ_{TL}= 0.4

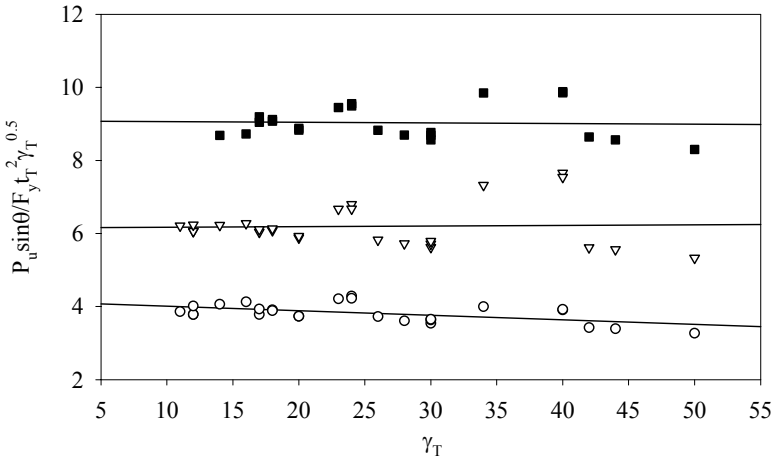

(b) τ_{TL}= 0.7

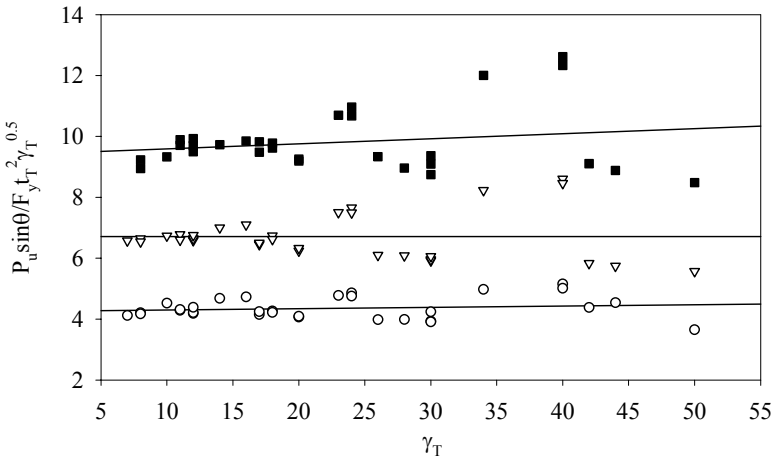

(c) τ_{TL}= 1.0

(Constants: g =51mm, θ= 45°)

Fig. 6.17 Non-dimensional ultimate strength of joints with varying γ_T (g =51mm)

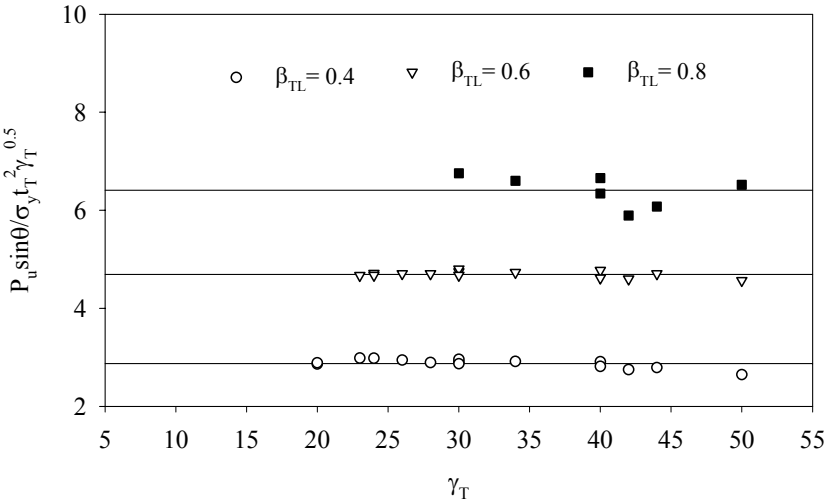

(a) τ_{TL}= 0.4

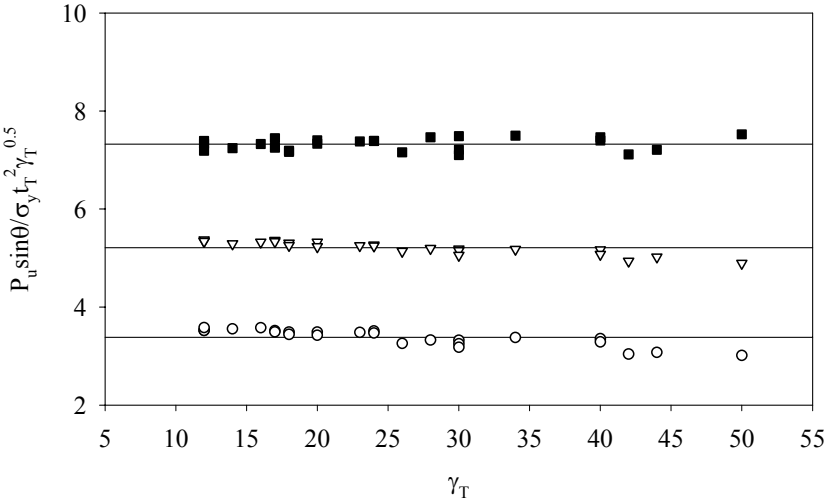

(b) τ_{TL}= 0.7

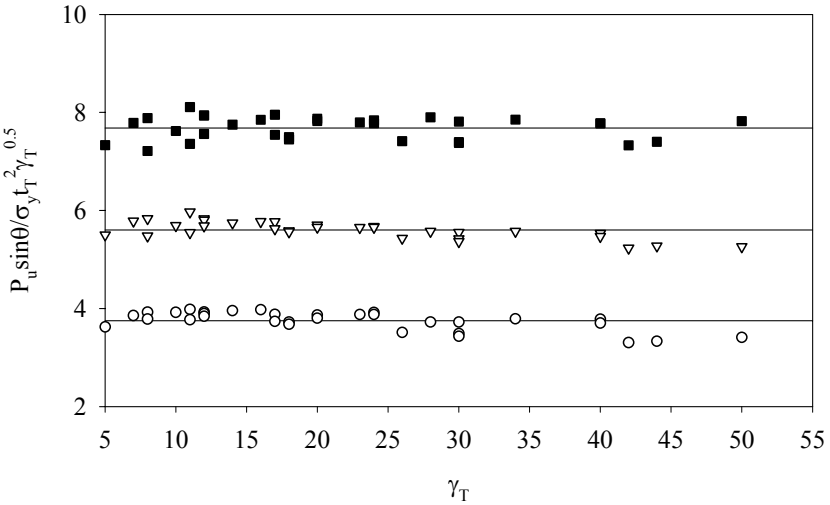

(c) τ_{TL}= 1.0

(Constants: ξ = 0.5, θ = 45°)

Fig. 6.18 Non-dimensional ultimate strength of joints with varying γ_T (ξ = 0.5)

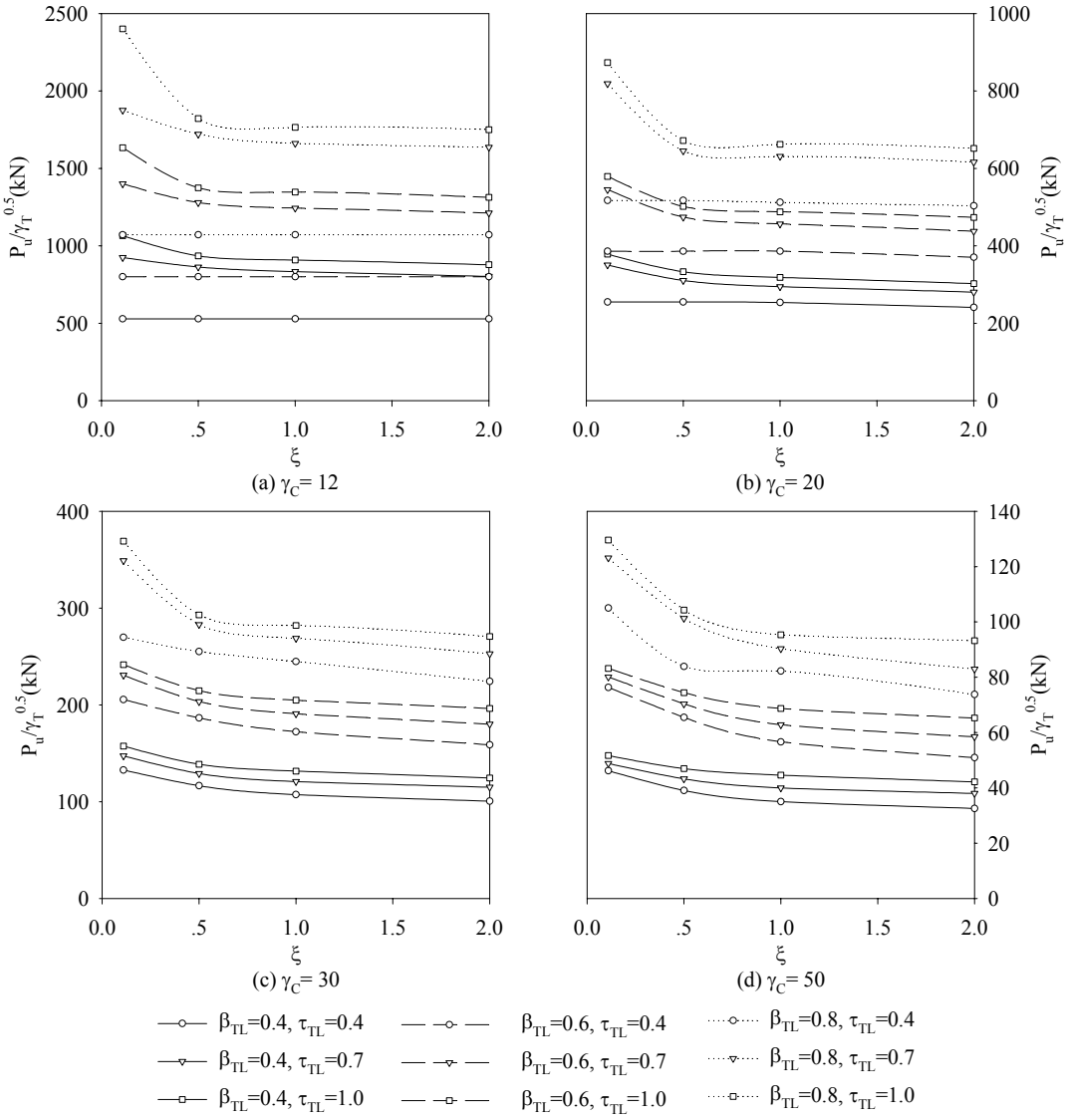

(Constants: $\beta_{CT} = 0.6,\ \tau_{CT} = 0.7,\ \theta = 45^o$)

Fig. 6.19 Ultimate strength (gap size-to-through brace diameter ratio, ξ)

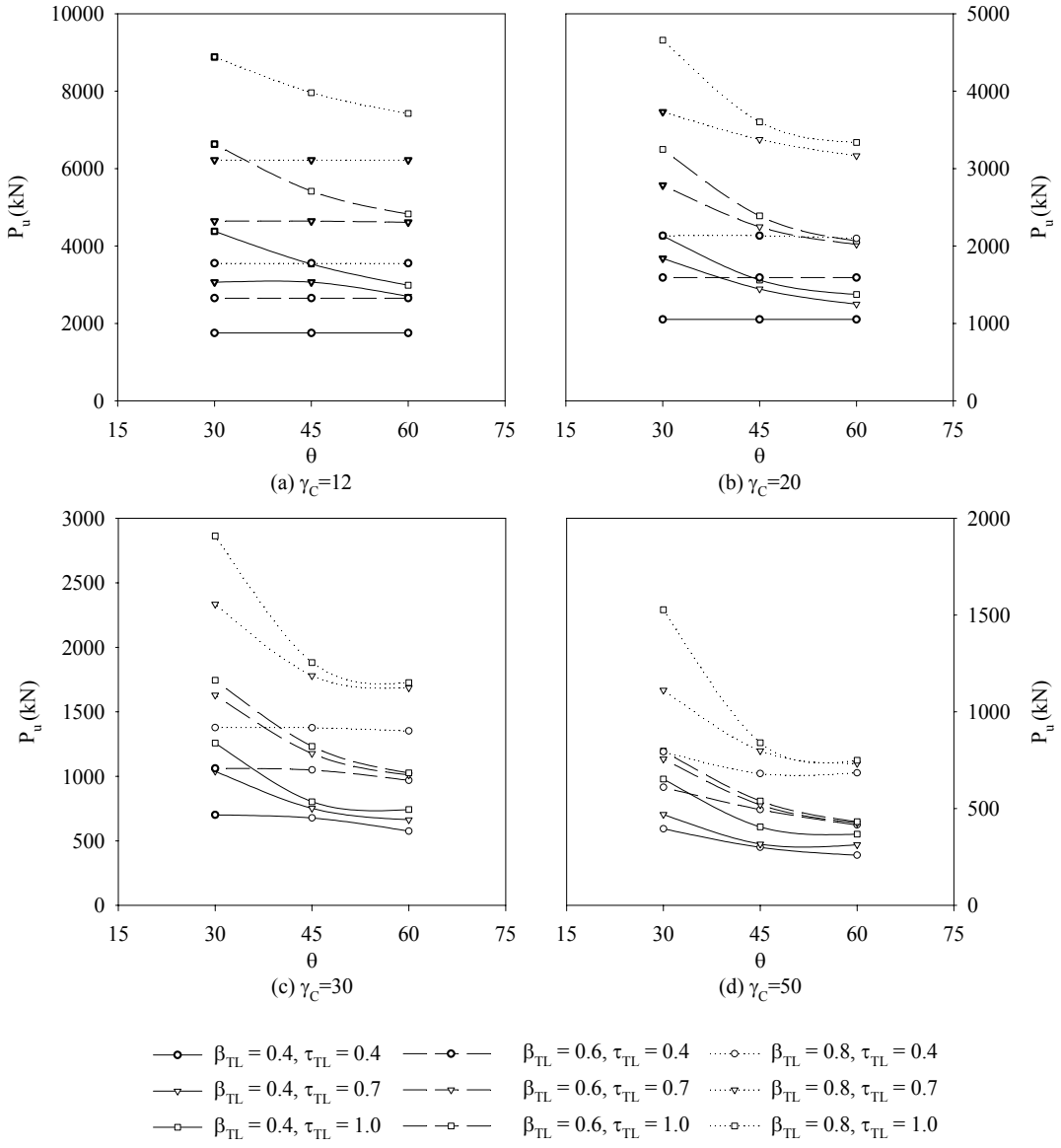

(Constants: $\beta_{CT} = 0.6,\ \tau_{CT} = 0.7, g = 51$mm)

Fig. 6.20 Ultimate strength (brace angle, θ, at small gap size)

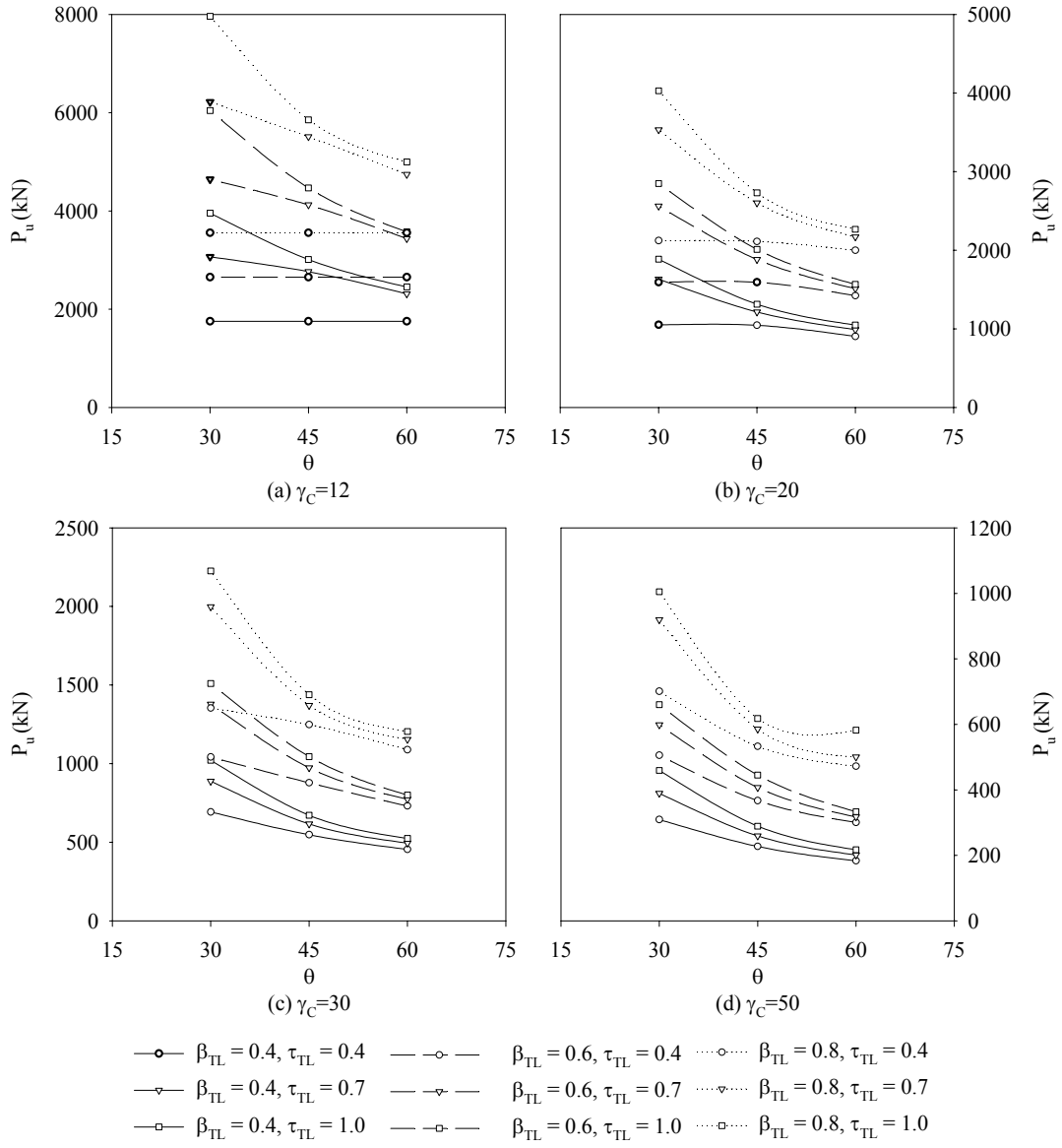

(Constants: $\beta_{CT} = 0.6,\ \tau_{CT} = 0.7,\ \xi = 1.0$)

Fig. 6.21 Ultimate strength (brace angle, θ, at large gap size)

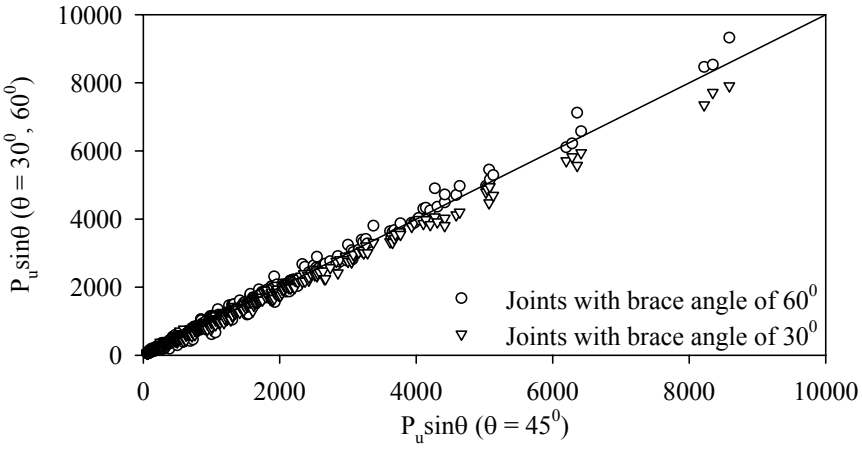

Fig. 6.22 Ultimate strength ($\sin\theta$ factor)

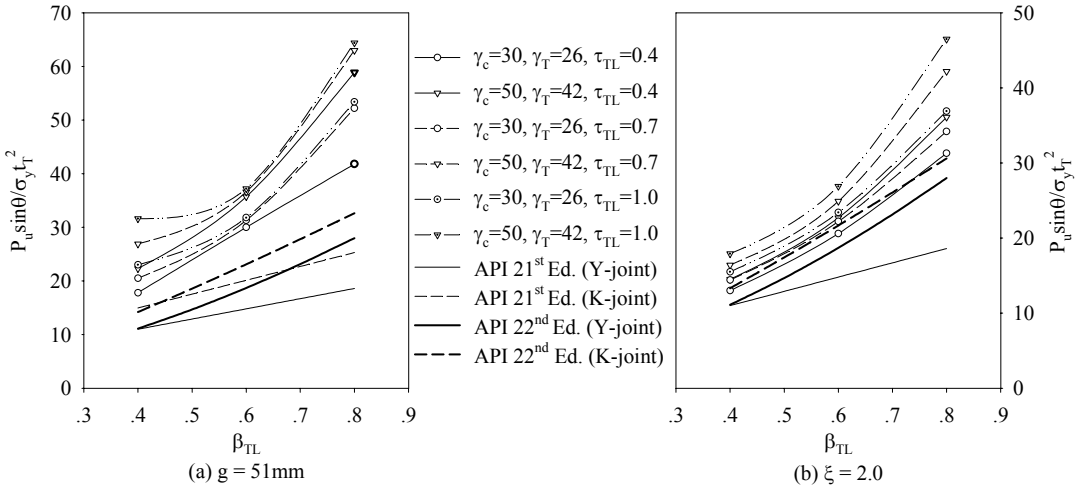

(Constants: $\beta_{CT} = 0.6,\ \tau_{CT} = 0.7,\ \theta = 60^0$)

Fig. 6.23 Comparison of ultimate strength with API RP2A (varying β_{TL})

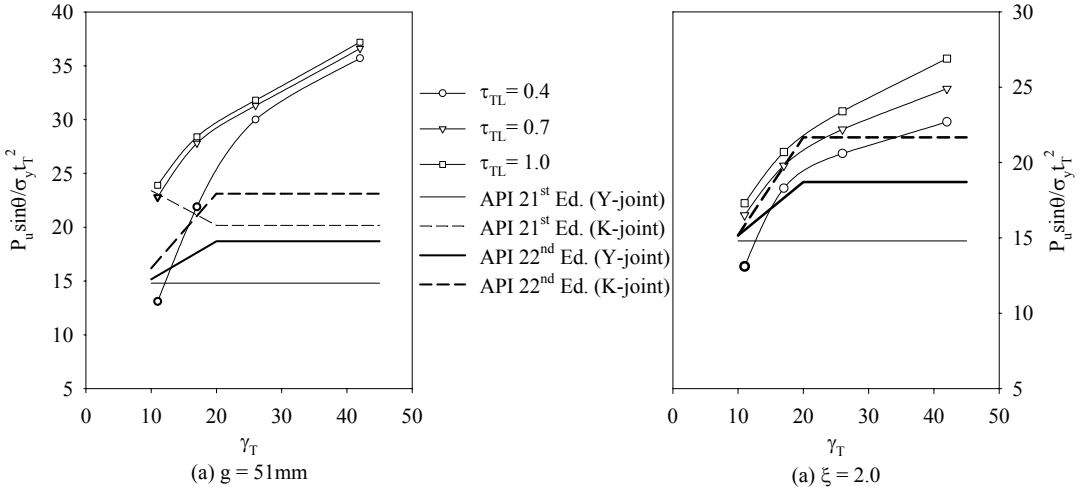

(Constants: $\beta_{CT} = 0.6,\ \tau_{CT} = 0.7,\ \beta_{TL} = 0.6,\ \theta = 60^0$)

Fig. 6.24 Comparison of ultimate strength with API RP2A (varying γ_T)

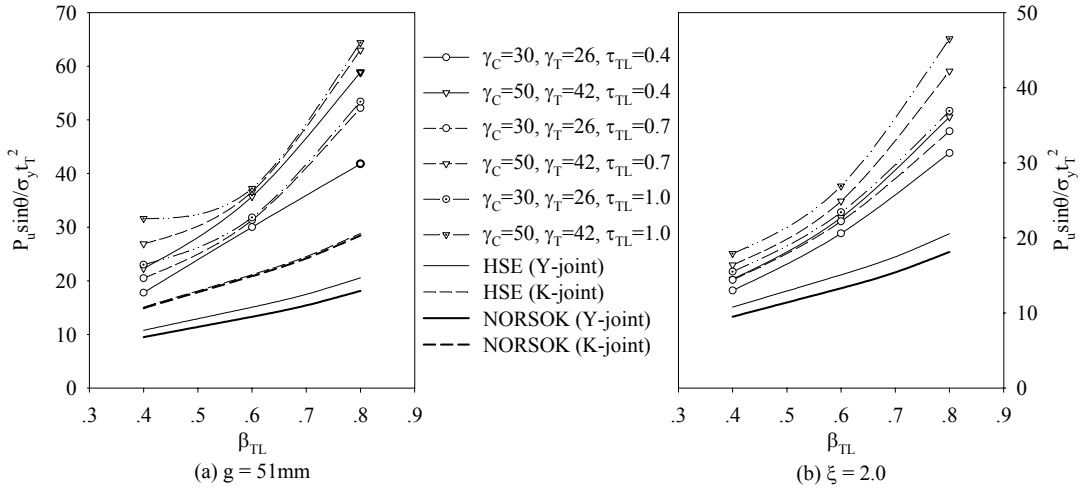

(Constants: $\beta_{CT} = 0.6$, $\tau_{CT} = 0.7$, $\beta_{TL} = 0.6$, $\theta = 60^0$)

Fig. 6.25 Comparison of ultimate strength with HSE and NORSOK (varying β_{TL})

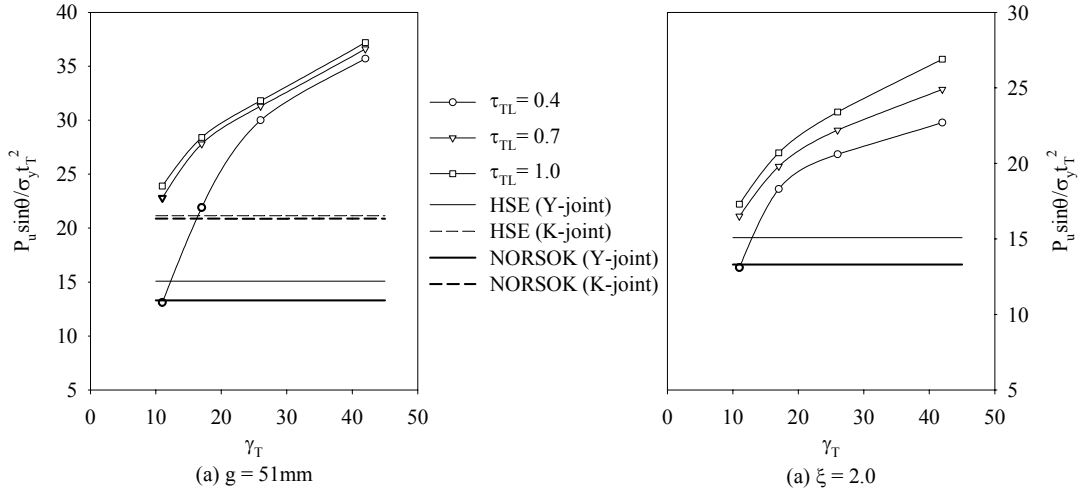

(Constants: $\beta_{CT} = 0.6$, $\tau_{CT} = 0.7$, $\beta_{TL} = 0.6$, $\theta = 60^0$)

Fig. 6.26 Comparison of ultimate strength with HSE and NORSOK (varying γ_T)

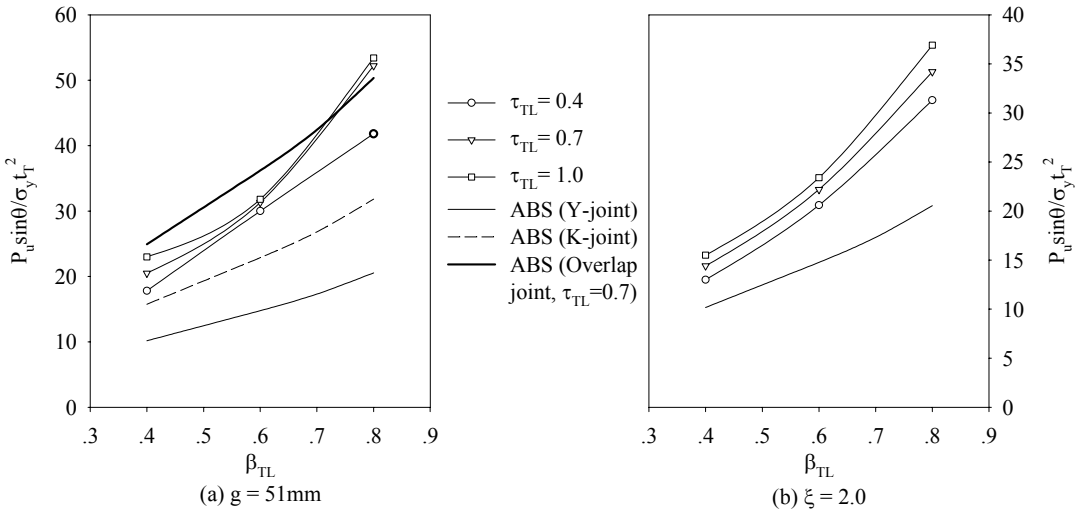

(Constants: $\beta_{CT} = 0.6$, $\tau_{CT} = 0.7$, $\gamma_C = 30$, $\gamma_T = 26$, $\theta = 60^0$)

Fig. 6.27 Comparison of ultimate strength with ABS (varying β_{TL})

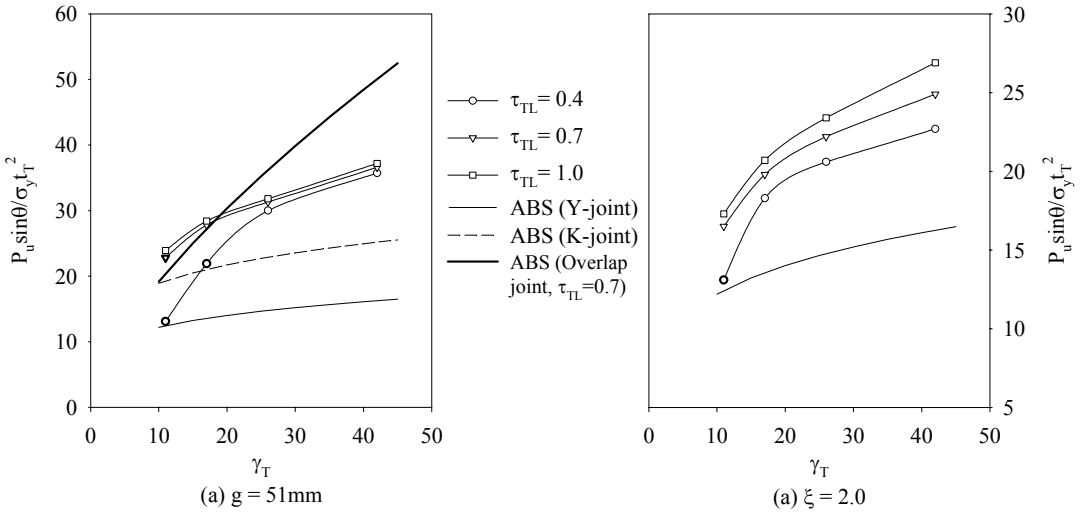

(Constants: $\beta_{CT} = 0.6$, $\tau_{CT} = 0.7$, $\gamma_C = 30$, $\beta_{TL} = 0.6$, $\theta = 60^0$)

Fig. 6.28 Comparison of ultimate strength with ABS (varying γ_T)

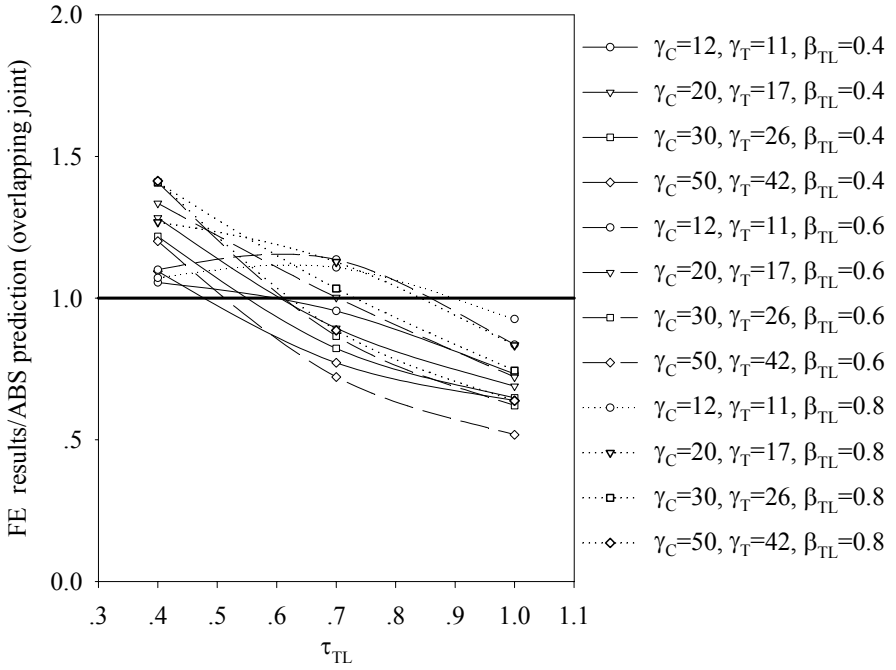

(Constants: $\beta_{CT} = 0.6$, $\tau_{CT} = 0.7$, $\theta = 60^0$)

Fig. 6.29 Comparison of ultimate strength with ABS (varying τ_{TL})

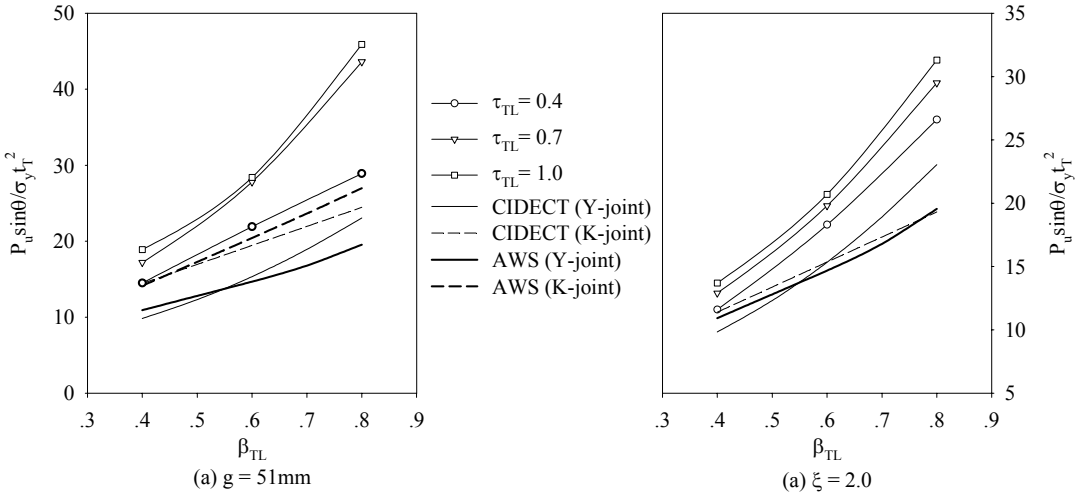

(Constants: $\beta_{CT} = 0.6$, $\tau_{CT} = 0.7$, $\gamma_C = 20$, $\gamma_T = 17$, $\theta = 60^0$)

Fig. 6.30 Comparison of ultimate strength with CIDECT and AWS (varying β_{TL})

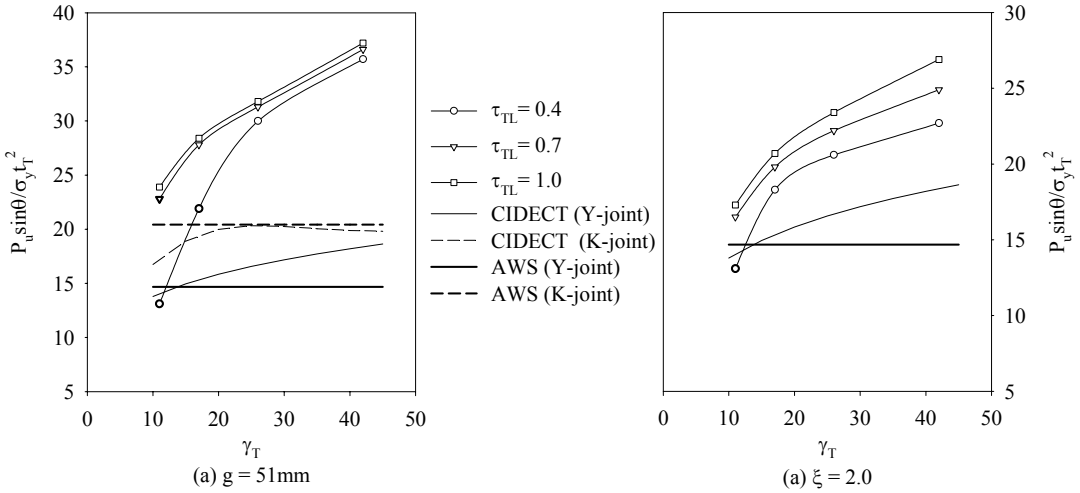

(Constants: $\beta_{CT} = 0.6$, $\tau_{CT} = 0.7$, $\beta_{TL} = 0.6$, $\theta = 60^0$)

Fig. 6.31 Comparison of ultimate strength with CIDECT and AWS (varying γ_T)

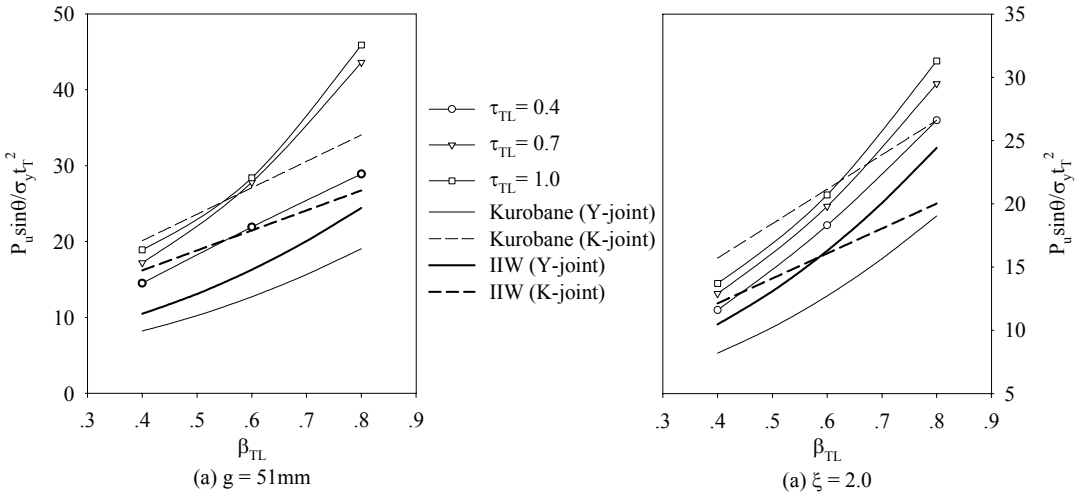

(Constants: $\beta_{CT} = 0.6$, $\tau_{CT} = 0.7$, $\gamma_C = 20$, $\gamma_T = 17$, $\theta = 60^0$)

Fig. 6.32 Comparison of ultimate strength with IIW and Kurobane et al (varying β_{TL})

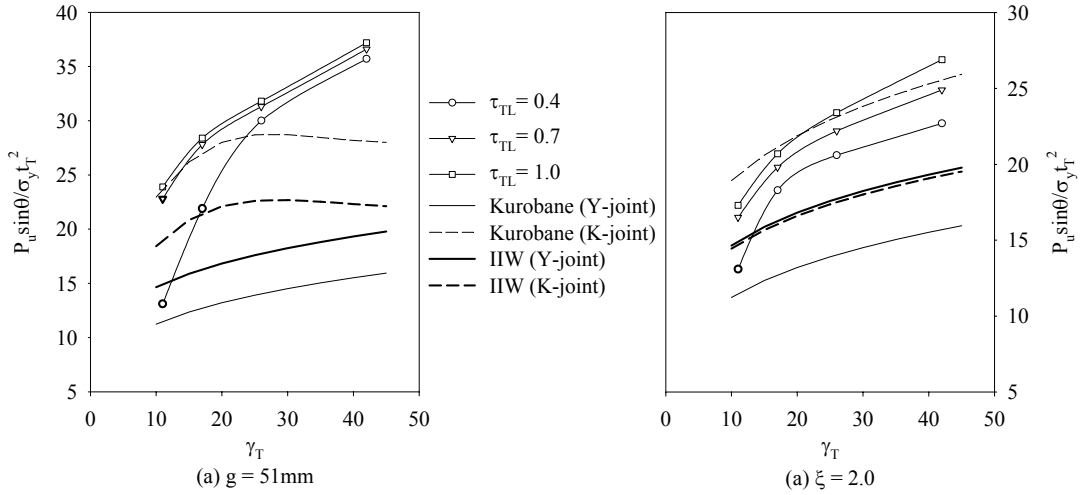

(a) g = 51mm (a) ξ = 2.0

(Constants: β_{CT} = 0.6, τ_{CT} = 0.7, β_{TL} = 0.6, θ = 60^0)

Fig. 6.33 Comparison of ultimate strength with IIW and Kurobane et al (varying γ_T)

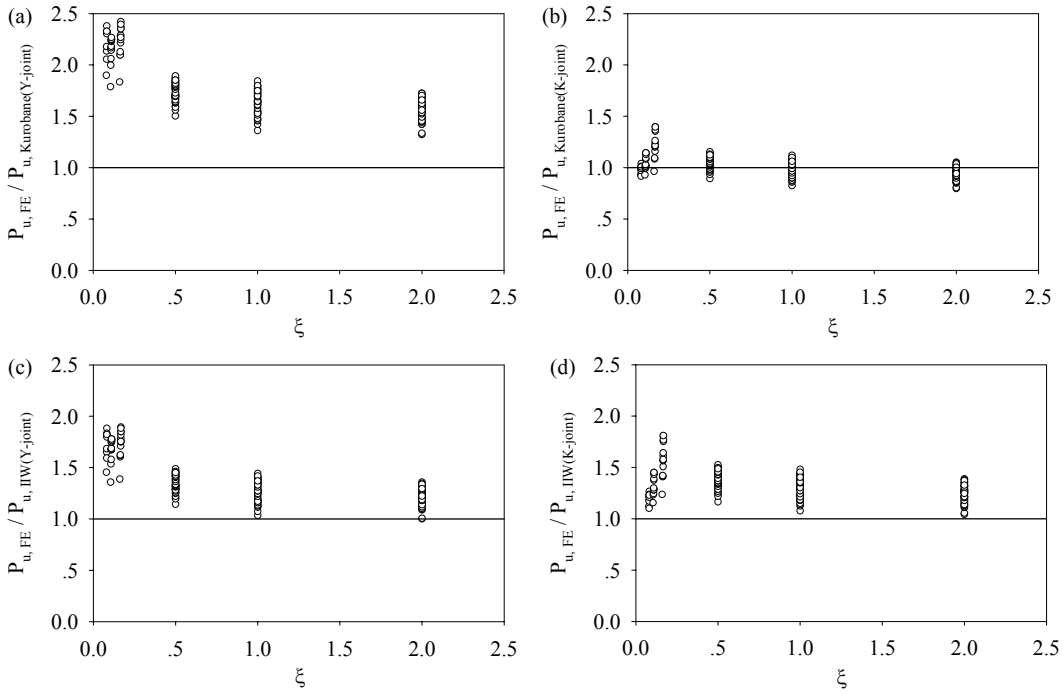

(Constants: β_{TL} = 0.6, θ = 60^0)

Fig. 6.34 Comparison of ultimate strength with IIW and Kurobane et al (varying ξ)

CHAPTER 7

PROPOSED ULTIMATE STRENGTH EQUATIONS

7.1 Introduction

Despite FE analysis has successfully been used as numerical tool for modelling and analysing tubular joints with various geometrical properties under different load conditions, the use of such method for predicting the joint strength in a normal day-to-day design office operation is still not feasible. The reason is that the time taken for modelling the joints can easily be a few hundreds for a typical offshore production steel jacket and the computation time for performing the analysis can be enormous. Instead, parametric equations are developed for predicting the ultimate capacity of tubular joints based on member forces obtained from structural analysis to achieve the time and cost savings.

Owing to the lack of understanding of the structural behaviour of completely overlapped tubular joint, this joint is commonly taken as two separate T/Y-joint configurations and continued with the use of available parametric equations for simple joint design in recommendations. However, it had been commented by Gho (2001) that the completely overlapped tubular joint should not be interpreted as two T/Y-joints as the interaction of stresses among members at the joints and the effect of shell membrane and bending stresses at the short segment of through brace should be considered. The parametric study performed in Chapter 6 showed that the existing equations failed to encompass all the effects of β_{TL}, γ_T, τ_{TL} and gap size in the strength calculation for predicting the ultimate capacity of the completely overlapped tubular joint. Therefore, it is necessary to propose new strength equations based on the FE and test data obtained in the current study to estimate the ultimate capacity of the joint for design. The current proposed strength equations have been verified against the existing database of previous test and FE analysis results.

7.2 Development of parametric equations

7.2.1 Validity ranges

A total of 3888 FE models with various geometrical parameters had been created for the development of parametric equations to anticipate the ultimate strength of completely overlapped tubular joints. The load condition was unbalanced with the joint subjected to lap brace axial compression. It should be noted that the lap-brace-in-compression gave the lowest failure load for the joint with complete overlap of braces (Gho 2001). The boundary conditions of the chord and the through brace were assumed fixed and pinned respectively. The length parameters of the chord (α_c=2L/D) and the through brace (α_T=2l_T/d_T) were set at 14 to eliminate any short member effects. The weld elements were excluded as the FE model without the welds showed reasonable result in comparison with the experimental values. The Young's modulus, the Poisson's ratio, the yield stress and the ultimate tensile stress of steel material were taken as 197kN/mm^2, 0.28, 355kN/mm^2 and 458kN/mm^2, respectively. These stresses were standardised based on that obtained from the experimental study. The ranges of geometrical parameters of the joints were limited as follow.

At the joint intersection of the chord and through brace,

$0.4 \le \beta_{CT} \le 0.8$

$0.4 \le \tau_{CT} \le 1.0$

$12 \le \gamma_C \le 50$

At the joint intersection of the through brace and lap brace,

$0.4 \le \beta_{TL} \le 0.8$

$0.4 \le \tau_{TL} \le 1.0$

$7 \le \gamma_T \le 50$

$30^0 \le \theta \le 60^0$

For the gap size,

$51 \le g \le 2d_T$

7.2.2 Proposed ultimate strength parametric equations

Based on the theoretical ring analogy, the following functions could be used as basis to determine the format of the joint strength equation for axially loaded joints (Wardenier 1982).

$$\begin{cases} P_u = \sigma_y \cdot T^2 \cdot f_1(\beta) \cdot f_2(\gamma) \cdot f_3(\xi) \cdot f_4(\alpha) \cdot f_5(\theta) \cdot f_6(\sigma_m/\sigma_y) \cdot f_7(\sigma_y/\sigma_u) \\ \beta = d/D, \quad \gamma = D/2T, \quad \xi = g/T, \quad \alpha = 2L/D \end{cases} \tag{7.1}$$

In the current study of completely overlapped tubular joint, the length parameters (α_C and α_T) and the material properties of the members were kept constant throughout the analysis. Some of the strength functions could be eliminated and thus, the equation EQ (7.1) could be re-arranged as follow.

$$\frac{P_u \sin\theta}{\sigma_y \cdot t_T^2} = F_1(\beta_{TL}) \cdot F_2(\gamma_T) \cdot F_3(\tau_{TL}) \cdot F_4(\xi) \tag{7.2}$$

A multiple nonlinear regression technique was adopted to define the influence functions F_1 to F_4 in EQ (7.2) based on the database of 2240 FE models obtained in the current analysis, excluding the joints with lap brace failure. The proposed parametric equation for predicting the mean ultimate strength of tubular joints with complete overlap of braces without considering the member failure could be derived as,

$$\frac{P_u \sin\theta}{\sigma_y \cdot t_T^2} = 3.813\left(0.216 + \beta_{TL}^{1.96}\right)\gamma_T^{0.539}\left(0.911 + \tau_{TL}^{0.382}\right)\left(1 + \frac{\gamma_C^{0.189}\tau_{CT}^{-0.228}}{\exp\left(0.06g/t_T + 1.398\right)}\right) \tag{7.3}$$

The comparison of the ultimate capacity of the joint with complete overlap of braces between the values predicted by EQ (7.3) and the FE data showed reasonable accuracy (Table 7.1). However, the ultimate capacity of most of the joints with lap brace failure was found over estimated (Fig. 7.1). In such a case, the joint strength

should be taken as the column strength of the lap brace under axial compression ($P_u \le \sigma_y A$). Furthermore, the equation EQ (7.3) over predicted the ultimate capacity of the joints with lap brace local buckling (Fig. 7.2). It could therefore be commented that EQ (7.3) was more suitable for predicting the ultimate capacity of the joint with through brace wall plastification. This was expected as the proposed equation EQ (7.3) was derived based on the ring model with the assumption of ring plastic collapse.

It should be noted that most of the completely overlapped tubular joints failed by through brace wall plastification under lap brace axial compression. For the joints failed by brace local buckling, Kurobane et al (1986) suggested that the brace local buckling parameter α (= $tE/d\sigma_y$) and the plastic bending deflection of chord wall should be included in the strength equation. The mathematical model below was proposed by Kurobane et al (1986) to calculate the ultimate capacity of the joint with brace local buckling.

$$\frac{P_b}{A\sigma_y} = a\left(\frac{tE}{d\sigma_y}\right)^b \left(\frac{P_u}{A\sigma_y}\right)^c \tag{7.4}$$

where P_b and P_u were the capacities of joints failed by brace local buckling and plastic bending of chord wall, respectively. P_b was obtained from the FE analysis while P_u could be computed from EQ (7.3). The parameters a, b and c were determined using the multiple nonlinear regression method and based on the database of 143 joints failed by lap brace local buckling. The form of the resulted equation for predicting the strength of the joint with local buckling was as follow.

$$\frac{P_b}{A\sigma_y} = 0.76\left(\frac{t_L E}{d_L \sigma_y}\right)^{0.07} \left(\frac{P_u}{A\sigma_y}\right)^{0.48} \tag{7.5}$$

The equation EQ (7.5) predicted very well the FE data (Table 7.1). The EQ (7.5) should be used, particularly, to check the strength of the joints associated with brace

local buckling with high γ_T (>20) and low τ_{TL} (< 0.7).

7.3 Assessment of proposed parametric equations

The joint strength predicted by EQ (7.3) compares reasonably well with the current FE data with average error of 5.3%, as shown in Fig. 7.3. The normal distribution of the resulting histogram of the ratio of current FE data to predicted capacity of the joint is presented in Fig. 7.4. The figure suggested that the proposed parametric equation EQ (7.3) could be converted to a characteristic format for design purpose. The joint strength predicted by EQ (7.3) also compares very well with the test data obtained from Tests 1 and 2 as shown in Fig. 7.3. It was noted from this figure that EQ(7.3) yielded lower but higher ultimate capacity of 6.5% and 4.2% in comparison with Test 1 (current test result) and Test 2 (Fung et al 2001a) respectively.

The FE results of 122 completely overlapped tubular joint models with 45-degree brace angle determined by Fung et al (2001b) were also used as reference for verification. The details of the geometrical parameters of the joints used in their study are summarised in Table 7.2. As could be seen in Fig. 7.5, EQ (7.3) predicts very well the FE data generated by Fung et al (2001b). The minimum and the maximum FE data to predicted mean strength ratios were determined as 0.81 and 1.11, and the mean and coefficient of variation (CoV) were found to be 0.974 and 7.07% respectively.

Dexter and Lee (1999a) carried out extensive FE study to determine the ultimate capacity of overlap tubular K-joints under balanced axial loading with through brace in compression. Thirty-six K-joints with more than 100% overlap were included in their investigation. The FE results of 23 number 60^0-60^0 axially loaded 100% overlap K-joints with $7<\gamma_T<50$ were used for verification of the current proposed equation EQ (7.3). Those joints failed by member collapse were excluded. The comparison of the ultimate capacity of the joint between the proposed parametric equation and the FE results of Dexter and Lee was shown in Table 7.3. It

could be commented from this table that the proposed equation predicted reasonably well most of the ultimate capacity of 100% overlap joints within 15% with mean error of 16.5%.

As shown in Fig. 7.6, EQ (7.3) gives better strength prediction for the joints with small γ_T. It was important to realise that the load condition of the joints investigated by Dexter and Lee (1999a) were balanced with through brace-in-compression and lap brace-in-tension. Furthermore, the geometrical properties of the two braces were identical. However, the reasonable prediction of joint strength implied that the proposed equation EQ (7.3) based on lap brace-in-compression was still applicable for predicting the ultimate capacity of the joints under balanced loading with through brace-in-compression and lap brace-in-tension.

The design guide CIDECT (Wardenier et al 1993) also provided formulation for predicting the strength of tubular joint with 100% overlap. However, the formulation was valid for joints with eccentricity of -0.55 times the chord diameter (D). For the 100% overlap joints investigated by Dexter and Lee (1999a), the eccentricity of -0.587D was outside the validity limit specified by CIDECT. If the CIDECT formulation was used for comparison, the ultimate capacity of the completely overlapped tubular joint would have been under estimated by about 38.7%.

For the joints failed by brace local buckling, the strength predicted by EQ (7.5) compares reasonably well with the current FE data with average difference of 4.3%, as shown in Fig. 7.7.

7.4 Simplification of proposed parametric equation

The proposed strength equation described in the previous section predicted very well the ultimate capacity of completely overlapped tubular joints. However, the constants in the formulation should be simplified so that the proposed equation EQ(7.3) could easily be used for design. In the process of simplification, an analysis

was conducted based on the statistical data generated from the predicted equation and the FE models so that the individual constant in the formulation could be adjusted with sufficient accuracy. The simplified strength equation with modification of individual constant could be seen below.

$$\frac{P_u \sin\theta}{\sigma_y \cdot t_T^2} = 3.78\gamma_T^{0.54}\left(0.2+\beta_{TL}^2\right)\left(1+\tau_{TL}^{0.4}\right)\left(1+\frac{\left(\gamma_C/\tau_{CT}\right)^{0.2}}{\exp\left(0.06g/t_T+1.4\right)}\right) \tag{7.6}$$

The constant 3.78 given in the above equation was included to maintain the same mean value with that of the original strength equation. The accuracy of this formula for predicting the ultimate capacity of the completely overlapped tubular joint is shown in Table 7.4. The overall performance of EQ (7.6) in comparison with the original equation against the FE database is illustrated in Table 7.5. It could be seen from these tables that the scatter of data with use of EQ (7.6) increased but the mean strength prediction remained as in the original proposed equation. However, the scatter of data increased was small, only about 4%. Hence, it could be concluded from the comparison of these two proposed equations that the simplified strength equation EQ (7.6) gave reasonable prediction of the ultimate capacity of the completely overlapped tubular joint under axial loading.

7.5 Determination of characteristic strength

In order for the proposed equation EQ (7.6) to be used in the limit state design, it should be converted to the characteristic format through a semi-probabilistic analysis. In the process, the mean bias factor was calculated based only on the test data. However, for the completely overlapped tubular joint, the available test data was very limited and was not sufficient to form a database for the derivation of strength equation in characteristic format. In the current study, the characteristic equation was evaluated based on the data obtained from the FE models calibrated against the experimental results. The comparison with the FE database and the experimental data revealed that the proposed simplified equation EQ (7.6) yielded mean strength value of 1.005 with CoV of 0.0673. Based on the semi-probabilistic

analysis, the lowest 5% fractile $x_{5\%}$ could be calculated as,

$$x_{5\%} = \mu(1-\kappa \cdot CoV) = 1.005(1-1.645\times 0.0673) = 0.89 \quad (7.7)$$

where μ and κ were the population mean and the probability of coefficient, respectively. As the previous study showed that the FE data to predicted strength ratio gave approximate normal distribution, κ could be taken as 1.645. Thus, the characteristic strength of the joint based on 5% probability could be obtained by multiplying the proposed simplified equation EQ (7.6) with 0.89.

7.6 Comparison with existing strength equations

A comparison of the ultimate capacity of the joint was conducted based on the proposed characteristic strength equation and the existing T/Y- and gap K-joint equations to investigate the difference. The joint strength predicted by T/Y-joint's equations versus the parameter β_{TL} of completely overlapped tubular joint is shown in Fig. 7.8. The geometrical parameters τ_{CT} (= 0.7), γ_C (= 17), τ_{TL} (= 0.7), γ_T (= 17) remained constant throughout the analysis. Two cases of gap sizes, g = 51mm and $2d_{T,}$ were considered. It was noted that the validity range of β_{TL} of these existing design codes was 0.2 to 1.0. Despite the proposed equation was developed based on the database of the joints with β_{TL} ranging from 0.4 to 0.8, the validity range of 0.2 and 1.0 were also considered in the comparison to assess the applicability of the proposed equation for predicting the ultimate strength of the joints.

It could be seen from Fig. 7.8 that the proposed characteristic equation predicts the joint strength with varying β similar to that of existing design formulae. The comparison of the joint strength from these equations suggested that the proposed equation could still be used for predicting the ultimate capacity of joints at β_{TL} = 0.2 and 1.0.

At small gap size (g = 51mm), all the existing T/Y-joint equations under predicted

the ultimate capacity of the completely overlapped joint. At large gap size ($g = 2d_T$), the joint could be regarded as two Y-joint configurations as the strength was equivalent to that predicted by T/Y-joint's equation. It should also be noted that the design formula of API RP2A (Marshall 2004) over predicted the ultimate capacity of the completely overlapped tubular joint particularly at large β_{TL}. The proposed equation showed almost the same strength as that predicted by IIW (1981). It could therefore be concluded from the above comparison that the proposed characteristic equation of completely overlapped tubular joint was applicable for predicting the ultimate capacity of simple Y/T-joints.

The joint strength predicted by K-joint's equation versus the parameter β_{TL} of completely overlapped tubular joint is shown in Fig. 7.9. The geometrical parameters were identical to those used in the comparison with Y/T-joints. For the joints at small gap size, the strength predicted by the proposed equation was similar to that by the existing equation with $\beta_{TL} < 0.6$. For the joints with $\beta_{TL} > 0.6$, the proposed equation yielded higher strength owing to parabolic relationship of β_{TL}. The strength increase of completely overlapped tubular joint at $\beta_{TL} > 0.6$ under lap brace axial compression was due to chord bending. A similar behaviour for the joints at large gap size was observed except the equation in API RP2A (Marshall 2004). Overall, the joint strength predicted by the proposed equation was closed to that by the existing K-joint's equation except the joints with $\beta_{TL} > 0.6$ (except for API equation).

The joint strength predicted by T/Y-joint's equation versus the parameter γ_T of completely overlapped tubular joint is shown in Fig. 7.10. The geometrical parameters τ_{CT} (= 0.7), γ_C (= 17), τ_{TL} (= 0.7) and β_{TL} (= 0.6) remained constant throughout the analysis. Two cases of gap size g = 51 and $2d_T$ were considered. For the onshore design guides, CIDECT (1991) and AISC (2003), the parameter γ_T was limited to 25.

The strength of the joint predicted by the proposed equation showed great difference with that computed by the existing equations specified in

recommendations, particularly for the joints with large γ_T. At small gap size, the proposed equation predicted higher strength for the completely overlapped tubular joint. However, at large gap size, the proposed equation only predicted higher strength for joints with $\gamma_T > 25$. Thus, the proposed equation could still be used for predicting the ultimate capacity of simple Y/T-joints provided that the parameter γ_T was less than 25. A similar result can be observed from the comparison of ultimate capacity with the K-joint equations shown in Fig. 7.11.

7.7 Concluding remarks

A new set of parametric equations has been proposed based on 3888 FE models for predicting the ultimate capacity of tubular joints with complete overlap of braces under lap brace axial loading. The validity ranges of the geometrical parameters of the joint are adequately covered for the parametric study. The comparison with the test and FE data showed that the proposed equations accurately predict the ultimate capacity of the joints. A simplified strength equation in characteristic format is also developed for limit state design. However, the proposed characteristic strength equation is only verified against the FE database as the experimental data is not sufficient for comparison. A comparison of the ultimate capacity between the proposed characteristic equation and the existing equations in recommendations indicated that the proposed equation is applicable for predicting the ultimate capacity of simple T/Y-joints with the condition that $\gamma_T < 25$.

Table 7.1 Regression analysis of FE model to predicted capacities

Failure type	Prediction equation	Number of data points	R^2 (%)	Min	Max	Mean	CoV
Through brace wall plastification	EQ (7.3)	2240	96.8	0.83	1.16	1.005	6.45×10^{-2}
Lap brace local buckling	EQ (7.5)	143	95.9	0.89	1.11	1.000	5.39×10^{-2}

Table 7.2 Geometrical parameters of joints (Fung et al 2001b)

β_{CT}	τ_{CT}	γ_C	β_{TL}	τ_{TL}	γ_T	g/t_T	P_u (kN)	β_{CT}	τ_{CT}	γ_C	β_{TL}	τ_{TL}	γ_T	g/t_T	P_u (kN)
0.29	0.29	12	0.77	0.76	11.8	5.4	1316	0.45	0.73	24	0.62	0.76	14.7	44	838
0.29	0.29	12	0.77	0.76	11.8	11.8	1126	0.45	0.73	24	0.62	0.76	14.7	58.7	822
0.29	0.29	12	0.77	0.76	11.8	23.6	1092	0.45	0.73	24	0.62	0.76	14.7	73.4	821
0.29	0.29	12	0.77	0.76	11.8	35.3	1093	0.45	0.73	24	0.62	0.76	14.7	88.1	826
0.29	0.37	15	0.77	0.76	11.8	5.4	1324	0.45	0.73	24	0.62	0.76	14.7	103	834
0.29	0.37	15	0.77	0.76	11.8	11.8	1132	0.53	0.37	15	0.41	0.76	21.8	5.4	835
0.29	0.37	15	0.77	0.76	11.8	23.6	1092	0.53	0.37	15	0.41	0.76	21.8	21.8	734
0.29	0.37	15	0.77	0.76	11.8	35.3	1088	0.53	0.37	15	0.41	0.76	21.8	43.7	687
0.29	0.37	15	0.77	0.76	11.8	47.1	1085	0.53	0.37	15	0.41	0.76	21.8	65.5	652
0.29	0.37	15	0.77	0.76	11.8	58.9	1086	0.53	0.37	15	0.41	0.76	21.8	87.4	630
0.29	0.37	15	0.77	0.76	11.8	70.7	1083	0.53	0.37	15	0.41	0.76	21.8	109	619
0.29	0.49	20	0.77	0.76	11.8	5.4	1328	0.53	0.37	15	0.41	0.76	21.8	131	617
0.29	0.49	20	0.77	0.76	11.8	11.8	1137	0.6	0.73	18	0.62	0.76	14.7	5.4	985
0.29	0.49	20	0.77	0.76	11.8	23.6	1088	0.6	0.73	18	0.62	0.76	14.7	14.7	906
0.29	0.49	20	0.77	0.76	11.8	35.3	1076	0.6	0.73	18	0.62	0.76	14.7	29.4	859
0.29	0.73	30	0.77	0.76	11.8	5.4	1319	0.6	0.73	18	0.62	0.76	14.7	44	830
0.29	0.73	30	0.77	0.76	11.8	11.8	1133	0.6	0.73	18	0.62	0.76	14.7	58.7	816
0.29	0.73	30	0.77	0.76	11.8	23.6	1068	0.6	0.73	18	0.62	0.76	14.7	73.4	815
0.29	0.73	30	0.77	0.76	11.8	35.3	1048	0.6	0.73	18	0.62	0.76	14.7	88.1	820
0.36	0.29	12	0.62	0.76	14.7	5.4	1046	0.6	0.73	18	0.62	0.76	14.7	103	828
0.36	0.29	12	0.62	0.76	14.7	14.7	925	0.67	0.29	12	0.33	0.76	27.3	5.4	724
0.36	0.29	12	0.62	0.76	14.7	29.4	893	0.67	0.29	12	0.33	0.76	27.3	27.3	616
0.36	0.29	12	0.62	0.76	14.7	44	871	0.67	0.29	12	0.33	0.76	27.3	54.6	564
0.36	0.37	15	0.62	0.76	14.7	5.4	1048	0.67	0.29	12	0.33	0.76	27.3	81.9	530
0.36	0.37	15	0.62	0.76	14.7	5.4	1056	0.67	0.37	15	0.33	0.76	27.3	5.4	725
0.36	0.37	15	0.62	0.76	14.7	14.7	926	0.67	0.37	15	0.33	0.76	27.3	27.3	610
0.36	0.37	15	0.62	0.76	14.7	14.7	926	0.67	0.37	15	0.33	0.76	27.3	54.6	557
0.36	0.37	15	0.62	0.76	14.7	14.7	927	0.67	0.37	15	0.33	0.76	27.3	81.9	524
0.36	0.37	15	0.62	0.76	14.7	29.4	880	0.67	0.37	15	0.33	0.76	27.3	109	505
0.36	0.37	15	0.62	0.76	14.7	29.4	890	0.67	0.37	15	0.33	0.76	27.3	137	497
0.36	0.37	15	0.62	0.76	14.7	29.4	892	0.67	0.37	15	0.33	0.76	27.3	164	496
0.36	0.37	15	0.62	0.76	14.7	44	862	0.67	0.49	20	0.33	0.76	27.3	5.4	728
0.36	0.37	15	0.62	0.76	14.7	44	867	0.67	0.49	20	0.33	0.76	27.3	27.3	603
0.36	0.37	15	0.62	0.76	14.7	58.7	845	0.67	0.49	20	0.33	0.76	27.3	54.6	544
0.36	0.37	15	0.62	0.76	14.7	73.4	841	0.67	0.49	20	0.33	0.76	27.3	81.9	514
0.36	0.37	15	0.62	0.76	14.7	88.1	843	0.67	0.5	15	0.33	0.56	20	3.9	1173
0.36	0.49	20	0.62	0.76	14.7	5.4	1050	0.67	0.5	15	0.33	0.56	20	20	992
0.36	0.49	20	0.62	0.76	14.7	14.7	928	0.67	0.5	15	0.33	0.56	20	40	918
0.36	0.49	20	0.62	0.76	14.7	29.4	887	0.67	0.5	15	0.33	0.56	20	60	875
0.36	0.49	20	0.62	0.76	14.7	44	858	0.67	0.5	15	0.33	0.56	20	80	838
0.36	0.5	15	0.62	0.56	10.8	3.9	1546	0.67	0.5	15	0.33	0.56	20	100	837
0.36	0.5	15	0.62	0.56	10.8	10.8	1466	0.67	0.5	15	0.33	0.56	20	120	838
0.36	0.5	15	0.62	0.56	10.8	21.5	1394	0.67	0.63	15	0.33	0.45	16	3.1	1584
0.36	0.5	15	0.62	0.56	10.8	32.3	1360	0.67	0.63	15	0.33	0.45	16	16	1388
0.36	0.5	15	0.62	0.56	10.8	43	1337	0.67	0.63	15	0.33	0.45	16	31.9	1317
0.36	0.5	15	0.62	0.56	10.8	53.8	1332	0.67	0.63	15	0.33	0.45	16	47.9	1271
0.36	0.5	15	0.62	0.56	10.8	64.5	1331	0.67	0.63	15	0.33	0.45	16	63.9	1245
0.36	0.73	30	0.62	0.76	14.7	5.4	1045	0.67	0.63	15	0.33	0.45	16	79.9	1234
0.36	0.73	30	0.62	0.76	14.7	14.7	921	0.67	0.63	15	0.33	0.45	16	95.8	1238
0.36	0.73	30	0.62	0.76	14.7	14.7	921	0.67	0.73	30	0.33	0.76	27.3	5.4	729
0.36	0.73	30	0.62	0.76	14.7	29.4	870	0.67	0.73	30	0.33	0.76	27.3	27.3	593
0.36	0.73	30	0.62	0.76	14.7	29.4	874	0.67	0.73	30	0.33	0.76	27.3	54.6	531
0.36	0.73	30	0.62	0.76	14.7	44	843	0.67	0.73	30	0.33	0.76	27.3	81.9	503
0.36	0.73	30	0.62	0.76	14.7	44	843	0.77	0.73	14	0.62	0.76	14.7	5.4	960
0.36	0.73	30	0.62	0.76	14.7	58.7	828	0.77	0.73	14	0.62	0.76	14.7	14.7	897
0.36	0.73	30	0.62	0.76	14.7	73.4	825	0.77	0.73	14	0.62	0.76	14.7	29.4	854
0.36	0.73	30	0.62	0.76	14.7	88.1	829	0.77	0.73	14	0.62	0.76	14.7	44	826
0.36	0.73	30	0.62	0.76	14.7	103	837	0.77	0.73	14	0.62	0.76	14.7	58.7	812
0.45	0.73	24	0.62	0.76	14.7	5.4	1016	0.77	0.73	14	0.62	0.76	14.7	73.4	811
0.45	0.73	24	0.62	0.76	14.7	14.7	915	0.77	0.73	14	0.62	0.76	14.7	88.1	817
0.45	0.73	24	0.62	0.76	14.7	29.4	865	0.77	0.73	14	0.62	0.76	14.7	103	825

Note: E=197GPa, σ_y=374MPa, σ_u=457MPa, $\alpha_C = \alpha_T$=12, α_L=6, $\theta = 45^0$.

Table 7.3 Assessment of equation with FE data of Dexter & Lee (1999a)

β_{CT}	τ_{CT}	γ_C	β_{TL}	τ_{TL}	γ_T	g (mm)	P_u (kN) (Dexter & Lee)	P_u (kN) (EQ7.3)	P_u (kN) (CIDECT)	Error (%)[a] (EQ7.3)	Error (%)[b] (CIDECT)
0.4	0.4	8	1	1	8	100	6530	6745	2108	3.3	-67.7
0.4	0.4	20	1	1	20	100	2360	1691	588	-28.3	-75.1
0.4	0.4	35	1	1	35	100	1310	698	311	-46.7	-76.3
0.4	1	20	1	1	8	100	6820	6682	3677	-2.0	-46.1
0.4	1	35	1	1	14	100	3490	2898	1942	-17.0	-44.3
0.4	1	50	1	1	20	100	2290	1677	1367	-26.7	-40.3
0.4	1.5	35	1	1	9	100	5220	5299	4370	1.5	-16.3
0.4	1.5	50	1	1	13	100	3510	3108	3075	-11.5	-12.4
0.7	0.4	8	1	1	14	100	10300	9125	3207	-11.4	-68.9
0.7	0.4	20	1	1	35	100	3910	2288	895	-41.5	-77.1
0.7	1	20	1	1	14	100	10400	9039	5591	-13.1	-46.2
0.7	1	35	1	1	25	100	5320	3920	2953	-26.3	-44.5
0.7	1	50	1	1	35	100	3530	2269	2078	-35.7	-41.1
0.7	1.5	20	1	1	9	100	15200	16284	12579	7.1	-17.2
0.7	1.5	35	1	1	16	100	7950	7168	6645	-9.8	-16.4
0.7	1.5	50	1	1	23	100	5290	4204	4675	-20.5	-11.6
1	0.4	8	1	1	20	100	12800	11063	4304	-13.6	-66.4
1	1	8	1	1	8	100	41100	41444	26903	0.8	-34.5
1	1	20	1	1	20	100	12200	10959	7504	-10.2	-38.5
1	1	35	1	1	35	100	6230	4753	3964	-23.7	-36.4
1	1.5	20	1	1	13	100	17700	19742	16885	11.5	-4.6
1	1.5	35	1	1	23	100	9100	8691	8919	-4.5	-2.0
1	1.5	50	1	1	33	100	5910	5097	6276	-13.7	6.2

[a]Mean of absolute value = 16.5%, [b]Mean of absolute value = 38.7%

Note: Joint material is ASTM A36, σ_y=254MPa, σ_u=405MPa (Dexter & Lee 1999a)

Table 7.4 Simplification of proposed mean strength equation

Constants		Statistics results for numerical/predicted ratios			
Original	Simplified	Min	Max	Mean	CoV
0.216	0.2	0.85	1.22	1.035	6.59
1.960	2	0.84	1.19	1.017	6.50
0.539	0.54	0.82	1.16	1.002	6.46
0.911	1	0.79	1.12	0.958	6.46
0.382	0.4	0.83	1.17	1.007	6.46
0.189	0.2	0.83	1.16	1.002	6.50
-0.228	-0.2	0.83	1.17	1.006	6.44
1.398	1.4	0.83	1.17	1.005	6.45
0.060	0.06	0.83	1.17	1.005	6.45
3.813	3.78	0.83	1.18	1.014	6.45

Table 7.5 Comparison of proposed with its simplified strength equation

Statistics	EQ(7.3)	EQ(7.6)
Data number	2240	2240
Mean	1.005	1.005
St Dev	6.49×10^{-2}	6.76×10^{-2}
CoV	6.45×10^{-2}	6.73×10^{-2}
Min	0.83	0.82
Max	1.16	1.18
Range	0.33	0.36

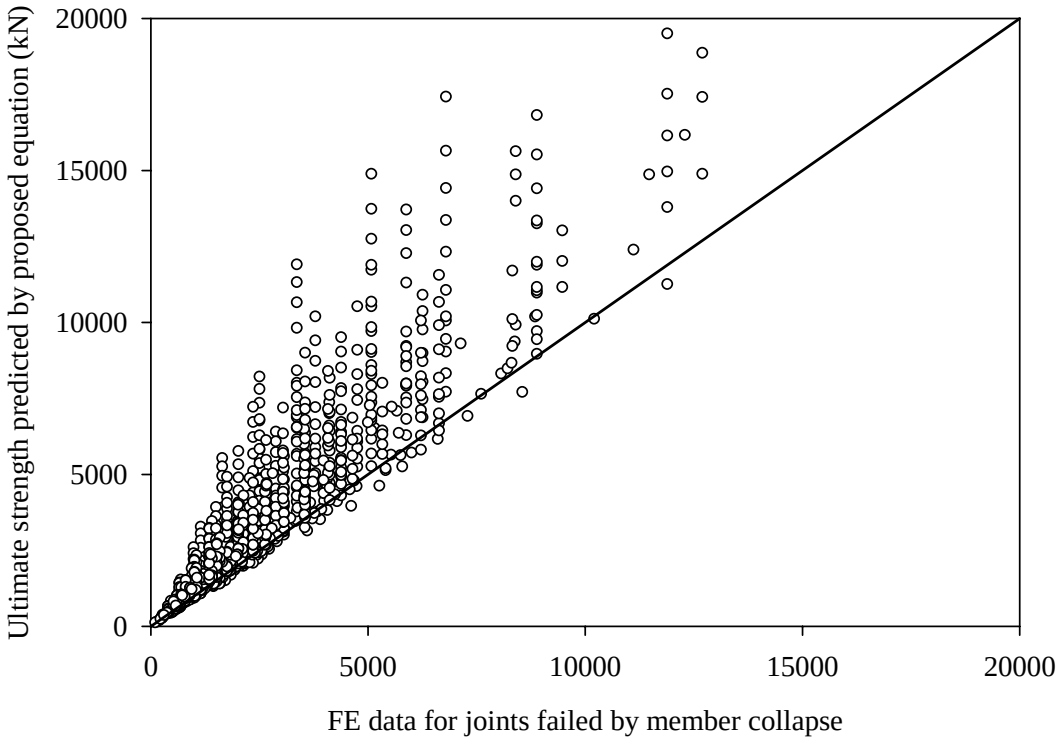

Fig. 7.1 Performance of proposed equation - prediction of ultimate capacity of joints failed by member collapse

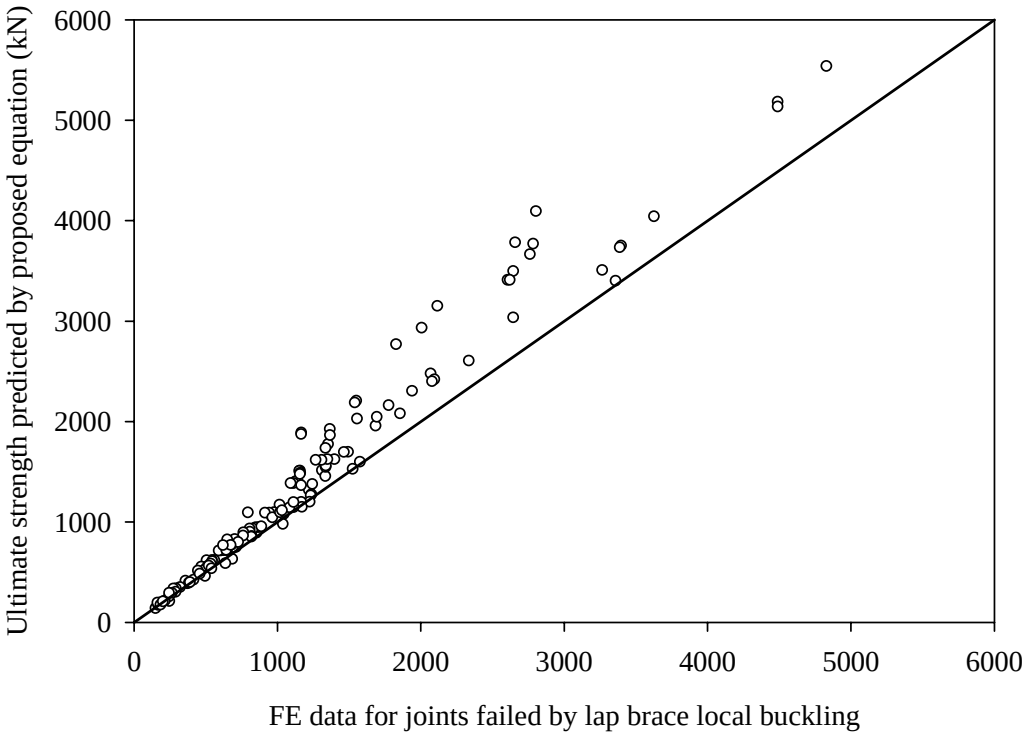

Fig. 7.2 Performance of proposed equation - prediction of ultimate capacity of joints failed by lap brace local buckling

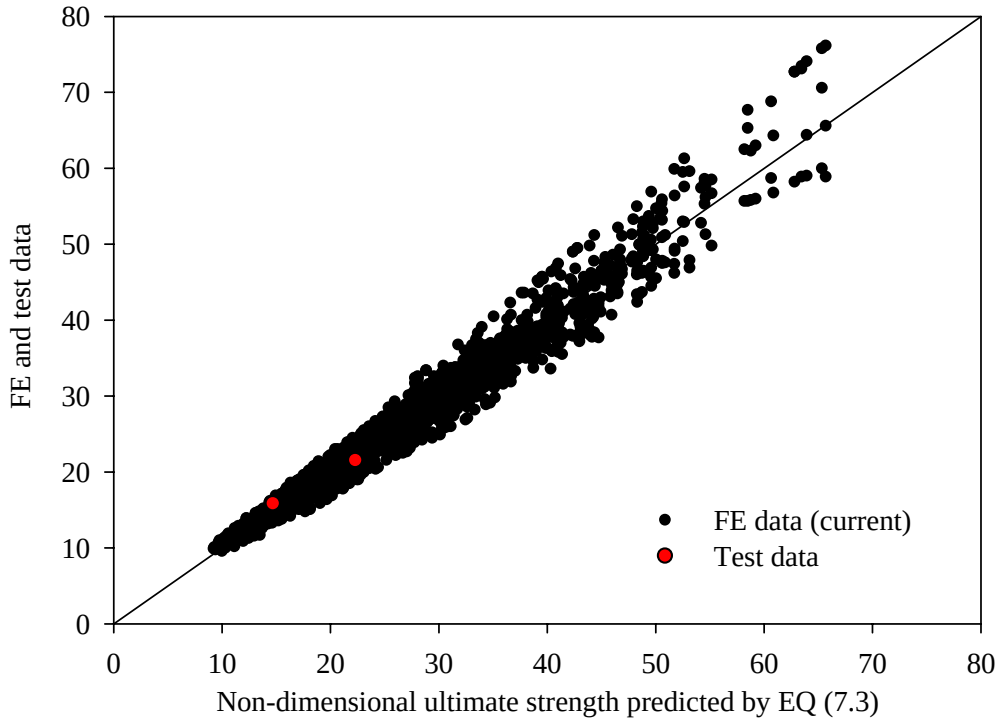

Fig. 7.3 Assessment of proposed equation with current FE and test data

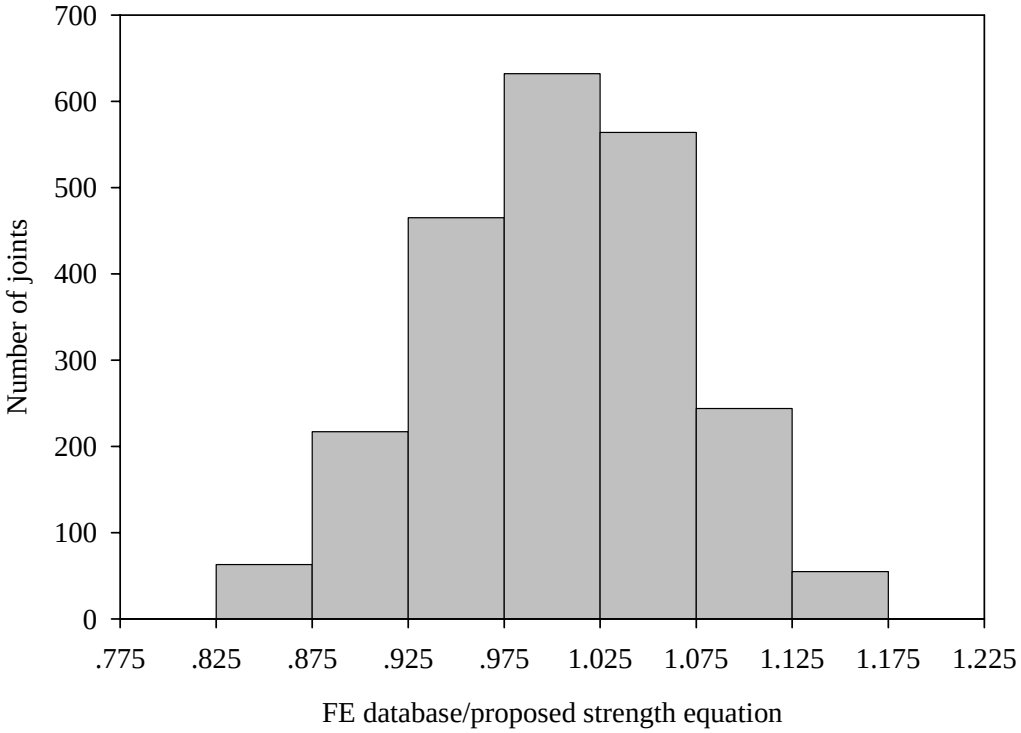

Fig. 7.4 Ultimate capacity of completely overlapped tubular joint – FE data/proposed equation

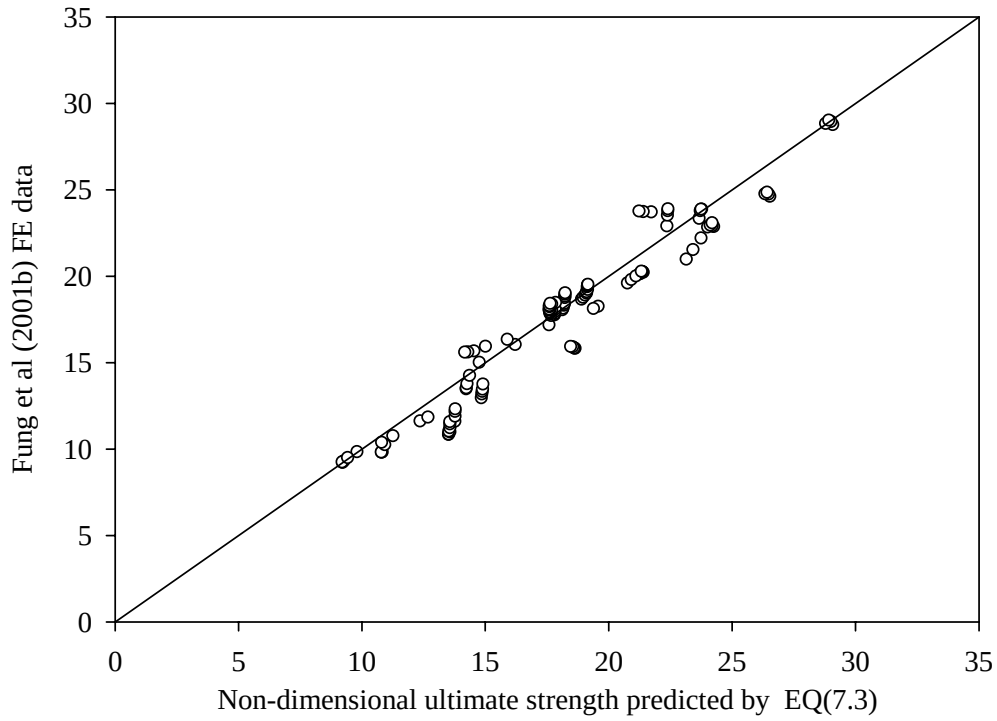

Fig. 7.5 Assessment of proposed equation with Fung et al (2001b) FE data

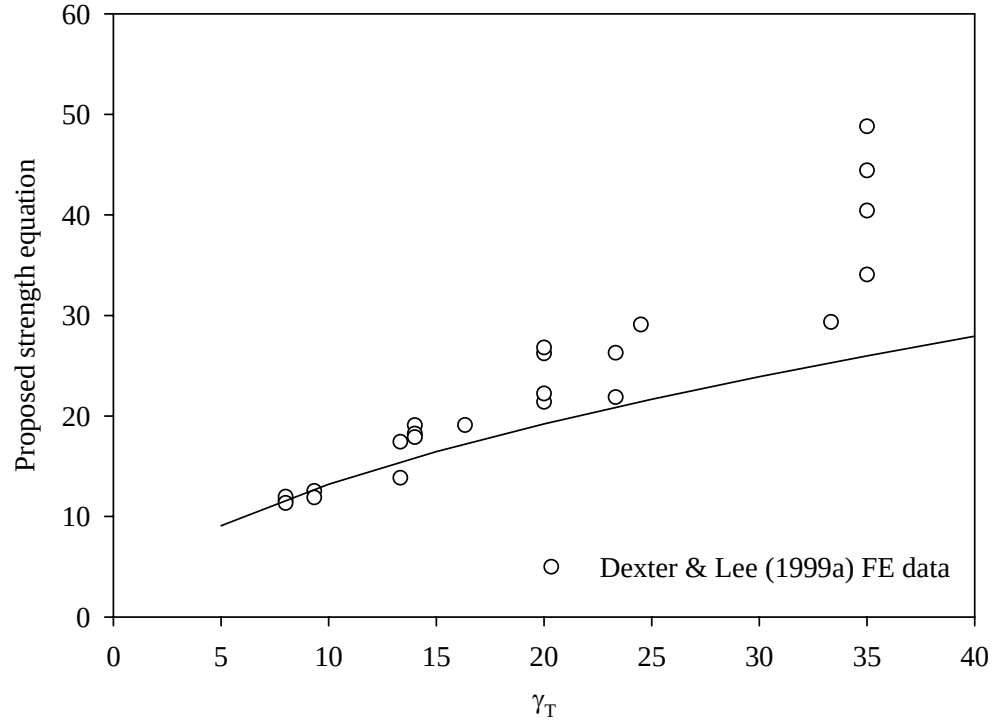

Fig. 7.6 Assessment of proposed equation with Dexter & Lee (1999a) FE data

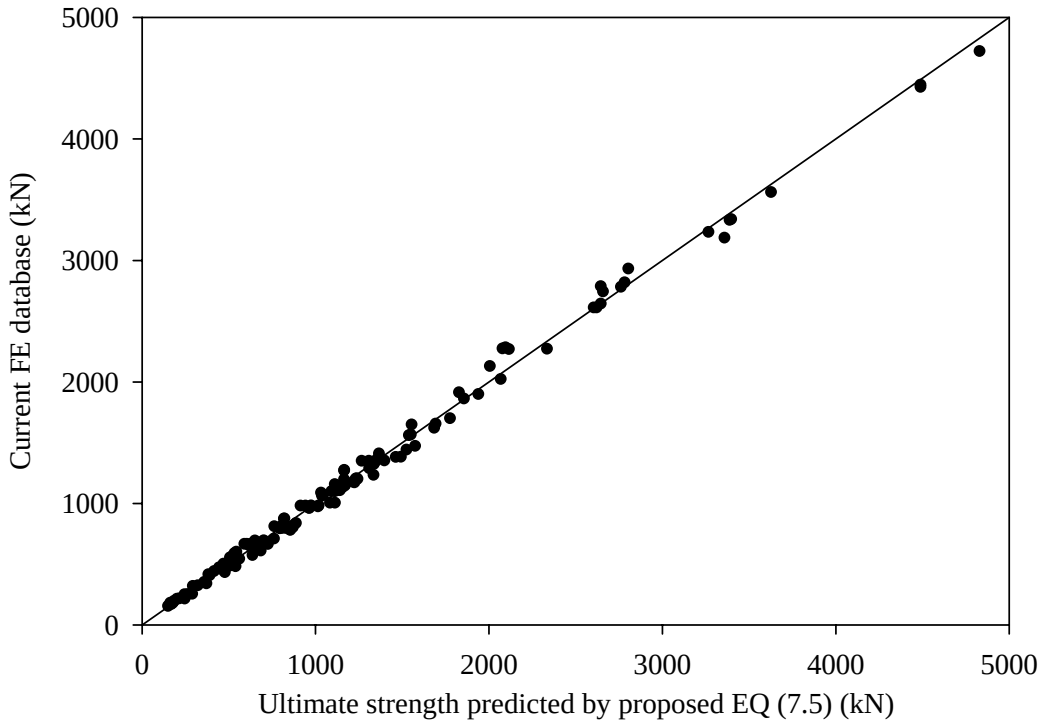

Fig. 7.7 Assessment of proposed equation with current FE data

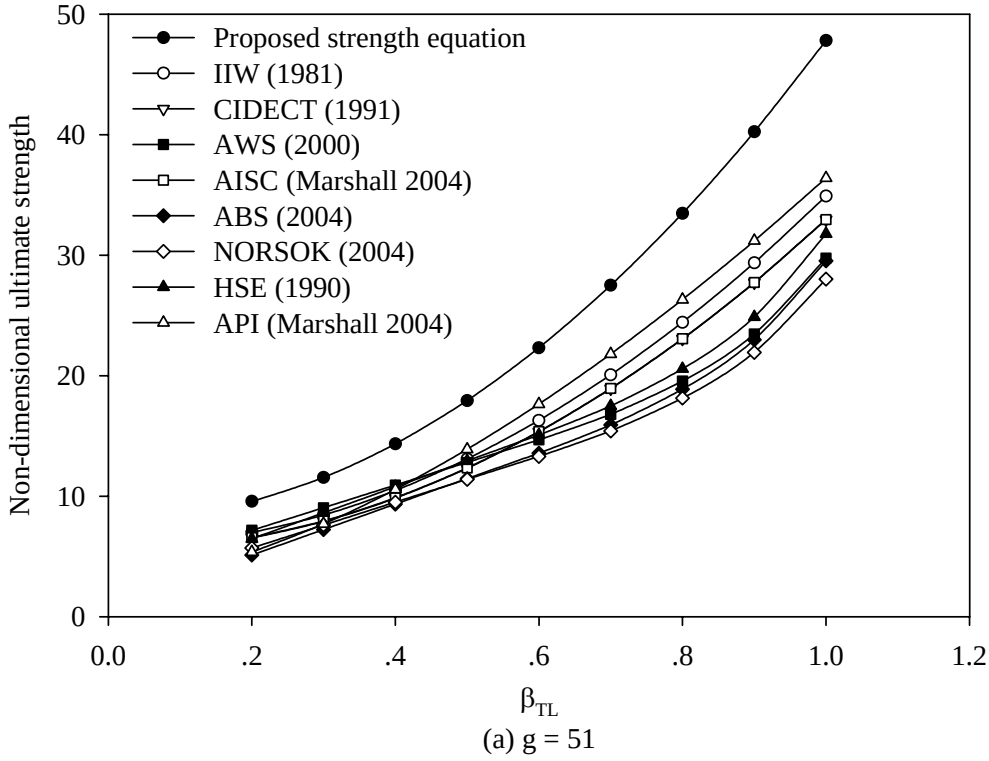

(a) g = 51

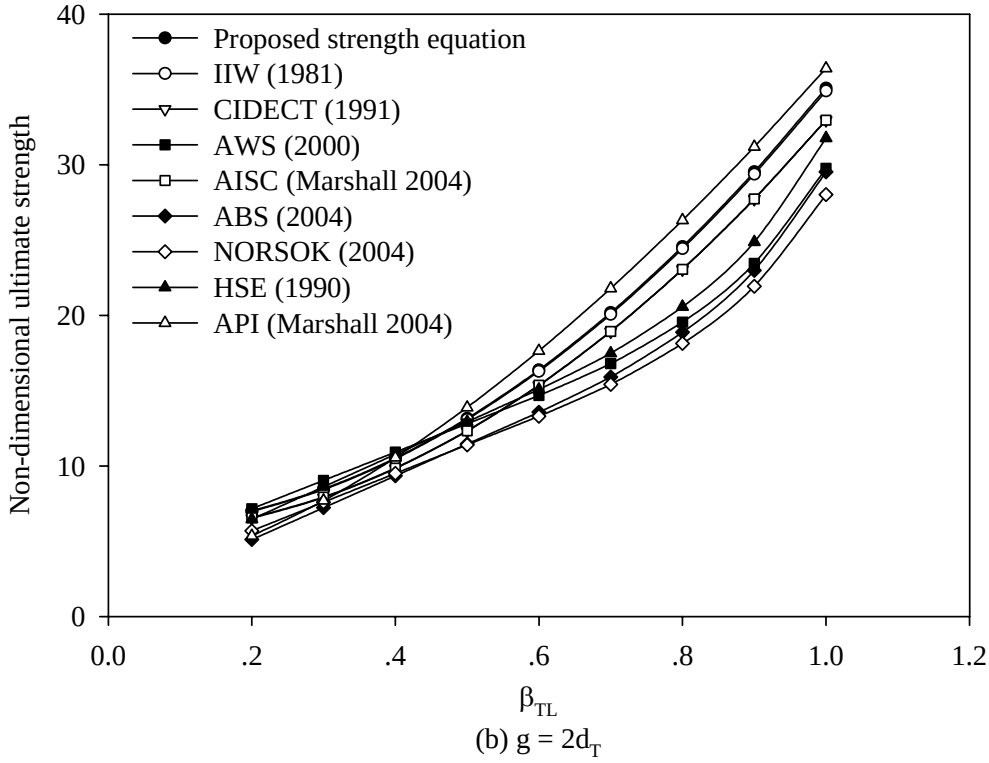

(b) g = $2d_T$

Fig. 7.8 Comparison with existing T/Y-joint strength equations (varying β_{TL})

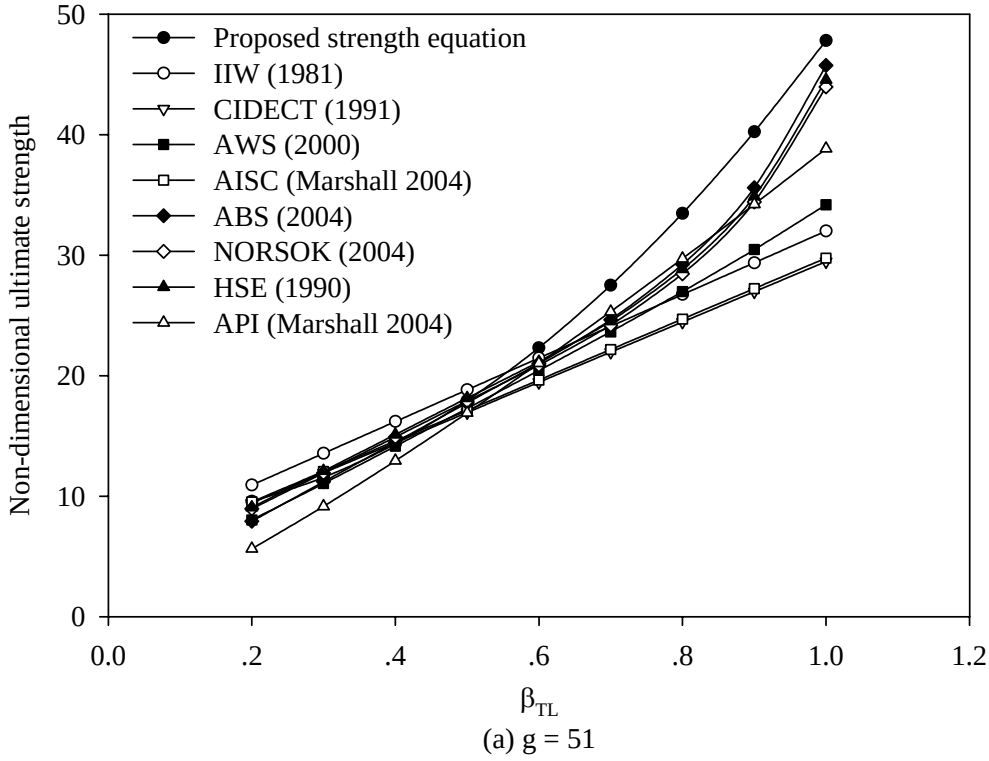

(a) g = 51

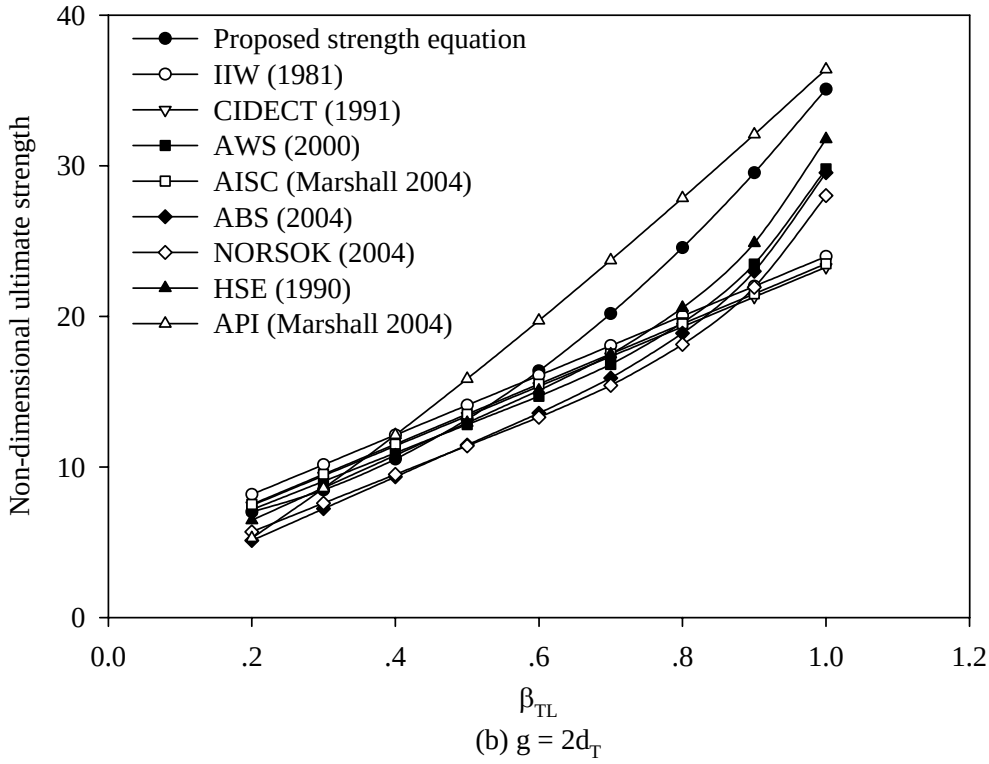

(b) g = $2d_T$

Fig. 7.9 Comparison with existing K-joint strength equations (varying β_{TL})

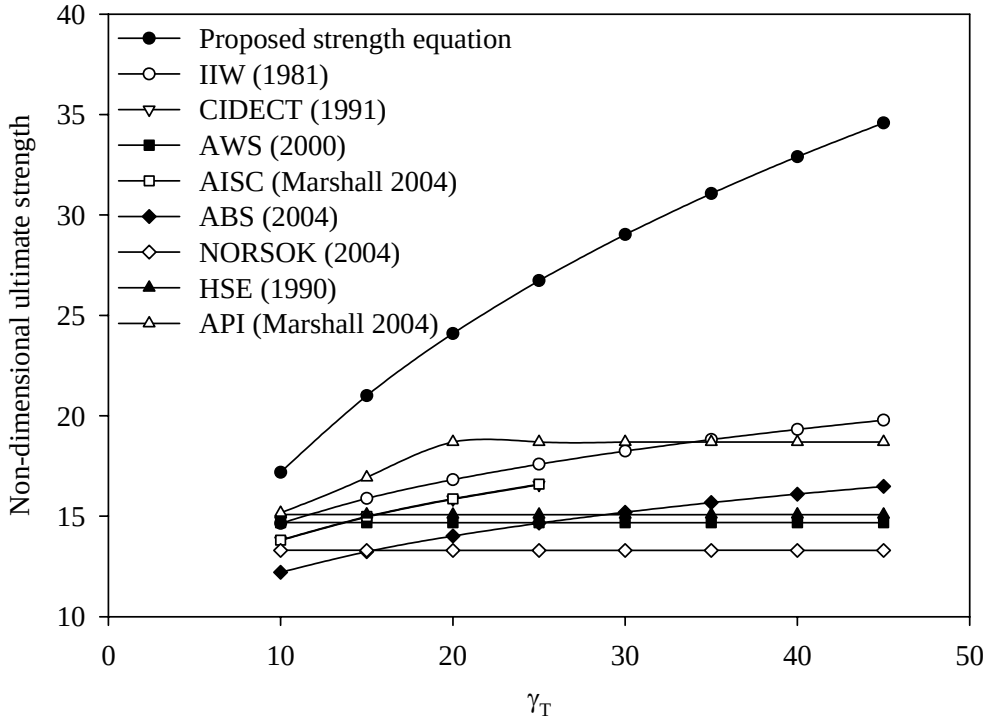

(a) g = 51

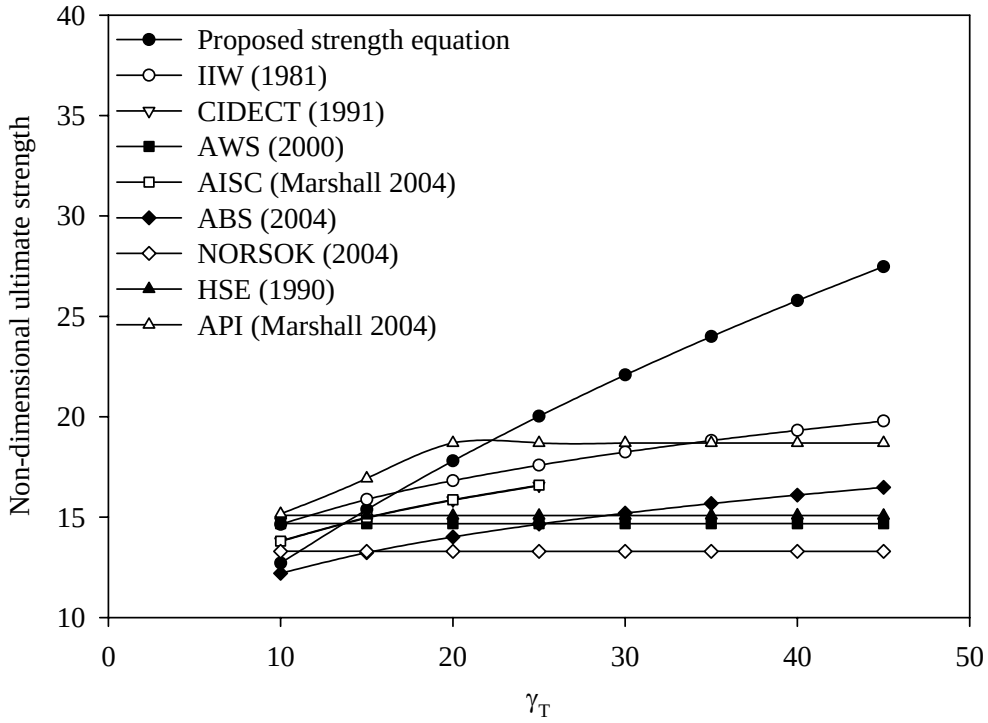

(b) g = $2d_T$

Fig. 7.10 Comparison with existing T/Y-joint strength equations (varying γ_T)

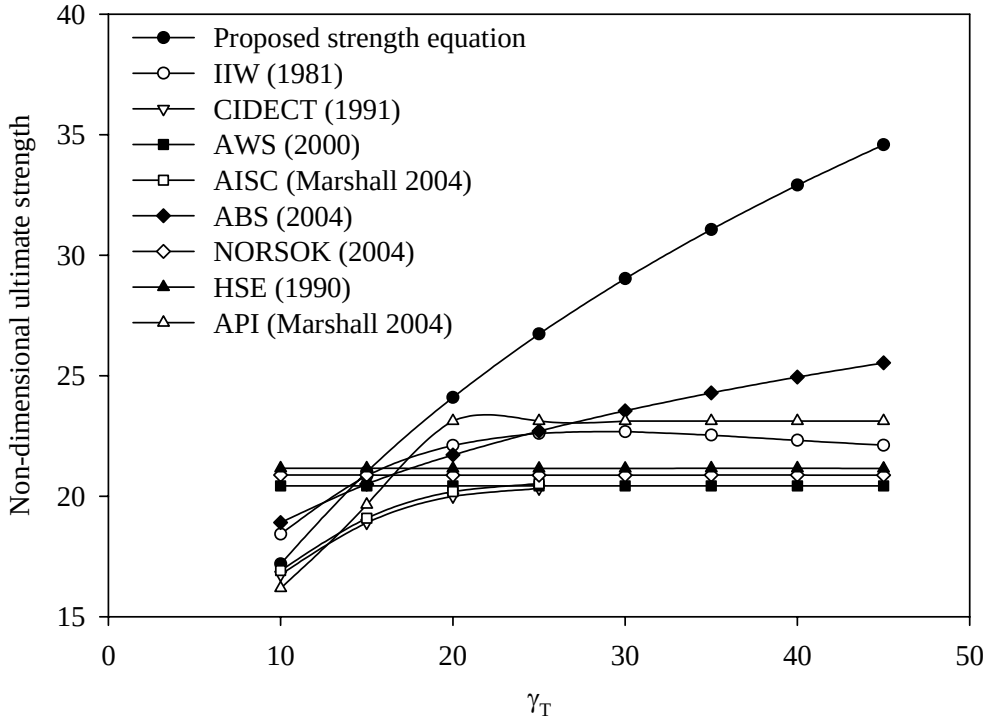

(a) g = 51

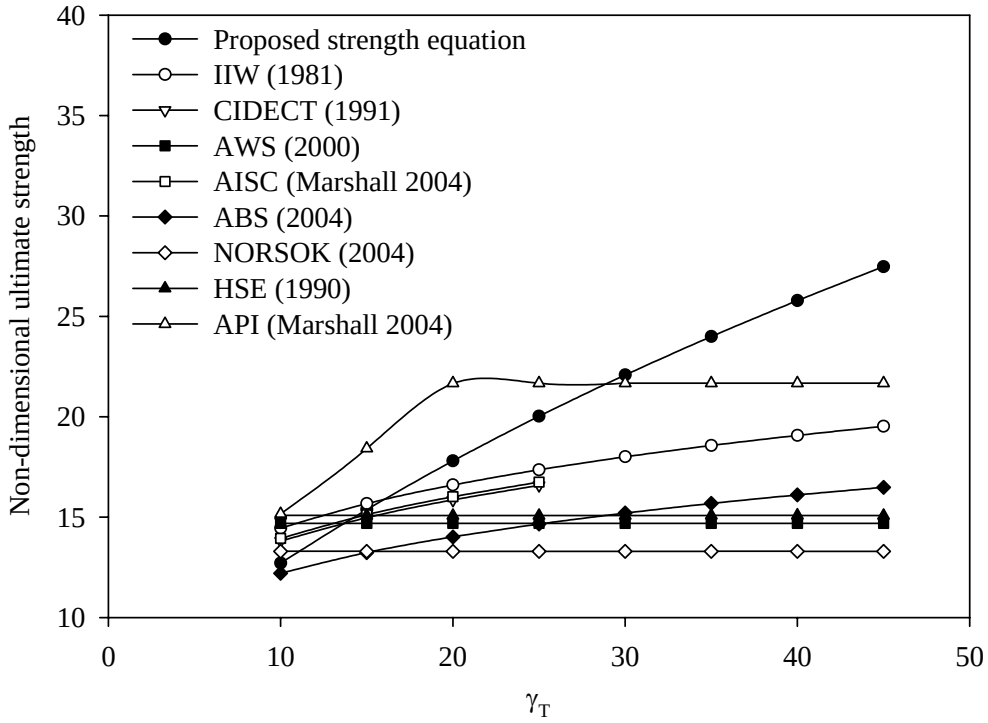

(b) g = $2d_T$

Fig. 7.11 Comparison with existing K-joint strength equations (varying γ_T)

CHAPTER 8

CYCLIC PERFORMANCE

8.1 Introduction

For the past two decades, most of the research activities have been focused on the ultimate strength and the stress and strain concentrations of tubular joints for design. The research on the cyclic performance of tubular joints is relatively less and is only limited to fatigue behaviour with large number of small amplitude loading applied within the elastic limit of material. The cyclic performance of tubular joints under large amplitude loading in the inelastic range has not been investigated in greater detail. A US government report stated that "*very little is known about the cyclic inelastic behaviour of joints in offshore platforms subjected to either extreme storms or earthquakes*" (Taylor 1996). Furthermore, this has also been pointed out in the standards and recommendations in the absence of provisions for seismic design of tubular joints.

Since 1960s, it has generally been accepted that the seismic performance of a structure depends on its inelastic cyclic response. The dissipative zone of a structure under hysteretic behaviour is designed based on material yielding and member buckling for dissipating the earthquake energy. The dissipative zone is designed to have adequate ductility and strength to resist the load (BSI 1996). The key parameter to measure the seismic efficiency of steel components in a frame is the ability to dissipate energy by undergoing a large plastic deformation without brittle failure. As the dissipative zones of a structure often locate near the ends of members, the ductility and the energy dissipation capacity of the joints under cyclic loading at large plastic deformation have to be intensively examined.

The need for reliable numerical technique to supplement experimental study for analysis of tubular joints under various kinds of loads has been emphasized in recent years. The FE modelling technique for simulating the static behaviour of

completely overlapped tubular joint has been discussed in detail in Chapter 3.

8.2 Assessment of cyclic behaviour

A tubular joint under cyclic loading can be considered stable if it exhibits the same behaviour as that under monotonic loading based on area of hysteresis loops with increasing load cycles. On the other hand, the joint behaviour under cyclic loading can be considered unstable if its stiffness decreases with load cycles characterized by continuously decreasing slope in hysteresis curves. Thus, the joint under cyclic loading can be commented ideal at specific strength level without stiffness deterioration after a number of load cycles.

The evaluation and the comparison of the joint performance under cyclic loading can be based on some behavioural parameters such as the ductility level, the energy dissipation capacity and the stiffness and strength deterioration during the load cycles. In the current study, several behavioural parameters namely the ductility, the strength resistance, the stiffness and the energy dissipation ratio were defined for assessing the joint capacity under cyclic loading. These parameters could be obtained through a comparison between the generic (Fig. 8.1a) and the corresponding elastic-perfectly plastic cycle (Fig. 8.1b) with the same displacement amplitude.

8.2.1 Ductility level

In capacity design, steel structures are generally classified based on ductility index (μ) into three categories namely the fully ductile, the limited ductility, and the fully elastic as specified in Canadian (1989) and New Zealand Standards (1997). Elchalakani et al (2002) used displacement ductility index to evaluate the ductility level of circular hollow sections. A similar indicator based on ductility ratio was used in the current study to determine the ductility performance of completely overlapped tubular joint under cyclic loading which could be defined as follow.

$$\mu = \delta_{\max} / \delta_y \tag{8.1}$$

where δ_{max} denoted the maximum deformation of joints prior to excessive loss of resistance. δ_y was the yield deformation for idealised elastic-perfectly plastic behaviour. In New Zealand standards (1992), the collapse of structures under cyclic loading was assessed based on 20% strength drop in load - deformation curve. For the cyclic behaviour of joint, the ductility ratio at *i*th half-cycle could be defined as,

$$\mu_i^+ = \delta_i^+ / \delta_y^+ \qquad \text{(Tension phase)} \tag{8.2}$$

$$\mu_i^- = \delta_i^- / \delta_y^- \qquad \text{(Compression phase)} \tag{8.3}$$

where δ_i^+ and δ_i^- were the maximum displacements at *i*th tension and compression, whilst δ_y^+ and δ_y^- were the yield displacements for idealised elastic-perfectly plastic behaviour in tension and compression half-cycle, respectively. It could be seen from the above that the joint capacity under large inelastic deformation increased with ductility ratio.

It was recommended to adopt the first development of localised inelastic strain, significant yielding or buckling in critical members, or overall stiffness loss of structures if δ_y could not be identified. From the load - deformation relationship obtained in the current test specimen, it was suggested that the overall loss of joint stiffness should be taken as the yield displacement.

European Convention for Constructed Steelwork (ECCS 1986) included several methods for determining the yield displacement of structures. The appropriate method adopted for assessing the joint capacity under cyclic loading according to the load - deformation curve under monotonic loading could be seen as follows.

(i) The value corresponding to the first yield of the test specimen (Fig. 8.2a)
(ii) The ultimate capacity of the test specimen (Fig. 8.2b)
(iii) The value corresponding to the yield deformation in the inelastic region of

load - deformation curve. An example is to define the yield deformation equivalent to two times the elastic deformation as illustrated in Fig. 8.2c.

(iv) The value corresponding to the intersection of two tangents plotted based on elastic and inelastic regions of the curves as shown in Fig. 8.2d. The tangent of the curve in inelastic range was based on a slope equivalent to 1/10 the tangent in elastic region.

(v) In some other cases, the yield displacement was obtained from computation.

The above mentioned methods for assessing the joint capacity under cyclic loading comprised some advantages and disadvantages. For method (i), the post yield region of the curve was ignored. For method (ii), the buckling mode was captured but this was corresponded to the excessive deformation in flexural behaviour of beams and joints. On the contrary, the deformation of beams and joints was well defined in method (iii). ECCS (1986) recommended the use of method (iv) for all cases. Method (v) was only applicable for cases where the design resistances had precisely been defined based on test data. In the current research on the structural behaviour of completely overlapped tubular joints under cyclic loading, the method (iv) recommended by ECCS was adopted.

It should be noted in some cases that the required level of displacement of the specimen could not be achieved owing to the limitation of test rig. In order to complete the full cycle of test, the loading was applied with identical displacement amplitude. Under this circumstance, the ductility ratio (μ) was not defined using the maximum displacement. A more realistic way to assess the cyclic performance was to measure the accumulative ductility of the joint under cyclic loading, which could be defined as the summation of ductility ratio of each cycle as shown below.

$$\mu_a = \sum_{i=1}^{N_c} \left(\mu_i^+ + \left| \mu_i^- \right| \right) \tag{8.4}$$

where N_c was the total number of load cycles.

8.2.2 Strength resistance

It could be seen from hysteresis curves that for large inelastic displacement cycle, the strength decreased after the material yielded due to damage of structural elements such as local buckling, cracking, etc. Under this circumstance, the reduction of strength resistance of the structural element could be evaluated using the strength resistance ratio as shown below.

$$\omega = P_i / P_y \tag{8.5}$$

where P_i was the force magnitude at point of unloading at ith cycle. P_y was the yield force for idealised elastic-perfectly plastic behaviour. Similar to the previous definition of μ_i^+ and μ_i^-, the respective strength resistance ratios in tension and compression half-cycle could be defined as follow.

$$\omega_i^+ = P_i^+ / P_y^+ \quad \text{(Tension phase)} \tag{8.6}$$

$$\omega_i^- = P_i^- / P_y^- \quad \text{(Compression phase)} \tag{8.7}$$

where P_i^+ and P_i^- were the force magnitudes at point of unloading at ith tension and compression half-cycle, whilst P_y^+ and P_y^- were the yield forces for idealised elastic-perfectly plastic behaviour in tension and compression half-cycle, respectively.

8.2.3 Joint stiffness

The deterioration of joint stiffness under cyclic loading increased with number of load cycles. The deterioration of joint stiffness was mainly caused by the global and local buckling, the Bauschinger effect exhibited in steel material subjected to inelastic load reversals or residual curvature during load cycles. The stiffness ratio for assessing this behaviour could be defined as follow.

$$\zeta_i^+ = \tan\alpha_i^+ \big/ \tan\alpha_y^+ \quad \text{(Tension phase)} \tag{8.8}$$

$$\zeta_i^- = \tan\alpha_i^- \big/ \tan\alpha_y^- \quad \text{(Compression phase)} \tag{8.9}$$

where $\tan\alpha_i^+$ and $\tan\alpha_i^-$ were the slope of tangent in hysteresis loops with forces changing from negative to positive and positive to negative respectively at *i*th load cycle. It should also be noted that $\tan\alpha_y^+$ and $\tan\alpha_y^-$ were the slope of tangent in hysteresis loops for idealised elastic-perfectly plastic behaviour when forces increased on positive and negative side respectively.

8.2.4 Energy dissipation capacity

In severe earthquake excitation, the elastic capacity of joint could be exceeded and the dynamic behaviour of structures became the energy dissipation mechanism. The area enclosed by hysteresis loop (E_i) at *i*th cycle was the amount of energy dissipated during the load history. The energy dissipation efficiency of the joint could be measured based on the energy dissipation ratio as shown below.

$$\eta_i^+ = E_i^+ \big/ E_y^+ \quad \text{(Tension phase)} \tag{8.10}$$

$$\eta_i^- = E_i^- \big/ E_y^- \quad \text{(Compression phase)} \tag{8.11}$$

where E_i^+ and E_i^- were the dissipated energy in tension and compression phase of *i*th cycle whilst E_y^+ and E_y^- were the dissipated energy in tension and compression phase under idealised elastic-perfectly plastic behaviour, respectively. They could be computed using the formulae as shown below.

$$E_y^+ = P_y^+(\delta_i^+ - \delta_y^+ + \delta_i^- - \delta_y^-) \tag{8.11}$$

$$E_y^- = P_y^-(\delta_i^- - \delta_y^- + \delta_i^+ - \delta_y^+) \tag{8.12}$$

Alternatively, a more useful and realistic parameter to determine the accumulative

energy dissipation ratio highlighted by Soh et al (2001) could be defined as follow.

$$\eta_a = \sum_{i=1}^{N_c} (E_i^+ + E_i^-) / E_y \tag{8.13}$$

where E_y was the energy absorption at first yield displacement (δy) defined as $E_y = P_y \delta_y / 2$.

It was noted from the above that all the parameters except those in accumulative ratio were defined based on the idealised elastic-perfectly plastic material behaviour. Indeed, the joint behaviour closely followed this idealised material condition when the above mentioned ratios for assessing the joint capacity under cyclic loading approached unity. Thus, the limiting values of these parameters could be used in the ultimate limit state for design of joint under cyclic loading. A small value of these ratios indicated a substantial loss of strength, stiffness or energy dissipation capacity.

8.3 Finite element modelling of cyclic behaviour

8.3.1 Modelling Technique

The commercial FE package MARC (2005a) with pre- and post-processing program MENTAT was adopted in the current study for the investigation of completely overlapped tubular joint behaviour under lap brace axial cyclic loading. For the purpose of verification, the geometrical, the material and the dimensional properties of the joint model are identical to those of the joint specimen, as shown in Fig. 3.1 and Table 3.1 in Chapter 3.

In the modelling of the joint specimen, the mid-plane of the member wall thickness was modelled using the shell element. By taking the advantage of symmetry in geometry and boundary conditions, only one-half of the joint was considered in the current FE analysis.

A numerical study on the effect of boundary conditions indicated that the steel flat plates at the end of the chord and the through brace should be modelled. The loading and the boundary conditions of the joint model are depicted in Fig. 8.3. The cyclic load was applied at the free end of the lap brace through displacement control mode. In the modelling, a high density of FE meshes was used at the joint intersections of members to account for the effect of high stress gradients. The sizes of the finite element increased with the distance outside the joint region. Transition elements between the fine and the coarse FE meshes are included in the model to reduce the number of elements for analysis as depicted in Fig. 8.4.

The weld element was included in the joint model. The sizes of the welds were modelled according to those measured in the test specimen. The method for modelling the weld elements at the joint intersections of the chord and through brace and the through brace and lap brace was based on the dihedral angles at the joint perimeters specified by AWS (2000).

Both the material and the geometric nonlinearities were considered in the FE analysis. The Young's modulus, the yield stress and the ultimate tensile stress of the members of the joint were obtained from the tensile coupon tests. The detail of the test results is summarized in Table 3.2. The Poisson's ratio was assumed to be 0.28. The true stress and the logarithm strain were adopted to account for large strain effect of material properties. The von Mises yield criterion and the multi-linear work hardening rule of plasticity were applied. The large displacement, the updated Lagrange procedure and the finite strain plasticity were activated in the analysis for a complete large strain plasticity formulation. A full Newton-Raphson method was adopted to reassemble the stiffness matrix of load iteration in displacement control mode. The convergence criteria for residual force and moment relative to reaction force and moment was set at 5%.

8.3.2 Convergence study

Prior to the actual FE analysis, a convergence study was conducted to obtain a sufficiently fine mesh of the joint model for accurate solutions. The ultimate capacity of the six different mesh densities of the joint models was considered in the study. The force response at the unloading point of each load cycle with different mesh layouts is presented in Fig. 8.5. It could be seen from the figure that the results converged as the FE mesh became finer. The FE mesh D of the joint model under axial compression was found suitable for simulating the joint model under cyclic loading with less computational effort.

8.3.3 Effect of element types

Three different types of shell elements (MARC element types 22, 72 and 75) previously discussed in Chapter 4 were assessed to determine the suitable element for modelling the completely overlapped tubular joint under cyclic loading. From the comparison of hysteresis loops as shown in Fig. 8.6, four-node thin shell element type 72 was unsuitable for modelling the joint as the effect of transverse shear was not considered. On the other hand, four- and eight-node thick shell elements 75 and 22 were found suitable for modelling the joint with sufficient accuracy.

It was noted that the joint model with eight-node thick shell element type 22 yielded lower force response. However, the average difference of cyclic response of the models using four- and eight-node thick shell finite elements was found less than 5%. In view of the computational effort, four-node thick shell element 75 was adopted in the current study for modelling the joint. The model showed to predict reasonably well the ultimate capacity of the test specimen with difference of approximately 5%. Despite Morgan (1997) showed that the geometrical stresses of the two K-joints modelled using the thin and the thick shell elements were about the same, the thin shell element seemed unsuitable for simulating the non-linear elastic-plastic behaviour of completely overlapped joints under both static and

cyclic loading.

8.3.4 Effect of weld elements

For the static strength analysis of T/Y-joints, the overall joint behaviour could be simulated without considering the weld effect. The behaviour of completely overlapped tubular joint was found similar to that of simple T/Y-joints in some ways. The current FE analysis indicated that the ultimate capacity of the completely overlapped joint without the weld was not significantly affected. For the joint under cyclic loading as shown in Fig. 8.7, the FE model without the weld elements gives lower response with average difference of 5.5% and 3.5% in compression and tension phase of the load cycle respectively in comparison to that with weld elements. In comparison with the experimental value, the difference was 7.5% and 5.7% for the model with and without the weld elements.

Although modelling of weld elements at the joint intersections produced reasonably accurate estimates of joint strength, the weld profile was somewhat arbitrary unless the actual weld size at the joint was measured. Thus, it was important to realise that in the current parametric study, the area of investigation was mainly focused on the effect of geometrical properties on the cyclic behaviour of the joint. The modelling of weld elements at the joint intersections of FE model was excluded so that the results obtained for comparison were more conservative.

8.3.5 Effect of material property

In the uni-axial test of joint specimen, the work hardening rule related the incremental stress to incremental plastic strain in the inelastic region after yielding. For the plastic analysis, there are two strain-hardening rules commonly applied for material properties namely the isotropic and the kinematic hardening rule. The isotropic work hardening model assumed the centre of the von Mises yield surface remained stationary in the stress space and the size of the yield surface expanded. On the other hand, the isotropic work hardening rule stated the reverse yield occured at

the same stress level in the reversed direction. However, it should be noted that the von Mises yield surface under the kinematic hardening rule did not change in size and shape and the centre of the yield surface moved in the stress space.

The isotropic and the kinematic hardening rule were considered in the current study for modelling the material post yield properties of the joint. As shown in Fig. 8.8, the isotropic hardening model overestimates the maximum load-carrying capacity of the joint. Furthermore, the deterioration of joint strength could not be identified with increasing load cycle. The reason was that the isotropic hardening model did not consider the Bauschinger effect due to plastic deformation and so the elastic range of the material expanded with equivalent plastic strain. In previous Chapter 4, it had been shown that the isotropic hardening model was suitable for strength analysis of tubular joints under monotonic axial loading. However, this was not the case for the joints under load reversals. On the other hand, the kinematic hardening model accurately predicted the cyclic behaviour of the joint. Thus, in the parametric study, a multi-linear kinematic hardening material model was adopted for modelling the post yield behaviour of the completely overlapped joint under cyclic loading.

8.3.6 Effect of failure criterion

It was noted in the experimental study that the joint specimen failed by crack initiation on the face of through brace. In order to simulate the effect of cracking, a failure criterion was proposed and included in the FE model. For strength analysis, Dexter and Lee (1999a) assumed a failure criterion of 20% tensile strain as the onset of cracking in the outer face of the joint. However, it should be noted that a crack for joints under cyclic loading took place due to accumulative effect of local strain reversals. In the current study, a maximum tensile stress of 486MPa, which was the ultimate tensile stress of through brace obtained from the coupon test, was taken as the failure criterion to simulate the crack initiation. This failure criterion was only applied to elements near the weld toe at the joint intersection of through brace and lap brace. At failure criterion, the material property of these elements was taken as 10% the Young’s modulus.

The hysteresis curves shown in Fig. 8.9 are the results obtained from the test specimen and the FE model with and without the failure criterion. It was noted from these curves that the tensile capacity of the joint with failure criterion was 3.3% lower. However, the compressive resistance of the joint was not affected as the failure criterion was associated with cracking with the joint under tensile load.

8.3.7 Effect of length parameters

It had been shown in the current study that the length parameters could have significant effects on the strength of the joint under static loading. In this section, the length parameters of the chord and the through brace were investigated to assess the impact on the joint capacity under cyclic loading. From the FE analysis results as shown in Fig. 8.10, the joint strength in the compression and tension phase is not significantly affected with varying chord length parameters. Owing to the reduction of bending stiffness, the joint stiffness decreased with increasing chord length parameter. This effect was found profound for the through brace member. As the failure mode of the completely overlapped tubular joint was associated with through brace wall plastification, the through brace member must have sufficient length to ensure unrestrained localized ovalisation of its cross section. In the current study, the assumption of length parameters of 14 ($\alpha_C = \alpha_T = 14$) was commented adequate to preclude any short member effect for the completely overlapped tubular joints under cyclic loading.

8.3.8 Comparison with conventional K(N)-Joints

Four different joint configurations were considered in the current study for comparison. They were the uni-planar tubular K(N)-joints with and without gap, 100% overlapped and complete overlap of braces with gap (Fig. 8.11). For the simple gap K(N)-joint, a slight change of the joint configuration was made by shifting the lap brace joining the chord. A gap size equivalent to that of the completely overlapped tubular joint was maintained between the two braces on the

chord face. These four joint configurations have identical dimensional properties, material properties and boundary conditions as summarised in Table 8.1. Eight load cycles were performed in the FE analysis so that the joint deformation was two times the excessive deformation limit specified by Yura et al (1980).

The axial load - displacement hysteresis curves under compression and tension are plotted in Fig. 8.12. As expected, the 100% overlapped tubular K(N)-joint provided the highest strength and initial stiffness. The completely overlapped tubular joint yielded larger but smaller compressive strength compared to K(N)-joint with and without gap respectively. A similar behaviour was observed for the joint under tension phase of the cyclic loading. From the axial load - displacement curves of the joints under monotonic loading, the yield force and the corresponding axial displacement could be determined using the method recommended by ECCS (1986), as shown in Table 8.2.

The comparison of normalized hysteresis curves as shown in Fig. 8.13 revealed that the completely overlapped tubular joint has similar behaviour with gap K(N)-joint. The hysteresis curve was found to be more stable in the compression phase. However, the 100% overlapped K(N)-joint showed to have more stable performance in the tension phase of the cyclic loading, but the strength deterioration in the compression phase was more severe with increasing load cycles.

It could been seen from Fig. 8.14 that the completely overlapped tubular joint dissipated more energy than 100% overlapped K(N)-joint, K(N)-joints with and without gap with differences of 6%, 18% and 32%, respectively. From Fig. 8.15, the completely overlapped tubular joint shows better ductility performance. The accumulative ductility ratio of the completely overlapped tubular was 9.3%, 16.2% and 23.4% more than those of 100% overlapped K(N)-joint, K(N)-joints with and without gap, respectively.

For strength resistance as shown in Fig. 8.16, all the joint configurations showed similar tensile strength resistance with increasing load cycles. However, for

compressive resistance in the subsequent load cycles, the 100% overlapped K(N)-joint exhibited strength deterioration due to buckling of lap brace member. On the contrary, the completely overlapped tubular joint and the gap K(N)-joint showed increasing compressive resistance in the subsequent phase of load cycles. The increase of compressive resistance of the joint was due to bending stiffness of the chord member at large displacement.

From the viewpoint of stress distribution as depicted in Fig. 8.17, the maximum von Mises stress for the conventional K(N)-joints is concentrated on the gap region between the two braces. For the completely overlapped tubular joint, it occurred on the face of the through brace in contact with the lap brace. It could therefore be concluded from the load transfer mechanism as shown in Fig. 8.17 that the completely overlapped tubular joint performs better than the conventional K(N)-joint with failure on the through brace instead the chord member.

8.4 Concluding remarks

In the current study, several behavioural parameters are considered for the evaluation of cyclic performance of completely overlapped tubular joints. These parameters include ductility, strength resistance, stiffness, and energy dissipation ratios. The FE model of the joint is calibrated against the test results with respect to the effect of finite element types, weld elements, material properties, and failure criteria. The results showed that thick shell finite elements are suitable for modelling the joint. The weld element has minimum impact on the joint capacity. For the material property, the kinematic hardening rule simulates very well the post yield behaviour of the joint.

The comparison of the cyclic behaviour indicated that the completely overlapped tubular joint attains higher strength resistance, dissipated more energy, and more ductility than the conventional K(N)-joints. Unlike the conventional K(N)-joints with the maximum stress occurring on the gap region of the chord face between the two braces, the maximum stress of the completely overlapped tubular joint is on the through brace instead the chord member.

Table 8.1 Properties used for comparison with conventional N-joints

Dimensions (mm)	L = 4890, D = 457.2, T = 12.7 l_T = 2407, d_T = 273.1, t_T = 9.3 l_L = 1520, d_L = 168.3, t_L = 7.1 g = 110 (if applicable)
Material properties	Young's modulus = 197GPa Poisson's ratio = 0.28 Yield stress = 355MPa Ultimate tensile stress = 458MPa
Boundary conditions	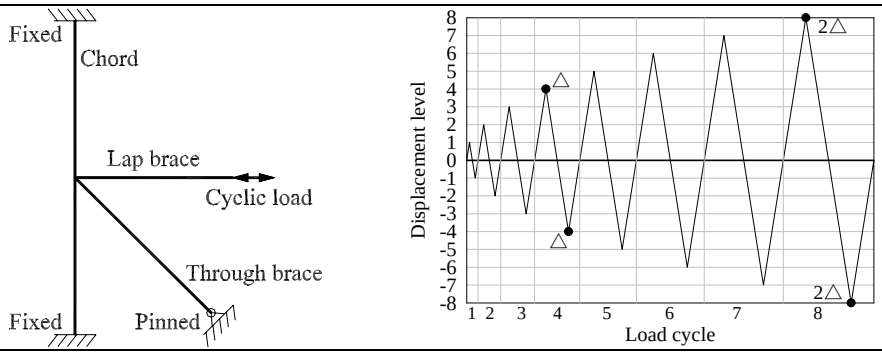

Table 8.2 Displacement and load at yield point

Joint configurations	P_y^-	δ_y^-	P_y^+	δ_y^+
N-joint with gap	630	4.95	1120	9.25
N-joint without gap	923	6.2	1160	7.65
100% overlapped N-joint	1135	5.9	1192	6.25
Completely overlapped joint	810	4.78	1135	6.62

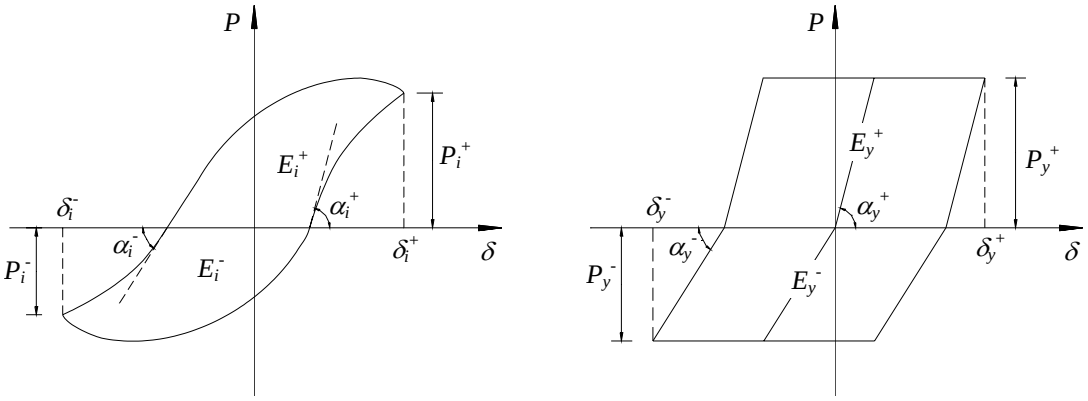

(a) True load cycle (b) idealised elastic-perfectly plastic load cycle

Fig. 8.1 Basic data for a cyclic test

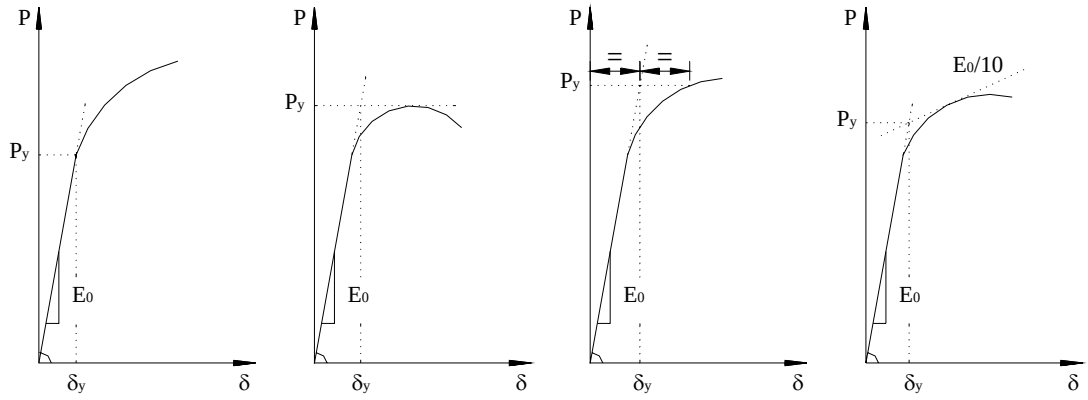

(a) (b) (c) (d)

Fig. 8.2 Determination of yield load and displacement

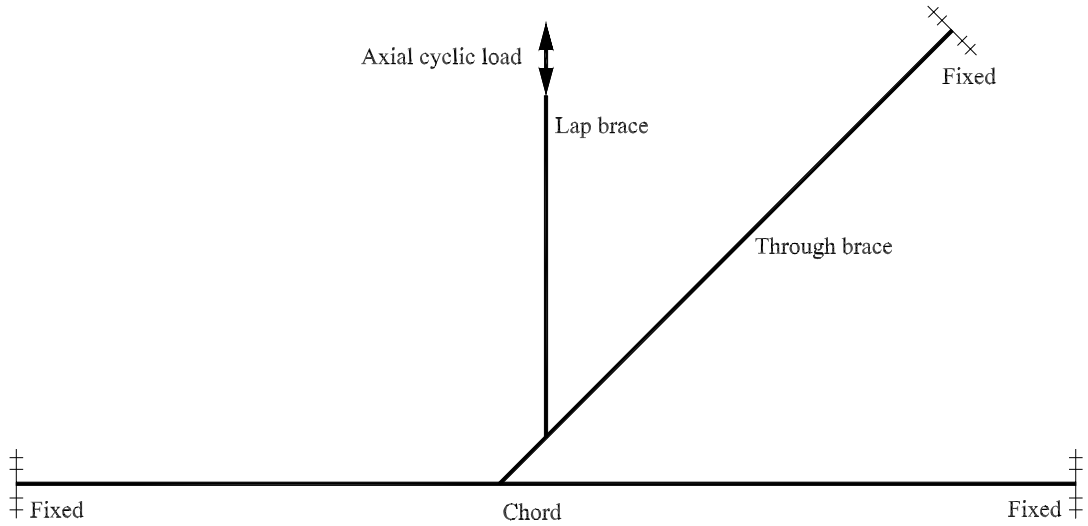

Fig. 8.3 Loading and boundary conditions

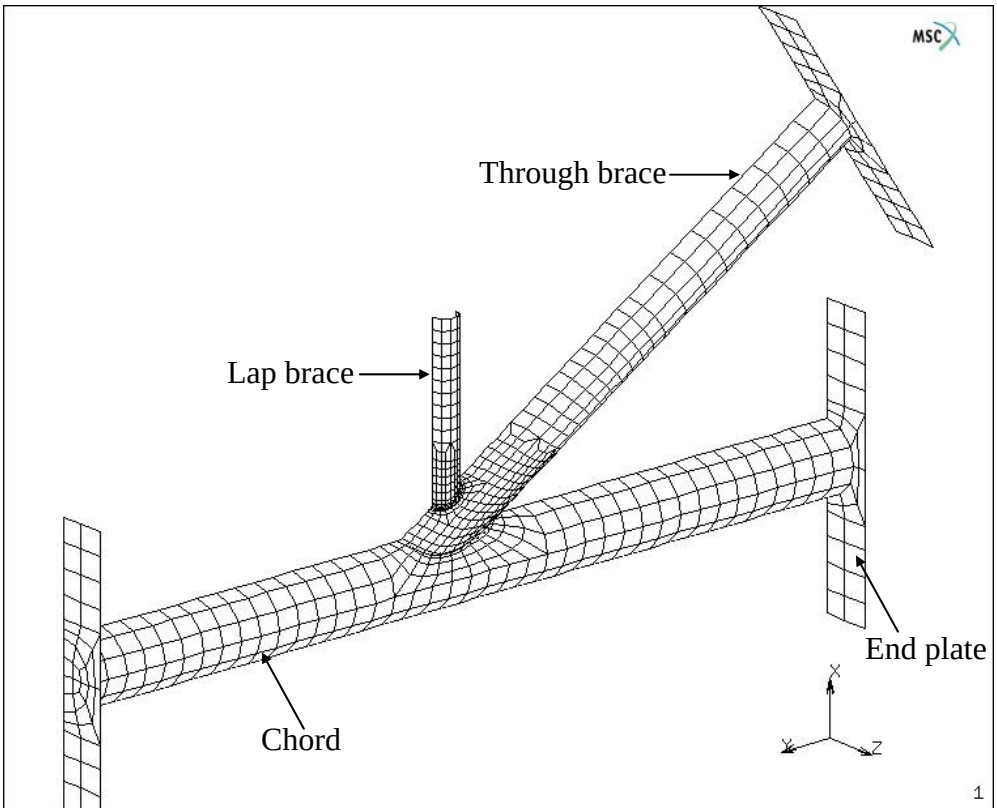

Fig. 8.4 FE model of test specimen under cyclic loading

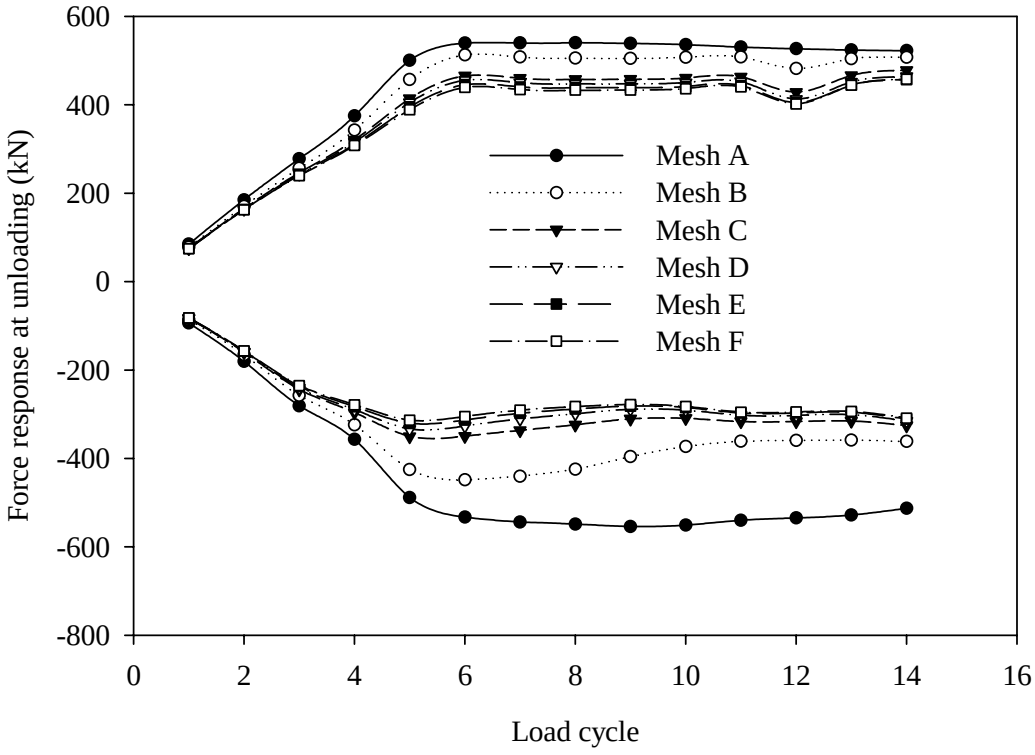

Fig. 8.5 Convergence study of FE models under cyclic loading

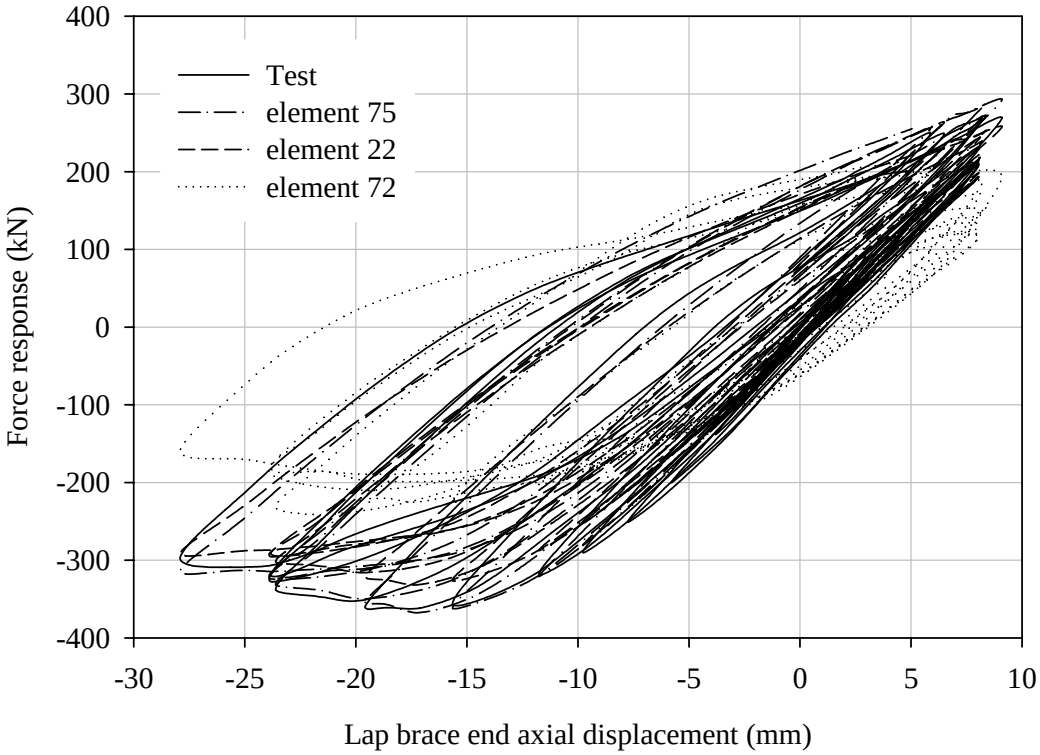

Fig. 8.6 Effect of element types

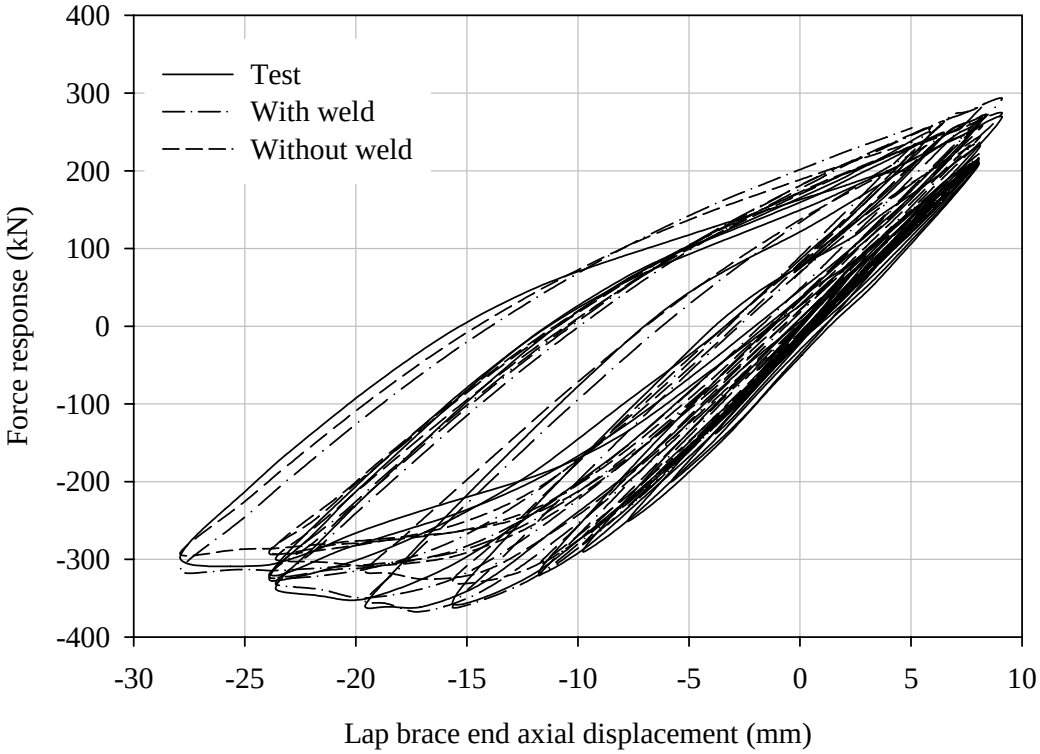

Fig. 8.7 Effect of weld elements

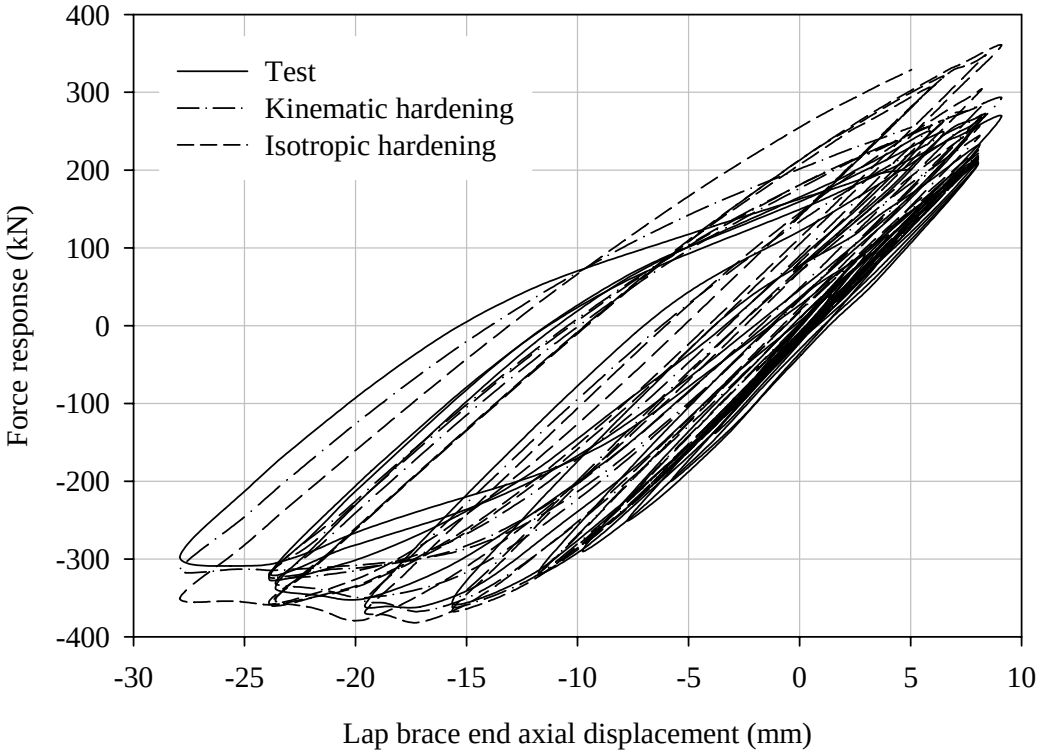

Fig. 8.8 Effect of material property

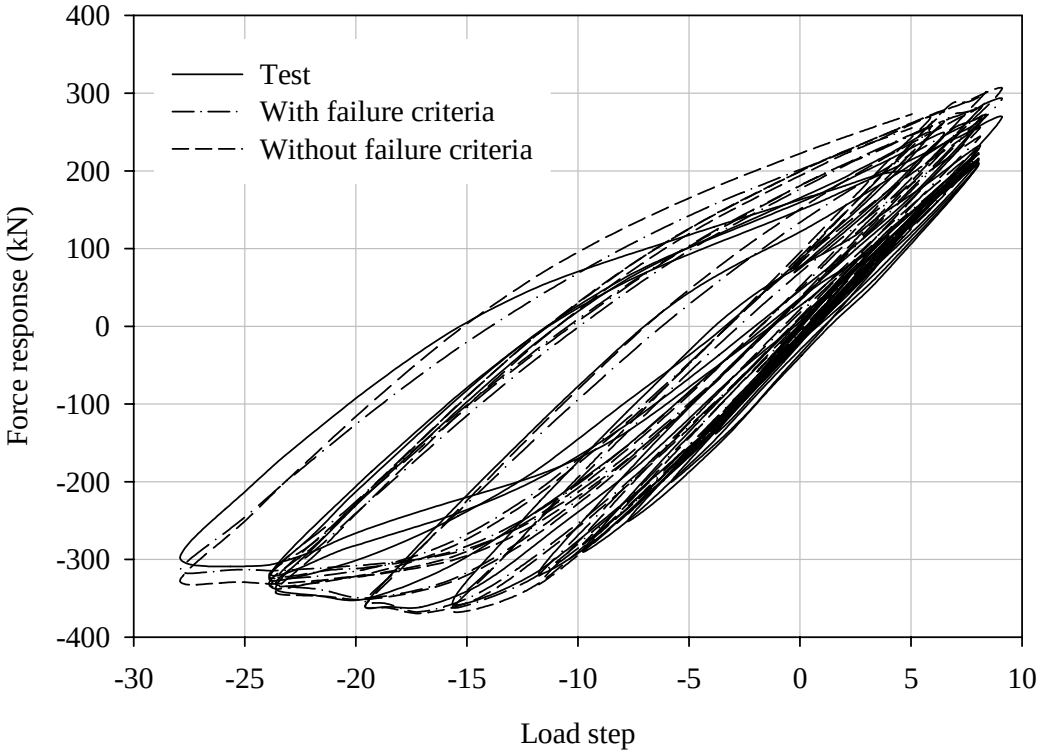

Fig. 8.9 Effect of failure criterion

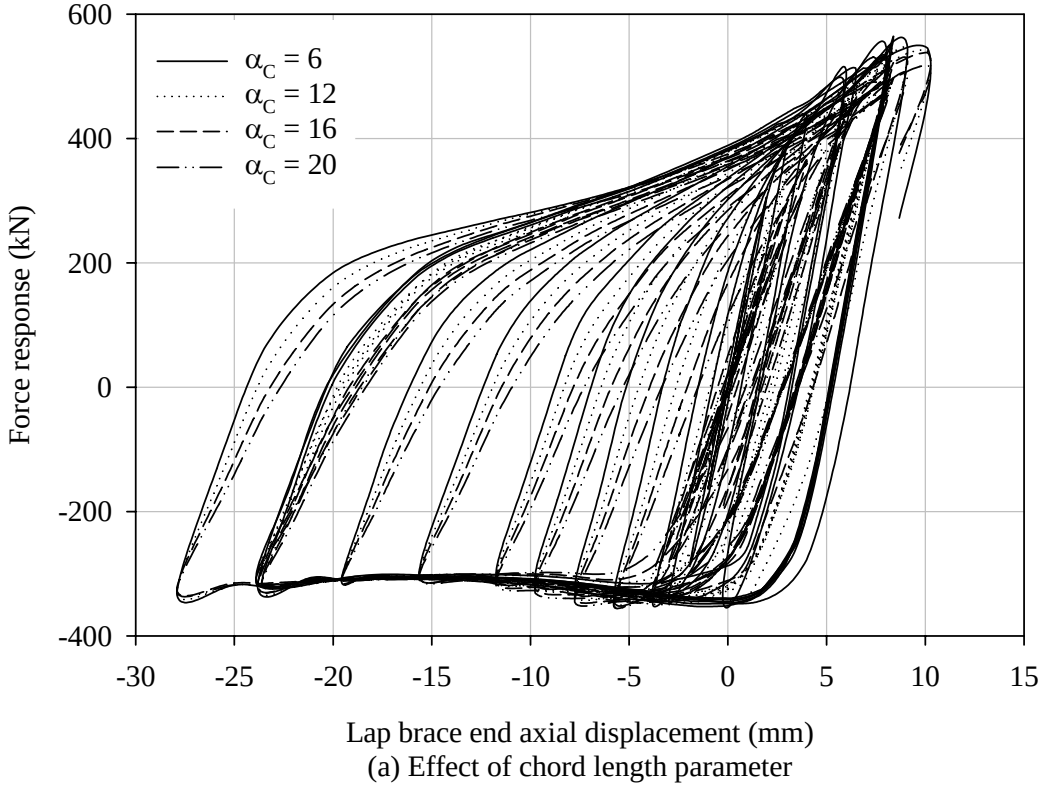

(a) Effect of chord length parameter

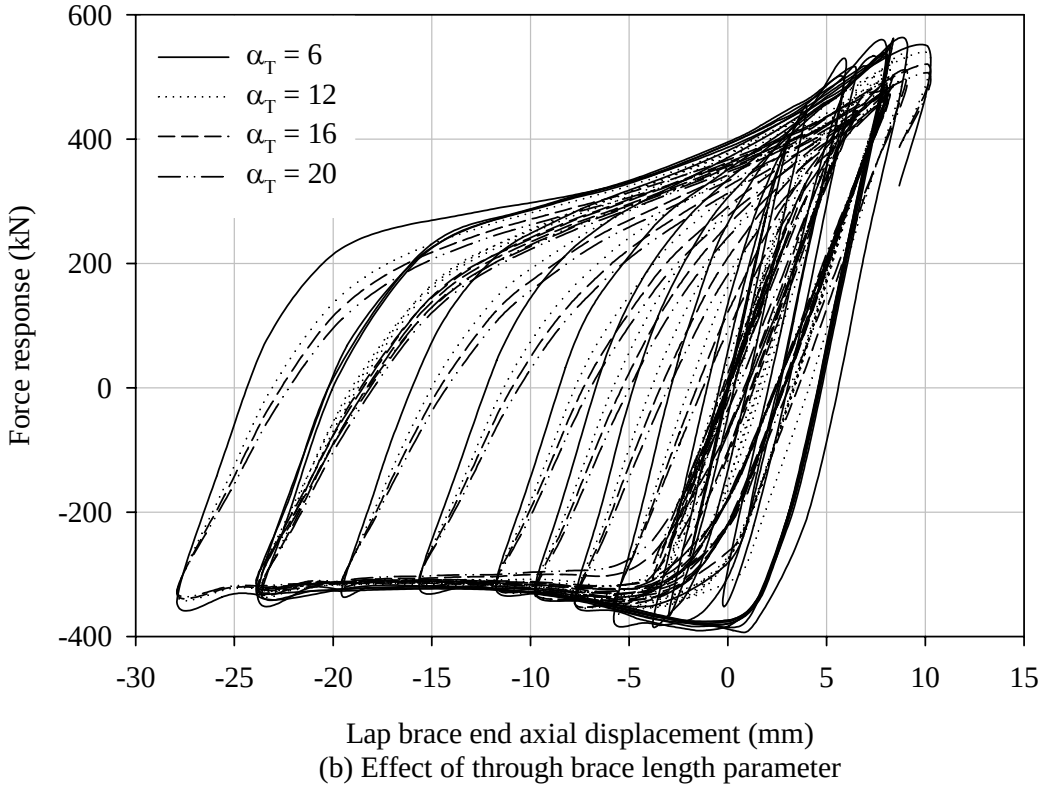

(b) Effect of through brace length parameter

Fig. 8.10 Effect of length parameters

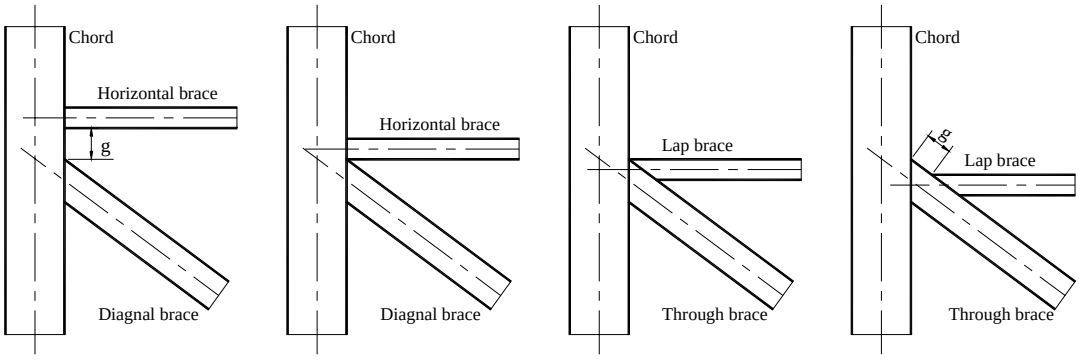

(a) N-joint with gap (b) N-joint without gap (c) 100% overlapped N-joint (d) Completely overlapped joint

Fig. 8.11 Configuration of N-joints

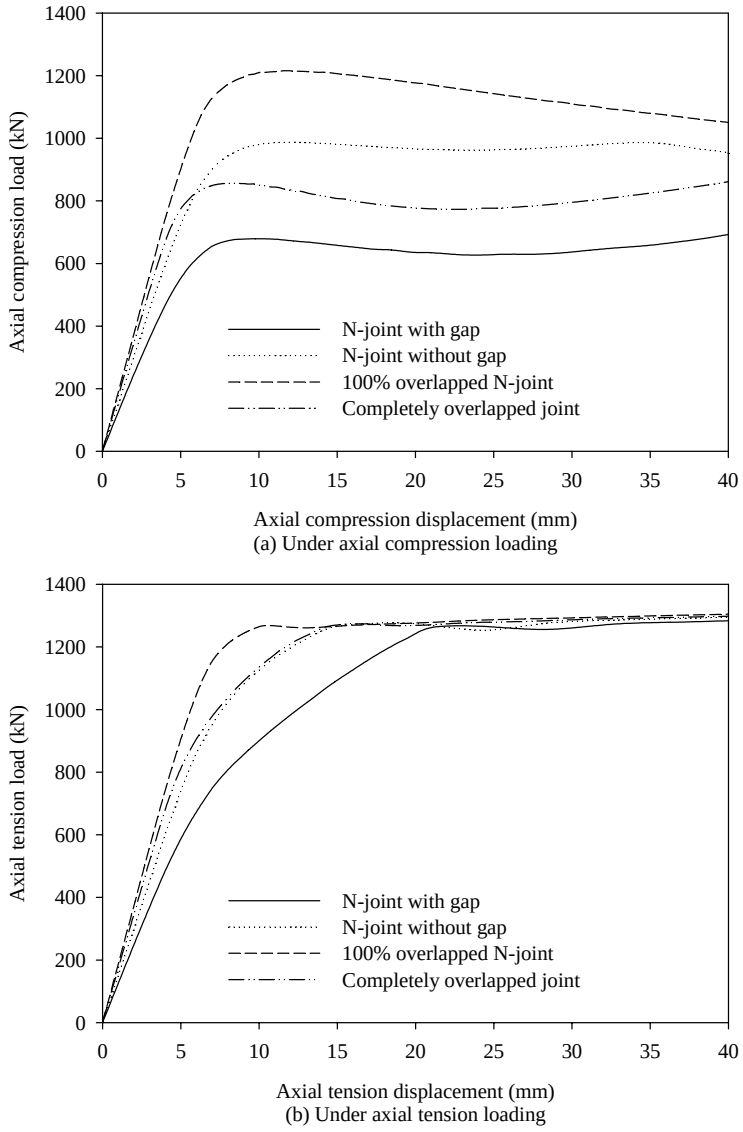

Fig. 8.12 Axial load - displacement curves of N-joints

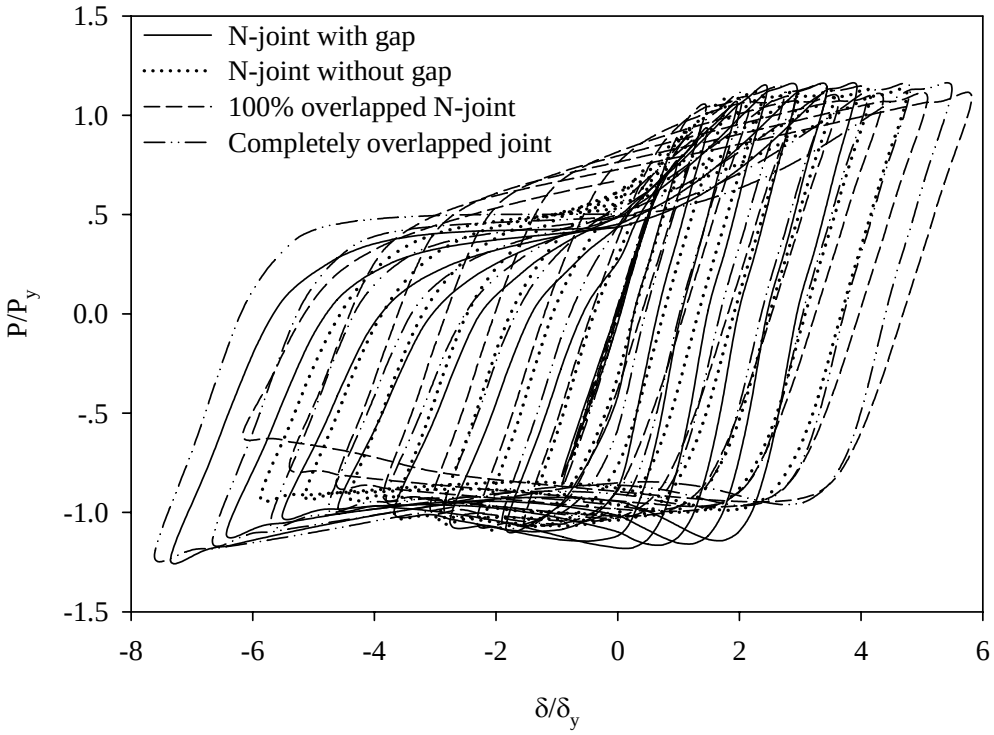

Fig. 8.13 Comparison of hysteresis curves between completely overlapped joint and conventional N-joints

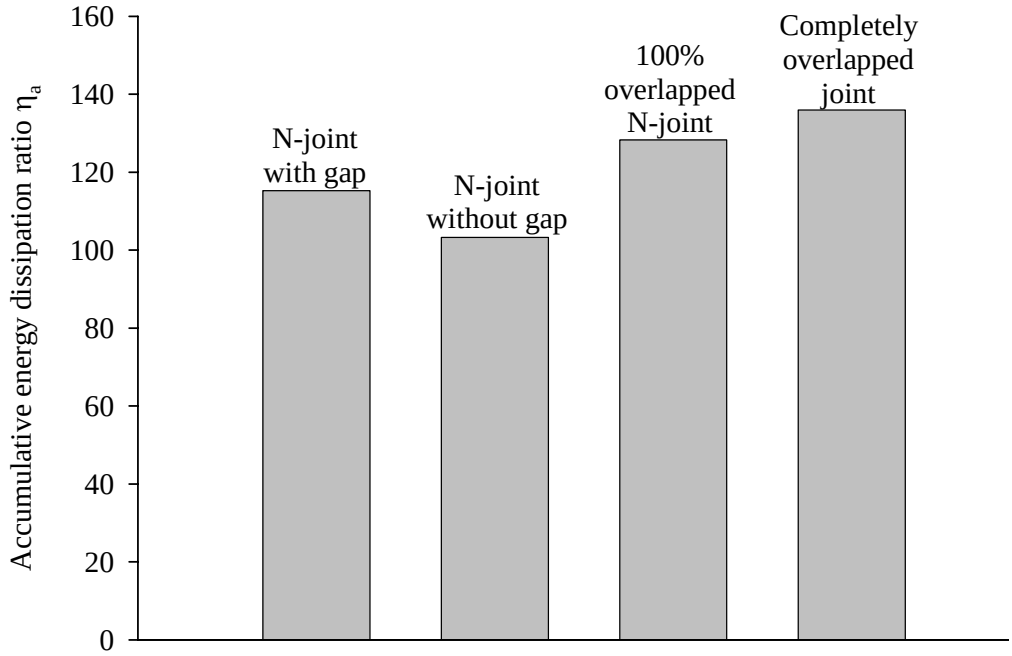

Fig. 8.14 Comparison of accumulative energy dissipation capacity between completely overlapped joint and conventional N-joints

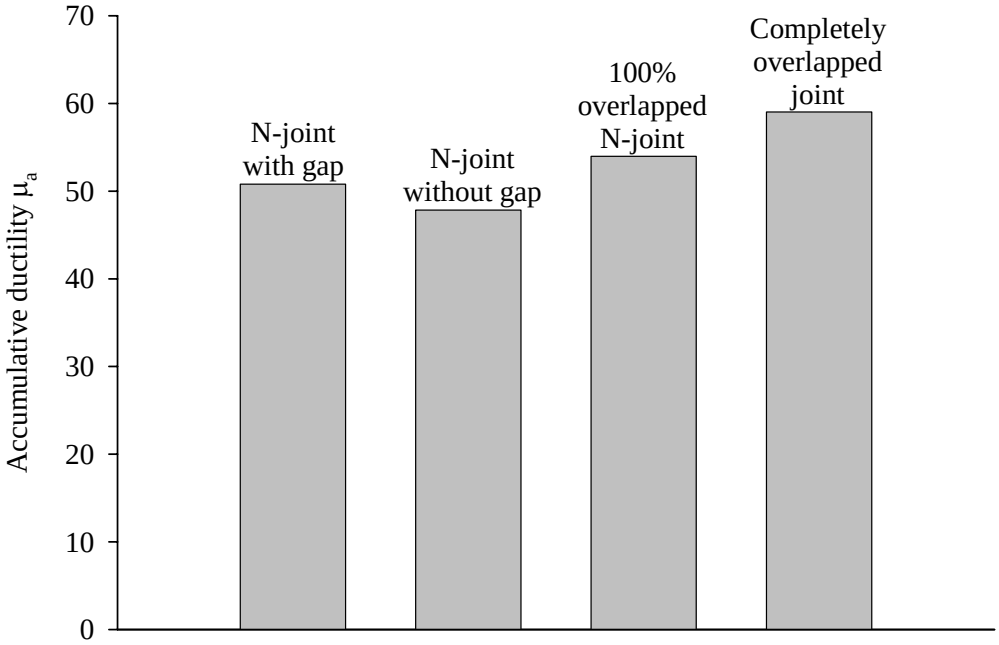

Fig. 8.15 Comparison of accumulative ductility between completely overlapped joint and conventional N-joints

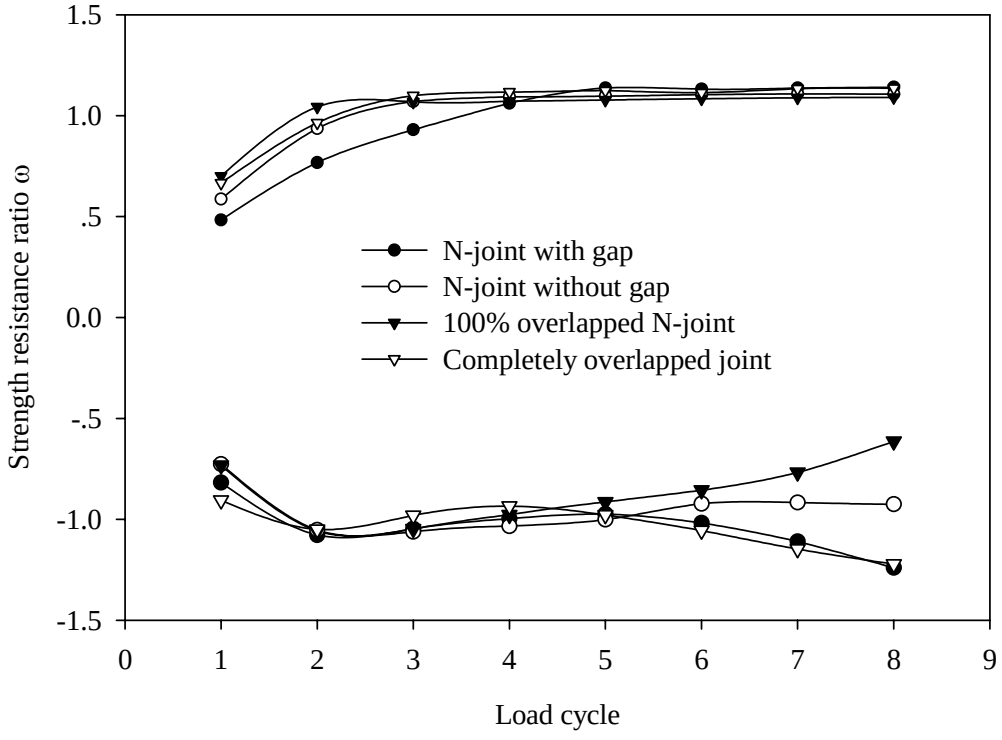

Fig. 8.16 Comparison of strength resistance between completely overlapped joint and conventional N-joints

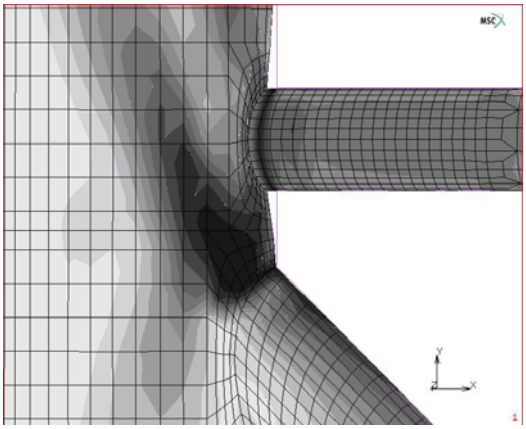

(a) N-joint with gap

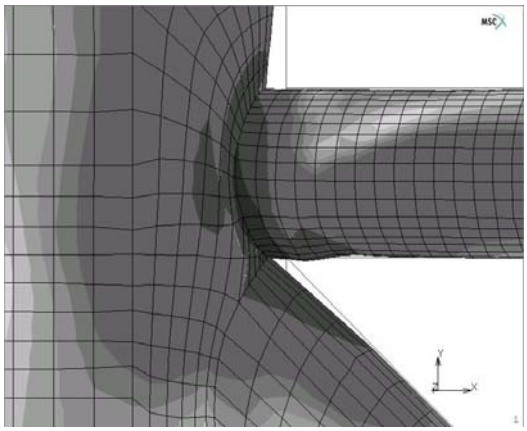

(b) N-joint without gap

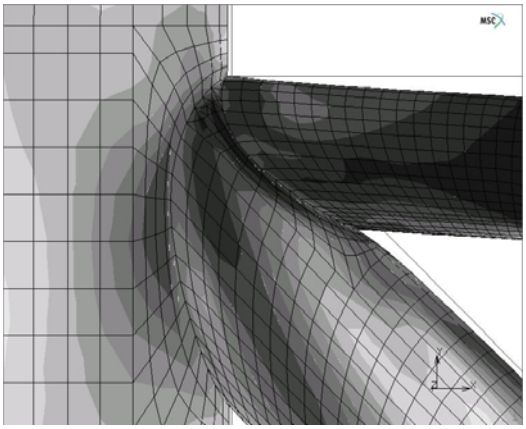

(c) 100% overlapped N-joint

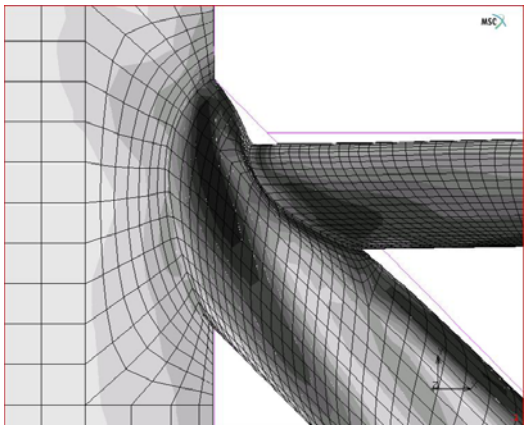

(d) Completely overlapped joint

Fig. 8.17 Equivalent von Mises stress distribution of N-joints

CHAPTER 9

PARAMETRIC STUDY OF CYCLIC BEHAVIOUR

9.1 Introduction

Steel structures are extensively used in earthquake sensitive areas owing to their excellent structural performance in terms of strength and ductility. However, the earthquakes of Northridge and Hyogoken-nanbu, Japan, 1994 and 1995 respectively, showed the unexpected damage and brittle failure at welded connections of moment resisting steel frames. This prompted a need for further investigation on the structural behaviour of steel connections under seismic loading. As a result, several studies have been carried out to clarify the inelastic cyclic behaviour of steel connections as well as to provide fundamental data for the development of seismic recommendations for design. Most of these research activities are concentrated on experimental investigation. Obviously, the excremental work is necessary but the research information is insufficient for design of steel structures.

With the advancement of computer technology, the use of FE method for the analysis of steel structures becomes common in both research and application because of the ability for modelling complicated geometrical configurations and boundary conditions. In order to examine the structural behaviour of completely overlapped tubular joint under cyclic loading, an extensive FE parametric study is conducted and the detailed results are presented in this chapter. The scope of the parametric study includes the hyteresis behaviour, the strength resistance, the ductility performance and the energy dissipation capacity of the joint.

9.2 Finite element models

In previous Chapter 8, the FE modelling technique was verified against the experimental results and was commended to be accurate and reliable for analysis of completely overlapped tubular joint under cyclic loading. Thus, the joint models

previously used for static analysis was adopted in the current parametric study. The analytical procedure for assessing the joint capacity under cyclic loading was different from that under static loading. The material properties of the joint model in the parametric study were identical to that in the static analysis. However, the plastic analysis considered a multi-linear kinematic hardening rule. Similar to the study reported in previous Chapter 8, a failure criterion based on maximum tensile stress of 458MPa, was imposed in finite elements along the intersection of through brace and lap brace to account for the effect of cracking.

The axial cyclic load was applied at the free end of lap brace through a fixed time stepping procedure with displacement control mode. Two types of load procedures namely the variable and the constant displacement amplitudes are adopted in the analysis, as shown in Fig. 9.1. For the case of variable displacement amplitude (Fig. 9.1a), six load cycles were performed based on stepwise increase for every load cycle at each displacement level until six times the yield deformation was attained. This analytical method for analysis was recommended by ECCS (1986). For the case of constant displacement amplitude, two parameters namely the normalized displacement $(\delta/\delta_y)_A$, and the normalized mean displacement $(\delta/\delta_y)_M$, are defined and used in the analysis as shown in Fig. 9.1b.

9.3 Effect of geometrical parameters

9.3.1 Effect of through brace-to-chord diameter ratio, β_{CT}

In the investigation of the effect of geometrical parameters, the variable displacement amplitude procedure was applied. In this section, the cyclic behaviour of completely overlapped tubular joints was studied by varying the parameters β_{CT} (0.4, 0.6 and 0.8) at different cases of γ_C (12 and 20) and τ_{CT} (0.4 and 1.0). The axial displacement - applied load relationship at the end of lap brace is plotted in Fig. 9.2. The displacement and the load level were normalized with respect to the yield displacement (δ_y) and the yield load (P_y), respectively, in order to examine the difference of behaviour. From the figure, β_{CT} showed little impact on the hysteresis

behaviour of the joint. It should be noted that the hysteresis curves of all the joint models showed almost the same behaviour.

The strength resistance versus the number of load cycles of the joint is plotted in Fig. 9.3. The strength of the joint was slightly affected with increasing β_{CT}. For the joints at τ_{CT} = 0.4 and γ_C = 12, significant reduction of strength due to lap brace member yielding at large displacement was specifically noted after fourth load cycle. It should be noted that the joints under monotonic compressive loading at τ_{CT} = 0.4 and γ_C = 12 also failed by lap brace member yielding. A sudden lost of strength for the joint at β_{CT} = 0.8 as shown in Fig. 9.3c indicates poor ductility performance.

The energy dissipation versus the number of load cycles of the joint is plotted in Fig. 9.4. The negative energy dissipation in the figure indicated the joint in compression phase. Despite the joint with higher β_{CT} showed lower energy dissipation efficiency, this effect was found insignificant. It could be concluded from the above study that the cyclic performance of the completely overlapped tubular joint would not be enhanced with increasing β_{CT}.

9.3.2 Effect of through brace-to-chord wall thickness ratio, τ_{CT}

In this section, the cyclic behaviour of the completely overlapped tubular joints was studied by varying the parameters τ_{CT} (0.4, 0.7 and 1.0) at different cases of γ_C (12 and 20) and β_{CT} (0.4 and 0.8). The normalized axial displacement and the applied load at the end of lap brace are plotted in Fig. 9.5. As shown in Fig. 9.5a, the hysteresis curves of the joints at τ_{CT} = 0.7 and 1.0 exhibit larger stiffness than the joint at τ_{CT} = 0.4. From the previous study of the failure mechanism of completely overlapped tubular joint under lap brace axial compression, it was commented that γ_T was one of the dominant parameters controlling the failure behaviour of the joint. The joints at τ_{CT} = 0.7 and 1.0 (β_{CT} = 0.4 and γ_C = 12) with smaller γ_T = 8 failed by lap brace local buckling. On the other hand, the joint at τ_{CT} = 0.4 (β_{CT} = 0.4 and γ_C = 12) with larger γ_T = 12 resulted in through brace wall plastification. It could be seen

from the above that the difference of cyclic behaviour could be attributed to the effect of γ_T. It is also noted that the joint with behaviour as shown in Fig. 9.5b has parameter $\gamma_T > 12$ with the failure associates with through brace wall plastification. This failure mode was similar to that observed for the joint under lap brace axial compression. Thus, the effect of τ_{CT} could be commented insignificant if the effect of γ_T was excluded.

The strength resistance versus the number of load cycles of the joint is plotted in Fig. 9.6. The joints with lap brace member failure revealed a significant reduction of strength resistance at large inelastic displacement. In this circumstance, the ductility performance of the joint was commented to be insufficient. The energy dissipation capacity of the joint under cyclic loading can be seen in Fig. 9.7. In the compression phase, the energy dissipation of the joint was not affected by varying τ_{CT}. However, in the tension phase, the energy dissipation of the joint increased with τ_{CT}. For the accumulative energy dissipation as shown in Fig. 9.8, the joints at higher τ_{CT} with lap brace member failure dissipate more energy after third load cycle. It should be realised from Fig. 9.8b that the accumulative energy dissipation of the joint with plastic formation in the through brace near the lap brace is not affected by $\tau_{CT.}$

9.3.3 Effect of chord radius-to-wall thickness ratio, γ_C

The hysteresis curves of the completely overlapped tubular joints with varying γ_C plotted in Fig. 9.9 showed that the behaviours are identical. The strength resistance versus the number of load cycles is plotted in Fig.9.10. A similar strength resistance was observed for joints with varying γ_C. However, a strength reduction after fifth load cycle is specifically noted for joints at $\gamma_C = 50$ as shown in Fig. 9.10c. This is not observed for the joint behaviour as shown in Fig.9.10b. The strength reduction could be attributed to the lap brace local buckling resulted from the effect of large γ_T. The energy dissipation capacity of the joint is not affected by varying γ_C as shown in Fig. 9.11.

9.3.4 Effect of lap brace-to-through brace diameter ratio, β_{TL}

In this section, the cyclic behaviour of the completely overlapped tubular joints was studied by varying the parameters β_{TL} (0.4, 0.6 and 0.8) at different cases of γ_T (11 and 26) and τ_{TL} (0.4 and 1.0). The normalized axial displacement and applied axial load relationship at the end of lap brace is shown in Fig. 9.12. For the joint with β_{TL} = 0.8, the analysis terminated at fifth load cycle owing to severe distortion of FE meshes. From the figure, the hysteresis behaviour of the joint at low τ_{TL} (= 0.4) is not affected by varying β_{TL}. In Figs. 9.12a and 9.12c, the joints at large β_{TL} show poor ductility performance with stiffness and strength reduction under inelastic load reversals.

For the joints at β_{TL} = 0.4, 0.6 and 0.8, the capacity at the first yield and the five times yield displacement in compression phase of the load cycle decreased by 38%, 58% and 70% respectively as shown in Fig. 9.13a, and 49%, 70% and 77% in Fig. 9.13c. The capacity reduction was due to the accumulated effect of yielding or local buckling of lap brace. The joint deformation at first load cycle was concentrated in the elastic limit of material. As the load cycle increased, the lap brace yielding or localised buckling of the joint became the main failure mode. However, the normalized strength of the joint in tension was not significantly affected by β_{TL} as the strength reduction was found less than 10%. In the tension phase of load cycle, the failure mechanism of the joint was controlled by cracking at the weld toe of the through brace in contact with the lap brace.

The hysteresis curves of the joints at large τ_{TL} (=1.0), as shown in Fig 9.12b, exhibit stable behaviour and thus the joint capacity is not significantly affected by β_{TL}. The capacity deterioration of the joint in compression phase of the load cycle was not observed. It was commended that a good ductility performance of the joint attained with failure due to through brace face plastification. However, at medium β_{TL} of 0.4 and 0.6, the joint exhibits significant reduction of tensile strength at fourth load cycle as shown in Fig. 13b. The strength reduction was attributed to the effect of

failure criteria and punching shear stress on the through brace face of the joint.

The energy dissipation versus the number of load cycles of the joint is plotted in Fig. 14. As shown in Fig. 14a, the energy dissipation of the joint with varying β_{TL} at low τ_{TL} and γ_T is almost identical. The energy dissipation in both compression and tension phase of the subsequent load cycle reduced with increasing β_{TL}. It was noted that the reduction of energy dissipation for the joints at large β_{TL} was more severe. This could be attributed to the yielding of lap brace member which accelerated the reduction of load carrying capacity at large displacement level.

As shown in Fig. 14a, the joints at low τ_{TL} (= 0.4), high γ_T (= 26) and high β_{TL} (= 0.8) yield the largest reduction of energy dissipation capacity of 36.7% and 61.8% in compression, and 2.4% and 39.9% in tension phase of third and fifth load cycle, respectively. This was attributed to the local buckling of lap brace prior to material yielding. As expected, the joint failure at τ_{TL} = 1.0 (in Fig. 14b) was associated with through brace wall plastification. The energy dissipation ratio did not exhibit any sign of reduction with load cycles. It was also noted that the energy dissipation capacity of the joint was slightly affected by β_{TL} at τ_{TL} = 1.0. The accumulative energy dissipation of the joint reduces with increasing β_{TL}, but this is only limited for the joints with lap brace local buckling or yielding, as shown in Fig. 9.15.

9.3.5 Effect of lap brace-to-through brace wall thickness ratio, τ_{TL}

In this section, the cyclic behaviour of the completely overlapped tubular joints was studied by varying the parameters τ_{TL} (0.4, 0.7 and 1.0) at different cases of γ_T (11 and 26) and β_{TL} (0.4 and 0.8). It had been reported from the previous Chapter 5 that the parameter τ_{TL} was one of the most crucial geometrical parameters controlling the failure behaviour of the joint under lap brace axial compression. In the current parametric study, the cyclic behaviour of the joint is also significantly affected by τ_{TL}, as shown in Fig. 9.16. The joint at low τ_{TL} (= 0.4) exhibited unstable cyclic behaviour with sudden lost of stiffness and strength due to premature yielding of lap

brace. The non uniform behaviour of the cyclic load carrying capacity of the joints is shown in Fig. 9.17. This behaviour was attributed to the interactive effect of joint parameters τ_{TL}, γ_T and β_{TL}. The compressive capacity of the joint at low τ_{TL} decreased at first few load cycles. It was specifically noted that the parameter τ_{TL} had less impact on tension in compared with that on compression phase of the joint under cyclic loading.

Similarly, the energy dissipation of the joint at low τ_{TL} decreased more rapidly at large displacement level due to stiffness and strength deterioration in subsequent load cycles (Fig. 9.18). The accumulative energy dissipation of the joint at large γ_T (= 26) increased with τ_{TL} (Fig. 9.19c). However, this is not the case for the joint at small γ_T (= 11) as shown in Fig. 9.19a.

The area enclosed by the hysteresis curves at *i*th load cycle for the joints with varying τ_{TL} is illustrated in Fig. 9.20. The joints at large τ_{TL} =1.0 dissipated more energy and did not exhibit any sign of reduction of energy dissipation with increasing load cycles. On the other hand, the joint at τ_{TL} = 0.4 dissipated least energy and exhibited reduction of energy dissipation, particularly for the joint at large β_{TL} (=0.8) in combined with small γ_T (=11) (Fig. 9.20b).

9.3.6 Effect of through brace radius-to-wall thickness ratio, γ_T

Apart from the parameter τ_{TL}, γ_T was also a crucial parameter influencing the failure mechanism of the joint. At large γ_T, the joint failure was associated with through brace wall plastification or lap brace local bucking. At small γ_T, the lap brace member failure under axial compression occurred as the member had lower strength than the joint.

In this section, the cyclic behaviour of completely overlapped tubular joints was studied by varying the parameters γ_T (11, 17, 26 and 42) at different cases of τ_{TL} (0.4 and 1.0) and β_{TL} (0.4 and 0.8). As shown in Fig. 9.21a, the joint at low β_{TL} (=0.4)

and τ_{TL} (=0.4) is associated with lap brace member failure. The stiffness of the joint decreased with increasing γ_T. However, this effect was not significant for the joints with γ_T greater than 17. The cyclic load carrying capacity of the joint in tension phase was not significantly affected by varying γ_T (Fig. 9.22a).

The joint at high β_{TL} (=0.8) and low τ_{TL} (=0.4) was associated with lap brace local buckling. The stiffness and the strength of the joint deteriorate with increasing γ_T, as shown in Fig. 9.21b. However, this effect became insignificant with γ_T greater than 26. For the joints with lower γ_T (=11 and 17), the failure in compression phase of load cycle was due to lap brace member yielding in combined with local buckling. On the other hand, for the joints with higher γ_T (=26 and 42), the failure was associated with lap brace local buckling. The deterioration of strength for the joint at large γ_T occurs in the earlier load cycle, as shown in Fig. 9.22b.

For the joint at large β_{TL} (=0.8) and τ_{TL} (=1.0), the failure was associated with through brace wall plastification. The hysteresis behaviour of the joint under cyclic loading was stable. The stiffness and the strength of the joint were not significantly affected by varying γ_T (Figs. 9.21c and 9.22c). As shown in Fig. 9.23, the energy dissipation capacity of the joint decreases with increasing γ_T. For the joints at large β_{TL} (=0.8) and τ_{TL} (=1.0), the effect of γ_T was not critical. The area enclosed by the hysteresis curves at *i*th load cycle also showed that the joints at small γ_T dissipated more energy (Fig. 9.24).

9.3.7 Effect of gap size parameter, ξ

In this section, the cyclic behaviour of the completely overlapped tubular joints was studied by varying the parameters ξ (0.11, 0.5, 1.0 and 2.0) at different cases of γ_T (11 and 26) and τ_{TL} (0.4 and 1.0). From the hysteresis curves as shown in Fig. 9.25, the stiffness of the joint decreases with increasing gap size. It was commented from this observation that the gap size could have significant impact on the capacity of the completely overlapped tubular joint under cyclic loading.

In Fig. 9.25b, it showed that the joint with minimum gap size exhibits unstable cyclic behaviour with lap brace local buckling. However, the local buckling failure of the lap brace could be avoided by increasing the gap size of the joint. It could be seen from Fig. 9.26 that the gap size could have significant impact on the strength resistance of the joint. For the joint at small gap size, the strength reduction occurred in earlier load cycles due to localised lap brace buckling under axial compression.

The gap size parameter (ξ) showed slight effect on the accumulative energy dissipation of the joint (Fig. 9.27). The joint at large gap size dissipated more energy than that at small gap size with the same ductility level (Fig. 9.28). This was attributed to the bending of through brace which dissipated more energy with increasing gap size. However, for the joints at large τ_{TL}, the impact of gap sizes was found less significant compared with the parameters τ_{TL} and γ_T.

9.3.8 Effect of brace angle, θ

In this section, the cyclic behaviour of the completely overlapped tubular joints was studied by varying the lap brace angle with respect to through brace, θ (30^0, 45^0 and 60^0) at different gap size parameters, ξ (0.11 and 1.0). It could be seen from Fig. 29 that the stiffness and the strength of the joint decreases with increasing θ. The joint at $\theta = 60^0$ exhibited lowest strength resistance and energy dissipation compared to that at small θ (Figs. 30 and 31).

9.4 Characteristics of load cycles

In this section, twenty-four FE models of the completely overlapped tubular joints subjected to constant displacement amplitude cyclic loading were analysed to study the effect of cyclic load sequence (tension and compression), normalized displacement amplitude, $(\delta/\delta_y)_A$, and mean displacement, $(\delta/\delta_y)_M$. The geometrical parameters of the joint β_{CT} (= 0.6), β_{TL} (= 0.6) and τ_{CT} (= 0.7) remained constant

throughout the analysis.

9.4.1 Effect of load sequence

The effect of load sequence on the tensile and compressive strength resistance of the joint with increasing load cycles can be seen in Fig. 9.32. In the figure, both FE models are subjected to the same load level. The load sequence of one model was initiated in tension while the other in compression. The results showed that the effect of load sequence was dependent upon the geometrical parameters of the joint. For the joint at low τ_{TL} (= 0.4) and γ_T (= 11), the load sequence showed slight effect on the strength resistance (Fig. 9.32a). This was attributed to the load level causing the lap brace member yielding prior to joint failure. Thus, the squash load of the lap brace member determined the strength resistance of the joint.

It could be seen from Figs. 9.32b and 9.32c that the joints with first load cycle in compression showed higher compressive resistance than that in tension. However, the compressive resistance of the joint rapidly deteriorated with increasing load cycle. For the joint at small τ_{TL} (= 0.4), the tensile resistance at both load sequences were almost identical. For the joints at large τ_{TL} (= 1.0), the first load cycle in tension resulted in higher tensile strength than that in compression. The reason was due to the through brace face plastification under first load cycle in compression which reduced the joint tensile resistance. At small τ_{TL} (= 0.4), the joint tensile capacity was limited by the lap brace member capacity, so the effect of load sequence was moderate. The energy dissipation capacity of the joint as shown in Fig. 9.33 is found not affected under different load sequences.

9.4.2 Effect of displacement amplitude

In this section, three levels of displacement amplitude ($(\delta/\delta_y)_A$= 4, 6, 8) with first load cycle in compression were considered to study the effect of $(\delta/\delta_y)_A$ on the strength resistance and the energy dissipation capacity of the joint. As shown in Fig. 34, the load carrying capacity of the joint decreases with increasing displacement

amplitude $(\delta/\delta_y)_A$. The deterioration rate of both tensile and compressive strength of the joint increased owing to severe damage at large displacement.

It could be seen from Fig. 9.35 that the accumulative energy dissipation increases with displacement amplitude of the joint. However, the rate of increasing energy dissipation capacity was not as large as that of displacement amplitude at $(\delta/\delta_y)_A = 6$. This was due to the reduced energy dissipation capacity at large displacement amplitude in subsequent load cycles.

9.4.3 Effect of mean displacement

In this section, five levels of normalized mean displacement ($(\delta/\delta_y)_M = 0, \pm1, \pm2$) with first load cycle in compression were considered to study the effect of $(\delta/\delta_y)_M$ on the strength resistance and the energy dissipation capacity of the joint. For the joints at small τ_{TL} (= 0.4) and γ_T (= 11), the effect of mean displacement on the strength resistance of the joint is moderate, as shown in Fig. 9.36a. The main reason was that the joint strength resistance was limited by the lap brace member squash load.

At small τ_{TL} (= 0.4) and large γ_T (= 26), both the compressive and the tensile resistance of the joint reduce as the mean displacement shifts toward the compressive load as shown in Fig. 9.36b. This caused a large displacement in the compression phase of load cycle. As a result, the load carrying capacity of the joint reduced due to local buckling failure of lap brace member.

At large τ_{TL} (= 1.0) and low γ_T (=11), the tensile strength resistance of the joint reduces as the mean displacement moves toward the compressive load as shown in Fig. 9.36c. The tensile load did not reach the maximum tensile capacity after the mean displacement shifted to the compression phase of the load cycle. On the other hand, the compressive strength of the joint increased as the mean displacement moved toward the compressive load due to the strain hardening effect of the through brace in contact with the lap brace.

At small τ_{TL} (= 0.4) and γ_T (= 11), the energy dissipation of the joint increases as the mean displacement moves toward the compressive load, as shown in Fig. 9.37a. This was because the joint dissipated more energy in compression than that in tension phase of the load cycle. However, the energy dissipation of the joint decreases at large compression displacement, as shown in Fig. 9.37b. This was due to the decrease of load carrying capacity after the lap brace local buckling took place. At large τ_{TL} (= 1.0) and small γ_T (=11), the cyclic behaviour of the joint was stable and the failure was associated with the through brace wall plastification. The effect of mean displacement on the energy dissipation capacity of the joint is moderate, as shown in Fig. 9.37c.

9.5 Discussions

In the seismic-resistant steel frames, two different approaches have been considered for connection design. The first approach is to ensure that the earthquake energy can be dissipated through the cyclic plastic bending behaviour at beam ends. This requires the connections to be designed to possess sufficient reserve strength to form plastic hinges. The second approach is to rely upon the energy dissipation through the cyclic plastic bending of connections. In this case, the dissipative zones are located in the connections and not in the beams.

In the current building design, the first approach mentioned above is generally adopted to ensure that the connections in dissipative zones have sufficient reserve strength for material yielding. The second approach is limited owing to the need of investigation to verify the effectiveness of connections under cyclic loading. However, it is important to note that if the recommendations for seismic design of building structures are to be adopted for that of offshore structures, the validity of using the recommendations must be thoroughly investigated since the offshore structures include some unique features which are not found in the building structures such as the use of large tubular hollow sections and welding connections.

From the current study of cyclic behaviour, the load carrying and the energy dissipation capacity of the completely overlapped tubular joint rapidly deteriorates after the lap brace member yields prior to joint failure. It is also noted that the joint associated with through brace wall plastification exhibits more stable and ductile cyclic behaviour. Thus, it can be commented from the above that the second approach with the design of completely overlapped tubular joint as dissipative zone is more appropriate for the proposed eccentrically braces offshore steel jacket structure.

9.6 Concluding remarks

The cyclic behaviour of the completely overlapped tubular joint is investigated through the nonlinear FE analyses with the model calibrated and verified against the current experimental results. The results obtained from the current study revealed that the influence of geometrical parameters (β_{CT}, τ_{CT} and γ_C) of the chord and the through brace is less significant compared to those of the through brace and the lap brace (β_{TL}, τ_{TL}, γ_T) for the joint under lap brace axial cyclic loading.

At low τ_{TL}, the cyclic behaviour of the completely overlapped tubular joint is rather unstable with failure associated with lap brace member yielding and local buckling prior to joint collapse. The stiffness, the compressive resistance and the dissipation capacity of the joint sharply reduce with increasing β_{TL} and decreasing τ_{TL}. However, the impact of these parameters on the tensile strength of the joint is minimal. At high τ_{TL}, the cyclic behaviour of the joint is very stable with failure associated with through brace wall plastification in contact with lap brace. The tensile strength of the joint in the subsequent load cycles increases with β_{TL}. The parameter β_{TL} shows minimum impact on the compressive resistance and the energy dissipation capacity of the joint. Among these geometrical parameters, γ_T is one of the critical parameters controlling the strength of the joint particularly at high β_{TL} and low τ_{TL}. It is found that the energy dissipation capacity of the joint increases with γ_T.

From the FE analysis results, the gap size parameter (ζ) showed significant impact on the cyclic performance of the completely overlapped tubular joint. The joint stiffness decreases with increasing gap size. The ductility and the energy dissipation capacity of the joint at large gap size enhance as the premature failure of lap brace local buckling is prevented. The strength and the energy dissipation capacity of the joint decrease with increasing brace angle (θ) but this is limited to angle of greater than 45^0.

For the cyclic load characteristics, the first load cycle in compression results in rapid deterioration of compressive strength of the joint. The load carrying capacity of the joint reduces and the reduction rate of both tensile and compressive strength increased with displacement amplitude. Furthermore, the energy dissipation capacity of the joint is found increased. The lap brace local buckling of the joint becomes predominant as the mean displacement moves toward the compression phase of load cycle. As a result, the load carrying capacity of the joint reduces but with small magnitude.

It is noted from the behaviour described above that the load carrying and the energy dissipation capacity of the completely overlapped tubular joint rapidly deteriorate if the lap brace yielding and local buckling take place prior to joint collapse. As such, the lap brace local buckling should be considered as one of the criteria for the design of completely overlapped tubular joint at low τ_{TL}, high β_{TL} and high γ_T under both static and cyclic loads. However, the joints failed by through brace wall plastification in contact with the lap brace exhibit more stable and ductile cyclic behaviour. In consideration of this failure mode, the energy dissipative zone of eccentrically braced offshore steel jacket under seismic loading should be designed at the short segment of the through brace joining the chord.

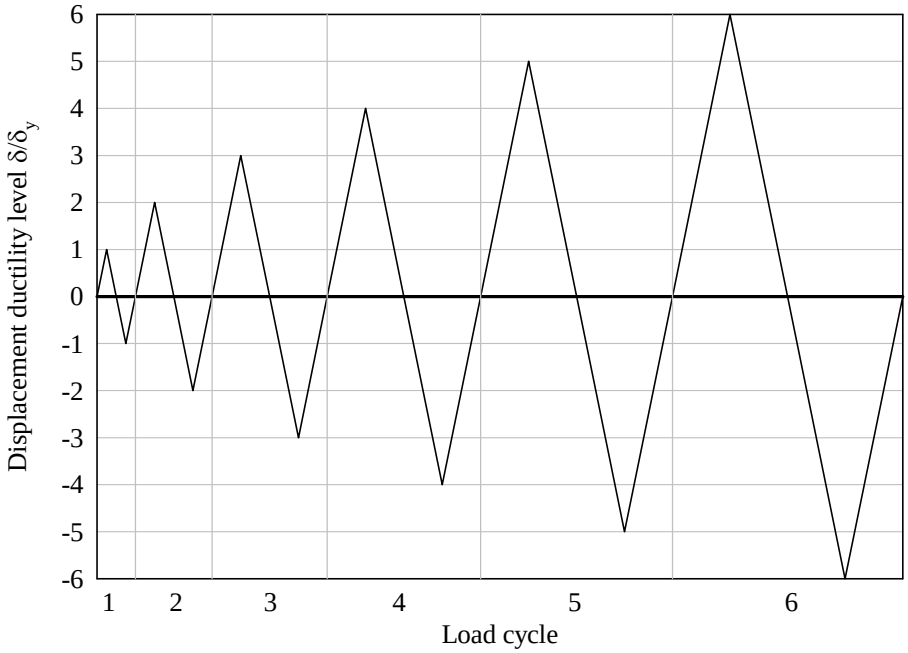

(a) Variable displacement amplitude

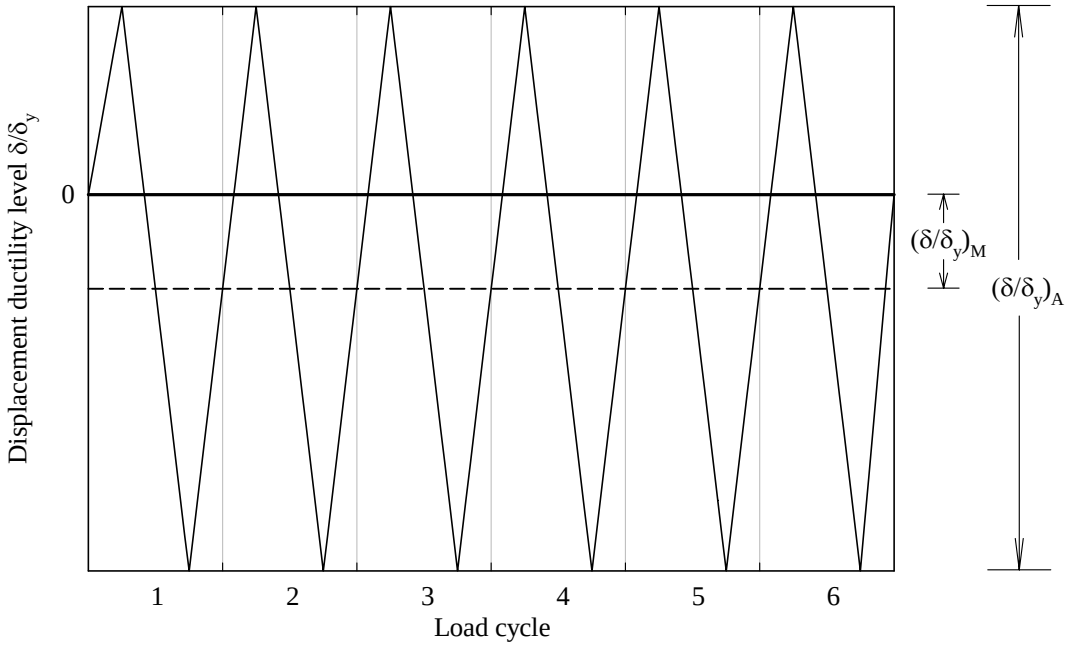

(b) Constant displacement amplitude

Fig. 9.1 Loading procedures in parametric study

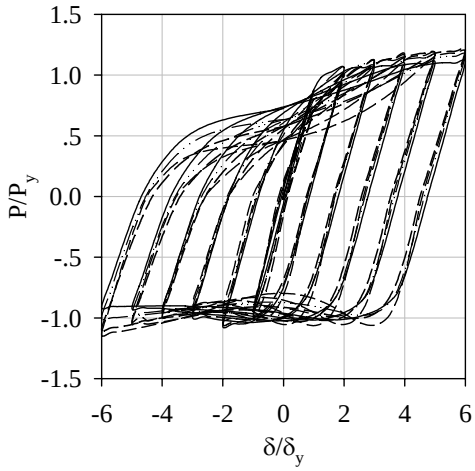

(a) τ_{CT} = 0.4, γ_C = 12

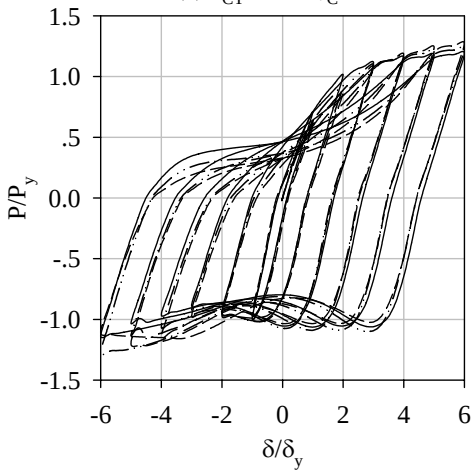

(b) τ_{CT} = 0.4, γ_C = 30

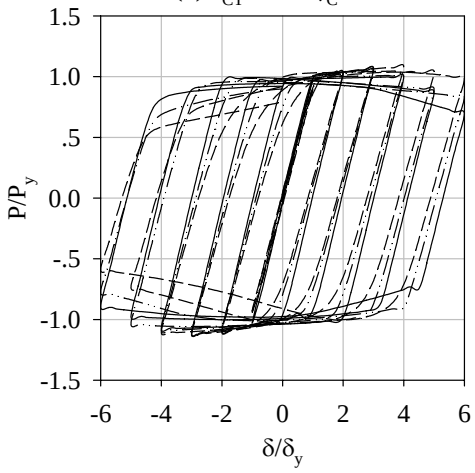

(c) τ_{CT} = 1.0, γ_C = 12

β_{CT} = 0.4 β_{CT} = 0.6 β_{CT} = 0.8

Constants: β_{TL} = 0.6, τ_{TL} = 0.7

Fig. 9.2 Hysteresis curve (through brace-to-chord diameter ratio, β_{CT})

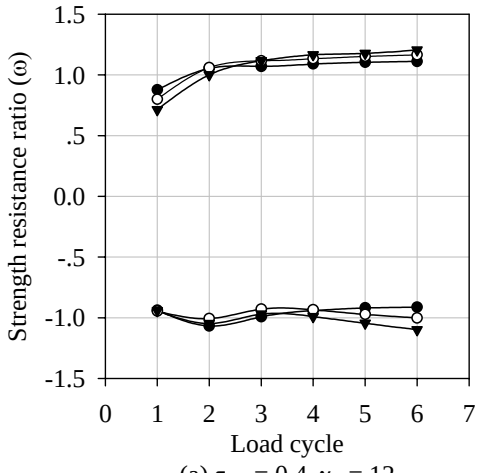

(a) τ_{CT} = 0.4, γ_C = 12

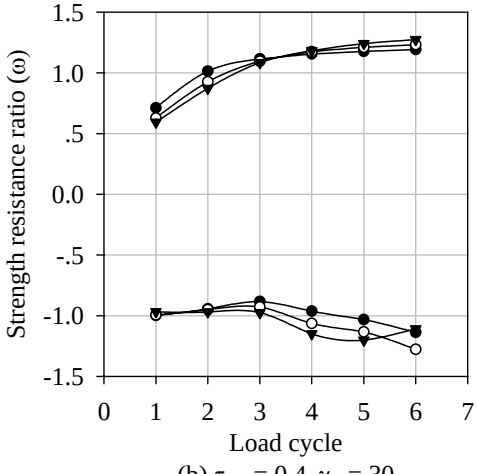

(b) τ_{CT} = 0.4, γ_C = 30

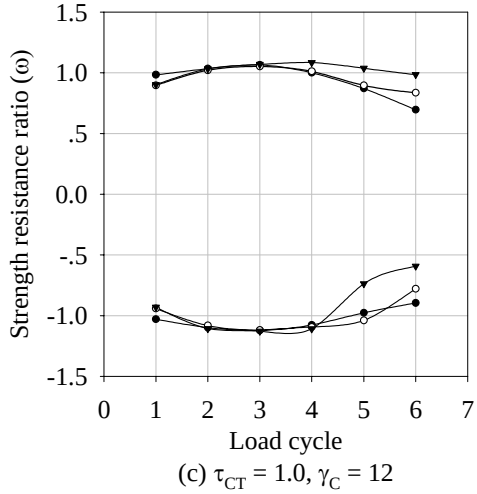

(c) τ_{CT} = 1.0, γ_C = 12

β_{CT} = 0.4 β_{CT} = 0.6 β_{CT} = 0.8

Constants: β_{TL} = 0.6, τ_{TL} = 0.7

Fig. 9.3 Strength resistance ratio (through brace-to-chord diameter ratio, β_{CT})

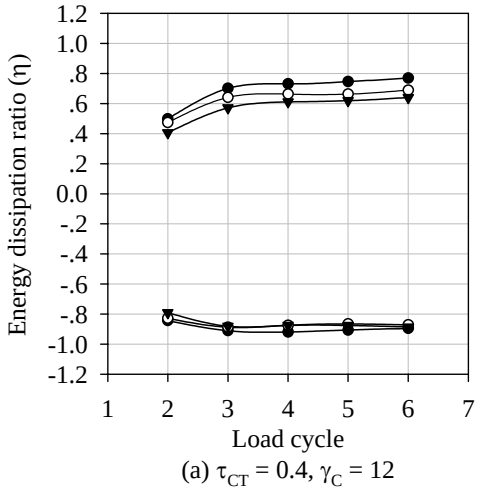

(a) τ_{CT} = 0.4, γ_C = 12

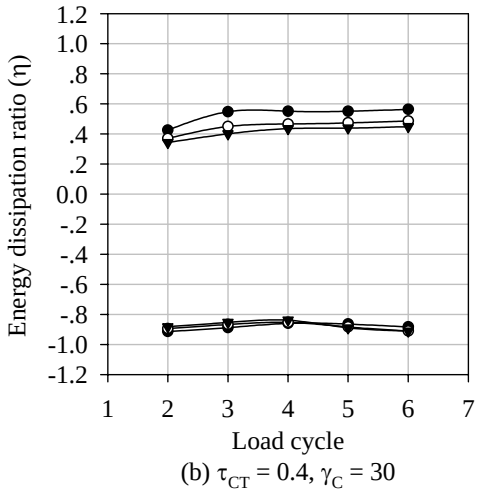

(b) τ_{CT} = 0.4, γ_C = 30

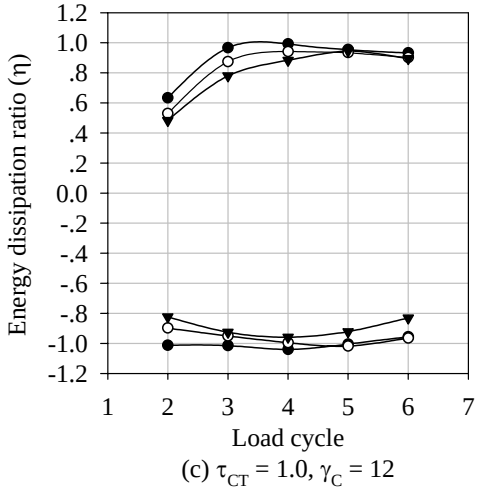

(c) τ_{CT} = 1.0, γ_C = 12

β_{CT} = 0.4 β_{CT} = 0.6 β_{CT} = 0.8

Constants: β_{TL} = 0.6, τ_{TL} = 0.7

Fig. 9.4 Energy dissipation ratio (through brace-to-chord diameter ratio, β_{CT})

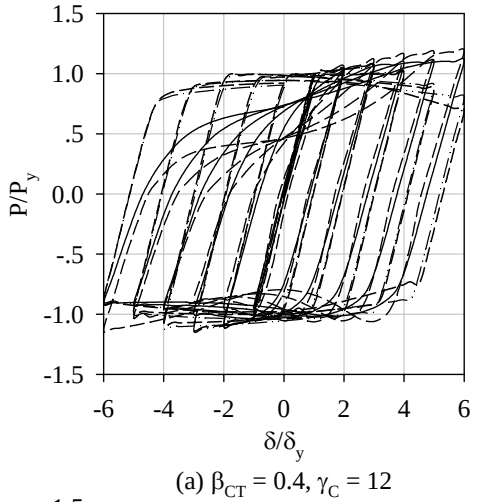

(a) β_{CT} = 0.4, γ_C = 12

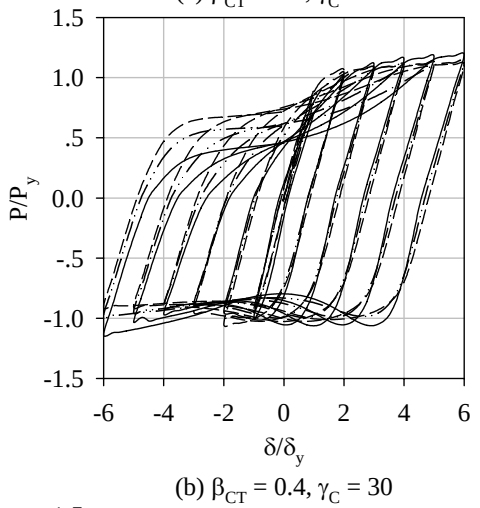

(b) β_{CT} = 0.4, γ_C = 30

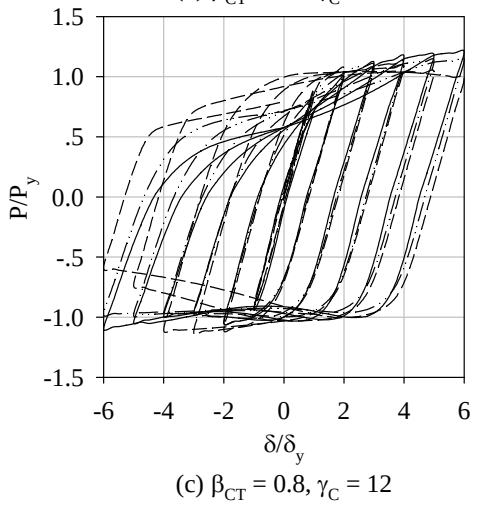

(c) β_{CT} = 0.8, γ_C = 12

τ_{CT} = 0.4 τ_{CT} = 0.7 τ_{CT} = 1.0

Constants: β_{TL} = 0.6, τ_{TL} = 0.7

Fig. 9.5 Hysteresis curve (through brace-to-chord wall thickness ratio, τ_{CT})

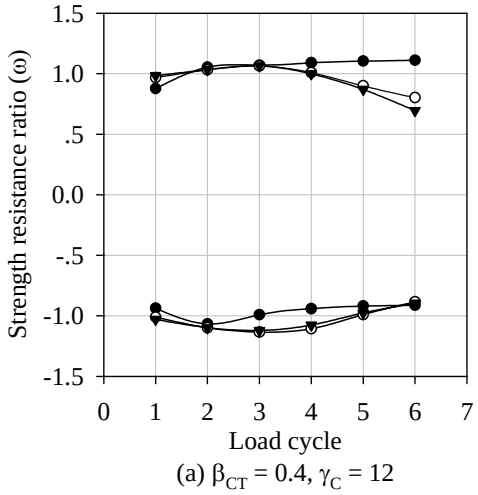

(a) β_{CT} = 0.4, γ_C = 12

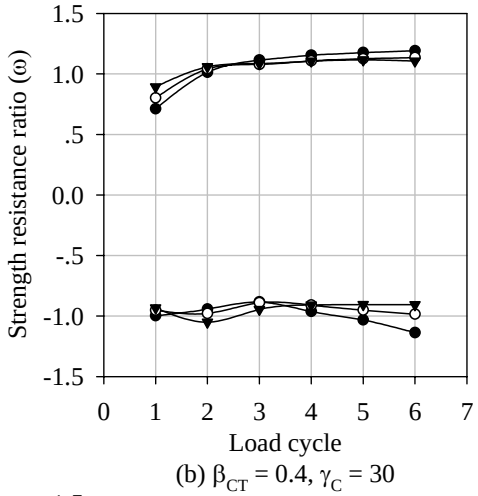

(b) β_{CT} = 0.4, γ_C = 30

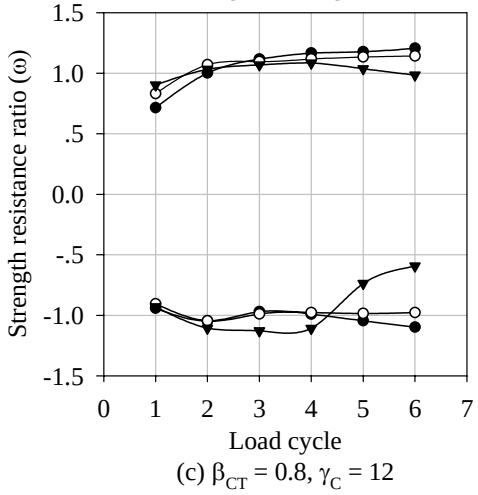

(c) β_{CT} = 0.8, γ_C = 12

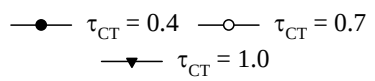

Constants: β_{TL} = 0.6, τ_{TL} = 0.7

Fig. 9.6 Strength resistance ratio (through brace-to-chord wall thickness ratio, τ_{CT})

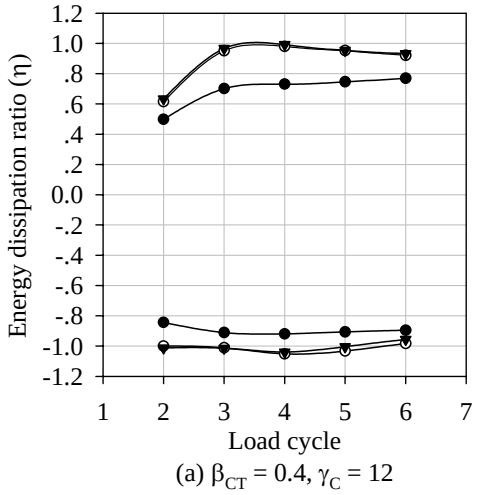

(a) β_{CT} = 0.4, γ_C = 12

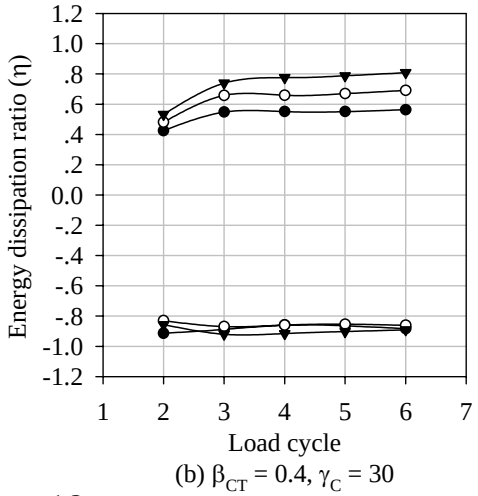

(b) β_{CT} = 0.4, γ_C = 30

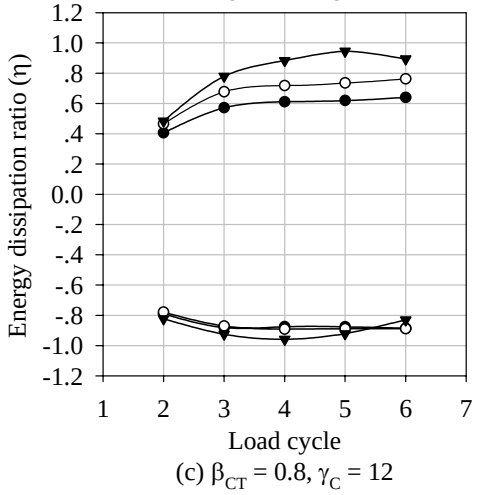

(c) β_{CT} = 0.8, γ_C = 12

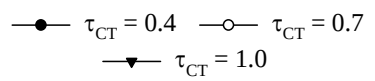

Constants: β_{TL} = 0.6, τ_{TL} = 0.7

Fig. 9.7 Energy dissipation ratio (through brace-to-chord wall thickness ratio, τ_{CT})

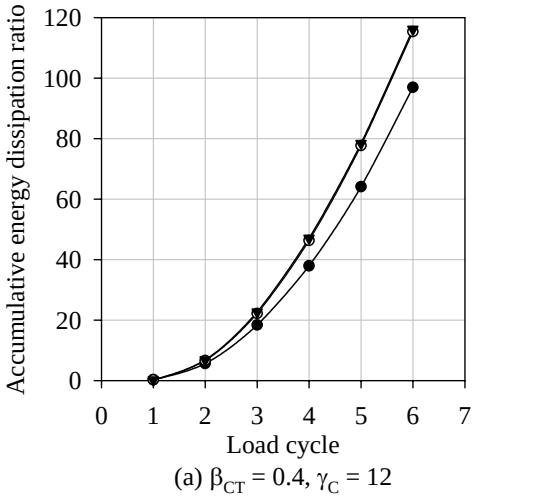

(a) β_{CT} = 0.4, γ_C = 12

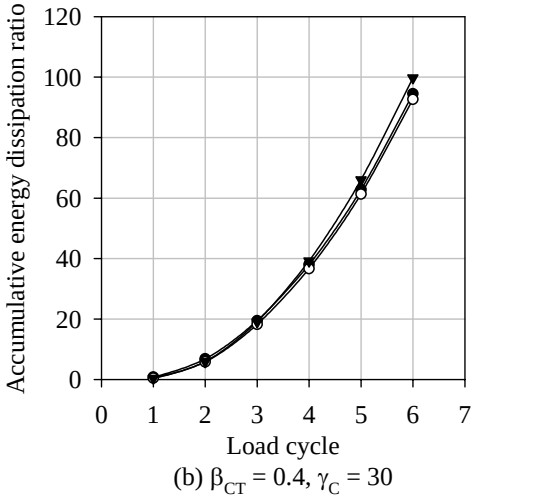

(b) β_{CT} = 0.4, γ_C = 30

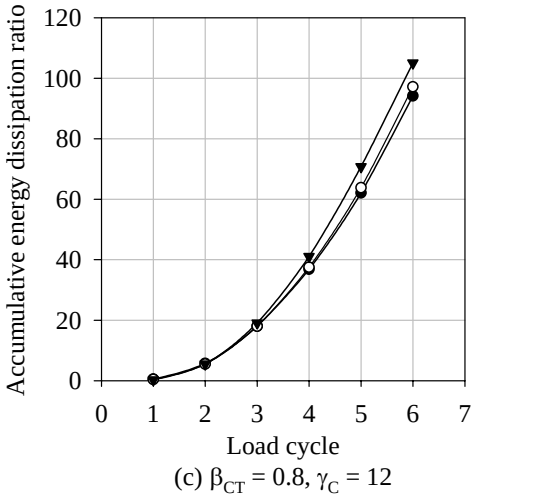

(c) β_{CT} = 0.8, γ_C = 12

τ_{CT} = 0.4 τ_{CT} = 0.7 τ_{CT} = 1.0

Constants: β_{TL} = 0.6, τ_{TL} = 0.7

Fig. 9.8 Accumulative energy dissipation ratio (through brace-to-chord wall thickness ratio, τ_{CT})

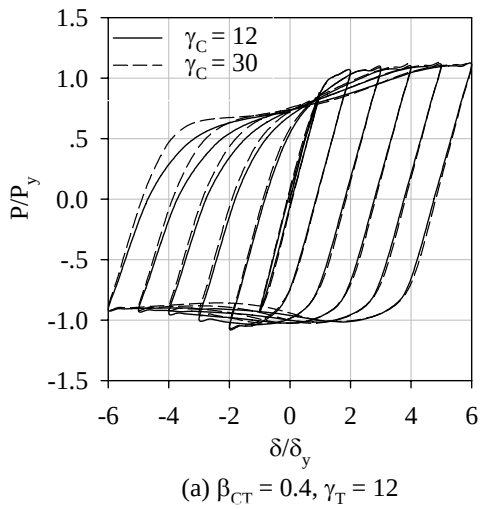

(a) β_{CT} = 0.4, γ_T = 12

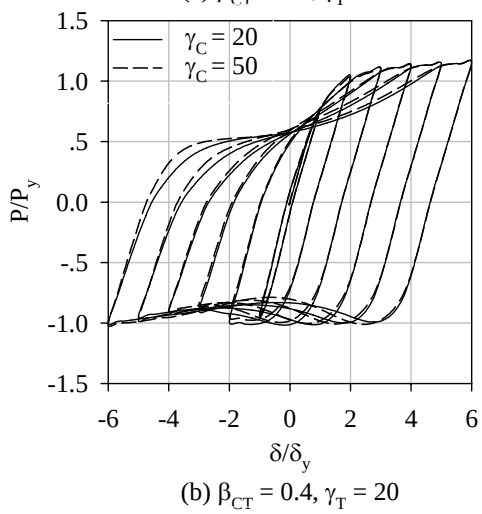

(b) β_{CT} = 0.4, γ_T = 20

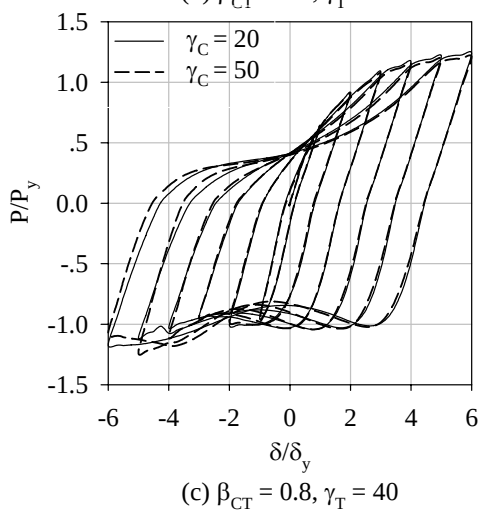

(c) β_{CT} = 0.8, γ_T = 40

Constants: β_{TL} = 0.6, τ_{TL} = 0.7

Fig. 9.9 Hysteresis curve (chord radius-to-wall thickness ratio, γ_C)

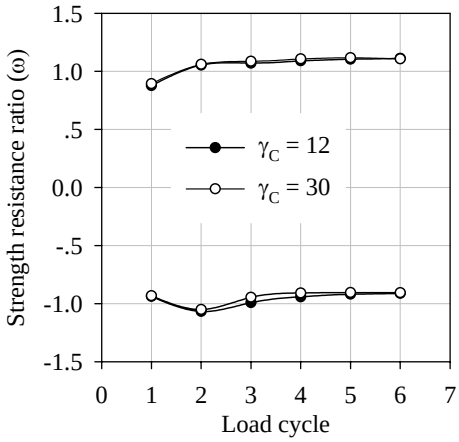

(a) $\beta_{CT} = 0.4$, $\gamma_T = 12$

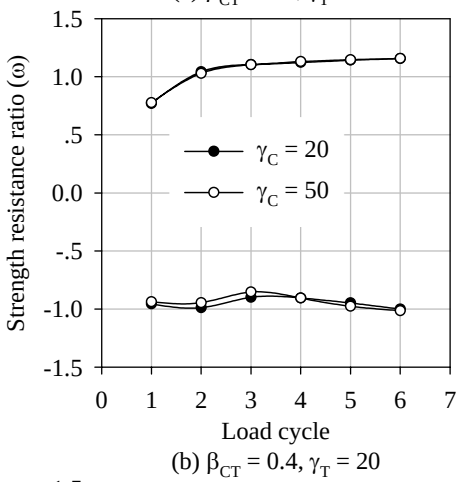

(b) $\beta_{CT} = 0.4$, $\gamma_T = 20$

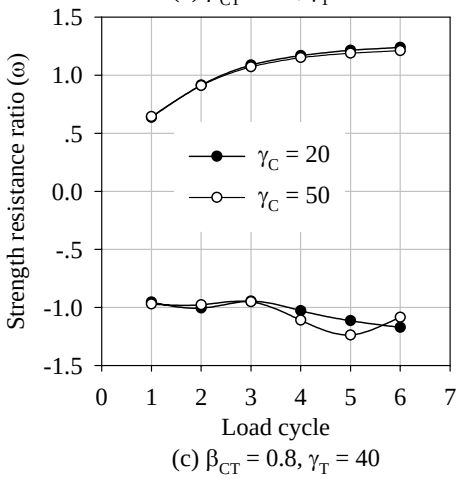

(c) $\beta_{CT} = 0.8$, $\gamma_T = 40$

Constants: $\beta_{TL} = 0.6$, $\tau_{TL} = 0.7$

Fig. 9.10 Strength resistance ratio (chord radius-to-wall thickness ratio, γ_C)

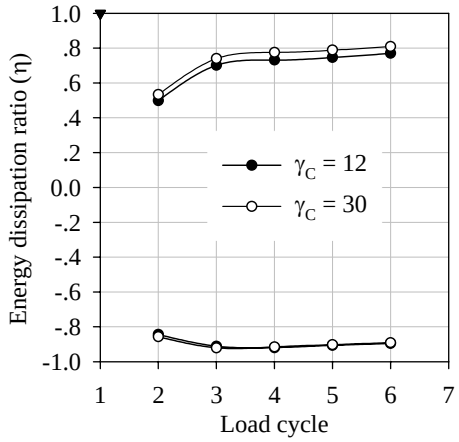

(a) $\beta_{CT} = 0.4$, $\gamma_T = 12$

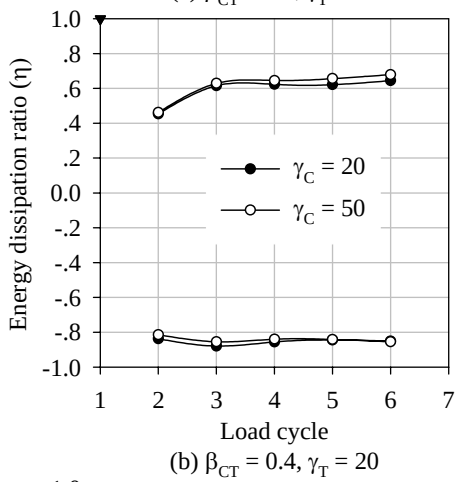

(b) $\beta_{CT} = 0.4$, $\gamma_T = 20$

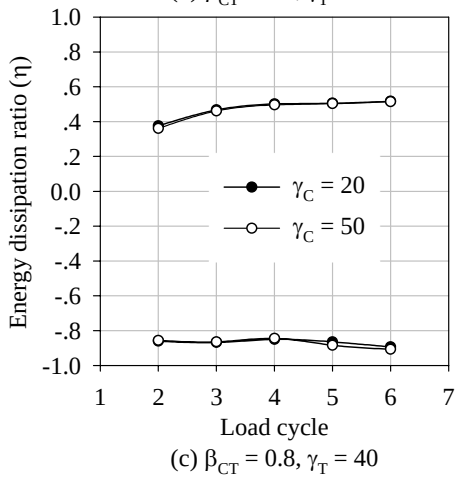

(c) $\beta_{CT} = 0.8$, $\gamma_T = 40$

Constants: $\beta_{TL} = 0.6$, $\tau_{TL} = 0.7$

Fig. 9.11 Energy dissipation ratio (chord radius-to-wall thickness ratio, γ_C)

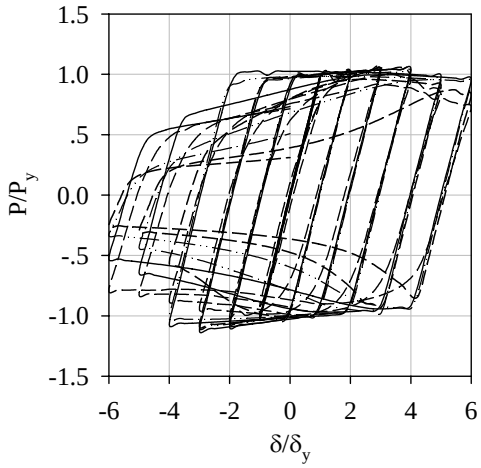

(a) τ_{TL} = 0.4, γ_C = 12, γ_T = 11

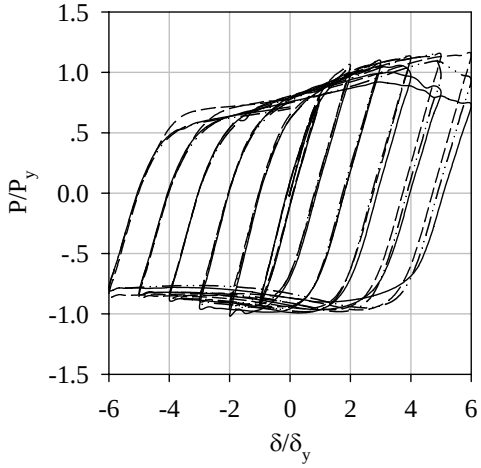

(b) τ_{TL} = 1.0, γ_C = 12, γ_T = 11

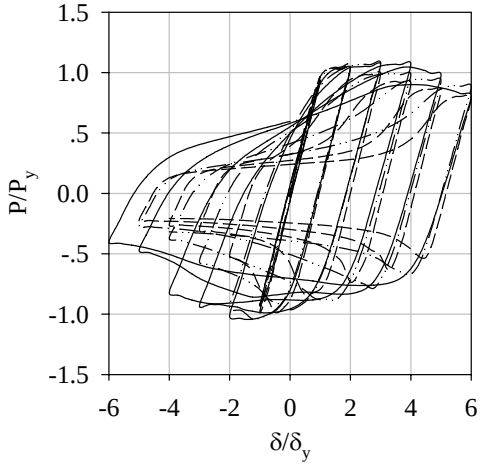

(c) τ_{TL} = 0.4, γ_C = 30, γ_T = 26

β_{TL} = 0.4 β_{TL} = 0.6 β_{TL} = 0.8

Constants: β_{CT} = 0.6, τ_{CT} = 0.7

Fig. 9.12 Hysteresis curve (lap brace-to-through brace diameter Ratio, β_{TL})

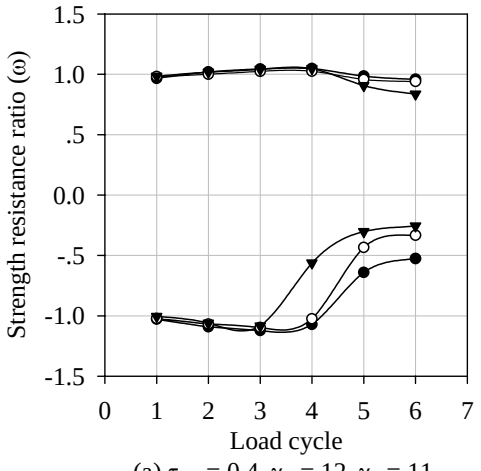

(a) τ_{TL} = 0.4, γ_C = 12, γ_T = 11

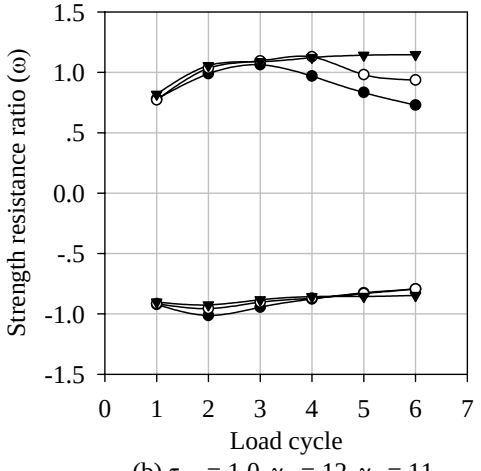

(b) τ_{TL} = 1.0, γ_C = 12, γ_T = 11

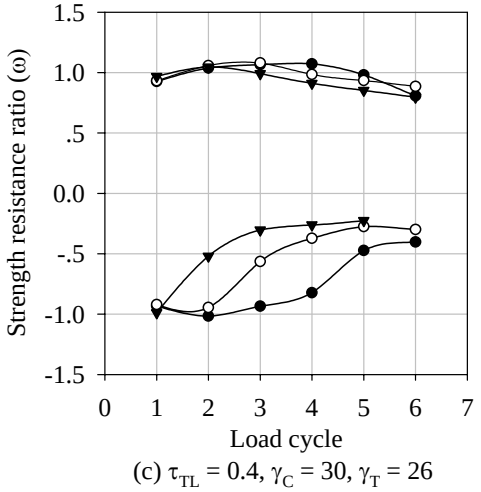

(c) τ_{TL} = 0.4, γ_C = 30, γ_T = 26

β_{TL} = 0.4 β_{TL} = 0.6 β_{TL} = 0.8

Constants: β_{CT} = 0.6, τ_{CT} = 0.7

Fig. 9.13 Strength resistance ratio (lap brace-to-through brace diameter ratio, β_{TL})

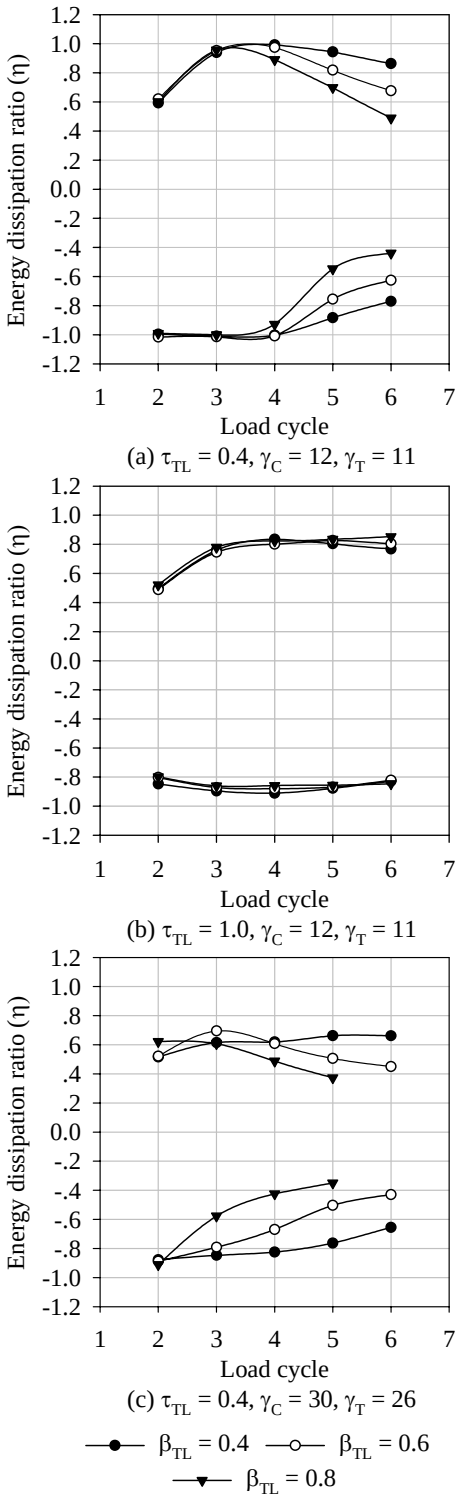

Constants: β_{CT} = 0.6, τ_{CT} = 0.7

Fig. 9.14 Energy dissipation ratio (lap brace-to-through brace diameter ratio, β_{TL})

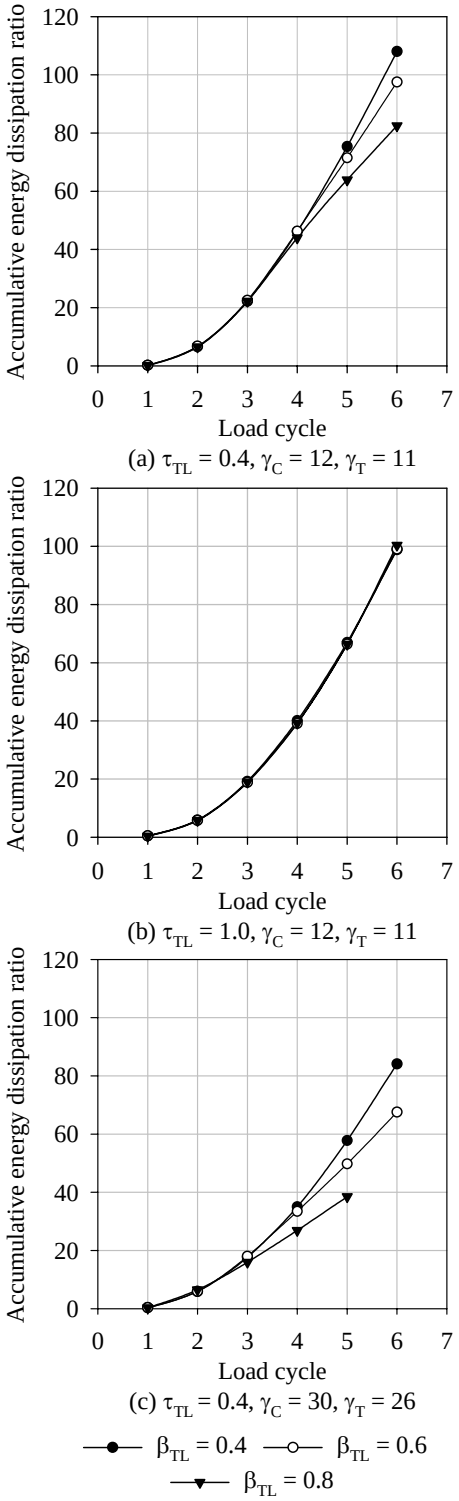

Constants: β_{CT} = 0.6, τ_{CT} = 0.7

Fig. 9.15 Accumulative energy dissipation ratio (lap brace-to-through brace diameter ratio, β_{TL})

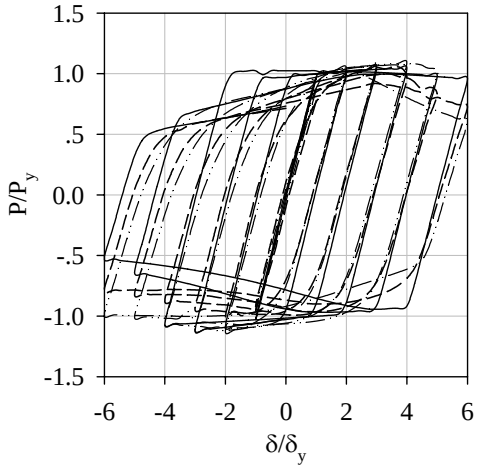

(a) β_{TL} = 0.4, γ_C = 12, γ_T = 11

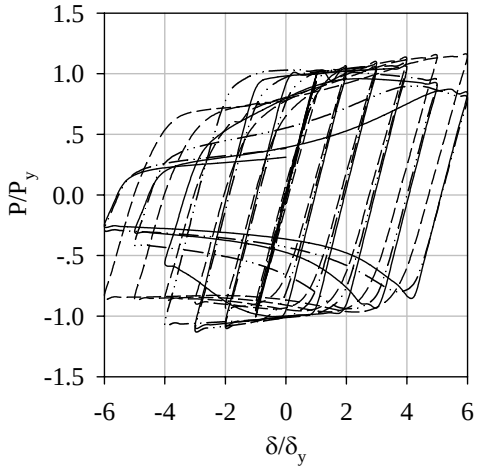

(b) β_{TL} = 0.8, γ_C = 12, γ_T = 11

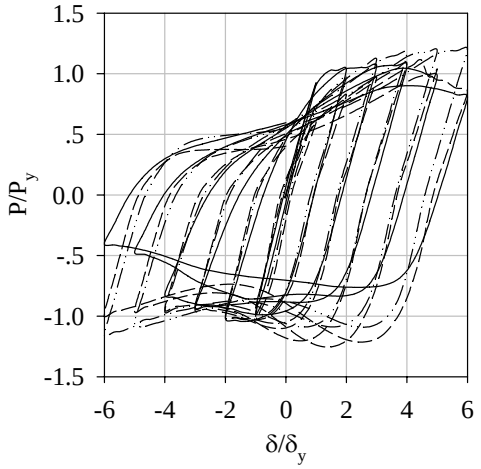

(c) β_{TL} = 0.4, γ_C = 30, γ_T = 26

τ_{TL} = 0.4 τ_{TL} = 0.7 τ_{TL} = 1.0

Constants: β_{CT} = 0.6, τ_{CT} = 0.7

Fig. 9.16 Hysteresis curve (lap brace -to-through brace wall thickness ratio, τ_{TL})

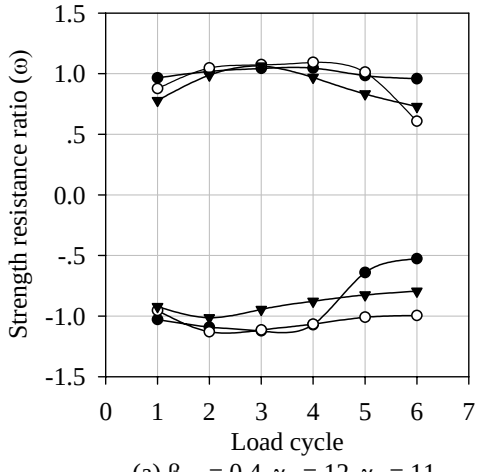

(a) β_{TL} = 0.4, γ_C = 12, γ_T = 11

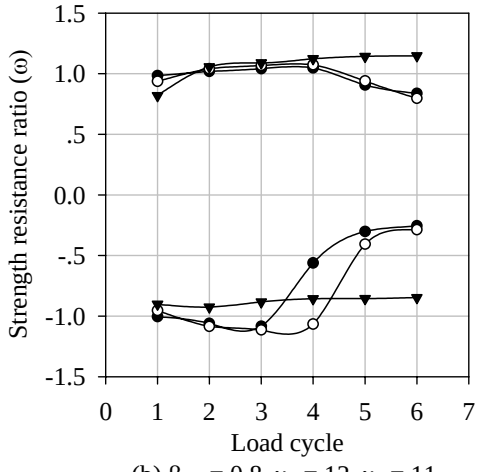

(b) β_{TL} = 0.8, γ_C = 12, γ_T = 11

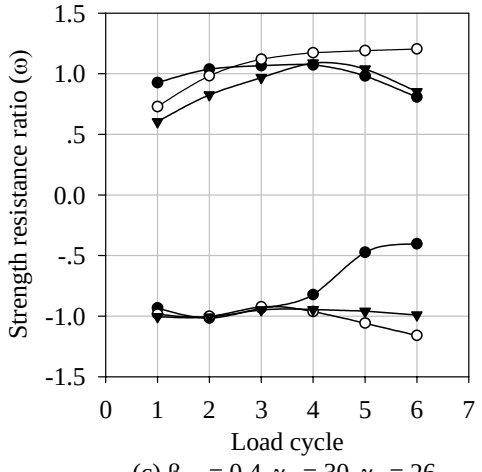

(c) β_{TL} = 0.4, γ_C = 30, γ_T = 26

τ_{TL} = 0.4 τ_{TL} = 0.7 τ_{TL} = 1.0

Constants: β_{CT} = 0.6, τ_{CT} = 0.7

Fig. 9.17 Strength resistance ratio (lap brace-to-through brace wall thickness ratio, τ_{TL})

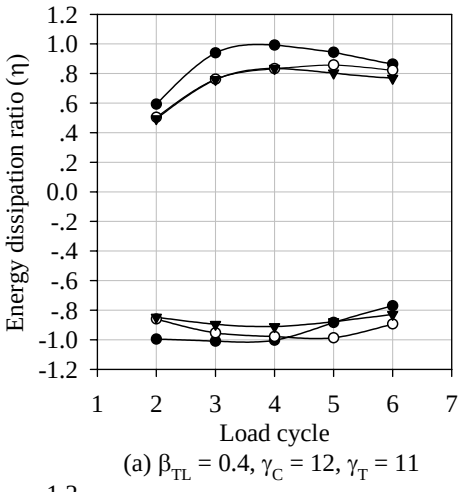

(a) β_{TL} = 0.4, γ_C = 12, γ_T = 11

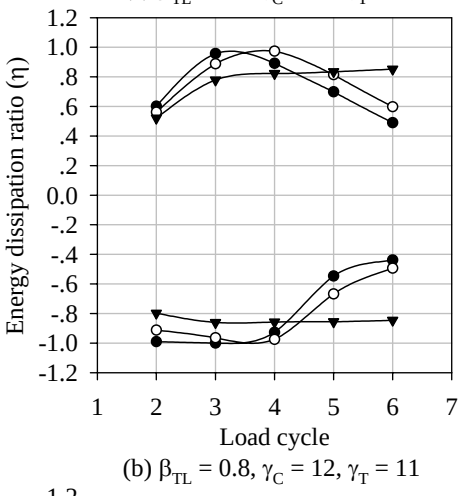

(b) β_{TL} = 0.8, γ_C = 12, γ_T = 11

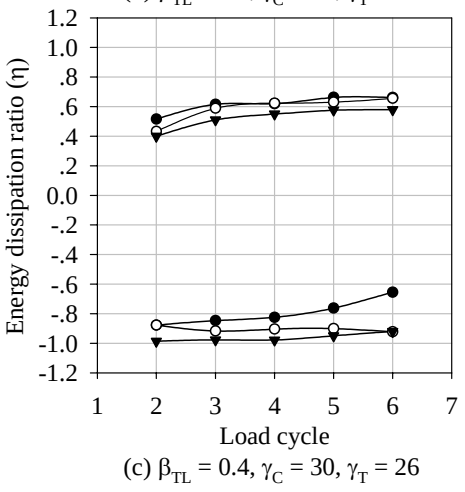

(c) β_{TL} = 0.4, γ_C = 30, γ_T = 26

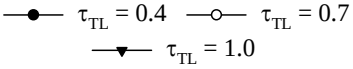

Constants: β_{CT} = 0.6, τ_{CT} = 0.7

Fig. 9.18 Energy dissipation ratio (lap brace-to-through brace wall thickness ratio, τ_{TL})

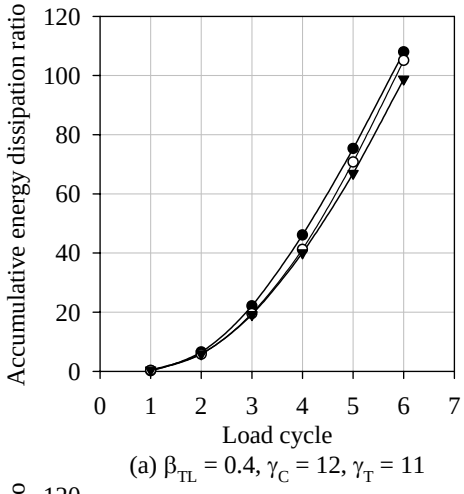

(a) β_{TL} = 0.4, γ_C = 12, γ_T = 11

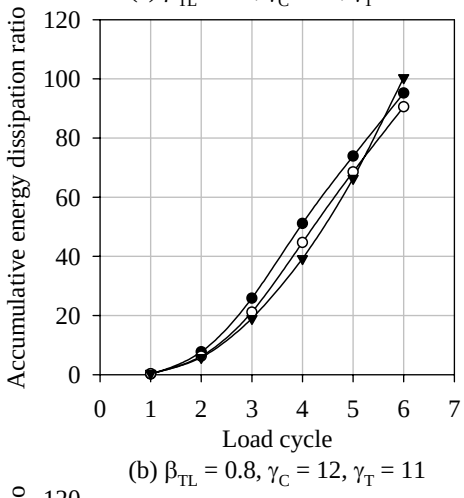

(b) β_{TL} = 0.8, γ_C = 12, γ_T = 11

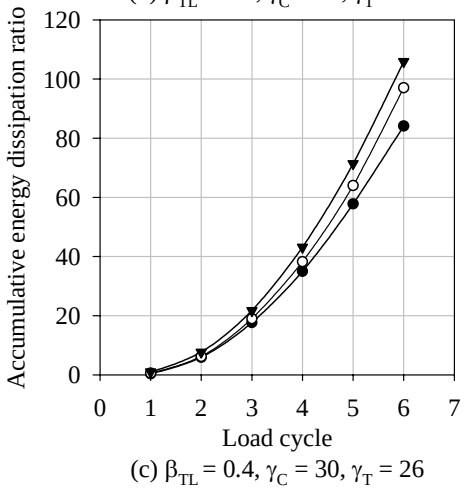

(c) β_{TL} = 0.4, γ_C = 30, γ_T = 26

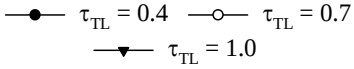

Constants: β_{CT} = 0.6, τ_{CT} = 0.7

Fig. 9.19 Accumulative energy dissipation ratio (lap brace-to-through brace wall thickness ratio, τ_{TL})

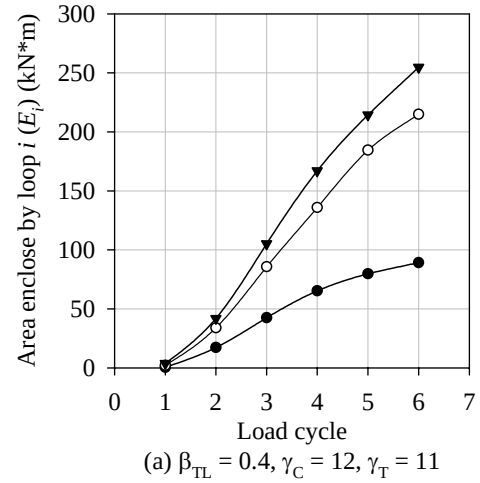

(a) β_{TL} = 0.4, γ_C = 12, γ_T = 11

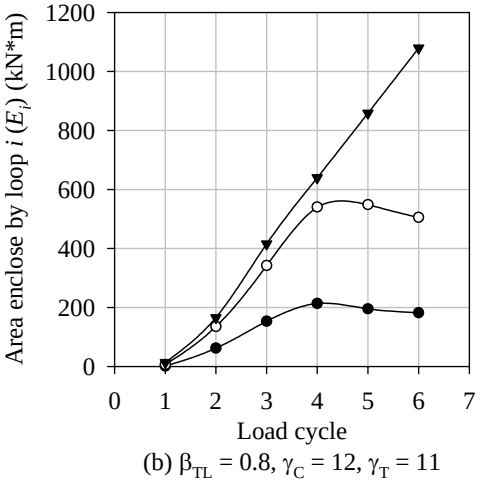

(b) β_{TL} = 0.8, γ_C = 12, γ_T = 11

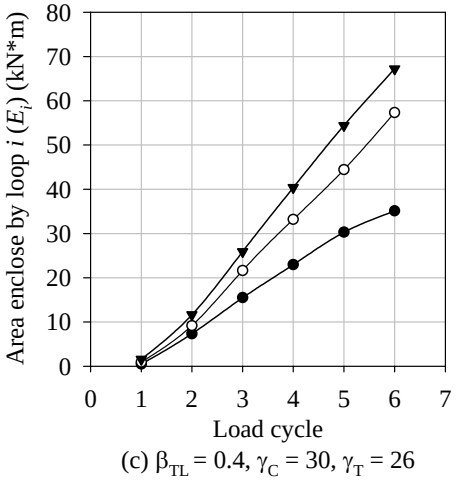

(c) β_{TL} = 0.4, γ_C = 30, γ_T = 26

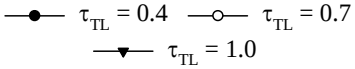

Constants: β_{CT} = 0.6, τ_{CT} = 0.7

Fig. 9.20 Area enclosed by hysteresis loop (lap brace-to-through brace wall thickness ratio, τ_{TL})

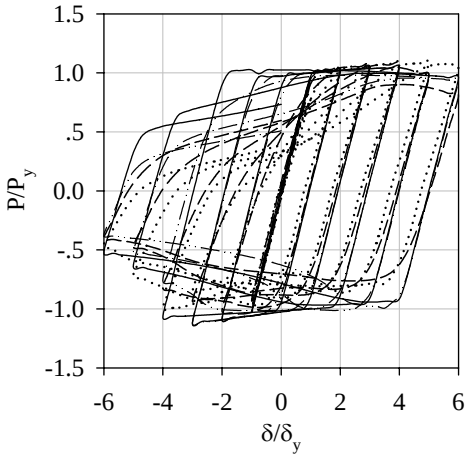

(a) β_{TL} = 0.4, τ_{TL} = 0.4

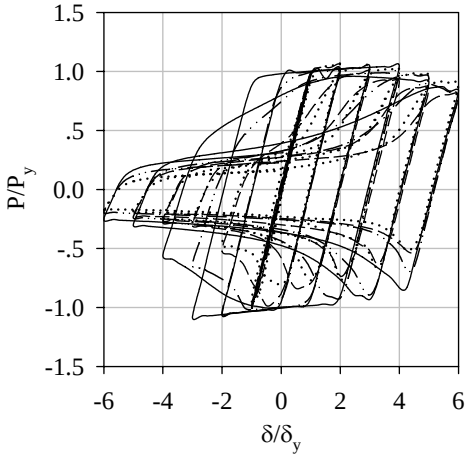

(b) β_{TL} = 0.8, τ_{TL} = 0.4

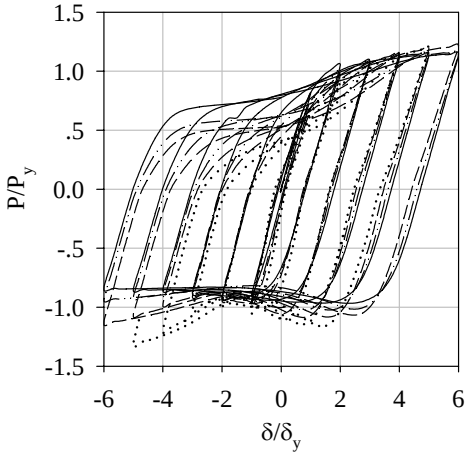

(c) β_{TL} = 0.8, τ_{TL} = 1.0

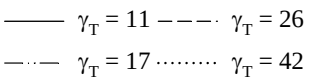

Constants: β_{CT} = 0.6, τ_{CT} = 0.7

Fig. 9.21 Hysteresis curve (through brace radius-to-wall thickness ratio, γ_T)

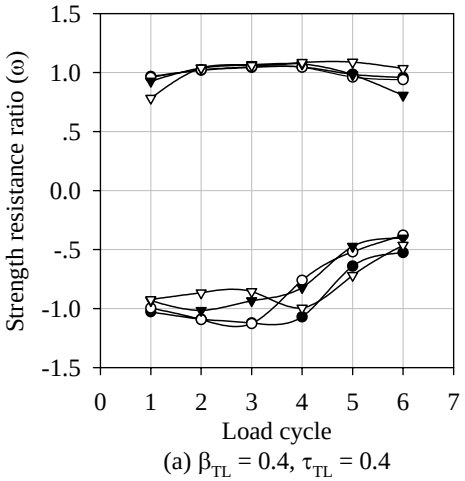

(a) β_{TL} = 0.4, τ_{TL} = 0.4

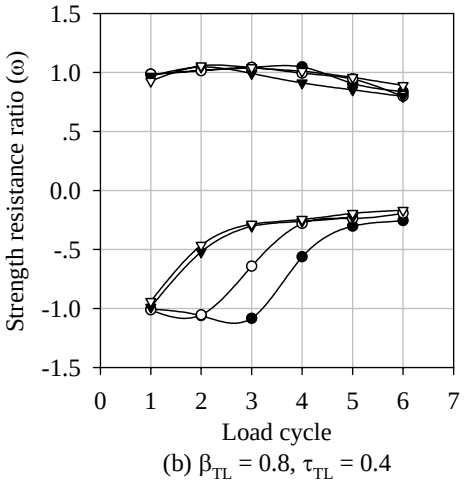

(b) β_{TL} = 0.8, τ_{TL} = 0.4

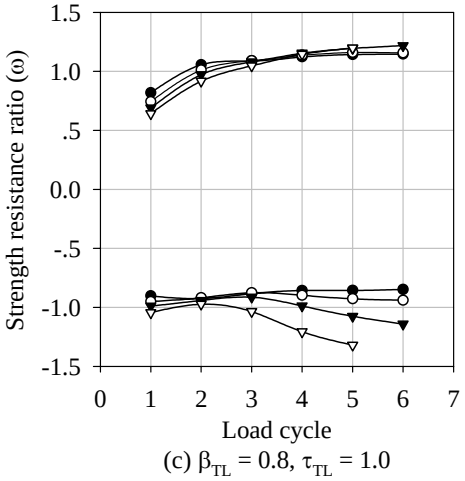

(c) β_{TL} = 0.8, τ_{TL} = 1.0

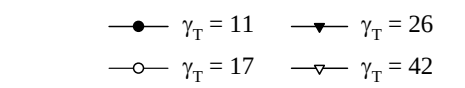

Constants: β_{CT} = 0.6, τ_{CT} = 0.7

Fig. 9.22 Strength resistance ratio (through brace radius-to-wall thickness ratio, γ_T)

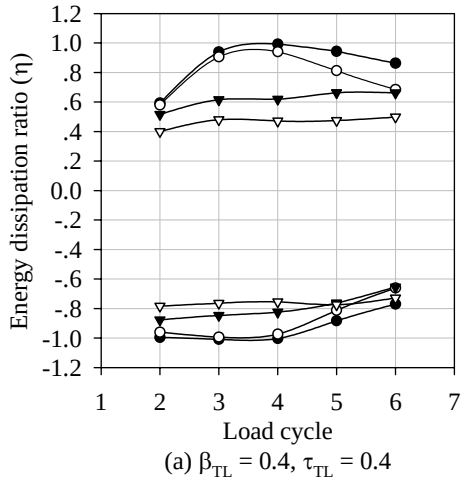

(a) β_{TL} = 0.4, τ_{TL} = 0.4

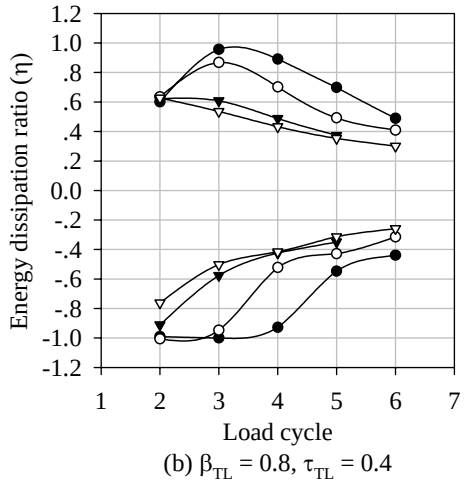

(b) β_{TL} = 0.8, τ_{TL} = 0.4

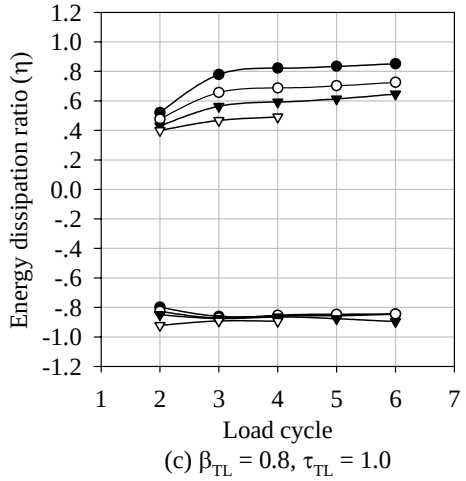

(c) β_{TL} = 0.8, τ_{TL} = 1.0

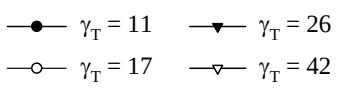

Constants: β_{CT} = 0.6, τ_{CT} = 0.7

Fig. 9.23 Accumulative energy dissipation ratio (through brace radius-to-wall thickness ratio, γ_T)

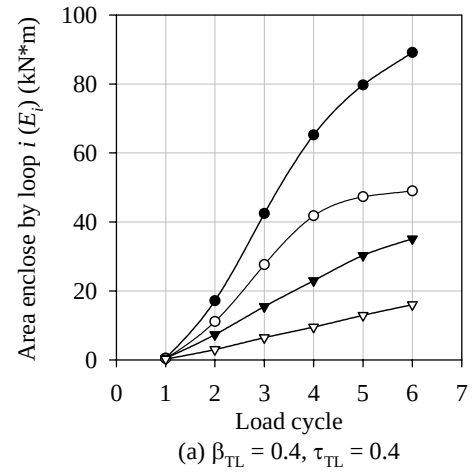

(a) β_{TL} = 0.4, τ_{TL} = 0.4

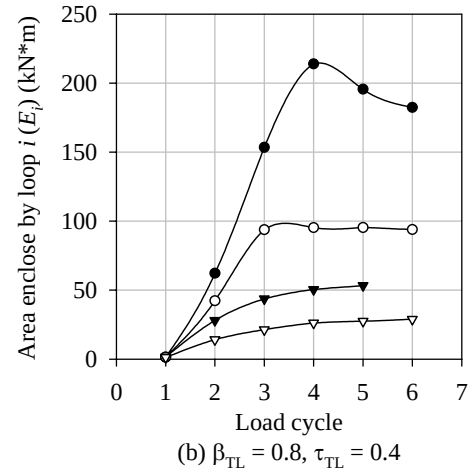

(b) β_{TL} = 0.8, τ_{TL} = 0.4

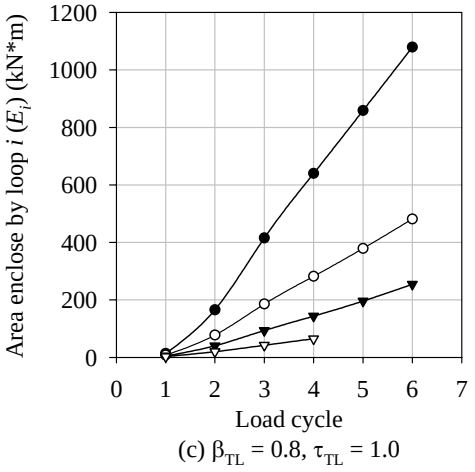

(c) β_{TL} = 0.8, τ_{TL} = 1.0

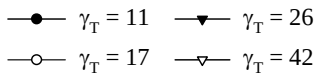

Constants: β_{CT} = 0.6, τ_{CT} = 0.7

Fig. 9.24 Area enclosed by hysteresis loop (through brace radius-to-wall thickness ratio, γ_T)

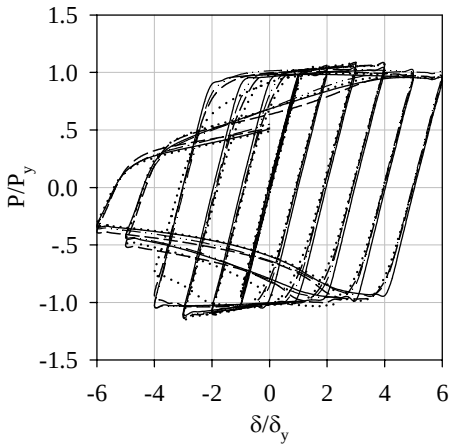

(a) τ_{TL} = 0.4, γ_T = 11

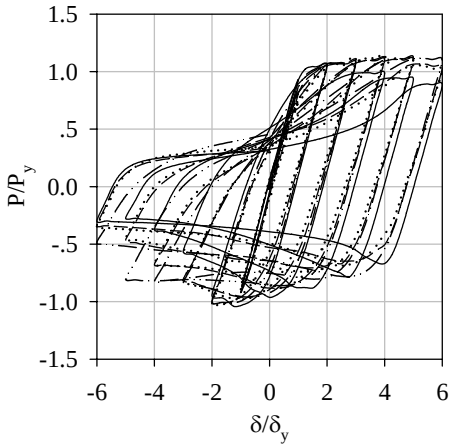

(b) τ_{TL} = 0.4, γ_T = 26

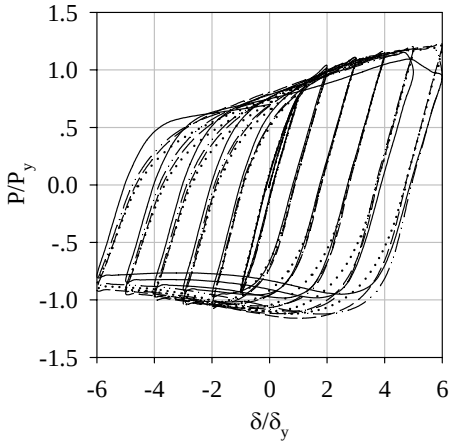

(c) τ_{TL} = 1.0, γ_T = 11

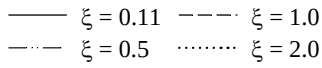

Constants: β_{CT} = 0.6, β_{TL} = 0.6, τ_{CT} = 0.7

Fig. 9.25 Hysteresis curves (gap size-to-through brace diameter ratio, ξ)

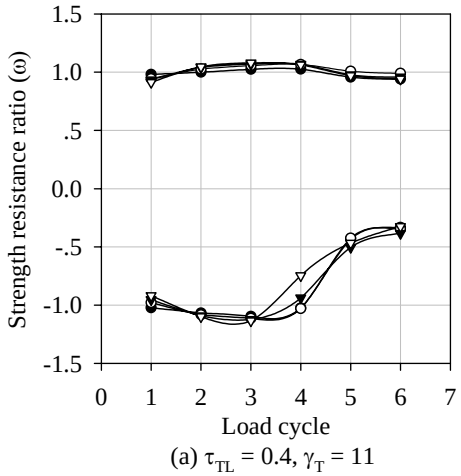

(a) τ_{TL} = 0.4, γ_T = 11

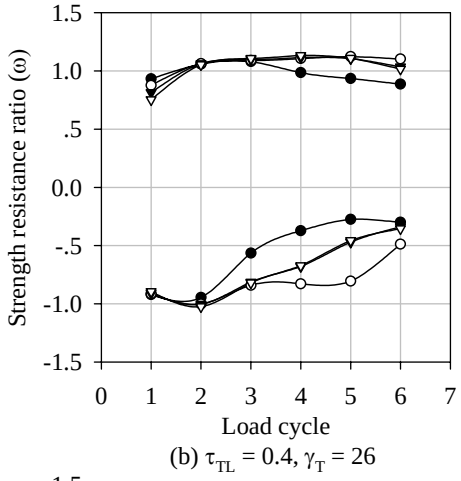

(b) τ_{TL} = 0.4, γ_T = 26

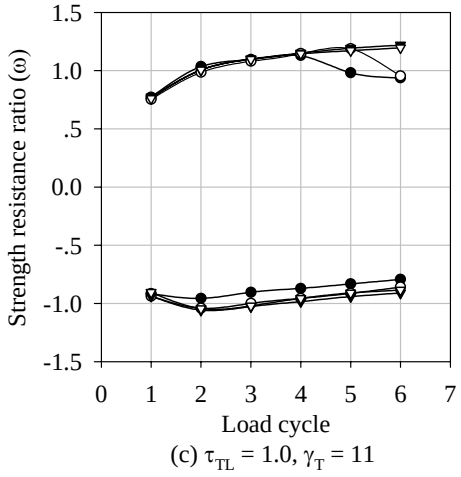

(c) τ_{TL} = 1.0, γ_T = 11

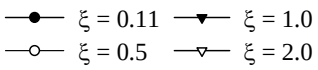

Constants: β_{CT} = 0.6, β_{TL} = 0.6, τ_{CT} = 0.7

Fig. 9.26 Strength resistance ratio (gap size-to-through brace diameter ratio, ξ)

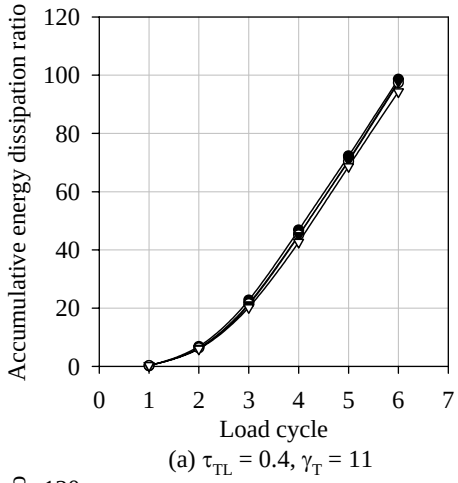

(a) τ_{TL} = 0.4, γ_T = 11

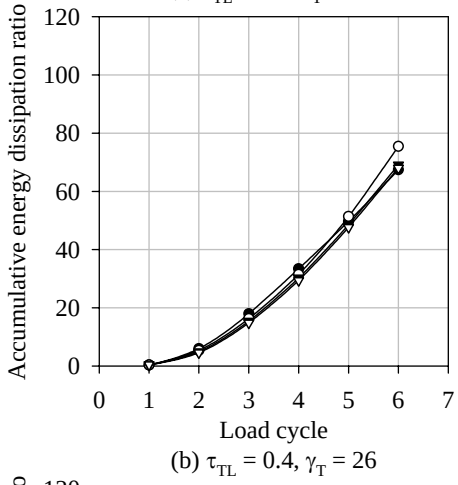

(b) τ_{TL} = 0.4, γ_T = 26

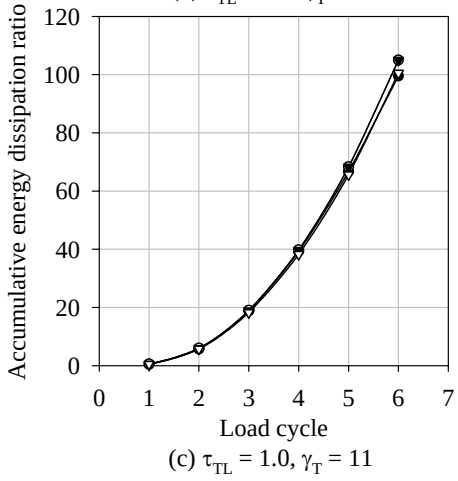

(c) τ_{TL} = 1.0, γ_T = 11

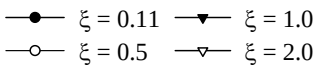

Constants: β_{CT} = 0.6, β_{TL} = 0.6, τ_{CT} = 0.7

Fig. 9.27 Accumulative energy dissipation ratio (gap size-to-through brace diameter ratio, ξ)

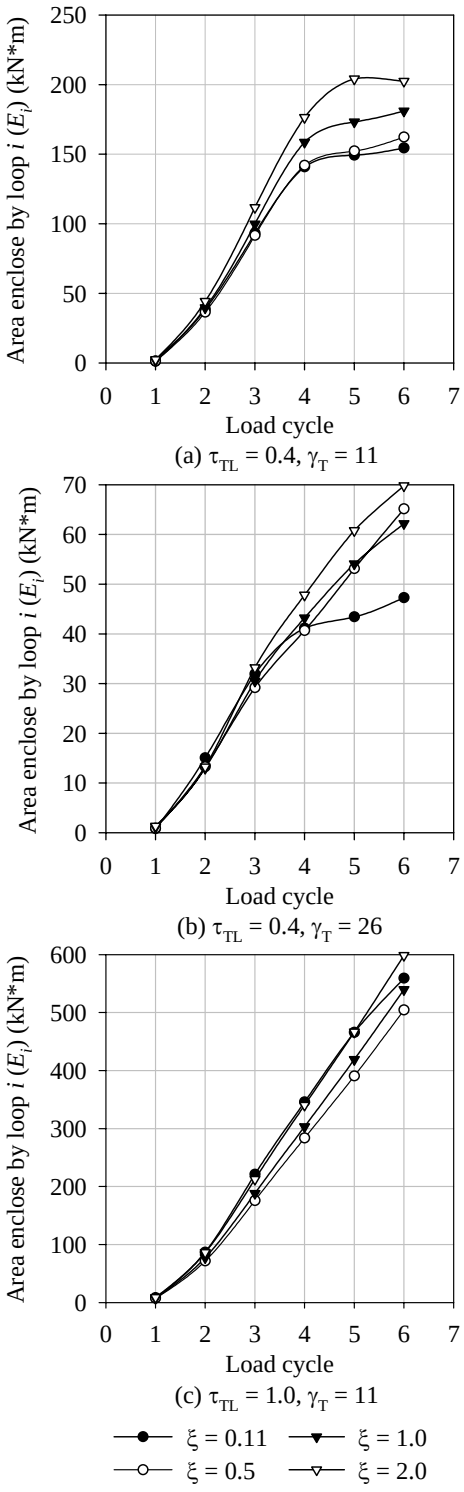

Constants: β_{CT} = 0.6, β_{TL} = 0.6, τ_{CT} = 0.7

Fig. 9.28 Area enclosed by hysteresis loop (gap size-to-through brace diameter ratio, ξ)

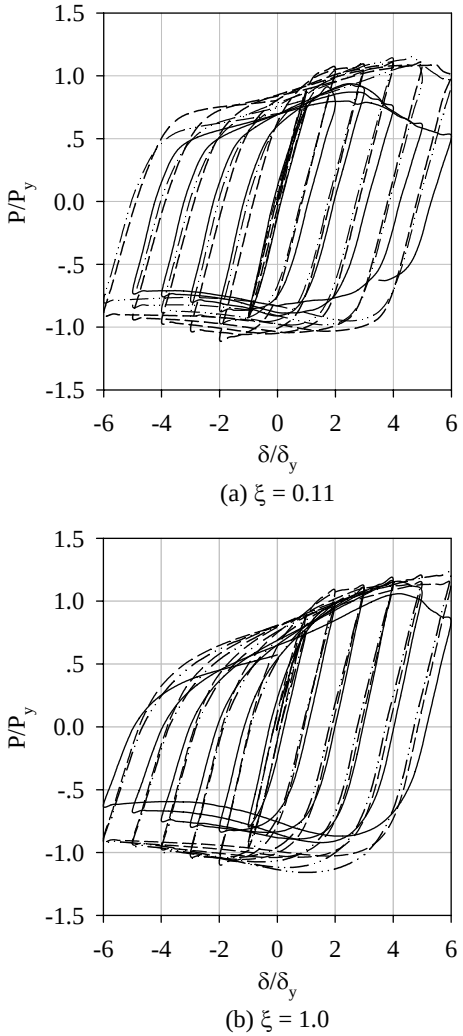

Constants: β_{CT} = 0.6, β_{TL} = 0.6, τ_{CT} = 0.7, τ_{TL} = 1.0, γ_C = 12, γ_T = 11

Fig. 9.29 Hysteresis curves (brace angle, θ)

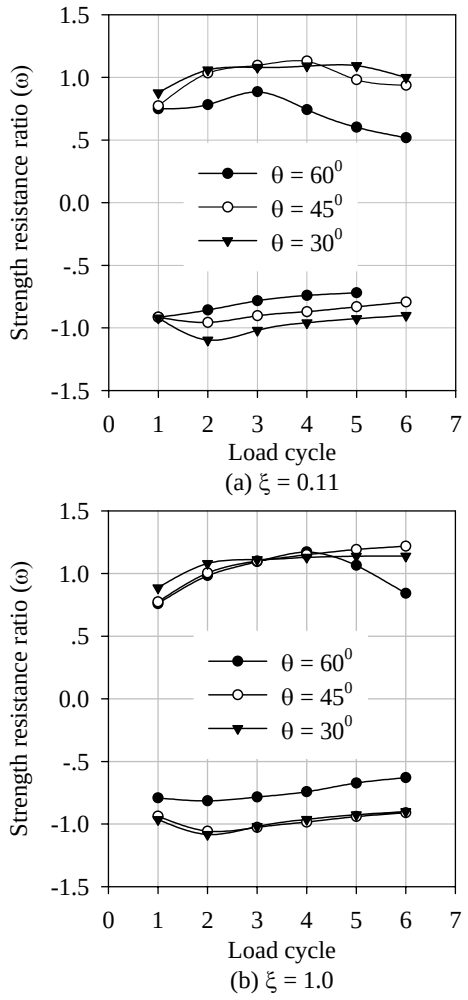

Constants: $\beta_{CT} = 0.6$, $\beta_{TL} = 0.6$, $\tau_{CT} = 0.7$, $\tau_{TL} = 1.0$, $\gamma_C = 12$, $\gamma_T = 11$

Fig. 9.30 Strength resistance ratio (brace angle, θ)

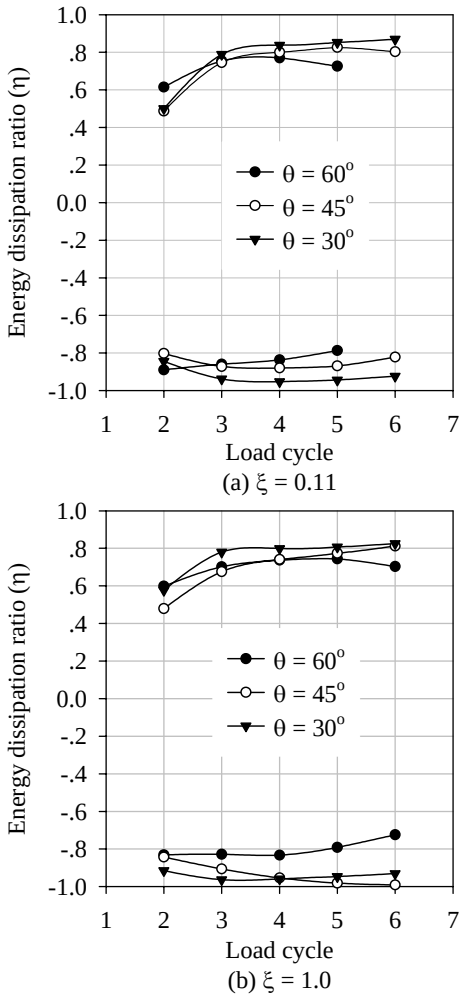

Constants: $\beta_{CT} = 0.6$, $\beta_{TL} = 0.6$, $\tau_{CT} = 0.7$, $\tau_{TL} = 1.0$, $\gamma_C = 12$, $\gamma_T = 11$

Fig. 9.31 Energy dissipation ratio (brace angle, θ)

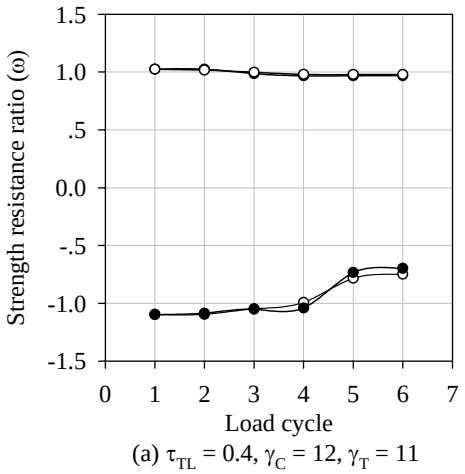

(a) τ_{TL} = 0.4, γ_C = 12, γ_T = 11

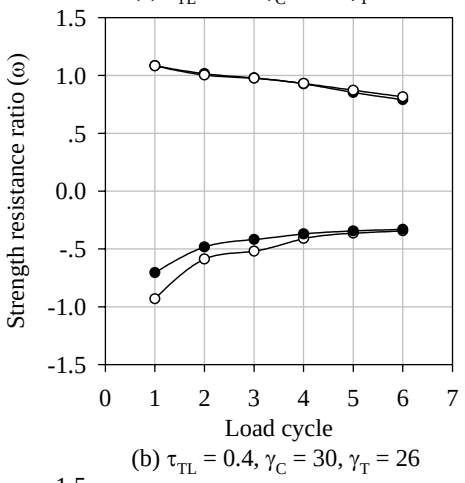

(b) τ_{TL} = 0.4, γ_C = 30, γ_T = 26

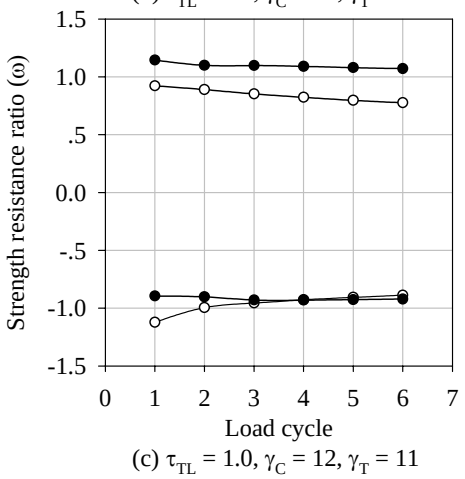

(c) τ_{TL} = 1.0, γ_C = 12, γ_T = 11

Tension first — Compression first

Constants: β_{CT} = 0.6, β_{TL} = 0.6, τ_{CT} = 0.7,

$(\delta/\delta_y)_A$ = 6, $(\delta/\delta_y)_M$ = 0

Fig. 9.32 Strength resistance ratio (load sequence)

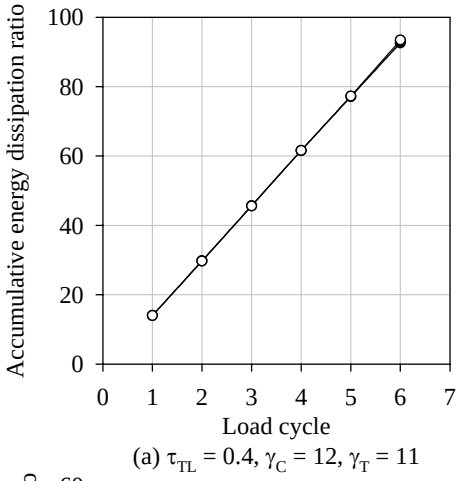

(a) τ_{TL} = 0.4, γ_C = 12, γ_T = 11

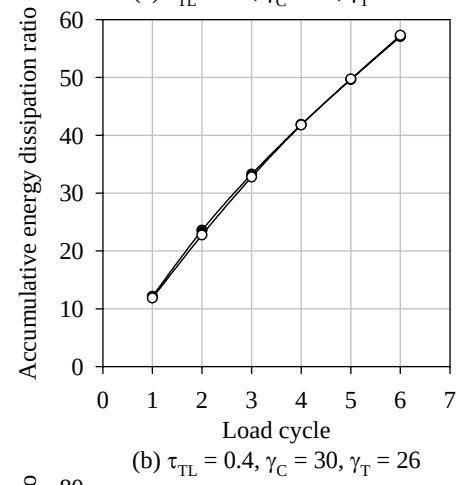

(b) τ_{TL} = 0.4, γ_C = 30, γ_T = 26

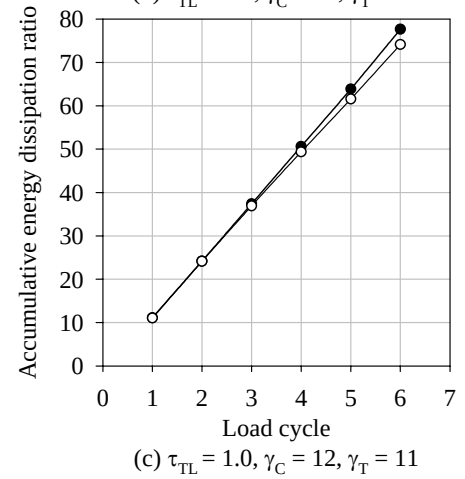

(c) τ_{TL} = 1.0, γ_C = 12, γ_T = 11

Tension first — Compression first

Constants: β_{CT} = 0.6, β_{TL} = 0.6, τ_{CT} = 0.7,

$(\delta/\delta_y)_A$ = 6, $(\delta/\delta_y)_M$ = 0

Fig. 9.33 Accumulative energy dissipation ratio (load sequence)

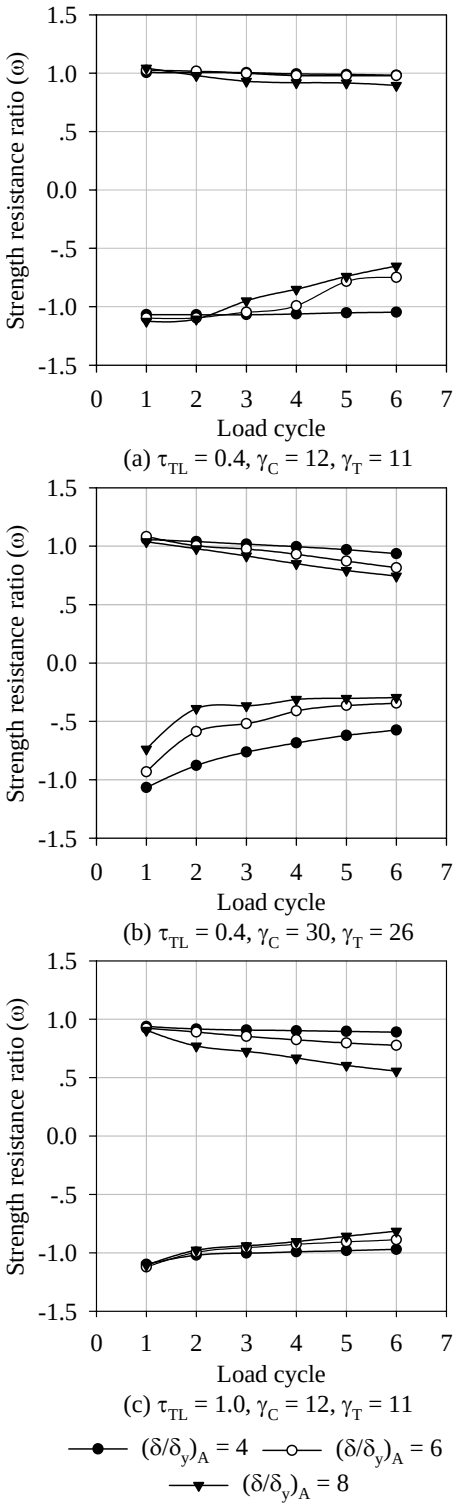

Constants: β_{CT} = 0.6, β_{TL} = 0.6, τ_{CT} = 0.7, $(\delta/\delta_y)_M$ = 0

Fig. 9.34 Strength resistance ratio (displacement amplitude)

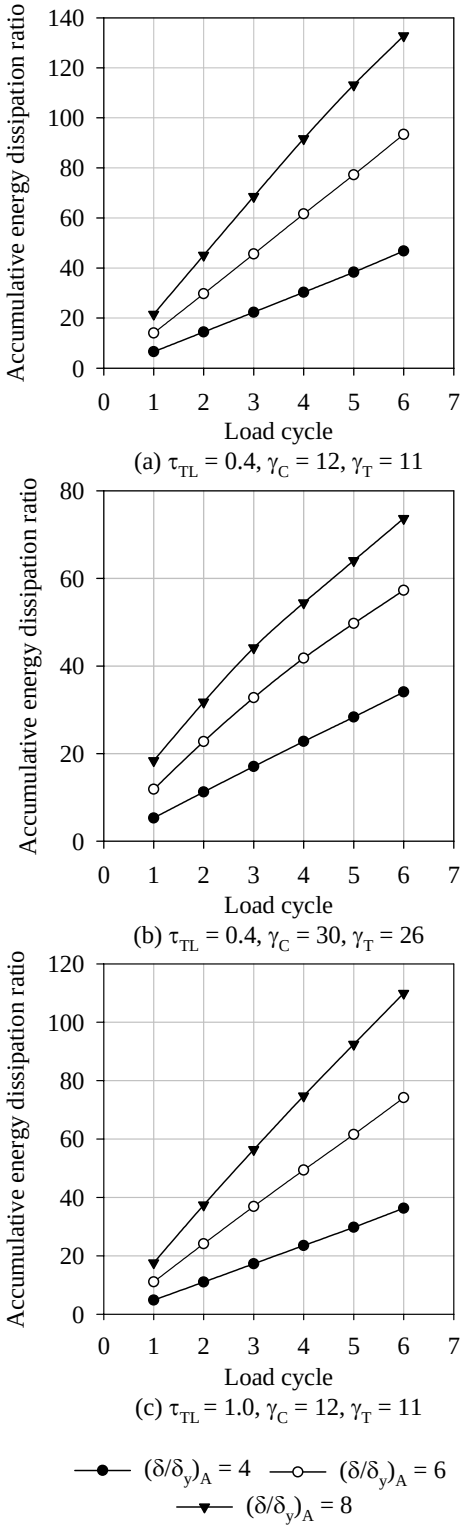

Constants: β_{CT} = 0.6, β_{TL} = 0.6, τ_{CT} = 0.7, $(\delta/\delta_y)_M$ = 0

Fig. 9.35 Accumulative energy dissipation ratio (displacement amplitude)

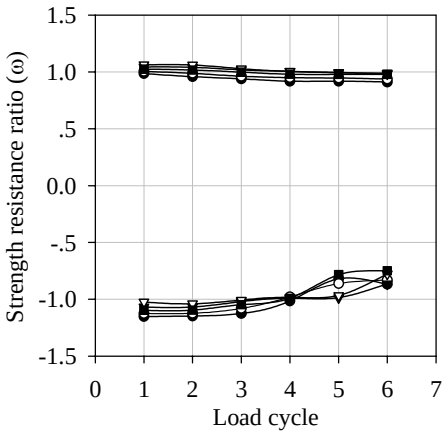

(a) τ_{TL} = 0.4, γ_C = 12, γ_T = 11

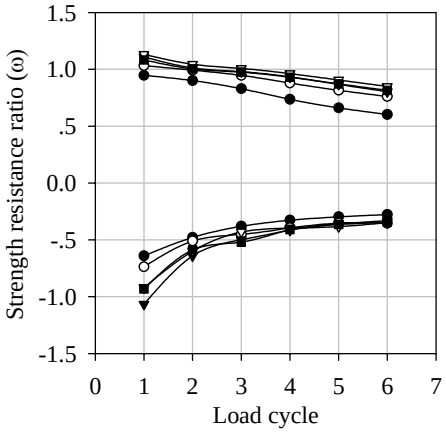

(b) τ_{TL} = 0.4, γ_C = 30, γ_T = 26

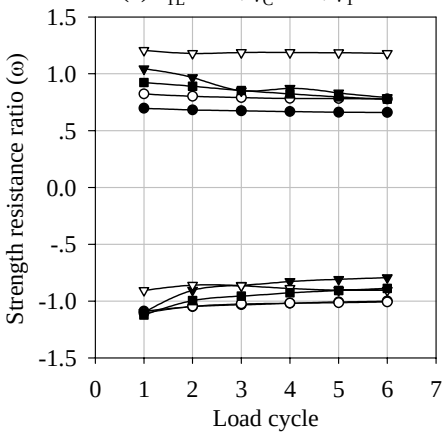

(c) τ_{TL} = 1.0, γ_C = 12, γ_T = 11

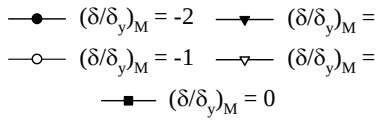

Constants: β_{CT} = 0.6, β_{TL} = 0.6, τ_{CT} = 0.7, $(\delta/\delta_y)_A$ = 6

Fig. 9.36 Strength resistance ratio (mean displacement)

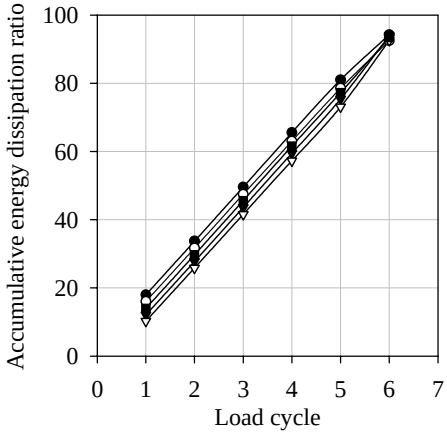

(a) τ_{TL} = 0.4, γ_C = 12, γ_T = 11

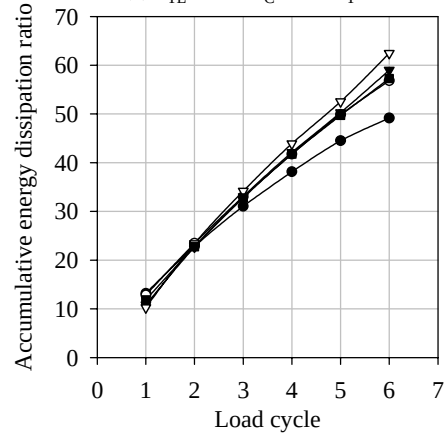

(b) τ_{TL} = 0.4, γ_C = 30, γ_T = 26

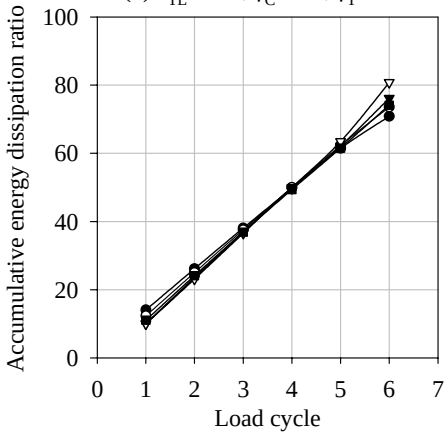

(c) τ_{TL} = 1.0, γ_C = 12, γ_T = 11

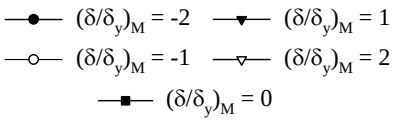

Constants: β_{CT} = 0.6, β_{TL} = 0.6, τ_{CT} = 0.7, $(\delta/\delta_y)_A$ = 6

Fig. 9.37 Accumulative energy dissipation ratio (mean displacement)

CHAPTER 10

CONCLUSIONS AND RECOMMENDATIONS

10.1 Conclusions

Experimental study

Two completely overlapped tubular joint specimens have been tested to failure under lap brace axial compression and quasi-static cyclic loading for the verification of FE models. For the joint specimen tested under lap brace axial compression, the ultimate capacity is determined as 380.5kN with the corresponding displacement of 5.83 mm. The failure mode of the joint specimen is associated with the through brace wall plastification. The load distribution showed that the joint specimen carries 60% and 40% the brace axial load of K- and Y-joint respectively. The comparison of the ultimate capacity showed that the existing strength equations in the codes such as API RP2A and CIDECT under-predict the test result of the joint specimen.

For the joint specimen tested under lap brace quasi-static cyclic loading, the failure mode of local buckling is first observed on the through brace near the chord and subsequently cracks at the weld toe of the through brace near the lap brace under compression and tension phase of the load cycle respectively. The hysteresis behaviour of the joint specimen showed that the applied load significantly reduces after the local buckling and the crack initiation take place. The axial load - displacement relationship revealed that the curve under monotonic loading can be used as envelope for that under cyclic loading before the crack initiation. However, the strength of the joint under cyclic loading will be overestimated because of the larger damage due to load reversal. Overall, the completely overlapped tubular joint specimen shows good ductility performance and energy dissipation capacity under cyclic loading. This is attributed to the inelastic local bucking deformation at the short segment of the through brace joining the chord.

Finite element modelling

The four-node thick shell finite element is found suitable for modelling the completely overlapped tubular joint specimens under both monotonic and cyclic loading. In the analysis, the weld element at the joint intersections is excluded. The material post yield property with the effect of strain hardening is adopted. The isotropic and the kinematic hardening rule simulate very well the static and cyclic behaviour of the joint, respectively. The comparison of the axial load - displacement curves and the failure behaviour showed that the FE models are suitable for predicting the ultimate strength of the joint specimens under static and cyclic loading. The maximum discrepancy of the ultimate capacity and the corresponding displacement is found not more than 5%.

The comparison of the cyclic behaviour indicated that the strength of the completely overlapped tubular joint can be higher than that of the simple gap K(N)-joint. The completely overlapped tubular joint dissipates more energy and better ductility than the simple gap K(N)-joint. For the completely overlapped tubular joint, the maximum stress occurs on the through brace in contact with the lap brace. For the simple gap K(N)-joint, the maximum stress is on the gap region between the braces of the chord.

Failure mechanism

From the results of the parametric study, the failure modes of the tubular joints with complete overlap of braces under lap brace axial compression can be characterised as the through brace wall plastification, the lap brace yielding, the lap brace local buckling, the lap brace member failure and the combination of these failure modes. Among these failure behaviours, the through brace wall plastification is the most common type of failure mode for the joints with high through brace-to-lap brace wall thickness ratio (τ_{TL}). For the through brace wall plastification failure, the load - displacement behaviour indicates significant post peak reserve capacity of the

completely overlapped joint. The failure mode of the joint is associated with the first peak load and the Yura et al's excessive deformation limit failure criteria.

The lap brace failure mainly occurs for the joints with low τ_{TL}, low through brace radius-to-thickness ratio (γ_T), small gap size parameter (ξ) and small brace angle (θ). The lap brace yielding or the localised buckling combined with the through brace wall plastification is the most prominent failure for the joints with high γ_T and lap brace-to-through brace diameter ratio (β_{TL}) but with low τ_{TL} and ξ. The lap brace local buckling only occurs for the joints with small τ_{TL} and large β_{TL}. The joints failed by lap brace local buckling exhibits sudden fall of load in the load - displacement curve with the peak load occurring at low displacement. Overall, τ_{TL}, γ_T, ξ and θ are the most crucial geometrical parameters controlling the failure behaviour of the completely overlapped tubular joint.

Ultimate capacity

The ultimate capacity of the joint with complete overlap of braces increases with increasing β_{CT}, τ_{CT}, β_{TL} and τ_{TL}, but decreases with increasing γ_T, γ_C, ξ and θ. The effects of geometric parameters of the joint are interactive. The joint capacity with small γ_T is significantly affected by β_{CT}. The strength increase of the joint with τ_{CT} and β_{TL} is dependent upon γ_C and γ_T and are found more significant with smaller γ_C and γ_T respectively.

The joints with small γ_C shows higher rate of strength decrease and this becomes insignificant with decreasing τ_{CT}. The strength of the joint with small γ_T and τ_T is affected by τ_{TL}. With decreasing gap size, the interactive effects of geometrical parameters of the joint become more significant. It is interesting to note that the strength of the joint with complete overlap of braces at a gap size larger than the through brace diameter is equivalent to that of the simple Y-joints. The comparison of the non-dimensional strength showed that the existing strength equations of simple T/Y- and gap K-joints do not consider the interactive effect of geometrical

parameters β_{TL}, γ_T, τ_{TL} and ξ of the completely overlapped tubular joint.

Strength equation

A new set of parametric equations has been proposed for predicting the ultimate capacity of completely overlapped tubular joints under brace axial compression. The reliability of this proposed equation is verified against the current FE models and the test data. A simplified characteristic strength equation is also proposed for the design of tubular joints with complete overlap of braces. The comparison of the ultimate capacity with the existing design strength equations in the codes such as API RP2A and CIDECT indicated that the proposed characteristic strength equation is also applicable for predicting the ultimate capacity of simple Y-joints with the condition that the through brace radius to wall thickness ratio (γ_T) (chord radius to wall thickness ratio for the case of simple Y-joints) is less than 25.

Cyclic behaviour

The FE analysis results showed that the geometrical parameters of the chord and the through brace (β_{CT}, τ_{CT}, γ_C) have minimal but the through brace and the lap brace (β_{TL}, τ_{TL}, γ_T) have significant effects on the cyclic behaviour of completely overlapped tubular joints. At low τ_{TL}, the hysteresis behaviour of the joint is unstable and the failure is associated with lap brace yielding and lap brace local buckling prior to joint failure. The stiffness and the compression strength of the joint rapidly deteriorate with increasing β_{TL} and decreasing τ_{TL} and so the dissipation capacity. However, the effect on the tensile strength of the joint is found less significant.

On the other hand, at high τ_{TL}, the hysteresis behaviour of the joint is stable and the failure is associated with through brace wall plastification. The tensile strength of the joints increases with increasing β_{TL}. The impact on the compressive strength and the energy dissipation capacity of the joint is minimal. At high β_{TL} and low τ_{TL}, the strength decrease of the joint is significantly affected by γ_T. It is noted that the

energy dissipation capacity of the joints increases with increasing γ_T.

The gap size parameter (ξ) has significant impact on the performance of the completely overlapped tubular joints under cyclic loading. The stiffness of the joints decreases with increasing gap size. At large gap size, the premature local buckling failure of the joint can be avoided. The strength and the energy dissipation increase with decreasing brace angle (θ) and this is limited to brace angle of greater than 45^0.

For the joint under cyclic loading, the loading at first load cycle in compression result in more rapid deterioration on the compressive strength. The effect of the load sequence on the energy dissipation capacity of the joint is limited. The load carrying capacity decreases but the accumulative energy dissipation of the joints increases with increasing displacement amplitude. The mean displacement in the compression load cycle aggravates the local buckling of lap brace resulting in the reduction of load carrying capacity.

It can be commented that the load carrying and the energy dissipation capacity of the joint rapidly deteriorate if the lap brace member fails prior to joint collapse. Thus, it is important to consider the effect of local buckling for the design of completely overlapped tubular joint at low τ_{TL}, high β_{TL} and high γ_T. The joint associated with through brace wall plastification failure exhibits more stable and ductile cyclic behaviour. It is highly recommended that the dissipative zone of the completely overlapped tubular joint under cyclic loading should be designed at the short segment of the through brace joining the chord.

10.2 Recommendations

In order to better understand the ultimate strength behaviour as well as the development of recommendations for design of completely overlapped tubular joints, the following areas are recommended for future research.

Static behaviour

The current research focuses on the strength behaviour of completely overlapped tubular joint under axial loading. The strength behaviour of the joint subjected to in-plane and out-of-plane bending as well as the combination of these loadings should be investigated. The impact on the failure mechanism and the ultimate capacity of the joint owing to the variation of material properties and post yield behaviour of members should be examined.

Cyclic behaviour

The research for the design of completely overlapped tubular joint under seismic loading is still insufficiently covered. Since ductility and strength are the two main criteria considered for seismic design, there is need to develop reliable formulae based on these two requirements so that the joint can effectively be used for economic design of offshore steel jackets in the earthquake sensitive areas. Hence, intensive experimental and numerical studies should be conducted to develop a set of reliable formulae for predicting the ultimate strength as well as the ductility of the completely overlapped tubular joints under cyclic loading.

In the practical design of structures, the required ductility and strength are determined at the level of full structural performance. In most research works, the ductility and the strength are obtained from the local behaviour of members and joints. Thus, it is essential and important that the relationship of the joints with and without the overall frame behaviour should be established for appropriate design.

REFERENCES

1. American Bureau of Shipping, ABS (2004), Guide for the Buckling and Ultimate Strength Assessment for Offshore Structures, Houston, USA.
2. American Institute of Steel Construction, AISC (1997), Seismic Provisions for Structural Steel Buildings, Chicago, USA.
3. American Institute of Steel Construction, AISC-LRFD (2000), Load and Resistance Factor Design Specification for the Design of Steel Hollow Structural Sections, Chicago, USA.
4. American Institute of Steel Construction, AISC (2000), Seismic Provisions for Structural Steel Buildings Supplement, No. 2, , Chicago, USA.
5. American Petroleum Institute, API RP2A (1984), Recommended Practice for Planning, Designing and Constructing Fixed Offshore Platforms-Load and Resistance Factor Design, 15th edition, Washington D.C., USA.
6. American Petroleum Institute, API RP2A-LRFD (1993), Recommended Practice for Planning, Designing and Constructing Fixed Offshore Platforms-Load and Resistance Factor Design, 1st edition, Washington D.C., USA.
7. American Petroleum Institute, API RP 2A-WSD (2000), Recommended practice for planning, designing and constructing fixed offshore platforms, 21st edition, Washington D.C., USA.
8. American Petroleum Institute, API 5L (1991), Specification for Line Pipe, 39th edition, Washington D.C., USA.
9. American Welding Society, AWS (2000), Structural Welding Code – Steel., ANSI/AWS, D1.1-2000, Miami, USA.
10. Bomel limited (2001), "Comparison of Tubular Joint Strength Provisions in Codes and Standards", Offshore Technological Report, Berkshire, UK.

11. Borst R. de (1991), "Computational Methods in Non-Linear Solid Mechanics, Part 1: Geometrical Non-Linearity and Solution Techniques", T. U. Delft Report 25-2-90-5-04, TNO-IBBC Report BI-90-069, Delft, The Netherlands.
12. British Standard Institution, BSI (1998), Metallic Materials-Tensile Testing, BS EN 10002-1: 1990, London, UK.
13. British Standard Institution, BSI (1996), Eurocode 8: Design Provisions for Earthquake Resistance of Structures, ENV 1998-1-3, London, UK.
14. Canadian Standards Associations (1989), Steel Structures for Buildings, Limit States Design, CAN-CSA S16.1, Canada.
15. Cheung, L.Y., Gho, W.M., Fung, T.C. and Soh, C.K. (1998), "Design Economics of Offshore Structure - eccentric jacket", Journal of the Institution of Engineers, Vol. 38, No. 3, pp.42-49.
16. Cofer, W.F., and Will, K.M. (1992), "A Finite element Technique for the Ultimate Strength Assessment of Tubular Joints." Engineering Computations, Vol. 9, pp. 345-358.
17. Coutie, M.G. and Saidani, M. (1989), "The Use of Finite Element Techniques for the Analysis of RHS Structures with Flexible Joints", The 3rd International Symposium On Tubular Structures, Lappeenranta, Finland, pp.224-231.
18. Crisfield, M.A. (1981), "A Fast Incremental iterative Procedure that Handles Snap-through", Computer & Structures, Vol. 13, pp.55-62.
19. Department of Energy, DEn (1984), Offshore Installations: Guidance on Design and Construction, HMSO, London, UK.
20. Department of Energy, (1993), Offshore Installations: Guidance on Design, Construction and Certification, 4th edition, HMSO, Consolidated Edition, plus mendment No. 3 (1995).
21. DET NORSKE VERITAS, DNV (1977), Rules for Design, Construction and Inspection of Fixed Offshore Structures, Norway.

22. DET NORSKE VERITAS, DNV (2004), Design of Offshore Steel Structures, General (LRFD Method), Offshore Standard, DNV-OS-C101, Norway.
23. Dexter, E.M. (1996), "Effects of Overlap on Behaviour and Strength of Steel Circular Hollow Section Joints", PhD thesis, University of Wales Swansea, UK.
24. Dexter, E.M. and Lee M.M.K. (1999a), "Static Strength of Axially Loaded Tubular K Joints I: Behavior", Journal of Structural Engineering, ASCE, Vol.125, No. 2, pp.194–201.
25. Dexter, E.M. and Lee M.M.K. (1999b), "Static Strength of Axially Loaded Tubular K Joints II: Ultimate Capacity", Journal of Structural Engineering, ASCE, Vol.125, No. 2, pp.202–210.
26. Dexter, E.M., Lee M.M.K. and Kirkwood, M.G. (1994), "Effect of Overlap on Strength of K Joints in CHS Tubular Members", Proceedings of the 6th International Symposium on Tubular Structures, Melbourne, Australia, pp.581–588.
27. Dexter, E.M., Lee M.M.K. and Kirkwood, M.G. (1996), "Overlapped K Joints in Circular Hollow Sections under Axial Loading", Journal of Offshore Mechanics and Arctic Engineering, Transactions of ASME, Vol.118, No. 1, pp.53–61.
28. Dier, A.F. and Lalani, M. (1998), "New Code Formulations for Tubular Joint Static Strength", Proceedings of 8th International Symposium on Tubular Structures, Singapore, pp.107-116.
29. Dowling, N.E. (1997), Mechanical Behaviour of Materials, Prentice Hall International, Inc, Singapore.
30. Elchalakani, M., Zhao X.L. and Grzebieta R. (2002), "Test of Cold-Formed Circular Tubular Braces Under Cyclic Axial Loading", Journal of Structural Engineering, Vol.129, No.4, pp.507-514.

31. European Convention for Constructed Steelwork Technical Committee 1 - Structural Safety and Loadings, ECCS (1986), Recommended Testing Procedure for Assessing the Behaviour of Structural Steel Elements under Cyclic Loads, Technical Working Group 1.3, Seismic Design.
32. Fung, T.C., Soh, C.K., Gho W.M. and Qin, F. (2001a), "Ultimate Capacity of Completely Overlapped Tubular Joint I: An Experimental Investigation", Journal of Constructional Steel Research, Vol.57, No. 8, pp.855-880.
33. Fung T.C., Soh C.K., Gho W.M. (2001b), "Ultimate capacity of completely overlapped tubular joints II: Behavioural study", Journal of Constructional Steel Research, Vol. 57, No. 8, pp.881-906
34. Fung, T.C., Soh, C.K. and Qin, F. (1999), "Seismic Behaviour of Completely Overlapped Tubular Joint", Computer Techniques for Civil and Structural Engineering, B.H.V. Topping and B. Kumar, Eds., Civil-Comp Press, Oxford, U.K., pp.139-146.
35. Gao, S., Usami, T. and Ge, H.B. (2000), "Eccentrically Loaded Steel Columns under Cyclic In-Plane Loading", Journal of Structural Engineering, Vol.126 (8), pp.964-973.
36. Gho, W.M. (2001), "Structural Behaviour of Completely Overlap Tubular Joints", PhD thesis, Nanyang Technological University, Singapore.
37. Goh, T.K., Grundy, P. (1994), "Capacity of CHS YT-joints under High Amplitude Cyclic Load". Tubular Structures VI, Grundy P., Holgate A. and Wong W. editors, Balkema, Rotterdam, pp.489-496.
38. Healy, B.E. (1994), "A Numerical Investigation into the Capacity of Overlapped Circular K-Joints", Proceedings of the 6th International Symposium on Tubular Structures, Melbourne, Australia, pp.563-571.
39. Health and Safety Executive, HSE (1990), Offshore Installations: Guidance on Design, Construction and Certification, 4th edition, HMSO, UK.

40. Health and Safety Executive, HSE (2002), Offshore Technology Report 01/015: Steel, edited under the HSE Technical Support Agreement by BOMEL Ltd, UK.
41. Hoadley, P.W. (1983), "Ultimate Strength of Tubular Joints Subjected to Combined Loads", PhD thesis, Unitverstiy of Texas at Austin, USA.
42. International Institute of Welding, IIW (1981), Design Recommendations for Hollow Section Joints in Predominantly Statically Loaded Joints, IIW Doc. XV-491-82, London, England.
43. International Standards Organization, ISO (2004), Petroleum and natural gas industries- Fixed steel offshore structures, Draft ISO/DIS 19902.
44. Kurobane, Y., Makino, Y. and Mitsui, Y. (1976), "Ultimate Strength Formula for Simple Tubular Joints", IIW Document XV-385-76, International Institute of Welding, London, England, pp.1-22.
45. Kurobane,Y., Makino,Y. and Mitsui, Y. (1980a), "Re-analysis of Ultimate Strength Data for Truss Connections in Circular Hollow Sections", IIW Document XV-461-80, International Institute of Welding, London, England, pp.1-42.
46. Kurobane,Y., Makino,Y., Honda, T. and Mitsui Y. (1980b), "Additional Test on Tubular K-joints with CHS Members under Static Loads", IIW Document XV-460-80, International Institute of Welding, London, England.
47. Kurobane, Y. (1981), "New Developments and Practices in Tubular Joint Design", IIW doc. XV-488-81 and XIII-1004-81, International Institute of Welding, London, England, pp.1-57.
48. Kurobane, Y, Makino, Y, Ochi, K. (1984) "Ultimate Resistance of Unstiffened Tubular Joints", Journal of Structural Engineering, ASCE, Vol. 110, No. 2, pp. 385–400.
49. Kurobane,Y., Ochi, K., Ogawa, K. and Makino,Y. (1986), "Local Buckling of Braces In Tubular K-joints", Thin-Walled Structures, Vol. 4, pp. 23-40.

50. Lalani, M. (1992), "Developments in Tubular Joints Technology for Offshore Structures", Proceedings of Second International Offshore and Polar Engineering Conference, International Society of Offshore and Polar Engineers, Golden (CO), pp. 260–274.
51. Lalani, M., Gholkar, S.F., and Ward, J.K. (1989), "Recent Developments in the Ultimate Strength Assessment of Tubular Joints: a nonlinear numerical treatment", Proceedings of 21st Annual Offshore Technological Conference, Houston, Texas, USA.
52. Lee, M.M.K. (1999), "Strength, Stress and Fracture Analysis of Offshore Tubular Joints Using Finite Elements", Journal of Constructional Steel Research, Vol. 51, No. 3, pp. 265-286.
53. Liu, Z.Y., and Goel, S. (1988), "Cyclic Load Behaviour of Concrete-Filled Tubular Braces", Journal of Structural Engineering, Vol. 114, No. 7, pp. 1488-1506.
54. Lu, L.H., de Winkel G.D., Yu, Y. and Wardenier, J. (1994), "Deformation Limit for the Ultimate Strength of Hollow Section Joints". Proceedings of 6th International Symposium on Tubular Structures, Melbourne, Australia, pp. 341-347.
55. MARC (2005a), User's Guide, MARC Analysis Research Corporation, Palo Alto, California, USA.
56. MARC (2005b), Element Library, Volume B, MARC Analysis Research Corporation, Palo Alto, California, USA.
57. Marshall, P.W. (1984), "Connections for Welded Tubular Structures", Proceedings of the 2nd International Conference on Welding of Tubular Structures, International Institute of welding, Boston, Massachusetts, pp. 1-54.
58. Marshall, P.W. (2004), "Review of tubular joint criteria", Connections in Steel Structures V: Innovative Steel Connections, ECCS/AISC Workshop, Amsterdam, The Netherlands.

59. Morgan, M.R. (1997), "Stress Fields in Tubular K-Joints for Fatigue Analysis of Offshore Structures", PhD thesis, University of Wales Swansea, UK.
60. New Zealand Standard (1992), Standards New Zealand, Code of Practice for General Structural Design and Design Loading for Buildings, and Commentary, Part1, 2, NZS 4203, Standards Association of New Zealand, Wellington, New Zealand.
61. New Zealand Standard (1997), Standards New Zealand, Steel Structures Standard, Part 1, NZS 3404, Standards Association of New Zealand, Wellington, New Zealand.
62. NORSOK Standard (2004), Design of Steel Structures, N-004. Rev 2.
63. Pan, R.B., Plummer, F.B., and Kuang, J.G. (1977), "Ultimate Strength of Tubular Joins", Journal of Petroleum Technology, Vol. 29, No. 4, pp. 449-460.
64. Paul, J.C. (1992), "The Ultimate Behaviour of Multiplanar TT- and KK-Joints Made of Circular Hollow Sections", PhD thesis, Kumanmoto University, Kumanmoto, Japan.
65. Philiastides, A. (1988), "Fully Overlapped Rolled Hollow Section Welded Joints in Trusses, PhD Thesis, University of Nottingham. UK.
66. Popov, E.P., Mahin, S.A. and Zayas, V.A. (1980), "Inelastic Cyclic Behavior of Tubular Braced Frames", Journal of the Structural Division, ASCE, Vol.106, pp.2375-2390.
67. Ramm, E. (1985), "Strategies for Tracing the Nonlinear Response Near Limit Points", Europe-US Workshop on Nonlinear Finite Element Analysis in Structural Mechanics, Ruhr University Bochum, Berlin, Germany, pp.63-89.
68. Reber, J.B. (1972), "Ultimate Strength Design of Tubular Joins", Proceedings of the 4th Annual Offshore Technology Conference, Houston, Texas, USA.
69. Sherman, D. and Sully, R.M. (1994), "Tubular Bracing Member under Cyclic Loading", Proceedings of 4th Pacific Structural Steel Conference, Singapore Society of Steel Structures, Singapore.

70. Skallerud, B. (1992), "On the Relationship between Low Cycle Fatigue and Crack Growth Rate Properties in Welded Steel Components", Fatigue and Fracture of Engineering Material Structures, Vol.15, pp. 43-56.
71. Skallerud, B. H., Eide, O. I., Amdahl, J. and Johansen, A. (1995), "On the Capacity of Tubular T-joints Subjected to Severe Cyclic Loading", Offshore Technology, OMAE-Volume I-B, ASME, pp. 133-142.
72. Soh, C.K., Fung, T.C., Qin, F., and Gho, W.M. (2001). "Behavior of Completely Overlapped Tubular Joints under Cyclic Loading", Journal of Structural Engineering, ASCE, Vol.127, No. 2, pp.122-128.
73. Taylor, A.W. (1996), Report of A Workshop on Requalification of Tubular Steel Joints in Offshore Structures, Rep. No. NISTIR 5877, Building and Fire Research Laboratory, National Institute of Standards and Technology, Maryland, USA.
74. Underwater Engineering Group, UEG (1985), Design of Tubular Joints for Offshore Structures, Volume 1 & 2, CIRIA.
75. Van der Vegte, G.J. (1995), "The Static Strength of Uniplanar and Multiplanar Tubular T- and X-Joints", PhD thesis, Delft University, The Netherlands.
76. Van der Vegte, G.J., De Koning, C.H.M., Puthli, R.S. and Wardenier, J. (1991), "Numerical Simulation of Experiments on Multiplanar Steel X-joints", International Journal of Offshore and Polar Engineering, Vol.1, No. 3, pp. 200-207.
77. Wadenier, J. (1982), Hollow Section Joints, Delf University Press, The Netherlands.
78. Wardenier, J., Kurobane, Y., Packer, J., Dutta, D. and Yeomans, N. (1993), Design Guide for Circular Hollow Section (CHS) Joints under Predominantly Static Loading, CIDECT, Koln, Verlag TUV Rheinland GmbH, Germany.

79. Walpole, W.P. (1995), "Behaviour of Cold-Formed Steel RHS Members under Cyclic Loading", Proceedings of Technical Conference of National Society for Earthquake Engineering, New Zealand Society for Earthquake Engineering, Waikanae, New Zealand, pp. 44-50.
80. Washio, K., Togo, T. and Mitsui, Y. (1968), "Experimental Study on Local Failure of Chords in Tubular Truss Joints" Technology Reports, Part I, Osaka University, Vol. 18, No. 850.
81. Washio, K., Togo, T. and Mitsui, Y. (1969), "Experimental Study on Local Failure of Chords in Tubular Truss Joints", Technology Reports, Part II, Osaka University, Vol. 19, No. 874.
82. Weinstein, R.M., and Yura, J.A. (1986), "The Effect of Chord Stresses on the Static Strength of DT Tubular Connections", Offshore Technology Conference 5135, Huston, USA.
83. Yura, J.A., Zettlemoyer, N, and Edwards, I.F. (1980), "Ultimate Capacity Equations for Tubular Joints". Offshore Technology Conference 3690, Houston, USA, pp. 113-126.
84. Zettlemoyer, N. (1988), "Development in Ultimate Strength Technology for Simple Tubular Joints", Proceedings of Offshore Tubular Joints Conference, OTJ88, Surrey, Paper No. 4.
85. Zhao, X.L., Grzebieta, R. and Lee. C. (2002), "Void-Filled Cold-Formed Rectangular Hollow Section Braces Subjected to Large Deformation Cyclic Axial Loading", Journal of Structural Engineering, Vol. 128, No. 6, pp. 746-753.
86. Zhu, K., AI-Bermani, F.G.A., Kitipornchai, S. and Li, B. (1995), "Dynamic Response of Flexibly Jointed Frames", Engineering Structures, Vol.17 (8), pp. 575-580.

APPENDIX A

Appendix A (a): Ultimate capacity of completely overlapped tubular joints ($\theta = 30^0$, g = 51mm)

Ultimate		β_{TL}	0.4						0.6						0.8					
Capacity		τ_{TL}	0.4		0.7		1		0.4		0.7		1		0.4		0.7		1	
β_{CT}	γ_C	τ_{CT}	FC	Load	FC	Load	FC	Load	FC	Load	FC	Load	FC	Load	FC	Load	FC	Load	FC	Load
0.4	12	0.4	MF	658	Peak	943	Yura	1030	MF	1001	Peak	1596	Peak	1705	MF	1344	MF	2353	Peak	2670
		0.7	MF	1151	MF	2015	Yura	2374	MF	1752	MF	3066	Peak	3922	MF	2353	MF	4117	Yura	5730
		1	MF	1645	MF	2878	Yura	3758	MF	2503	MF	4380	Yura	6000	MF	3361	MF	5882	Yura	7734
	20	0.4	Peak	373	Peak	417	Yura	459	MF	596	Peak	713	Peak	737	Peak	774	Peak	1127	Peak	1216
		0.7	Peak	642	Peak	1017	Yura	1113	MF	1051	Peak	1714	Peak	1853	MF	1412	MF	2470	Peak	2845
		1	MF	987	Yura	1672	Yura	1903	MF	1502	MF	2628	Yura	3099	MF	2016	Yura	3529	Yura	3973
	30	0.4	Peak	194	Peak	210	Yura	242	Peak	343	Peak	362	Peak	372	Peak	501	Peak	600	Peak	628
		0.7	Peak	426	Peak	541	Yura	585	MF	701	Peak	922	Peak	967	Peak	915	Peak	1412	Peak	1555
		1	MF	658	Peak	943	Yura	1033	MF	1001	Peak	1580	Yura	1713	MF	1344	Yura	2176	Yura	2322
	50	0.4	Peak	82	Peak	88	Yura	117	Peak	149	Peak	154	Peak	159	Peak	245	Peak	261	Peak	268
		0.7	Peak	210	Peak	231	Yura	259	Peak	368	Peak	395	Peak	409	Peak	525	Peak	648	Peak	696
		1	Peak	370	Peak	421	Yura	458	Peak	593	Peak	714	Peak	753	Peak	771	Yura	1101	Yura	1181
0.6	12	0.4	Peak	1000	Peak	1157	Peak	1269	MF	1516	Peak	1856	Peak	1882	Peak	1990	Peak	2982	Peak	3087
		0.7	MF	1752	Peak	2698	Peak	2988	MF	2653	Peak	4612	Peak	4827	MF	3554	MF	6220	Peak	7425
		1	MF	2503	Yura	4311	Yura	4996	MF	3790	MF	6633	Yura	8266	MF	5077	MF	8885	Yura	11310
	20	0.4	Peak	454	Peak	514	Yura	599	Peak	753	Peak	776	Peak	787	Peak	1152	Peak	1314	Peak	1345
		0.7	Peak	1052	Peak	1249	Peak	1374	MF	1592	Peak	2022	Peak	2065	Peak	2097	Peak	3165	Peak	3338
		1	MF	1502	Peak	2126	Peak	2358	MF	2274	Peak	3600	Peak	3739	MF	3046	Yura	5262	Peak	5446
	30	0.4	Peak	239	Yura	300	Yura	352	Peak	383	Peak	392	Peak	398	Peak	636	Peak	678	Peak	692
		0.7	Peak	575	Peak	663	Peak	742	Peak	968	Peak	1010	Peak	1026	Peak	1350	Peak	1685	Peak	1726
		1	Yura	982	Peak	1151	Peak	1275	MF	1516	Peak	1852	Peak	1899	Peak	1986	Peak	2870	Peak	2996
	50	0.4	Peak	105	Yura	161	Yura	190	Peak	164	Peak	167	Peak	171	Peak	283	Peak	296	Peak	303
		0.7	Peak	259	Yura	313	Yura	368	Peak	415	Peak	425	Peak	432	Peak	685	Peak	733	Peak	749
		1	Peak	451	Peak	521	Peak	592	Peak	746	Peak	773	Peak	787	Peak	1147	Peak	1299	Peak	1335
0.8	12	0.4	Peak	1152	Yura	1390	Yura	1567	Peak	1838	Yura	2194	Peak	2160	Peak	2602	Peak	3099	Peak	3249
		0.7	MF	2353	Peak	3206	Yura	3561	MF	3554	Peak	5028	Yura	5433	MF	4756	Peak	7740	Peak	8220
		1	MF	3361	Yura	5404	Yura	6035	MF	5077	Peak	8548	Peak	9247	MF	6794	MF	11889	Peak	13992
	20	0.4	Peak	515	Yura	677	Yura	762	Peak	820	Peak	879	Peak	901	Peak	1237	Peak	1324	Peak	1398
		0.7	Peak	1239	Yura	1482	Yura	1655	Peak	1967	Yura	2306	Peak	2346	Peak	2741	Peak	3357	Peak	3499
		1	MF	2017	Yura	2515	Yura	2773	MF	3046	Peak	3871	Yura	4173	Peak	4062	Peak	5951	Peak	6288
	30	0.4	Peak	272	Yura	401	Yura	449	Peak	436	Peak	453	Peak	481	Peak	662	Peak	695	Peak	713
		0.7	Peak	660	Yura	824	Yura	922	Peak	1043	Peak	1150	Peak	1203	Peak	1575	Peak	1707	Peak	1800
		1	Peak	1143	Yura	1365	Yura	1520	Peak	1811	Yura	2095	Peak	2152	Peak	2595	Peak	3066	Peak	3206
	50	0.4	Peak	123	Yura	217	Yura	243	Peak	200	Peak	208	Peak	214	Peak	310	Peak	323	Peak	333
		0.7	Peak	296	Yura	417	Yura	465	Peak	471	Peak	500	Peak	532	Peak	716	Peak	752	Peak	772
		1	Peak	518	Yura	654	Yura	732	Peak	817	Peak	870	Peak	899	Peak	1231	Peak	1323	Peak	1381

Note: FC = Failure criteria; Peak = First peak load; Yura = Yura's deformation limit; MF = Member failure
Load unit: kN

Appendix A (b): Ultimate capacity of completely overlapped tubular joints ($\theta = 30^0$, $\xi = 0.5$)

Ultimate Capacity		β_{TL}	0.4						0.6						0.8					
		τ_{TL}	0.4		0.7		1		0.4		0.7		1		0.4		0.7		1	
β_{CT}	γ_C	τ_{CT}	FC	Load	FC	Load	FC	Load	FC	Load	FC	Load	FC	Load	FC	Load	FC	Load	FC	Load
0.4	12	0.4	MF	658	Peak	847	Peak	888	MF	1001	Peak	1326	Peak	1366	Peak	1332	Peak	1896	Peak	2024
		0.7	MF	1151	MF	2015	Yura	2222	MF	1752	MF	3066	Peak	3473	MF	2353	MF	4117	Peak	4928
		1	MF	1645	MF	2878	Yura	3738	MF	2503	MF	4380	Yura	5900	MF	3361	MF	5881	Yura	7390
	20	0.4	Peak	336	Peak	362	Peak	377	Peak	536	Peak	563	Peak	574	Peak	737	Peak	818	Yura	902
		0.7	MF	691	Peak	919	Peak	965	MF	1051	Peak	1442	Peak	1491	MF	1412	Peak	2058	Peak	2234
		1	MF	987	Peak	1619	Yura	1735	MF	1502	Peak	2558	Peak	2699	MF	2017	Yura	3325	Yura	3796
	30	0.4	Peak	172	Peak	182	Peak	190	Peak	278	Peak	288	Peak	294	Peak	405	Peak	425	Yura	504
		0.7	Peak	429	Peak	468	Peak	489	MF	683	Peak	729	Peak	749	Peak	878	Peak	1063	Yura	1144
		1	MF	658	Peak	846	Peak	889	MF	1001	Peak	1323	Peak	1370	Peak	1331	Peak	1893	Yura	2078
	50	0.4	Peak	72	Peak	76	Peak	79	Peak	121	Peak	125	Peak	128	Peak	184	Peak	193	Yura	221
		0.7	Peak	183	Peak	196	Peak	205	Peak	295	Peak	308	Peak	315	Peak	430	Peak	458	Yura	532
		1	Peak	331	Peak	358	Peak	375	Peak	524	Peak	555	Peak	572	Peak	724	Peak	820	Yura	900
0.6	12	0.4	Peak	893	Peak	967	Peak	1011	Peak	1395	Peak	1465	Peak	1496	Peak	1970	Peak	2143	Peak	2187
		0.7	MF	1752	Peak	2440	Peak	2565	MF	2653	Peak	3718	Peak	3838	MF	3554	Peak	5406	Peak	5656
		1	MF	2503	Peak	4290	Yura	4610	MF	3790	Peak	6605	Peak	6944	MF	5077	MF	8885	Peak	10136
	20	0.4	Peak	385	Peak	410	Peak	427	Peak	616	Peak	635	Peak	648	Peak	922	Peak	951	Peak	968
		0.7	Peak	963	Peak	1048	Peak	1097	Peak	1507	Peak	1592	Peak	1631	Peak	2092	Peak	2338	Peak	2397
		1	MF	1502	Peak	1896	Peak	1987	MF	2274	Peak	2882	Peak	2969	MF	3046	Peak	4202	Peak	4385
	30	0.4	Peak	194	Peak	205	Peak	213	Peak	321	Peak	330	Peak	337	Peak	495	Peak	510	Peak	521
		0.7	Peak	491	Peak	527	Peak	551	Peak	782	Peak	814	Peak	831	Peak	1166	Peak	1213	Peak	1239
		1	Peak	885	Peak	961	Peak	1008	Peak	1387	Peak	1464	Peak	1503	Peak	1961	Peak	2154	Peak	2222
	50	0.4	Peak	78	Peak	83	Peak	88	Peak	137	Peak	142	Peak	147	Peak	226	Peak	233	Peak	240
		0.7	Peak	205	Peak	218	Peak	228	Peak	339	Peak	350	Peak	360	Peak	525	Peak	543	Peak	556
		1	Peak	375	Peak	402	Peak	422	Peak	602	Peak	626	Peak	642	Peak	903	Peak	941	Peak	967
0.8	12	0.4	Peak	999	Peak	1112	Peak	1222	Peak	1580	Peak	1654	Peak	1694	Peak	2242	Peak	2336	Peak	2392
		0.7	Yura	2339	Peak	2721	Yura	2967	MF	3554	Peak	4084	Peak	4219	MF	4756	Peak	5718	Peak	5955
		1	MF	3361	Peak	4736	Yura	5182	MF	5077	Peak	7290	Peak	7592	MF	6794	Peak	10207	Peak	10765
	20	0.4	Peak	445	Peak	486	Peak	541	Peak	719	Peak	740	Peak	757	Peak	1048	Peak	1078	Peak	1100
		0.7	Peak	1074	Peak	1199	Peak	1316	Peak	1706	Peak	1792	Peak	1839	Peak	2420	Peak	2538	Peak	2606
		1	Peak	1844	Peak	2129	Peak	2320	Peak	2964	Peak	3188	Peak	3290	Peak	3990	Peak	4473	Peak	4647
	30	0.4	Peak	229	Peak	249	Peak	283	Peak	382	Peak	395	Peak	405	Peak	573	Peak	595	Peak	609
		0.7	Peak	562	Peak	620	Peak	685	Peak	907	Peak	938	Peak	961	Peak	1316	Peak	1360	Peak	1392
		1	Peak	990	Peak	1106	Peak	1213	Peak	1578	Peak	1658	Peak	1703	Peak	2245	Peak	2357	Peak	2428
	50	0.4	Peak	96	Yura	123	Yura	145	Peak	167	Peak	174	Peak	181	Peak	269	Peak	281	Peak	289
		0.7	Peak	241	Peak	265	Peak	297	Peak	403	Peak	418	Peak	430	Peak	609	Peak	632	Peak	649
		1	Peak	433	Peak	479	Peak	528	Peak	706	Peak	733	Peak	753	Peak	1038	Peak	1074	Peak	1104

Note: *FC = Failure criteria; Peak = First peak load; Yura = Yura's deformation limit; MF = Member failure*
Load unit: kN

Appendix A (c): Ultimate capacity of completely overlapped tubular joints ($\theta = 30^0$, $\xi = 1.0$)

Ultimate		β_{TL}	0.4						0.6						0.8					
Capacity		τ_{TL}	0.4		0.7		1		0.4		0.7		1		0.4		0.7		1	
β_{CT}	γ_C	τ_{CT}	FC	Load	FC	Load	FC	Load	FC	Load	FC	Load	FC	Load	FC	Load	FC	Load	FC	Load
0.4	12	0.4	MF	658	Peak	802	Peak	849	MF	1001	Peak	1215	Peak	1263	Peak	1312	Peak	1634	Yura	1782
		0.7	MF	1151	Yura	1930	Yura	2080	MF	1752	Peak	2904	Yura	3081	MF	2353	Peak	3671	Yura	4108
		1	MF	1645	MF	2878	Yura	3531	MF	2503	MF	4380	Yura	5290	MF	3361	Yura	5660	Yura	6538
	20	0.4	Peak	317	Peak	344	Peak	363	Peak	507	Peak	538	Peak	556	Peak	689	Peak	758	Yura	838
		0.7	MF	691	Peak	863	Yura	917	MF	1051	Peak	1310	Peak	1365	Peak	1391	Peak	1772	Yura	1940
		1	MF	987	Yura	1518	Yura	1622	MF	1502	Peak	2279	Yura	2400	MF	2017	Yura	2930	Yura	3246
	30	0.4	Peak	160	Peak	173	Peak	183	Peak	262	Peak	276	Peak	286	Peak	383	Peak	411	Yura	463
		0.7	Peak	401	Peak	440	Peak	466	Peak	636	Peak	682	Peak	709	Peak	843	Peak	965	Yura	1063
		1	MF	658	Peak	791	Yura	841	MF	1001	Peak	1195	Peak	1250	Peak	1300	Yura	1640	Yura	1810
	50	0.4	Peak	65	Peak	71	Peak	76	Peak	108	Peak	114	Yura	125	Peak	172	Yura	201	Yura	233
		0.7	Peak	169	Peak	184	Peak	196	Peak	273	Peak	291	Peak	304	Peak	398	Peak	439	Peak	499
		1	Peak	307	Peak	336	Peak	356	Peak	486	Peak	519	Peak	542	Peak	661	Peak	755	Yura	847
0.6	12	0.4	Peak	847	Peak	925	Peak	977	Peak	1331	Peak	1409	Peak	1454	Peak	1876	Peak	2013	Peak	2092
		0.7	MF	1752	Peak	2312	Yura	2453	MF	2653	Peak	3437	Peak	3573	MF	3554	Peak	4744	Peak	4997
		1	MF	2503	Yura	4064	Yura	4361	MF	3790	Peak	6000	Yura	6307	MF	5077	Peak	8064	Yura	8670
	20	0.4	Peak	358	Peak	388	Peak	410	Peak	581	Peak	610	Peak	628	Peak	877	Peak	918	Peak	945
		0.7	Peak	903	Peak	990	Peak	1048	Peak	1421	Peak	1512	Peak	1565	Peak	1998	Peak	2170	Peak	2267
		1	MF	1502	Peak	1783	Peak	1890	MF	2274	Peak	2664	Peak	2770	MF	3046	Peak	3732	Peak	3936
	30	0.4	Peak	174	Peak	190	Peak	204	Peak	289	Peak	303	Peak	315	Peak	458	Peak	478	Yura	550
		0.7	Peak	454	Peak	494	Peak	524	Peak	730	Peak	773	Peak	800	Peak	1088	Peak	1154	Peak	1204
		1	Peak	822	Peak	902	Peak	955	Peak	1295	Peak	1378	Peak	1429	Peak	1825	Peak	1985	Peak	2093
	50	0.4	Peak	69	Peak	76	Peak	84	Peak	116	Yura	140	Yura	158	Peak	196	Yura	256	Yura	289
		0.7	Peak	183	Peak	201	Peak	217	Peak	300	Peak	317	Peak	333	Peak	472	Peak	500	Yura	582
		1	Peak	341	Peak	373	Peak	398	Peak	549	Peak	583	Peak	608	Peak	822	Peak	880	Peak	942
0.8	12	0.4	Peak	952	Peak	1076	Peak	1189	Peak	1520	Peak	1608	Peak	1664	Peak	2170	Peak	2294	Peak	2385
		0.7	Peak	2218	Peak	2629	Yura	2892	Peak	3546	Peak	3919	Peak	4083	Peak	4677	Peak	5402	Peak	5698
		1	MF	3361	Yura	4559	Yura	5034	MF	5077	Peak	6848	Peak	7178	MF	6794	Peak	9266	Peak	9849
	20	0.4	Peak	410	Peak	466	Peak	524	Peak	661	Peak	697	Peak	723	Peak	987	Peak	1030	Yura	1138
		0.7	Peak	1010	Peak	1149	Peak	1270	Peak	1614	Peak	1718	Peak	1785	Peak	2311	Peak	2461	Peak	2578
		1	Peak	1755	Peak	2036	Peak	2242	Peak	2807	Peak	3037	Peak	3165	Peak	3827	Peak	4239	Peak	4485
	30	0.4	Peak	205	Peak	237	Peak	274	Peak	329	Peak	349	Yura	382	Peak	517	Yura	600	Yura	670
		0.7	Peak	516	Peak	590	Peak	661	Peak	823	Peak	875	Peak	913	Peak	1221	Peak	1292	Yura	1403
		1	Peak	921	Peak	1050	Peak	1157	Peak	1466	Peak	1564	Peak	1630	Peak	2101	Peak	2251	Peak	2381
	50	0.4	Peak	85	Peak	105	Peak	124	Peak	134	Yura	172	Yura	186	Peak	225	Yura	309	Yura	358
		0.7	Peak	216	Peak	252	Peak	291	Peak	340	Peak	363	Peak	387	Peak	532	Yura	637	Yura	709
		1	Peak	391	Peak	452	Peak	512	Peak	617	Peak	660	Peak	695	Peak	926	Peak	987	Yura	1119

Note: *FC = Failure criteria; Peak = First peak load; Yura = Yura's deformation limit; MF = Member failure*
Load unit: kN

Appendix A (d): Ultimate capacity of completely overlapped tubular joints

($\theta = 30^0$, $\xi = 2.0$)

Ultimate		β_{TL}	0.4						0.6						0.8					
Capacity		τ_{TL}	0.4		0.7		1		0.4		0.7		1		0.4		0.7		1	
β_{CT}	γ_C	τ_{CT}	FC	Load	FC	Load	FC	Load	FC	Load	FC	Load	FC	Load	FC	Load	FC	Load	FC	Load
0.4	12	0.4	MF	658	Yura	764	Peak	817	MF	1001	Peak	1159	Peak	1218	Peak	1287	Peak	1636	Peak	1796
		0.7	MF	1151	Yura	1840	Yura	1985	MF	1752	Yura	2722	Yura	2890	MF	2353	Yura	3452	Yura	3849
		1	MF	1645	MF	2878	Yura	3320	MF	2503	Yura	4320	Yura	4690	MF	3361	Yura	5150	Yura	5735
	20	0.4	Peak	295	Peak	325	Peak	348	Peak	466	Peak	503	Peak	529	Peak	670	Peak	762	Peak	846
		0.7	MF	691	Yura	820	Yura	878	MF	1051	Peak	1241	Peak	1308	Peak	1362	Peak	1748	Yura	1933
		1	MF	987	Yura	1441	Yura	1545	MF	1502	Yura	2130	Yura	2260	MF	2017	Yura	2750	Yura	3037
	30	0.4	Peak	147	Peak	163	Peak	176	Peak	232	Peak	252	Peak	267	Peak	357	Peak	405	Peak	463
		0.7	Peak	375	Peak	417	Peak	445	Peak	588	Peak	639	Peak	674	Peak	816	Peak	960	Yura	1069
		1	Yura	654	Yura	750	Yura	802	Yura	1000	Peak	1131	Peak	1195	Peak	1271	Yura	1606	Yura	1774
	50	0.4	Peak	60	Peak	68	Peak	74	Peak	93	Peak	103	Peak	113	Peak	157	Yura	196	Yura	226
		0.7	Peak	157	Peak	175	Peak	188	Peak	243	Peak	265	Peak	284	Peak	372	Yura	433	Peak	496
		1	Peak	287	Peak	318	Peak	340	Peak	444	Peak	484	Peak	514	Peak	640	Yura	743	Yura	840
0.6	12	0.4	Peak	792	Peak	874	Peak	932	Peak	1254	Peak	1345	Peak	1405	Peak	1824	Peak	2000	Peak	2109
		0.7	MF	1752	Yura	2216	Yura	2368	MF	2653	Peak	3334	Peak	3497	MF	3554	Peak	4671	Peak	4960
		1	MF	2503	Yura	3899	Yura	4173	MF	3790	Yura	5790	Yura	6105	MF	5077	Yura	7604	Yura	8165
	20	0.4	Peak	328	Peak	363	Peak	390	Peak	524	Peak	563	Peak	594	Peak	806	Peak	875	Peak	941
		0.7	Peak	846	Peak	937	Peak	998	Peak	1333	Peak	1437	Peak	1505	Peak	1931	Peak	2145	Peak	2273
		1	Peak	1491	Peak	1696	Peak	1807	MF	2274	Peak	2568	Peak	2694	Peak	3026	Peak	3674	Peak	3910
	30	0.4	Peak	159	Peak	178	Peak	195	Peak	252	Peak	274	Peak	297	Peak	405	Yura	472	Yura	520
		0.7	Peak	420	Peak	466	Peak	500	Peak	665	Peak	717	Peak	757	Peak	1010	Peak	1104	Peak	1191
		1	Peak	769	Peak	853	Peak	910	Peak	1209	Peak	1306	Peak	1372	Peak	1759	Peak	1947	Peak	2078
	50	0.4	Peak	63	Peak	73	Peak	82	Peak	100	Yura	120	Yura	136	Peak	184	Yura	234	Yura	262
		0.7	Peak	168	Peak	190	Peak	208	Peak	264	Peak	289	Peak	313	Peak	420	Yura	491	Yura	541
		1	Peak	316	Peak	353	Peak	380	Peak	495	Peak	537	Peak	573	Peak	751	Peak	834	Peak	913
0.8	12	0.4	Peak	892	Peak	1035	Peak	1148	Peak	1404	Peak	1519	Peak	1599	Peak	2064	Peak	2242	Peak	2393
		0.7	Peak	2125	Peak	2535	Peak	2802	Peak	3406	Peak	3792	Peak	3988	Peak	4581	Peak	5400	Peak	5742
		1	MF	3361	Yura	4421	Yura	4904	MF	5077	Peak	6668	Yura	7047	MF	6794	Peak	9119	Yura	9775
	20	0.4	Peak	379	Peak	451	Peak	508	Peak	580	Peak	633	Peak	681	Peak	875	Yura	993	Peak	1095
		0.7	Peak	950	Peak	1108	Peak	1226	Peak	1486	Peak	1617	Peak	1709	Peak	2181	Peak	2395	Peak	2581
		1	Peak	1670	Peak	1962	Peak	2164	Peak	2651	Peak	2910	Peak	3068	Peak	3709	Peak	4198	Peak	4491
	30	0.4	Peak	190	Peak	232	Peak	266	Peak	281	Peak	316	Yura	348	Peak	470	Yura	562	Yura	627
		0.7	Peak	482	Peak	573	Peak	639	Peak	731	Peak	801	Peak	860	Peak	1090	Yura	1237	Peak	1366
		1	Peak	867	Peak	1017	Peak	1124	Peak	1340	Peak	1464	Peak	1556	Peak	1961	Peak	2171	Peak	2365
	50	0.4	Peak	81	Peak	101	Peak	120	Yura	127	Yura	148	Yura	169	Peak	219	Yura	288	Yura	328
		0.7	Peak	203	Peak	247	Peak	282	Peak	294	Peak	330	Peak	361	Peak	488	Yura	585	Yura	654
		1	Peak	367	Peak	441	Peak	494	Peak	544	Peak	601	Peak	651	Peak	822	Yura	959	Yura	1060

Note: *FC = Failure criteria; Peak = First peak load; Yura = Yura's deformation limit; MF = Member failure*
Load unit: kN

Appendix A (e): Ultimate capacity of completely overlapped tubular joints ($\theta = 45^0$, g = 51mm)

Ultimate		β_{TL}	0.4						0.6						0.8					
Capacity		τ_{TL}	0.4		0.7		1		0.4		0.7		1		0.4		0.7		1	
β_{CT}	γ_C	τ_{CT}	FC	Load	FC	Load	FC	Load	FC	Load	FC	Load	FC	Load	FC	Load	FC	Load	FC	Load
0.4	12	0.4	MF	658	Peak	1057	Yura	1172	MF	1001	Peak	1693	Peak	1841	MF	1344	MF	2353	Peak	2716
		0.7	MF	1151	MF	2015	Yura	2701	MF	1752	MF	3066	Yura	4308	MF	2353	MF	4117	MF	5882
		1	MF	1645	MF	2878	MF	4112	MF	2503	MF	4380	MF	6257	MF	3361	MF	5882	MF	8403
	20	0.4	MF	395	Peak	484	Peak	529	MF	601	Peak	764	Peak	810	MF	807	Peak	1155	Peak	1195
		0.7	MF	691	Peak	1137	Peak	1267	MF	1051	Peak	1835	Peak	1999	MF	1412	MF	2470	Peak	2922
		1	MF	987	MF	1727	Yura	2165	MF	1502	MF	2628	Yura	3420	MF	2017	MF	3529	Yura	4750
	30	0.4	Peak	224	Peak	251	Peak	278	Peak	371	Peak	398	Peak	419	Peak	525	Peak	606	Peak	618
		0.7	MF	461	Peak	619	Peak	676	MF	701	Peak	986	Peak	1051	MF	941	Peak	1477	Peak	1547
		1	MF	658	Peak	1058	Peak	1178	MF	1001	Peak	1694	Peak	1854	MF	1344	MF	2353	Peak	2660
	50	0.4	Peak	99	Peak	107	Peak	120	Peak	169	Peak	175	Peak	183	Peak	245	Peak	273	Peak	279
		0.7	Peak	241	Peak	272	Peak	300	Peak	399	Peak	432	Peak	458	Peak	551	Peak	655	Peak	675
		1	MF	395	Peak	486	Peak	532	MF	601	Peak	770	Peak	823	MF	807	Peak	1148	Peak	1204
0.6	12	0.4	MF	1001	Peak	1341	Yura	1459	MF	1516	Peak	2086	Yura	2306	MF	2031	Peak	3110	Peak	3297
		0.7	MF	1752	MF	3066	Peak	3535	MF	2653	MF	4643	Peak	5418	MF	3554	MF	6220	Peak	7961
		1	MF	2503	MF	4380	Yura	5962	MF	3790	MF	6633	Yura	9342	MF	5077	MF	8885	Yura	12780
	20	0.4	Peak	532	Peak	578	Peak	622	Peak	852	Peak	910	Peak	949	Peak	1167	Peak	1384	Peak	1448
		0.7	MF	1051	Peak	1445	Peak	1560	MF	1592	Peak	2247	Peak	2388	MF	2133	Peak	3375	Peak	3601
		1	MF	1502	Peak	2523	Yura	2763	MF	2274	Peak	3928	Peak	4245	MF	3046	MF	5331	Peak	6249
	30	0.4	Peak	277	Peak	290	Yura	389	Peak	458	Peak	477	Peak	492	Peak	643	Peak	734	Peak	761
		0.7	Peak	677	Peak	751	Peak	803	Peak	1048	Peak	1176	Peak	1232	Peak	1376	Peak	1780	Peak	1882
		1	MF	1001	Peak	1336	Peak	1443	MF	1516	Peak	2100	Yura	2268	MF	2031	Peak	3121	Peak	3353
	50	0.4	Peak	117	Peak	123	Yura	202	Peak	206	Peak	216	Peak	224	Peak	288	Peak	338	Peak	351
		0.7	Peak	300	Peak	316	Yura	405	Peak	495	Peak	519	Peak	539	Peak	681	Peak	798	Peak	840
		1	Peak	533	Peak	581	Peak	622	Peak	854	Peak	920	Peak	965	Peak	1146	Peak	1396	Peak	1491
0.8	12	0.4	MF	1344	Yura	1697	Yura	1918	Peak	2002	Yura	2687	Yura	3028	Peak	2650	Peak	3777	Yura	4339
		0.7	MF	2353	Peak	3764	Yura	4319	MF	3554	Peak	5750	Yura	6485	MF	4756	Peak	8049	Yura	8990
		1	MF	3361	MF	5882	Yura	7228	MF	5077	MF	8885	Peak	10771	MF	6794	MF	11889	Peak	14899
	20	0.4	Peak	621	Peak	719	Yura	949	Peak	961	Yura	1406	Yura	1465	Peak	1337	Peak	1811	Yura	2181
		0.7	MF	1412	Yura	1800	Yura	2038	Peak	2121	Yura	2845	Yura	3202	Peak	2796	Yura	4035	Yura	4569
		1	MF	2017	Yura	2997	Yura	3431	MF	3046	Peak	4554	Yura	5168	MF	4076	Peak	6342	Yura	7165
	30	0.4	Peak	332	Peak	373	Yura	574	Peak	510	Peak	836	Yura	978	Peak	733	Yura	1011	Yura	1415
		0.7	Peak	789	Peak	920	Yura	1149	Peak	1218	Yura	1673	Yura	1843	Peak	1684	Peak	2271	Yura	2728
		1	MF	1344	Yura	1670	Yura	1882	Peak	2002	Yura	2637	Yura	2964	Peak	2649	Yura	3756	Yura	4223
	50	0.4	Peak	148	Peak	168	Yura	314	Peak	234	Peak	412	Yura	540	Peak	349	Peak	511	Peak	708
		0.7	Peak	358	Peak	404	Yura	597	Peak	547	Peak	887	Yura	1031	Peak	779	Peak	1068	Yura	1497
		1	Peak	623	Peak	720	Yura	921	Peak	964	Yura	1332	Yura	1455	Peak	1336	Peak	1817	Yura	2154

Note: *FC = Failure criteria; Peak = First peak load; Yura = Yura's deformation limit; MF = Member failure*
Load unit: kN

Appendix A (f): Ultimate capacity of completely overlapped tubular joints

($\theta = 45^0$, $\xi = 0.5$)

Ultimate Capacity		β_{TL}	0.4						0.6						0.8					
		τ_{TL}	0.4		0.7		1		0.4		0.7		1		0.4		0.7		1	
β_{CT}	γ_C	τ_{CT}	FC	Load	FC	Load	FC	Load	FC	Load	FC	Load	FC	Load	FC	Load	FC	Load	FC	Load
0.4	12	0.4	MF	658	Peak	987	Peak	1096	MF	1001	Peak	1504	Peak	1628	MF	1344	Peak	2064	Peak	2217
		0.7	MF	1151	MF	2015	Yura	2524	MF	1752	MF	3066	Peak	3778	MF	2353	MF	4117	Yura	5098
		1	MF	1645	MF	2878	Yura	4112	MF	2503	MF	4380	Yura	6214	MF	3361	MF	5882	Yura	8290
	20	0.4	Peak	371	Peak	453	Peak	502	Peak	596	Peak	691	Peak	741	Peak	798	Peak	963	Peak	1017
		0.7	MF	691	Peak	1060	Peak	1179	MF	1051	Peak	1617	Peak	1759	MF	1412	Peak	2221	Peak	2397
		1	MF	987	MF	1727	Yura	2010	MF	1502	MF	2628	Peak	2999	MF	2017	MF	3529	Yura	4043
	30	0.4	Peak	206	Peak	235	Peak	263	Peak	336	Peak	367	Peak	393	Peak	478	Peak	529	Peak	553
		0.7	MF	461	Peak	572	Peak	632	MF	701	Peak	875	Peak	942	MF	941	Peak	1216	Peak	1298
		1	MF	658	Peak	981	Peak	1090	MF	1001	Peak	1494	Peak	1626	MF	1344	Peak	2051	Peak	2218
	50	0.4	Peak	87	Peak	99	Peak	112	Peak	150	Peak	161	Peak	173	Peak	214	Peak	247	Peak	257
		0.7	Peak	218	Peak	251	Peak	280	Peak	354	Peak	391	Peak	420	Peak	504	Peak	563	Peak	596
		1	Peak	374	Peak	446	Peak	494	Peak	587	Peak	681	Peak	735	Peak	793	Peak	954	Peak	1024
0.6	12	0.4	MF	1001	Peak	1192	Peak	1276	MF	1516	Peak	1815	Peak	1917	Peak	2024	Peak	2462	Peak	2555
		0.7	MF	1752	Peak	2863	Peak	3100	MF	2653	Peak	4241	Peak	4557	MF	3554	Peak	5706	Peak	6042
		1	MF	2503	MF	4380	Yura	5390	MF	3790	MF	6633	Yura	7840	MF	5077	MF	8885	Peak	10285
	20	0.4	Peak	471	Peak	518	Peak	556	Peak	764	Peak	821	Peak	863	Peak	1031	Peak	1147	Peak	1175
		0.7	MF	1051	Peak	1280	Peak	1373	MF	1592	Peak	1954	Peak	2067	MF	2133	Peak	2659	Peak	2770
		1	MF	1502	Peak	2254	Peak	2425	MF	2274	Peak	3360	Peak	3586	MF	3046	Peak	4528	Peak	4768
	30	0.4	Peak	240	Peak	263	Peak	285	Peak	403	Peak	430	Peak	452	Peak	521	Peak	618	Peak	635
		0.7	Peak	594	Peak	659	Peak	707	Peak	951	Peak	1037	Peak	1094	Peak	1301	Peak	1443	Peak	1494
		1	MF	1001	Peak	1177	Peak	1263	MF	1516	Peak	1801	Peak	1907	Peak	2014	Peak	2455	Peak	2568
	50	0.4	Peak	98	Peak	111	Peak	123	Peak	171	Peak	183	Peak	194	Peak	236	Peak	278	Peak	289
		0.7	Peak	253	Peak	280	Peak	304	Peak	424	Peak	456	Peak	482	Peak	544	Peak	657	Peak	676
		1	Peak	457	Peak	507	Peak	546	Peak	744	Peak	806	Peak	853	Peak	992	Peak	1131	Peak	1176
0.8	12	0.4	Peak	1199	Peak	1392	Peak	1552	Peak	1868	Peak	2083	Peak	2243	Peak	2601	Peak	2922	Peak	3075
		0.7	MF	2353	Peak	3286	Peak	3655	MF	3554	Peak	4902	Peak	5316	MF	4756	Peak	6700	Peak	7181
		1	MF	3361	Peak	5529	Peak	6248	MF	5077	Peak	8214	Peak	9074	MF	6794	Peak	11111	Peak	12145
	20	0.4	Peak	535	Peak	617	Peak	693	Peak	877	Peak	950	Peak	1017	Peak	1225	Peak	1373	Peak	1429
		0.7	Peak	1275	Peak	1490	Peak	1660	Peak	1991	Peak	2241	Peak	2414	Peak	2745	Peak	3150	Peak	3327
		1	MF	2017	Peak	2592	Peak	2880	MF	3046	Peak	3875	Peak	4193	MF	4076	Peak	5330	Peak	5705
	30	0.4	Peak	271	Peak	319	Peak	363	Peak	454	Peak	499	Peak	539	Peak	641	Peak	741	Peak	772
		0.7	Peak	672	Peak	779	Peak	873	Peak	1093	Peak	1196	Peak	1285	Peak	1524	Peak	1727	Peak	1812
		1	Peak	1179	Peak	1374	Peak	1531	Peak	1848	Peak	2075	Peak	2235	Peak	2587	Peak	2926	Peak	3100
	50	0.4	Peak	113	Peak	139	Peak	165	Peak	193	Peak	216	Peak	243	Peak	297	Peak	334	Peak	352
		0.7	Peak	286	Peak	338	Peak	386	Peak	478	Peak	529	Peak	573	Peak	679	Peak	785	Peak	822
		1	Peak	516	Peak	604	Peak	680	Peak	848	Peak	933	Peak	1007	Peak	1166	Peak	1362	Peak	1431

Note: FC = Failure criteria; Peak = First peak load; Yura = Yura's deformation limit; MF = Member failure
Load unit: kN

Appendix A (g): Ultimate capacity of completely overlapped tubular joints

($\theta = 45^0$, $\xi = 1.0$)

Ultimate		β_{TL}	0.4						0.6						0.8					
Capacity		τ_{TL}	0.4		0.7		1		0.4		0.7		1		0.4		0.7		1	
β_{CT}	γ_C	τ_{CT}	FC	Load	FC	Load	FC	Load	FC	Load	FC	Load	FC	Load	FC	Load	FC	Load	FC	Load
0.4	12	0.4	MF	658	Peak	960	Yura	1075	MF	1001	Peak	1469	Peak	1605	MF	1344	Peak	2009	Peak	2169
		0.7	MF	1151	MF	2015	Yura	2463	MF	1752	MF	3066	Yura	3617	MF	2353	MF	4117	Yura	4702
		1	MF	1645	MF	2878	Yura	4009	MF	2503	MF	4380	Yura	5850	MF	3361	MF	5882	Yura	7367
	20	0.4	Peak	364	Peak	435	Peak	485	Peak	576	Peak	674	Peak	730	Peak	788	Peak	953	Peak	1016
		0.7	MF	691	Peak	1021	Yura	1147	MF	1051	Peak	1564	Peak	1717	MF	1412	Peak	2130	Peak	2313
		1	MF	987	Yura	1720	Yura	1955	MF	1502	Yura	2569	Yura	2875	MF	2017	Yura	3378	Yura	3752
	30	0.4	Peak	191	Peak	225	Peak	254	Peak	312	Peak	350	Peak	382	Peak	465	Peak	512	Peak	545
		0.7	Peak	449	Peak	546	Peak	609	Peak	695	Peak	844	Peak	918	Peak	934	Peak	1187	Peak	1277
		1	MF	658	Peak	941	Peak	1054	MF	1001	Peak	1438	Peak	1578	MF	1344	Peak	1952	Peak	2125
	50	0.4	Peak	79	Peak	94	Peak	110	Peak	130	Peak	147	Peak	166	Peak	202	Peak	225	Yura	268
		0.7	Peak	202	Peak	239	Peak	269	Peak	324	Peak	367	Peak	405	Peak	476	Peak	534	Peak	576
		1	Peak	354	Peak	423	Peak	472	Peak	554	Peak	650	Peak	712	Peak	769	Peak	919	Peak	996
0.6	12	0.4	Peak	988	Peak	1142	Peak	1233	Peak	1515	Peak	1771	Peak	1886	Peak	2007	Peak	2442	Peak	2549
		0.7	MF	1752	Peak	2764	Peak	3011	MF	2653	Peak	4123	Peak	4467	MF	3554	Peak	5510	Peak	5855
		1	MF	2503	MF	4380	Yura	5236	MF	3790	MF	6633	Peak	7529	MF	5077	Yura	8845	Yura	9570
	20	0.4	Peak	434	Peak	487	Peak	531	Peak	710	Peak	778	Peak	833	Peak	1013	Peak	1104	Peak	1148
		0.7	Peak	1045	Peak	1214	Peak	1312	MF	1592	Peak	1882	Peak	2011	Peak	2112	Peak	2601	Peak	2730
		1	MF	1502	Peak	2146	Peak	2326	MF	2274	Peak	3236	Peak	3476	MF	3046	Peak	4359	Peak	4611
	30	0.4	Peak	215	Peak	244	Peak	272	Peak	353	Peak	390	Peak	423	Peak	506	Peak	564	Yura	637
		0.7	Peak	547	Peak	616	Peak	671	Peak	878	Peak	973	Peak	1044	Peak	1248	Peak	1370	Peak	1438
		1	Peak	960	Peak	1107	Peak	1198	Peak	1476	Peak	1712	Peak	1834	Peak	1982	Peak	2367	Peak	2495
	50	0.4	Peak	87	Peak	103	Peak	118	Peak	144	Peak	161	Peak	181	Peak	223	Peak	239	Yura	322
		0.7	Peak	227	Peak	259	Peak	289	Peak	367	Peak	407	Peak	445	Peak	533	Peak	585	Peak	618
		1	Peak	416	Peak	470	Peak	515	Peak	667	Peak	739	Peak	801	Peak	955	Peak	1040	Peak	1100
0.8	12	0.4	Peak	1134	Peak	1337	Peak	1500	Peak	1786	Peak	2023	Peak	2206	Peak	2547	Peak	2878	Peak	3059
		0.7	MF	2353	Peak	3168	Peak	3555	MF	3554	Peak	4782	Peak	5227	MF	4756	Peak	6620	Peak	7129
		1	MF	3361	Peak	5366	Peak	6095	MF	5077	Peak	7994	Peak	8885	MF	6794	Peak	10741	Peak	11803
	20	0.4	Peak	487	Peak	583	Peak	668	Peak	783	Peak	886	Peak	983	Peak	1171	Peak	1289	Yura	1433
		0.7	Peak	1196	Peak	1417	Peak	1589	Peak	1870	Peak	2143	Peak	2349	Peak	2662	Peak	3051	Peak	3269
		1	MF	2017	Peak	2470	Peak	2768	Peak	3046	Peak	3728	Peak	4077	Peak	4057	Peak	5204	Peak	5615
	30	0.4	Peak	241	Peak	300	Peak	352	Peak	389	Peak	450	Peak	516	Peak	607	Peak	661	Yura	840
		0.7	Peak	613	Peak	734	Peak	834	Peak	975	Peak	1106	Peak	1230	Peak	1455	Peak	1598	Peak	1731
		1	Peak	1094	Peak	1297	Peak	1455	Peak	1707	Peak	1953	Peak	2153	Peak	2451	Peak	2777	Peak	2996
	50	0.4	Peak	102	Peak	133	Peak	160	Peak	164	Peak	200	Yura	277	Peak	262	Peak	359	Yura	435
		0.7	Peak	256	Peak	319	Peak	373	Peak	407	Peak	472	Peak	539	Peak	632	Peak	691	Yura	883
		1	Peak	466	Peak	566	Peak	648	Peak	736	Peak	844	Peak	949	Peak	1107	Peak	1218	Yura	1377

Note: *FC = Failure criteria; Peak = First peak load; Yura = Yura's deformation limit; MF = Member failure*
Load unit: kN

Appendix A (h): Ultimate capacity of completely overlapped tubular joints

($\theta = 45^0$, $\xi = 2.0$)

Ultimate	β_{TL}	0.4						0.6						0.8					
Capacity	τ_{TL}	0.4		0.7		1		0.4		0.7		1		0.4		0.7		1	
β_{CT}	γ_C	τ_{CT}	FC	Load	FC	Load	FC	Load	FC	Load	FC	Load	FC	Load	FC	Load	FC	Load	FC	Load
0.4	12	0.4	MF	658	Peak	926	Yura	1045	MF	1001	Peak	1433	Peak	1582	MF	1344	Peak	1990	Peak	2167
		0.7	MF	1151	MF	2015	Yura	2415	MF	1752	MF	3066	Yura	3556	MF	2353	Yura	4047	Yura	4508
		1	MF	1645	MF	2878	Yura	3929	MF	2503	MF	4380	Yura	5536	MF	3361	MF	5882	Yura	6557
	20	0.4	Peak	347	Peak	418	Peak	464	Peak	543	Peak	646	Peak	713	Peak	765	Peak	935	Peak	1012
		0.7	MF	691	Peak	986	Yura	1116	MF	1051	Peak	1521	Peak	1687	MF	1412	Peak	2093	Peak	2295
		1	MF	987	Yura	1656	Yura	1907	MF	1502	Peak	2490	Yura	2815	MF	2017	Yura	3215	Yura	3527
	30	0.4	Peak	180	Peak	218	Peak	241	Peak	285	Peak	331	Peak	370	Peak	417	Peak	481	Peak	532
		0.7	Peak	428	Peak	527	Peak	587	Peak	667	Peak	814	Peak	899	Peak	916	Peak	1162	Peak	1264
		1	MF	658	Peak	908	Peak	1025	MF	1001	Peak	1400	Peak	1551	MF	1344	Peak	1910	Peak	2085
	50	0.4	Peak	74	Peak	92	Peak	105	Peak	117	Peak	140	Peak	160	Peak	177	Yura	215	Yura	247
		0.7	Peak	192	Peak	233	Peak	257	Peak	301	Peak	351	Peak	391	Peak	434	Peak	504	Peak	559
		1	Peak	339	Peak	411	Peak	453	Peak	527	Peak	628	Peak	694	Peak	746	Peak	893	Peak	977
0.6	12	0.4	Peak	935	Peak	1083	Peak	1169	Peak	1450	Peak	1696	Peak	1832	Peak	1971	Peak	2400	Peak	2530
		0.7	MF	1752	Peak	2661	Peak	2911	MF	2653	Peak	4020	Peak	4355	MF	3554	Peak	5425	Peak	5805
		1	MF	2503	MF	4380	Yura	5105	MF	3790	MF	6633	Peak	7252	MF	5077	Yura	8376	Yura	8987
	20	0.4	Peak	402	Peak	460	Peak	501	Peak	642	Peak	724	Peak	794	Peak	920	Peak	1023	Peak	1099
		0.7	Peak	993	Peak	1156	Peak	1247	Peak	1527	Peak	1804	Peak	1952	Peak	2075	Peak	2540	Peak	2687
		1	MF	1502	Peak	2055	Peak	2236	MF	2274	Peak	3141	Peak	3410	MF	3046	Peak	4259	Peak	4528
	30	0.4	Peak	197	Peak	231	Peak	257	Peak	312	Peak	357	Peak	400	Peak	458	Yura	526	Yura	591
		0.7	Peak	513	Peak	586	Peak	635	Peak	810	Peak	918	Peak	1001	Peak	1144	Peak	1289	Peak	1380
		1	Peak	912	Peak	1057	Peak	1139	Peak	1404	Peak	1644	Peak	1779	Peak	1936	Peak	2299	Peak	2440
	50	0.4	Peak	81	Peak	98	Peak	113	Peak	127	Peak	149	Peak	171	Peak	190	Peak	250	Yura	293
		0.7	Peak	211	Peak	246	Peak	273	Peak	330	Peak	379	Peak	423	Peak	478	Yura	538	Yura	604
		1	Peak	390	Peak	448	Peak	488	Peak	612	Peak	696	Peak	764	Peak	866	Peak	967	Peak	1043
0.8	12	0.4	Peak	1066	Peak	1285	Peak	1422	Peak	1662	Peak	1937	Peak	2156	Peak	2397	Peak	2781	Peak	3027
		0.7	MF	2353	Peak	3053	Peak	3433	MF	3554	Peak	4649	Peak	5142	MF	4756	Peak	6550	Peak	7105
		1	MF	3361	Yura	5211	Yura	5947	MF	5077	Peak	7828	Peak	8766	MF	6794	Peak	10524	Peak	11624
	20	0.4	Peak	452	Peak	559	Peak	628	Peak	701	Peak	831	Peak	943	Peak	1041	Peak	1197	Peak	1344
		0.7	Peak	1132	Peak	1369	Peak	1510	Peak	1750	Peak	2056	Peak	2286	Peak	2502	Peak	2939	Peak	3220
		1	Peak	1922	Peak	2383	Peak	2656	Peak	2929	Peak	3617	Peak	4001	Peak	3986	Peak	5115	Peak	5561
	30	0.4	Peak	226	Peak	287	Peak	332	Peak	347	Peak	423	Peak	488	Peak	519	Yura	667	Yura	770
		0.7	Peak	577	Peak	706	Peak	788	Peak	887	Peak	1050	Peak	1182	Peak	1283	Peak	1482	Peak	1662
		1	Peak	1037	Peak	1255	Peak	1383	Peak	1596	Peak	1877	Peak	2086	Peak	2272	Peak	2660	Peak	2931
	50	0.4	Peak	98	Peak	128	Peak	153	Peak	148	Peak	186	Peak	220	Peak	225	Peak	312	Yura	396
		0.7	Peak	241	Peak	305	Peak	352	Peak	367	Peak	447	Peak	516	Peak	544	Yura	680	Yura	785
		1	Peak	440	Peak	543	Peak	612	Peak	670	Peak	802	Peak	909	Peak	979	Peak	1121	Peak	1265

Note: *FC = Failure criteria; Peak = First peak load; Yura = Yura's deformation limit; MF = Member failure*
Load unit: kN

Appendix A (i): Ultimate capacity of completely overlapped tubular joints ($\theta = 60^0$, g = 51mm)

Ultimate Capacity		β_{TL}	0.4			0.6			0.8		
		τ_{TL}	0.4	0.7	1	0.4	0.7	1	0.4	0.7	1
β_{CT}	γ_C	τ_{CT}	MF 658	MF 1151	Peak 1579	MF 1001	MF 1752	Peak 2336	MF 1344	MF 2353	Peak 3327
0.4	12	0.4	MF 1151	MF 2015	MF 2878	MF 1752	MF 3066	MF 4380	MF 2353	MF 4117	MF 5882
		0.7	MF 1645	MF 2878	MF 4112	MF 2503	MF 4380	MF 6257	MF 3361	MF 5882	MF 8403
		1	MF 395	Peak 666	Peak 734	MF 601	Peak 998	Peak 1104	MF 807	MF 1412	Peak 1580
	20	0.4	MF 691	MF 1209	Peak 1707	MF 1051	MF 1840	Peak 2515	MF 1412	MF 2470	MF 3529
		0.7	MF 987	MF 1727	MF 2467	MF 1502	MF 2628	MF 3754	MF 2017	MF 3529	MF 5042
		1	MF 263	Peak 362	Peak 391	Peak 393	Peak 554	Peak 592	Peak 525	Peak 813	Peak 857
	30	0.4	MF 461	MF 806	Peak 933	MF 701	MF 1226	Peak 1401	MF 941	MF 1647	Peak 2002
		0.7	MF 658	MF 1151	Peak 1587	MF 1001	MF 1752	Peak 2345	MF 1344	MF 2353	Peak 3304
		1	Peak 143	Peak 162	Peak 174	Peak 222	Peak 259	Peak 271	Peak 302	Peak 389	Yura 510
	50	0.4	MF 276	Peak 390	Peak 423	Peak 415	Peak 597	Peak 643	Peak 553	Peak 874	Peak 930
		0.7	MF 395	Peak 668	Peak 738	MF 601	Peak 1003	Peak 1114	MF 807	MF 1412	Peak 1591
		1	MF 1001	MF 1752	Yura 2016	MF 1516	MF 2653	Yura 3124	MF 2031	MF 3554	Peak 4326
0.6	12	0.4	MF 1752	MF 3066	MF 4380	MF 2653	MF 4643	MF 6633	MF 3554	MF 6220	MF 8885
		0.7	MF 2503	MF 4380	MF 6257	MF 3790	MF 6633	MF 9475	MF 5077	MF 8885	MF 12693
		1	Peak 598	Peak 818	Yura 1042	Peak 907	Peak 1283	Peak 1362	Peak 1165	Peak 1855	Yura 2404
	20	0.4	MF 1051	MF 1840	Peak 2131	MF 1592	MF 2786	Peak 3250	MF 2133	MF 3732	Peak 4660
		0.7	MF 1502	MF 2628	Peak 3564	MF 2274	MF 3980	Peak 5514	MF 3046	MF 5331	Peak 7604
		1	Peak 374	Peak 433	Yura 618	Peak 579	Peak 700	Peak 734	Peak 724	Peak 1031	Yura 1420
	30	0.4	MF 701	Peak 1039	Yura 1258	MF 1061	Peak 1629	Peak 1744	Peak 1377	Peak 2334	Yura 2863
		0.7	MF 1001	MF 1752	Peak 1989	MF 1516	MF 2653	Peak 3029	Peak 2010	MF 3554	Peak 4350
		1	Peak 178	Peak 195	Yura 335	Peak 263	Peak 325	Peak 339	Peak 384	Peak 489	Peak 762
	50	0.4	Peak 395	Peak 469	Yura 652	Peak 609	Peak 756	Peak 797	Peak 793	Peak 1111	Yura 1527
		0.7	Peak 598	Peak 823	Yura 1008	Peak 904	Peak 1296	Peak 1381	Peak 1164	Peak 1870	Yura 2373
		1	MF 1344	Peak 2137	Yura 2612	Peak 2022	Peak 3265	Yura 4060	Peak 2667	Peak 4488	Yura 5685
0.8	12	0.4	MF 2353	MF 4117	Peak 5476	MF 3554	MF 6220	Peak 8233	MF 4756	MF 8322	Peak 11144
		0.7	MF 3361	MF 5882	MF 8403	MF 5077	MF 8885	MF 12693	MF 6794	MF 11889	MF 16984
		1	Peak 778	Peak 1000	Yura 1351	Peak 1159	Peak 1513	Yura 2075	Peak 1550	Peak 2095	Yura 3006
	20	0.4	MF 1412	Peak 2295	Yura 2760	Peak 2129	Peak 3512	Yura 4300	Peak 2806	Peak 4828	Yura 6003
		0.7	MF 2017	MF 3529	Yura 4405	MF 3046	MF 5331	Peak 6623	MF 4076	MF 7133	Peak 8946
		1	Peak 469	Peak 528	Yura 839	Peak 705	Peak 826	Yura 1328	Peak 924	Peak 1136	Peak 1668
	30	0.4	MF 941	Peak 1262	Yura 1637	Peak 1366	Peak 1920	Yura 2590	Peak 1827	Peak 2644	Yura 3653
		0.7	MF 1344	Peak 2145	Yura 2572	Peak 2020	Peak 3277	Yura 4024	Peak 2668	Peak 4488	Yura 5610
		1	Peak 219	Peak 239	Yura 463	Peak 290	Peak 382	Peak 674	Peak 408	Peak 520	Peak 777
	50	0.4	Peak 500	Peak 570	Yura 880	Peak 744	Peak 887	Yura 1409	Peak 962	Peak 1204	Peak 1780
		0.7	Peak 777	Peak 994	Yura 1332	Peak 1156	Peak 1517	Yura 2058	Peak 1539	Peak 2078	Yura 2987
		1	MF 658	MF 1151	Peak 1579	MF 1001	MF 1752	Peak 2336	MF 1344	MF 2353	Peak 3327

Note: *FC = Failure criteria; Peak = First peak load; Yura = Yura's deformation limit; MF = Member failure*
Load unit: kN

Appendix A (j): Ultimate capacity of completely overlapped tubular joints

($\theta = 60^0$, $\xi = 0.5$)

Ultimate	β_{TL}	0.4						0.6						0.8					
Capacity	τ_{TL}	0.4		0.7		1		0.4		0.7		1		0.4		0.7		1	
β_{CT}	γ_C	τ_{CT}	FC	Load	FC	Load	FC	Load	FC	Load	FC	Load	FC	Load	FC	Load	FC	Load	FC	Load
0.4	12	0.4	MF	658	MF	1151	Peak	1484	MF	1001	MF	1752	Peak	2174	MF	1344	MF	2353	Peak	2963
		0.7	MF	1151	MF	2015	MF	2878	MF	1752	MF	3066	MF	4380	MF	2353	MF	4117	MF	5882
		1	MF	1645	MF	2878	MF	4112	MF	2503	MF	4380	MF	6257	MF	3361	MF	5882	MF	8403
	20	0.4	MF	395	Peak	626	Peak	693	MF	601	Peak	943	Peak	1046	MF	807	Peak	1331	Peak	1458
		0.7	MF	691	MF	1209	Peak	1591	MF	1051	MF	1840	Peak	2324	MF	1412	MF	2470	Peak	3144
		1	MF	987	MF	1727	MF	2467	MF	1502	MF	2628	MF	3754	MF	2017	MF	3529	Peak	4997
	30	0.4	MF	263	Peak	335	Peak	366	Peak	388	Peak	520	Peak	565	Peak	522	Peak	766	Peak	812
		0.7	MF	461	Peak	780	Peak	871	MF	701	Peak	1161	Peak	1307	MF	941	Peak	1630	Peak	1813
		1	MF	658	MF	1151	Peak	1477	MF	1001	MF	1752	Peak	2166	MF	1344	MF	2353	Peak	2915
	50	0.4	Peak	123	Peak	145	Peak	160	Peak	202	Peak	234	Peak	253	Peak	289	Peak	367	Peak	385
		0.7	MF	276	Peak	355	Peak	390	Peak	409	Peak	551	Peak	601	Peak	549	Peak	807	Peak	866
		1	MF	395	Peak	617	Peak	682	MF	601	Peak	930	Peak	1033	MF	807	Peak	1314	Peak	1448
0.6	12	0.4	MF	1001	Peak	1600	Peak	1831	MF	1516	Peak	2500	Peak	2747	Peak	2014	Peak	3396	Peak	3822
		0.7	MF	1752	MF	3066	Peak	4047	MF	2653	MF	4643	Peak	6154	MF	3554	MF	6220	Peak	8117
		1	MF	2503	MF	4380	MF	6257	MF	3790	MF	6633	MF	9475	MF	5077	MF	8885	MF	12693
	20	0.4	Peak	592	Peak	750	Peak	843	Peak	894	Peak	1190	Peak	1271	Peak	1156	Peak	1709	Peak	1843
		0.7	MF	1051	Peak	1705	Peak	1957	MF	1592	Peak	2673	Peak	2950	Peak	2124	Peak	3626	Peak	4103
		1	MF	1502	MF	2628	Peak	3259	MF	2274	MF	3980	Peak	4943	MF	3046	MF	5331	Peak	6606
	30	0.4	Peak	322	Peak	388	Peak	438	Peak	540	Peak	634	Peak	676	Peak	725	Peak	974	Peak	1031
		0.7	MF	701	Peak	942	Peak	1060	MF	1061	Peak	1481	Peak	1595	Peak	1365	Peak	2100	Peak	2301
		1	MF	1001	Peak	1587	Peak	1815	MF	1516	Peak	2484	Peak	2728	Peak	2017	Peak	3387	Peak	3819
	50	0.4	Peak	141	Peak	168	Peak	194	Peak	242	Peak	278	Peak	299	Peak	310	Peak	456	Peak	485
		0.7	Peak	340	Peak	413	Peak	468	Peak	563	Peak	673	Peak	720	Peak	760	Peak	1030	Peak	1097
		1	Peak	588	Peak	734	Peak	828	Peak	889	Peak	1164	Peak	1251	Peak	1151	Peak	1684	Peak	1834
0.8	12	0.4	MF	1344	Peak	1915	Peak	2136	Peak	2018	Peak	2916	Peak	3182	Peak	2663	Peak	4102	Peak	4435
		0.7	MF	2353	MF	4117	Peak	4859	MF	3554	MF	6220	Peak	7251	MF	4756	MF	8322	Peak	9888
		1	MF	3361	MF	5882	Peak	8041	MF	5077	MF	8885	Peak	11883	MF	6794	MF	11889	Peak	15807
	20	0.4	Peak	711	Peak	865	Peak	966	Peak	1112	Peak	1364	Peak	1467	Peak	1493	Peak	1987	Peak	2102
		0.7	MF	1412	Peak	2040	Peak	2279	Peak	2128	Peak	3119	Peak	3416	Peak	2803	Peak	4391	Peak	4777
		1	MF	2017	Peak	3401	Peak	3876	MF	3046	Peak	5143	Peak	5796	MF	4076	Peak	7089	Peak	7969
	30	0.4	Peak	375	Peak	450	Peak	509	Peak	656	Peak	724	Peak	784	Peak	754	Peak	1058	Peak	1122
		0.7	Peak	887	Peak	1088	Peak	1216	Peak	1334	Peak	1704	Peak	1841	Peak	1775	Peak	2482	Peak	2638
		1	MF	1344	Peak	1886	Peak	2108	Peak	2018	Peak	2891	Peak	3162	Peak	2658	Peak	4086	Peak	4445
	50	0.4	Peak	164	Peak	198	Peak	230	Peak	267	Peak	321	Peak	353	Peak	336	Peak	473	Peak	505
		0.7	Peak	395	Peak	479	Peak	543	Peak	675	Peak	768	Peak	835	Peak	765	Peak	1127	Peak	1202
		1	Peak	688	Peak	846	Peak	950	Peak	1084	Peak	1335	Peak	1446	Peak	1463	Peak	1956	Peak	2083

Note: *FC = Failure criteria; Peak = First peak load; Yura = Yura's deformation limit; MF = Member failure*
Load unit: kN

Appendix A (k): Ultimate capacity of completely overlapped tubular joints ($\theta = 60^0$, $\xi = 1.0$)

Ultimate	β_{TL}	0.4						0.6						0.8					
Capacity	τ_{TL}	0.4		0.7		1		0.4		0.7		1		0.4		0.7		1	
β_{CT}	γ_C	τ_{CT}	FC	Load	FC	Load	FC	Load	FC	Load	FC	Load	FC	Load	FC	Load	FC	Load	FC	Load
0.4	12	0.4	MF	658	MF	1151	Peak	1447	MF	1001	MF	1752	Peak	2147	MF	1344	MF	2353	Peak	2923
		0.7	MF	1151	MF	2015	MF	2878	MF	1752	MF	3066	MF	4380	MF	2353	MF	4117	MF	5882
		1	MF	1645	MF	2878	MF	4112	MF	2503	MF	4380	MF	6257	MF	3361	MF	5882	MF	8403
	20	0.4	MF	395	Peak	597	Peak	664	MF	601	Peak	911	Peak	1020	MF	807	Peak	1309	Peak	1447
		0.7	MF	691	MF	1209	Peak	1537	MF	1051	MF	1840	Peak	2278	MF	1412	MF	2470	Peak	3059
		1	MF	987	MF	1727	MF	2467	MF	1502	MF	2628	Peak	3655	MF	2017	MF	3529	Peak	4750
	30	0.4	Peak	255	Peak	312	Peak	349	Peak	377	Peak	488	Peak	542	Peak	516	Peak	731	Peak	786
		0.7	MF	461	Peak	739	Peak	829	MF	701	Peak	1114	Peak	1265	MF	941	Peak	1581	Peak	1765
		1	MF	658	MF	1151	Peak	1417	MF	1001	MF	1752	Peak	2106	MF	1344	MF	2353	Peak	2805
	50	0.4	Peak	111	Peak	133	Peak	152	Peak	178	Peak	210	Peak	236	Peak	263	Peak	325	Peak	348
		0.7	Peak	269	Peak	330	Peak	369	Peak	396	Peak	511	Peak	572	Peak	542	Peak	756	Peak	822
		1	MF	395	Peak	579	Peak	645	MF	601	Peak	880	Peak	990	MF	807	Peak	1256	Peak	1391
0.6	12	0.4	MF	1001	Peak	1546	Peak	1780	MF	1516	Peak	2432	Peak	2688	Peak	2013	Peak	3358	Peak	3809
		0.7	MF	1752	MF	3066	Peak	3955	MF	2653	MF	4643	Peak	6043	MF	3554	MF	6220	Peak	7961
		1	MF	2503	MF	4380	MF	6257	MF	3790	MF	6633	MF	9475	MF	5077	MF	8885	Yura	12292
	20	0.4	Peak	560	Peak	710	Peak	817	Peak	869	Peak	1112	Peak	1210	Peak	1140	Peak	1643	Peak	1799
		0.7	MF	1051	Peak	1633	Peak	1887	MF	1592	Peak	2561	Peak	2848	Peak	2122	Peak	3533	Peak	4028
		1	MF	1502	MF	2628	Peak	3154	MF	2274	MF	3980	Peak	4799	MF	3046	MF	5331	Peak	6420
	30	0.4	Peak	292	Peak	365	Peak	430	Peak	484	Peak	570	Peak	625	Peak	674	Peak	888	Peak	962
		0.7	Peak	692	Peak	889	Peak	1021	Peak	1042	Peak	1378	Peak	1510	Peak	1353	Peak	1997	Peak	2226
		1	MF	1001	Peak	1510	Peak	1740	MF	1516	Peak	2355	Peak	2611	Peak	2013	Peak	3259	Peak	3703
	50	0.4	Peak	126	Peak	158	Peak	194	Peak	212	Peak	243	Peak	271	Peak	313	Peak	401	Peak	434
		0.7	Peak	309	Peak	389	Peak	459	Peak	505	Peak	599	Peak	660	Peak	701	Peak	919	Peak	1005
		1	Peak	542	Peak	690	Peak	800	Peak	850	Peak	1061	Peak	1165	Peak	1126	Peak	1558	Peak	1733
0.8	12	0.4	MF	1344	Peak	1824	Peak	2063	Peak	2000	Peak	2810	Peak	3107	Peak	2644	Peak	4017	Peak	4376
		0.7	MF	2353	MF	4117	Peak	4713	MF	3554	MF	6220	Peak	7101	MF	4756	MF	8322	Peak	9751
		1	MF	3361	MF	5882	Peak	7829	MF	5077	MF	8885	Peak	11656	MF	6794	MF	11889	Peak	15430
	20	0.4	Peak	648	Peak	809	Peak	935	Peak	1018	Peak	1252	Peak	1392	Peak	1397	Peak	1837	Peak	1974
		0.7	MF	1412	Peak	1926	Peak	2186	Peak	2108	Peak	2956	Peak	3290	Peak	2783	Peak	4220	Peak	4643
		1	MF	2017	Peak	3238	Peak	3719	MF	3046	Peak	4935	Peak	5603	MF	4076	Peak	6860	Peak	7766
	30	0.4	Peak	334	Peak	418	Peak	496	Peak	557	Peak	645	Peak	728	Peak	751	Peak	948	Peak	1021
		0.7	Peak	807	Peak	1015	Peak	1170	Peak	1242	Peak	1558	Peak	1737	Peak	1692	Peak	2264	Peak	2455
		1	MF	1344	Peak	1769	Peak	2014	Peak	1986	Peak	2705	Peak	3018	Peak	2631	Peak	3860	Peak	4254
	50	0.4	Peak	146	Peak	186	Peak	228	Peak	242	Peak	284	Peak	338	Peak	348	Peak	419	Peak	454
		0.7	Peak	352	Peak	444	Peak	528	Peak	579	Peak	679	Peak	769	Peak	795	Peak	996	Peak	1078
		1	Peak	624	Peak	786	Peak	915	Peak	974	Peak	1197	Peak	1345	Peak	1348	Peak	1742	Peak	1889

Note: *FC = Failure criteria; Peak = First peak load; Yura = Yura's deformation limit; MF = Member failure*
Load unit: kN

Appendix A (l): Ultimate capacity of completely overlapped tubular joints

($\theta = 60^0$, $\xi = 2.0$)

Ultimate		β_{TL}	0.4						0.6						0.8					
Capacity		τ_{TL}	0.4		0.7		1		0.4		0.7		1		0.4		0.7		1	
β_{CT}	γ_C	τ_{CT}	FC	Load	FC	Load	FC	Load	FC	Load	FC	Load	FC	Load	FC	Load	FC	Load	FC	Load
0.4	12	0.4	MF	658	MF	1151	Peak	1400	MF	1001	MF	1752	Peak	2112	MF	1344	MF	2353	Peak	2868
		0.7	MF	1151	MF	2015	MF	2878	MF	1752	MF	3066	MF	4380	MF	2353	MF	4117	Yura	5545
		1	MF	1645	MF	2878	MF	4112	MF	2503	MF	4380	MF	6257	MF	3361	MF	5882	Yura	8403
	20	0.4	MF	395	Peak	568	Peak	636	MF	601	Peak	874	Peak	996	MF	807	Peak	1265	Peak	1412
		0.7	MF	691	MF	1209	Peak	1488	MF	1051	MF	1840	Peak	2224	MF	1412	MF	2470	Peak	2934
		1	MF	987	MF	1727	MF	2467	MF	1502	MF	2628	Peak	3517	MF	2017	MF	3529	Yura	5042
	30	0.4	Peak	239	Peak	296	Peak	332	Peak	358	Peak	462	Peak	529	Peak	505	Peak	681	Peak	747
		0.7	MF	461	Peak	709	Peak	800	MF	701	Peak	1077	Peak	1241	MF	941	Peak	1521	Peak	1709
		1	MF	658	MF	1151	Peak	1372	MF	1001	MF	1752	Peak	2051	MF	1344	MF	2353	Peak	2648
	50	0.4	Peak	102	Peak	127	Peak	145	Peak	162	Peak	198	Peak	232	Peak	244	Peak	287	Yura	332
		0.7	Peak	254	Peak	316	Peak	353	Peak	378	Peak	491	Peak	562	Peak	532	Peak	710	Peak	781
		1	MF	395	Peak	556	Peak	622	MF	601	Peak	852	Peak	974	MF	807	Peak	1203	Peak	1337
0.6	12	0.4	MF	1001	Peak	1486	Peak	1728	MF	1516	Peak	2338	Peak	2620	Peak	2008	Peak	3279	Peak	3770
		0.7	MF	1752	MF	3066	Peak	3867	MF	2653	MF	4643	Peak	5918	MF	3554	MF	6220	Peak	7729
		1	MF	2503	MF	4380	MF	6257	MF	3790	MF	6633	Yura	9393	MF	5077	MF	8885	Yura	11475
	20	0.4	Peak	527	Peak	682	Peak	791	Peak	828	Peak	1042	Peak	1161	Peak	1111	Peak	1549	Peak	1742
		0.7	MF	1051	Peak	1577	Peak	1840	MF	1592	Peak	2473	Peak	2786	Peak	2115	Peak	3426	Peak	3949
		1	MF	1502	MF	2628	Peak	3078	MF	2274	MF	3980	Peak	4687	MF	3046	MF	5331	Peak	6152
	30	0.4	Peak	274	Peak	356	Peak	417	Peak	444	Peak	526	Peak	597	Peak	620	Peak	802	Peak	924
		0.7	Peak	654	Peak	859	Peak	994	Peak	1014	Peak	1314	Peak	1465	Peak	1336	Peak	1908	Peak	2159
		1	MF	1001	Peak	1460	Peak	1704	MF	1516	Peak	2277	Peak	2557	Peak	2006	Peak	3148	Peak	3612
	50	0.4	Peak	118	Peak	157	Peak	190	Peak	189	Peak	224	Peak	262	Peak	294	Peak	354	Peak	398
		0.7	Peak	292	Peak	382	Peak	444	Peak	469	Peak	559	Peak	635	Peak	650	Peak	840	Peak	959
		1	Peak	517	Peak	671	Peak	776	Peak	806	Peak	1009	Peak	1131	Peak	1091	Peak	1470	Peak	1668
0.8	12	0.4	Peak	1339	Peak	1742	Peak	1991	Peak	1959	Peak	2684	Peak	3031	Peak	2620	Peak	3878	Peak	4293
		0.7	MF	2353	Peak	3940	Peak	4585	MF	3554	Peak	6006	Peak	6987	MF	4756	Peak	8304	Peak	9576
		1	MF	3361	MF	5882	Peak	7660	MF	5077	MF	8885	Peak	11415	MF	6794	MF	11889	Peak	14696
	20	0.4	Peak	603	Peak	775	Peak	891	Peak	942	Peak	1170	Peak	1350	Peak	1308	Peak	1679	Peak	1881
		0.7	MF	1412	Peak	1852	Peak	2118	Peak	2068	Peak	2845	Peak	3227	Peak	2761	Peak	4068	Peak	4525
		1	MF	2017	Peak	3130	Peak	3625	MF	3046	Peak	4796	Peak	5514	MF	4076	Peak	6657	Peak	7564
	30	0.4	Peak	310	Peak	406	Peak	476	Peak	500	Peak	602	Peak	709	Peak	716	Peak	850	Peak	1005
		0.7	Peak	762	Peak	980	Peak	1117	Peak	1165	Peak	1476	Peak	1696	Peak	1555	Peak	2107	Peak	2350
		1	Peak	1309	Peak	1707	Peak	1948	Peak	1938	Peak	2609	Peak	2968	Peak	2604	Peak	3708	Peak	4124
	50	0.4	Peak	138	Peak	184	Peak	223	Peak	220	Peak	268	Peak	315	Peak	331	Peak	381	Peak	427
		0.7	Peak	330	Peak	434	Peak	507	Peak	527	Peak	640	Peak	754	Peak	748	Peak	903	Peak	1010
		1	Peak	589	Peak	764	Peak	873	Peak	913	Peak	1136	Peak	1316	Peak	1267	Peak	1606	Peak	1797

Note: *FC = Failure criteria; Peak = First peak load; Yura = Yura's deformation limit; MF = Member failure*
Load unit: kN

APPENDIX B

Source Program written in Visual C Language

Post-Processing of Output Data from FE Analysis

```
#include "stdafx.h"
#include "stdio.h"
#include "stdlib.h"
#include "string.h"
#include "math.h"

main()
{
      float x[300], y[300];
      float temp;
      FILE *fp_in,*fp_out;
while(1)
{
      char in[40],c,file[40]="e:/results/",file_o[40]="e:/results/";
      int i,j,times,joint,mod,max=-999, flag=0;
      puts("File name:");
       gets(in);
       strcat(file,in);
      strcat(file_o,in);
       strcat(file,".txt");
      strcat(file_o,"_out.txt");
      puts(file);
       if ((fp_in=fopen(file,"r"))==NULL)
      {
            printf("File openning error!");
      }
            if ((fp_out=fopen(file_o,"w"))==NULL)
      {
            printf("File openning error!");
      }
//new
      puts("");
      puts("");
      puts("File mode...");
      puts("4 node element——press 1    ");
      puts("8 node element——press 2    ");
      scanf("%d",&mod);
//new end
      puts("");
      puts("Increment number!");
```

```
        scanf("%d",&times);

        puts("");
        puts("Node number!");
        scanf("%d",&joint);
//new
        if (mod==2)
        {
            joint=joint/2+1;
        }
//new end
        while(c!='-')
        {
            fscanf(fp_in,"%c",&c );
        }
        while(c=='-')
        {
            fscanf(fp_in,"%c",&c );
        }

        for(i=1;i<=times;i++)
        {
             fscanf(fp_in,"%f",&temp );
              x[i]=temp;
             fscanf(fp_in,"%f",&temp );
            y[i]=temp/2;
        }
        for (j=2; j<=joint-1;j++)
        {
            while(c!='-')
            {
                fscanf(fp_in,"%c",&c );
            }
            while(c=='-')
            {
                 fscanf(fp_in,"%c",&c );
            }

             for(i=1;i<=times;i++)
            {
                 fscanf(fp_in,"%f",&temp );
                 x[i]=x[i]+temp;
                  fscanf(fp_in,"%f",&temp );
                 y[i]=y[i]+temp;
            }
        }
        while(c!='-')
        {
```

```
            fscanf(fp_in,"%c",&c );
        }
        while(c=='-')
        {
            fscanf(fp_in,"%c",&c );
        }
        for(i=1;i<=times;i++)
        {
            fscanf(fp_in,"%f",&temp );
            x[i]=x[i]+temp;
            fscanf(fp_in,"%f",&temp );
            y[i]=2*y[i];
        }
      //    for (i=1;i<=times;i++)
//    {
//        x[i]=x[i]/joint;
//        y[i]=2*y[i];
//    }
//new
if (mod==2)
{
      for (j=joint+1; j<=2*joint-1;j++)
      {
          while(c!='-')
          {
              fscanf(fp_in,"%c",&c );
          }
          while(c=='-')
          {
              fscanf(fp_in,"%c",&c );
          }

          for(i=1;i<=times;i++)
          {
              fscanf(fp_in,"%f",&temp );
              x[i]=x[i]+temp;
              fscanf(fp_in,"%f",&temp );
              y[i]=2*y[i];
          }
      }
      joint=2*joint-1;
}
//new end
//new
      for (i=1;i<=times;i++)
      {
          x[i]=x[i]/joint;
          y[i]=2*y[i];
```

```
        }

        for(i=1;i<=times;i++)
        {
                if (fabs(y[i])>max)
                {
                        flag=i;
                        max=fabs(y[i]);
                }
                else
                {
                        i=999999;
                }
        }
//new end
        temp=0;
        fprintf(fp_out,"%f",temp);
         fprintf(fp_out,"    %f\n",temp);

        for(i=1;i<=times;i++)
        {
                fprintf(fp_out,"%f",fabs(x[i]));
                fprintf(fp_out,"    %f\n",fabs(y[i]));
        }

         fprintf(fp_out,"\nMax\n");
         fprintf(fp_out,"%f",fabs(x[flag]));
         fprintf(fp_out,"    %f\n",fabs(y[flag]));

        fclose(fp_in);
        fclose(fp_out);

        puts("");
        puts("Output File: ");
        puts(file_o);
        puts("Thanks!");

        scanf("%c",&c);
        scanf("%c",&c);
}
        return 0;
}
```

PUBLICATIONS

Journal papers

1. Wie-Min Gho and Ye Yang, "Parametric Equation for Static Strength of Completely Overlapped Tubular Joints", Journal of Structural Engineering, ASCE, 2006. (revised version submitted for possible publication)
2. Wie-Min Gho, Ye Yang and Fei Gao, "Failure Mechanisms of Tubular Joint with Complete Overlap of Braces", Thin-Walled Structures, 44(6), pp. 655-666, 2006.
3. Wie-Min Gho, Fei Gao and Ye Yang, "Stress and Strain Concentration of Completely Overlapped Tubular K(N)-Joints under Basic Loadings", Journal of Constructional Steel Research, 62(7), pp. 656-674, 2006.
4. Wie-Min Gho, Fei Gao and Ye Yang, "Load Combination Effects on Stress and Strain Concentration of Completely Overlapped Tubular K(N)-Joints", Thin-Walled Structures, 43(8), pp. 1243-1263, 2005.

Conference papers

5. Wie-Min Gho and Ye Yang, "Cyclic Performance of Completely Overlapped Tubular Joints", Proceedings of The 15th International Offshore and Polar Engineering Conference, Seoul, Korea, pp.320-324, 2005.
6. Ye Yang, Wie-Min Gho and Fei Gao, "Assessment of Cyclic Behaviour of Completely Overlapped Tubular Joints Based on Strength Resistance", Proceedings of the International Conference on Structural and Foundation Failures, Singapore, pp.239-246, 2004.
7. Wie-Min Gho, Fei Gao and Ye Yang, "Stress and Strain Concentrations of Completely Overlapped Tubular Joints under Lap Brace Axial Compression", Proceedings of The 18th Australia Conference on the Mechanics of Structures & Materials, Western Australia, pp.1115-1120, 2004.